UNIVERSITY OF CINCINNATI

16 Mrch 19 92

I hereby recommend that the thesis prepared under my supervision by ALI TOLO HERFAT

entitled ULTRASOUND SURFACE FINISH MEASUREMENT DURING THE PRECISION GRINDING PROCESS

be accepted as fulfilling this part of the requirements for the degree of DOCTOR OF PHILOSOPHY

Approved by:

A STUDY OF THE ULTRASOUND SURFACE FINISH MEASUREMENT DURING THE PRECISION GRINDING PROCESS

A Dissertation submitted to the

Department of Mechanical, Industrial
and Nuclear Engineering
College of Engineering

Division of Graduate Studies and Research

UNIVERSITY OF CINCINNATI

in partial fulfillment of the
requirements for the degree of

DOCTOR OF PHILOSOPHY

1992

by

ALI TOLO HERFAT

B.S. University of Tehran, Iran 1973

M.S. University of Cincinnati 1987

ADVISOR: DR.MAX L. BROWN

ABSTRACT

This research studied the methods and techniques that can be applied to measure the surface finish of a cylindrical part during the grinding process. The applicability, capability, and feasibility of the techniques and roughness measurement methods are the main research objectives. Through a literature survey and various technique investigations, it was estabilished that an ultrasonic technique has the greatest promise.

The research consists of both theoretical and experimental aspects. The theoretical work includes the study of wave propagation in two phase flow (emulsion), fluid dynamics and acoustic theories for the waveguide components of different geometry. The attenuated ultrasonic wave portion versus the waveguide system geometry, surface roughness, coolant (emulsion) properties, ultrasonic wave properties and modeling the surface finish measurement are also covered as a portion of the theoretical task of this work.

In the final section of the theoretical work, a code is written to predict the problem parameters utilizing a parameter estimation technique. The experimental part of this research deals with selecting required commercial devices, designing and building of test equipment, developing the test plan, performing the various test procedures for obtaining a maximum sensitivity and better resolution in surface finish measurement during the grinding process.

The scope of the research is to establish a correlation between experimental and theoretical results, analyze the data, optimize the prototype system, and recommend a product through the performing extensive test work.

GLOSSARY

Acoustics: The science of sound including its production, transmission and effects.

Attenuation: Loss of intensity in an ultrasonic wave.

Couplant: Material through which an ultrasonic wave may pass from a source to another material.

The Eulerian Description: This description, appropriate to fluid mechanics, is concerned with the field of flow. In Eulerian method, the pressure field of the fluid flow pattern is calculated, not the pressure changes which a particle experiences as it moves through the field.

Free Progressive Wave: A wave in a medium free from boundary effects.

Frequency: For a periodic quantity, in which time is independent variable, the number of periods occurring in a unit of time.

Intensity: The average rate of flow of energy through a unit area normal to the direction of wave propagation.

The Lagrangian Description: This method follows an individual particle motion in fluid flow.

Longitudinal Wave: A wave in which the direction of displacement at each point of the medium is normal to the wave front.

Monochromatic Wave: A monochromatic wave is a wave in which the pressure and velocity are periodic functions of time of a single frequency.

Piezo Electricity: Electric charges that appear on the parallel surfaces of a piezoelectric crystal when the crystal is subjected to a mechanical stress.

Plane Wave: A wave in which the wave fronts are everywhere parallel planes normal to the direction of propagation.

Rayleigh Wave: Type of surface wave in which the particle motion is elliptical about axes that are parallel to the wave front.

Reflection Coefficient: The ratio of acoustic intensity of the reflected wave to that of the incident wave at a boundary between two media of different acoustic impedances.

Resonance: Condition of vibration at which the absolute value of the driving-point impedance is a minimum. Velocity resonance exists between a body, or system, and an applied sinusoidal force if any small change in the frequency of the applied force causes a decrease in velocity at the driving point. Except for simple systems, such as pendulums, it is usually necessary to specify the type of resonance or resonant frequency.

Shear Wave: Transverse wave; a wave in which the particle motion is normal to the direction of propagation.

Sound Absorption: Dissipation or conversion of sound energy into other forms of energy, such as heat, either within the medium or attendant upon a reflection, molecular exchanges of energy and viscous losses.

Stress Waves: Any wave in a medium which is dependent upon the elastic nature of the medium.

Surface Waves: Waves that propagate along the surface of a medium and penetrate the medium only to shallow depths.

Transducer: A device that converts one energy form into a second energy form. The types most commonly used in ultrasonics convert electrical energy to ultrasonic energy and vice versa.

Transmission Coefficient: The ratio of the intensity of the transmitted wave to that of the incident wave at a boundary between two media of different characteristic impedances.

Ultrasonics: The general subject of sound in the frequency range above the average audible range of human beings. In general, sonic waves whose frequencies are greater than 20 KHZ.

Wave: A disturbance which is propagated within a medium in such a manner that for any point in the medium the displacement is a function of the time.

Wave Front: a) For a progressive wave in space, a continuous surface which is a locus of points having the same phase at a given instant; b) For a progressive surface wave, a continuous line which is a locus of points having the same phase at a given instant.

LIST OF SYMBOLS

a: tube radius ($1.59*10^{-3}$ m).
B_t: blockage factor for diffuser.
c: speed of ultrasonic wave in the coolant.
C_p: pressure recovery coefficient.
c_p: specific heat.
d: feedrate.
e: base of natural logarithms, 2.71828.
f: frequency, HZ.
g: acceleration due to gravity.
I: ultrasonic wave intensity, energy/area.
J_{nm}: Bessel's function.
k: wave number, ω/c.
K_n: eigenvalues.
L: a certain length of a grinding part.
n: normal to the waveguide assembly wall.
N: discrete sample points.
m: grating slope.
M_a: Mack number.
P_o: the mean pressure of medium.
P': ultrasonic wave pressure.
R: reflection coefficient.
r: lateral variable in the tube radius direction.
R: grid radius or approximately cutting depth.
R_{nm}: eigen-function, for lateral modes in tube shape path.
s: specific entropy.
t: time.
T: temperature.
u: internal energy.
v: medium local velocity.
x: distance variable along grinding part, horizontal.
z: distance variable along path.
α: absorption coefficient.
α_n: eigenvalue.
β: expansion coefficient.
2Θ: diffuser angle, degree.
θ: scattering angle.
η: effectiveness of a diffuser.
κ: thermal conductivity.
λ: grating wavelength.
π: pi, 3.141592654.
ρ: coolant density.
σ: surface roughness.
σ: summation sign.
φ: velocity potential.
ω: transducer frequency.

LIST OF FIGURES

LIST OF TABLES

ACKNOWLEDGEMENTS

A great debt is owed to Dr. Max L. Brown for his advice, guidance, encouragement and financial support throughout the Masters and Ph.D. programs.

The author is deeply indebted to Dr. Ivan E. Morse for his guidance, encouragement, discussion throughout the preparation of this dissertation, and use of his computer.

The author wishes to thank Dr. Ronald L. Huston for his enthusiasm and guidance during the preparation of this dissertation.

The author wishes to thank Dr. Phillip Quo for his guidance and serving in my committee.

A great debt is owed to Dr. Randall J. Allemang for his financial support, guidance, and enthusiasm. Also his great directory of graduate study program.

It was the author's extreme good fortune to have the collaboration of Dr. Noor Khadri for his literary comments in this dissertation.

Special thanks to all my colleagues who helped me in preparation of this dissertation, particularly Young Cho and Wang Chen-Hua.

Finally, the author's largest debt of thanks is owed to his wife Poran and his sons (Farokh and Safa) for their patience, sacrifice, and understanding during almost six years of hard pursual.

The financial support for Experimental part of this research was awarded in March 1988 by Ohio's Thomas Edison Program to the Department of Mechanical and Industrial Engineering of The University of Cincinnati.

CONTENTS

CHAPTER 1

1-1 INTRODUCTION:

Surface finish measurement during the precision grinding process is proposed for high-precision grinding of parts and specifically for cylindrical parts. Realization of the surface finish quality is dependent upon the development and integration of the grinding process feedback control devices.

The detection and control of the grinding process parameters on the CNC grinder can be equipped with integration of the ultrasonic sensor signal and four other sensor signals (acoustic emission, normal force, grinding power and vibration) to protect the surface finish measurement from undesired environmental input signals. It should be noted that the research works for those four sensors which were entitled as SBIR-I & II awarded to Metcut Research Associated, INC. by United State Air Force (USAF).

1-2 PROBLEM SIGNIFICANCE AND DESCRIPTION:

The proposed research answers an urgent need of the aerospace and associated industry to produce high technology and high quality products. The Metcut estimate states that the U.S. spends about $125 billion annually on removing metal by conventional machining. Another similar estimate states that the U.S. Air Force expense for machining is $12 to $13 billion annually. One reason for this high cost is that the existing technology cannot control surface finish during the grinding process. Precision grinding of parts is still considered an art and not a science.

Traditionally, a machine tool operator evaluates the surface roughness of a machined part by tactile sensing and visual observation of the stationary part. A stylus gauge is used to provide a more precise roughness measure by traversing in direct contact with a section of the stationary part. The direct contact approach has limitations. It is not practical to completely characterize a surface with the stylus because the small area scanned and the size of the probe tip limit the results to three to four thousand scanned points. Therefore, the stylus measuring method is not capable of measuring surface finish during the grinding process, Fig.(1-1).

Ultrasonic techniques are a more powerful approach to work in the grinding process. The ultrasonic wave is able to propagate inside the liquid which is used for cooling during the grinding operation. For this reason it is preferable to the other techniques such as lasers and fiber optics. The measurement is accomplished by the propagation of a high frequency ultrasonic wave through the coolant. The impinging wave at the grinding surface area is scattered in different directions. Rougher surfaces cause more ultrasonic energy dissipation, thus, the amplitude of the reflected signal decreases as the surface finish become rougher. The advantage with an on-line ultrasonic approach is not only real-time evaluation of surface finish quality, but also, the capability to provide sensor feed back for machine control and a criteria to evaluate tool condition in term of its performance on the part. A worn tool cuts or grinds a surface to different finish quality than a sharp tool. The ultrasonic system components are less expensive, consisting basically of a pulse generator and receiver (analyzer), transducers and some instruments to have signal measurement ability. The ultrasonic system process is not complicated. The transducer is exited by an electrical pulse

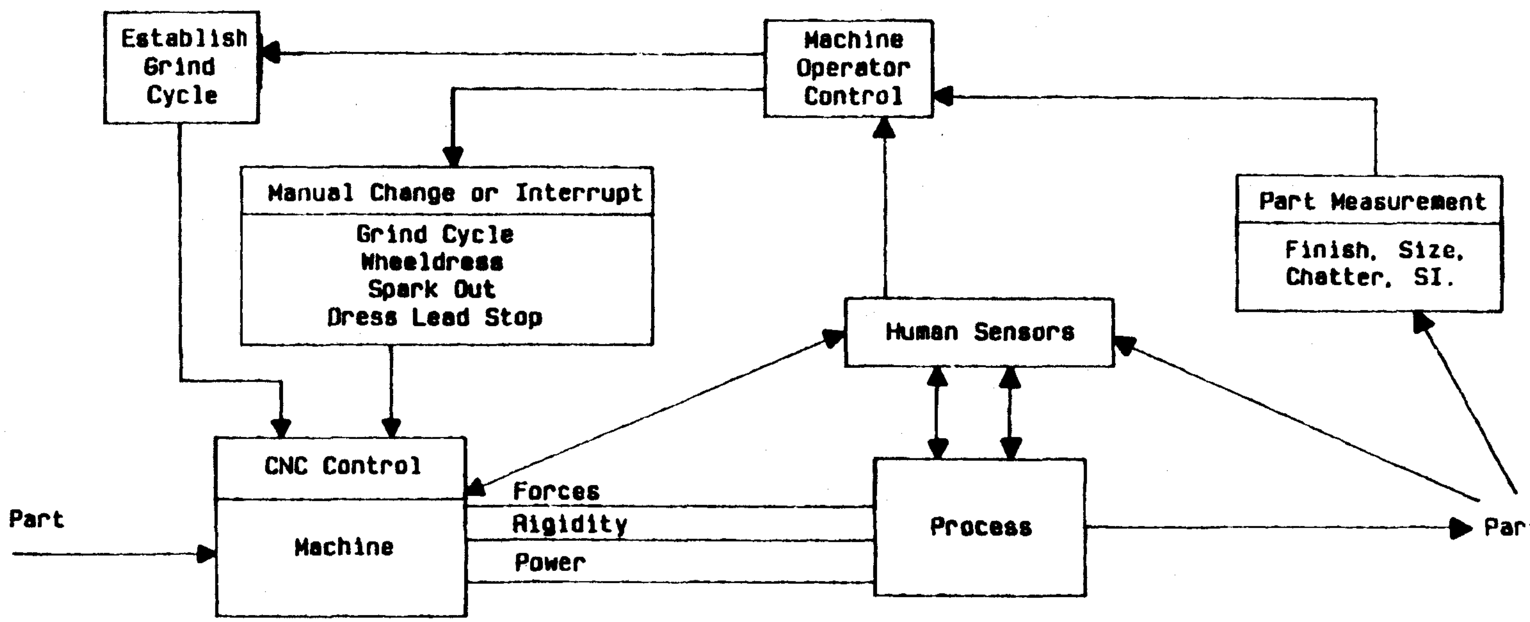

Grinding system model.

Fig.1-1

which comes from the pulse generator. Thus the transducer converts its input pulse to a vibrational wave. The reflected or echo wave is changed to an electrical pulse signal through either another transducer or the same transducer. The amount of echo signal energy measurement states the surface finish condition. Therefore, the pulse-echo technique can be applied to analyze a wide range of surface roughnesses by monitoring the peak amplitude of the echo signal. An ultrasonic wave with higher frequency has more capability to scan a finer surface discontinuity, therefore, a proper wave frequency which is proportional to the range of the precision surface finish measurement, is optimized through the experimental tests.

Choosing the right medium between transducer and grinding part for ultrasound propagation is one of the important parts of this research. Several commercial oils which can be mixed with tap water and form a homogeneous liquid were tested and finally an oil commercially known as Interlub-Bestcut was chosen based on: 1) higher wave energy transmission , or low energy attenuation; 2) no corrosive effect on the grinder components or grinding part in the range 3-5% oil volume fraction and 4) reasonable price. In fact, much of the original motivation for applying the ultrasonic technique in high speed grinding relied on the liquid jet (squirter) to flood the tool-part site for cooling and lubrication process. Both bubbling and cavitation inside two phase fluid flow (coolant) generate some problems such as opaque media for ultrasonic wave propagation, heat generation and possible turbulence. It is, however, possible to get rid of these undesired problems by controlling the temperature, pressure and oil volume fraction coolant. The fluid pattern study specifies the fluid characteristics through the wave guide. Analysis of waveguide geometries enables us to investigate the reflected wave conditions inside the coolant system. A portion of ultrasonic energy is attenuated in the waveguide system which, in this experiment consists of the squirter and the diffuser, and the transducer fixed inside the squirter, Fig.(1-2).

It should be noted that ultrasonic waves can be propagated efficiently through tap water, but it cannot be used as a proper coolant for a grinder due to its corrosive property.

Surface finish measurements, during the precision grinding process, are performed by integration of the ultrasonic signal with an accelerometer, normal force, acoustic emission, and grinding power wheel signals. Schematically the process diagram is shown in Fig. (1-3).

1-3 The Theoretical Development of the Waveguide Assembly:

This portion of the research is mainly based upon the acoustic theory and the sonic properties of the various materials for waveguide assembly design and development. The fluid flow pattern and the characteristics of the coolant are also studied in this section of research. The theoretical research part is summarized as follows:

- Survey through well documented researches of recent developments in the surface roughness measurement are currently available. The ultrasonic approach is recognized as a reliable and repeatable technique which has a strong capability for surface finish detection of the grinding part.
- Design and build a waveguide system which is matched with a grinder coolant system. Develope a waveguide assembly with different components such as squirter, diffuser and nozzle for obtaining the most powerful signal amplitude, refer to Appendix-A.
- The pattern of fluid flow is analyzed to determine the coolant properties and boundary layer conditions. Some of the fluid flow problems such as fluid separation, bubbling and increasing oil volume fractions are studied in this research. The attenuation rate of the

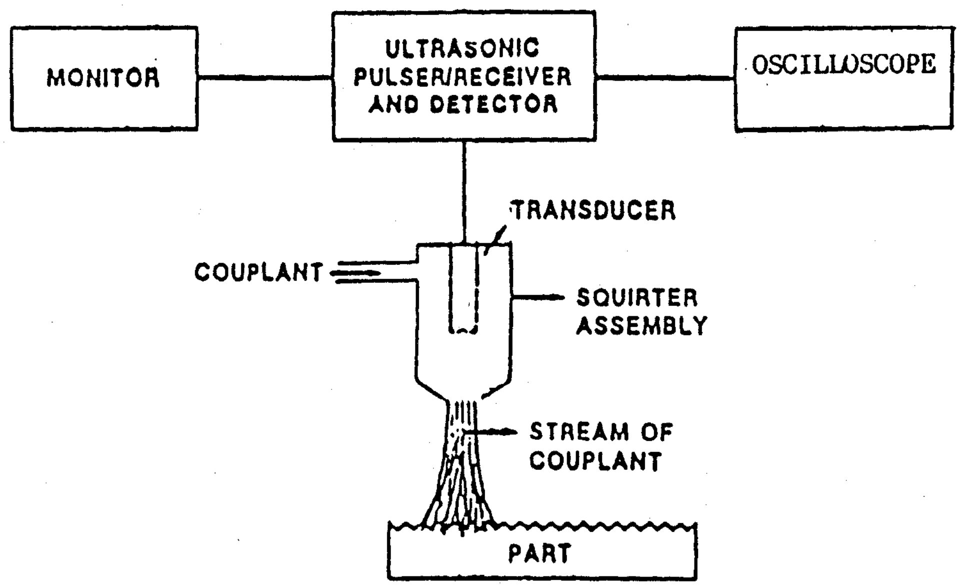

Ultrasonic pulse-echo approach to monitoring surface roughness, using a squirter assembly to couple the ultrasound between the transducer and part.

Fig. 1-2

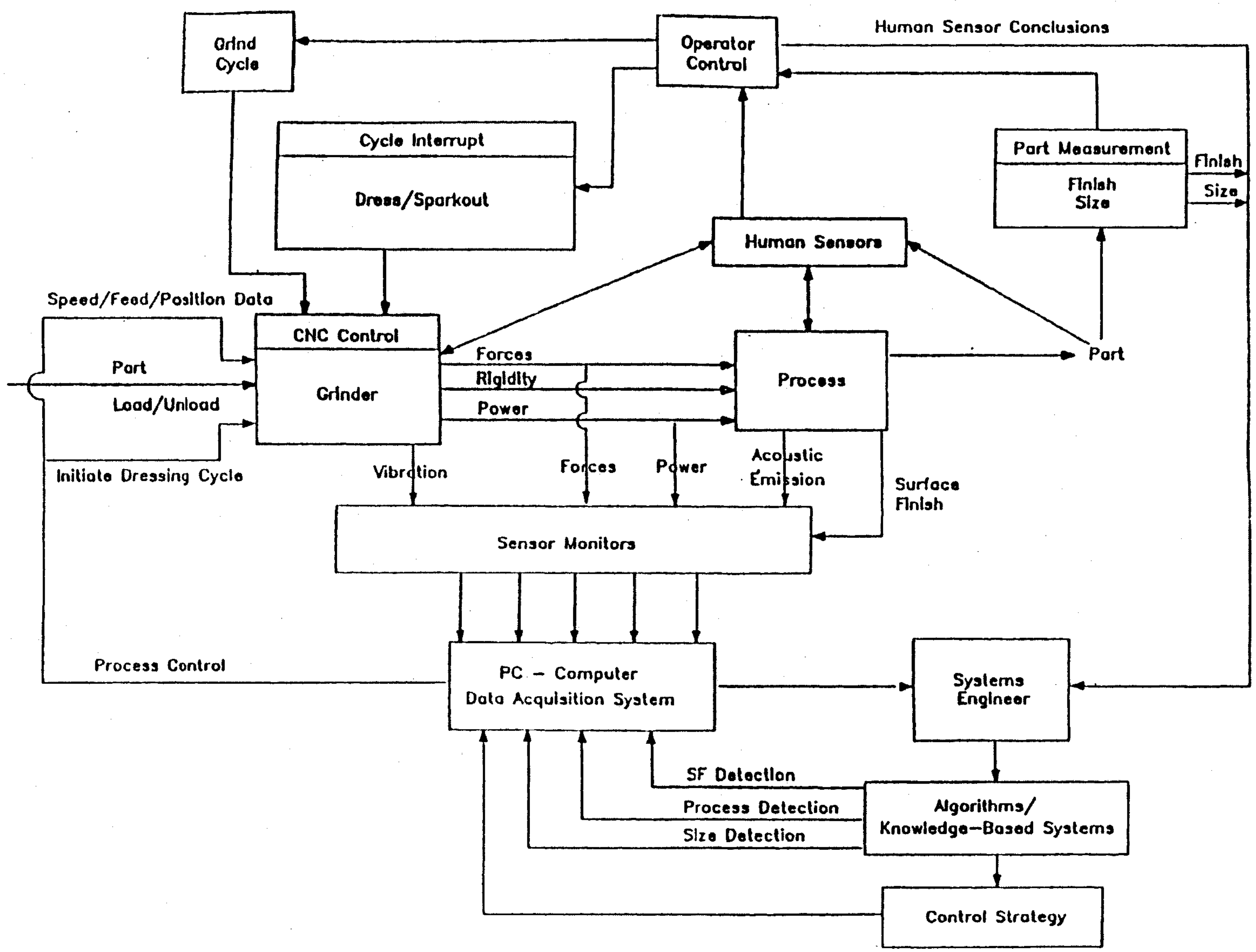

UNATTENDED GRINDING PROCESS

Fig. 1-3

ultrasonic wave is considered and calculated due to these undesired phenomena, see Chapter 2.

- The acoustic wave propagation in the waveguide assembly of the coolant system is studied and the wave propagation model obtained through the acoustic theory development for this research work. The multi-mode analysis enables us to find that the fundamental mode is much greater than the lateral modes, thus, it controls the propagation process in z-axis direction, refer to Chapter 3 .
- Mathematical surface finish analysis is accomplished through the statistical theories and equations developed which enable us to obtain a sinusoidal surface finish model for the precision grinding process. It should be noted that the finishing method of most grinding machines is in the form of a sinusoidal surface topography, see Chapter 4.
- Scattering phenomenon from the part surface (interface between media 1 and 2) is a function of surface finish quality. This phenomenon is studied by considering the surface finish model and applying the field equation which is presented in a Bessel-Fourier series form. The rate of reflected waves which can be captured by the waveguide assembly is investigated through the geometrical analysis of the waveguide assembly. The diffuser angle plays an important role to maximize the rate of reflected waves which are able to impinge upon the transducer face (piezoelectric crystal). The reflected ultrasonic velocity potential model is obtained based on the optimization of reflected angle versus part surface length (x) and distance from the part to the diffuser mouth. The parameter estimation theory finalizes the attenuation percentage rate for the different sample points along the interface and various standard distances from the part surface to the diffuser mouth. The empirical expressions derived for the standard part positions are

applied to determine the reflection coefficient for the reflection part of the field equation (field parameter is equal to summation of propagated wave parameter and reflected wave parameter), see Chapters 5 & 6.

- A proper code is written in linkage with the MATLAB software to specify the global solution of the research problem. This code is based on the theoretical results and empirical equations which are obtained in Chapters 2 through 6. The parameter estimation theory enables user to compute any variable parameter using this code when the rest are constant.
- The analysis of the experimental and theoretical results shows that the ideal diffuser is the diffuser with an angle of 10 degrees or less due to the following standpoints: 1) There is no fluid flow separation and 2) an increase in the rate of the reflected wave. But the capability of available machine tools in the machine shops and machinist were limited even the expertise machinist to make a diffuser with an angle less than about 30 degrees and with the same dimensions. Manufacturing of the stainless steel diffuser is very expensive compared to a similar diffuser made from aluminum, see Chapter 8.

1-4 RESEARCH OBJECTIVES AND METHOD OF INVESTIGATION:

The major objectives of this research titled as *surface finish measurement during the precision grinding process* are explained in two parts, an experimental part and a theoretical part as follows:

- The research concentrates on the round part (such as a shaft), the surface finish measurement, and the use of the standard grinder coolants. To verify the accuracy of the equipment and instrumentation in the required range for this research, several set tests were done for a flat plate with tap water. The acquired data must be compared with the similar experiments done for the flat plate in the past. This comparison proves the capability and accuracy of the experiment prototype. The ultrasonic frequency is optimized through testing of several transducers with various frequency (10 MHZ, 20 MHZ, and 30 MHZ).

- Design and fabrication of a non-contacting surface finish measurement device and installing and testing for reliability, repeatability and efficiency of the device. This device should be developed for more accuracy and capability. It can be done by adding other auxiliary components such as a diffuser or nozzle attached to the squirter.
- Obtaining the empirical equations for propagated wave, reflected wave , field and the attenuation expressions through model analysis, geometric analysis and parameter estimation theories.
- Surface finish model for this research which can be used in the precision range (4 to 75 μin) surface finish measurement of the round parts (cylindrical).

CHAPTER 2

FLOW PATTERN AND ATTENUATION IN TWO PHASE FLOW (EMULSION):

2-1 INTRODUCTION:

The purpose of this fluids study is to optimize the variables that influence the fluid flow and the ultrasonic waves in the region between the transducer and the work surface. A layout of the experimental set-up is shown in Fig. (A-1), Appendix A . This test plan is approved by the National Institute of Standards Technology (N.I.S.T.).

Important components of the fluid flow path include the squirter and conical diffuser. The conditions of the fluid inside the squirter were controlled by the geometry of stream lines inside the squirter, Fig. (2-1). The properties of the coolant (such as inlet pressure, temperature, and density) to satisfy a desired flow pattern (such as free of bubbling and laminar flow) were analyzed. These conditions enabled the ultrasonic wave propagation to be studied in a proper process.

In order to improve the quality of the sensor signal measurements, different short narrow pipes (called nozzles) and short diffusers were designed. Figures (2-2, 3). Each nozzle or diffuser was carefully expoxied to the squirter assembly, leaving no leakage or build up through the fluid passage hole. The mouth surface of the nozzles and diffusers were in contact with a flat stationary surface for these comparitive tests.

The conical diffusers performed better than the nozzles (higher sensitivity and amplitudes ratio). The reasons for these better performance values are associated with their

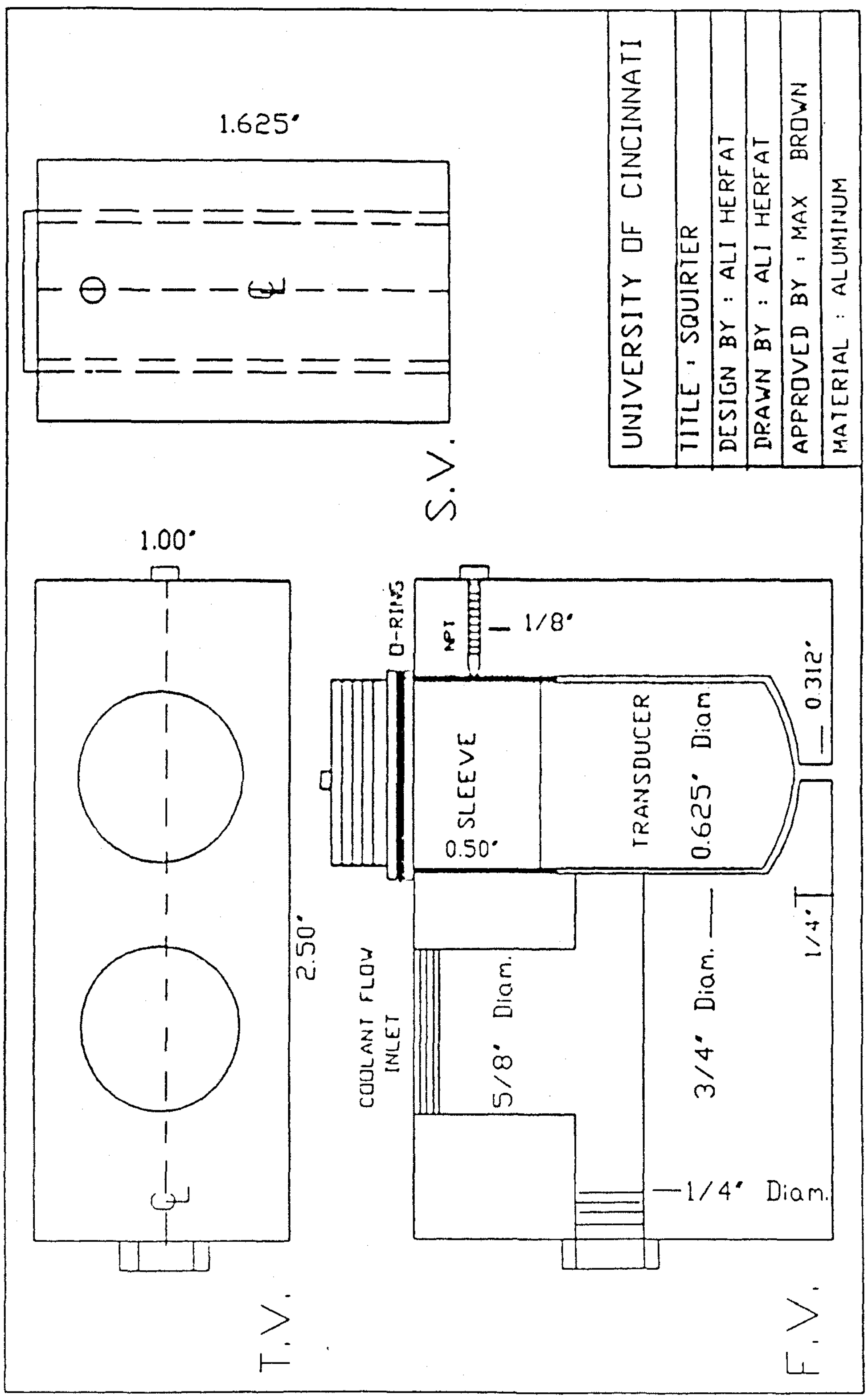
UNIVERSITY OF CINCINNATI
TITLE : SQUIRTER
DESIGN BY : ALI HERFAT
DRAWN BY : ALI HERFAT
APPROVED BY : MAX BROWN
MATERIAL : ALUMINUM
1.625'
S.V.
1.00'
2.50'
T.V.
O-RING
NPT
1/8'
SLEEVE
0.50'
TRANSDUCER
0.625' Diam.
0.312'
1/4'
COOLANT FLOW
INLET
5/8' Diam.
3/4' Diam.
1/4' Diam.
F.V.

FIG. 2-1

Fig. 2-2

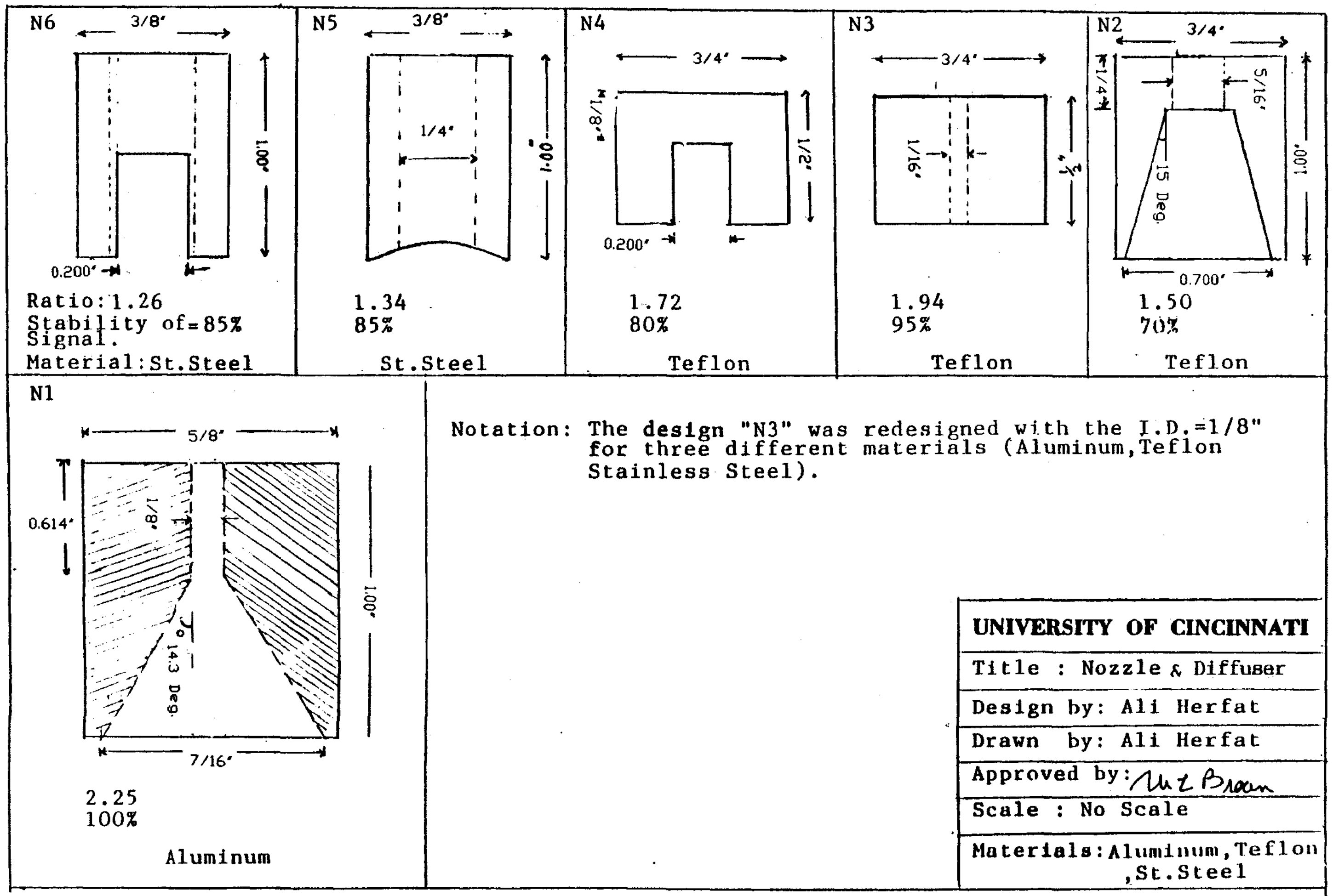
N6
3/8'
1.00'
0.200'
Ratio: 1.26
Stability of = 85%
Signal.
Material: St.Steel
N5
3/8'
1/4'
1.00"
1.34
85%
St.Steel
N4
3/4'
1/8"
1/2'
0.200'
1.72
80%
Teflon
N3
3/4'
1/16'
1/2'
1.94
95%
Teflon
N2
3/4'
1/4'
5/16'
15 Deg.
1.00'
0.700'
1.50
70%
Teflon
N1
5/8'
0.614'
1/8'
14.3 Deg.
1.00'
7/16'
2.25
100%
Aluminum
Notation: The design "N3" was redesigned with the I.D.=1/8" for three different materials (Aluminum, Teflon Stainless Steel).
UNIVERSITY OF CINCINNATI
Title : Nozzle & Diffuser
Design by: Ali Herfat
Drawn by: Ali Herfat
Approved by:
Scale : No Scale
Materials: Aluminum, Teflon ,St.Steel

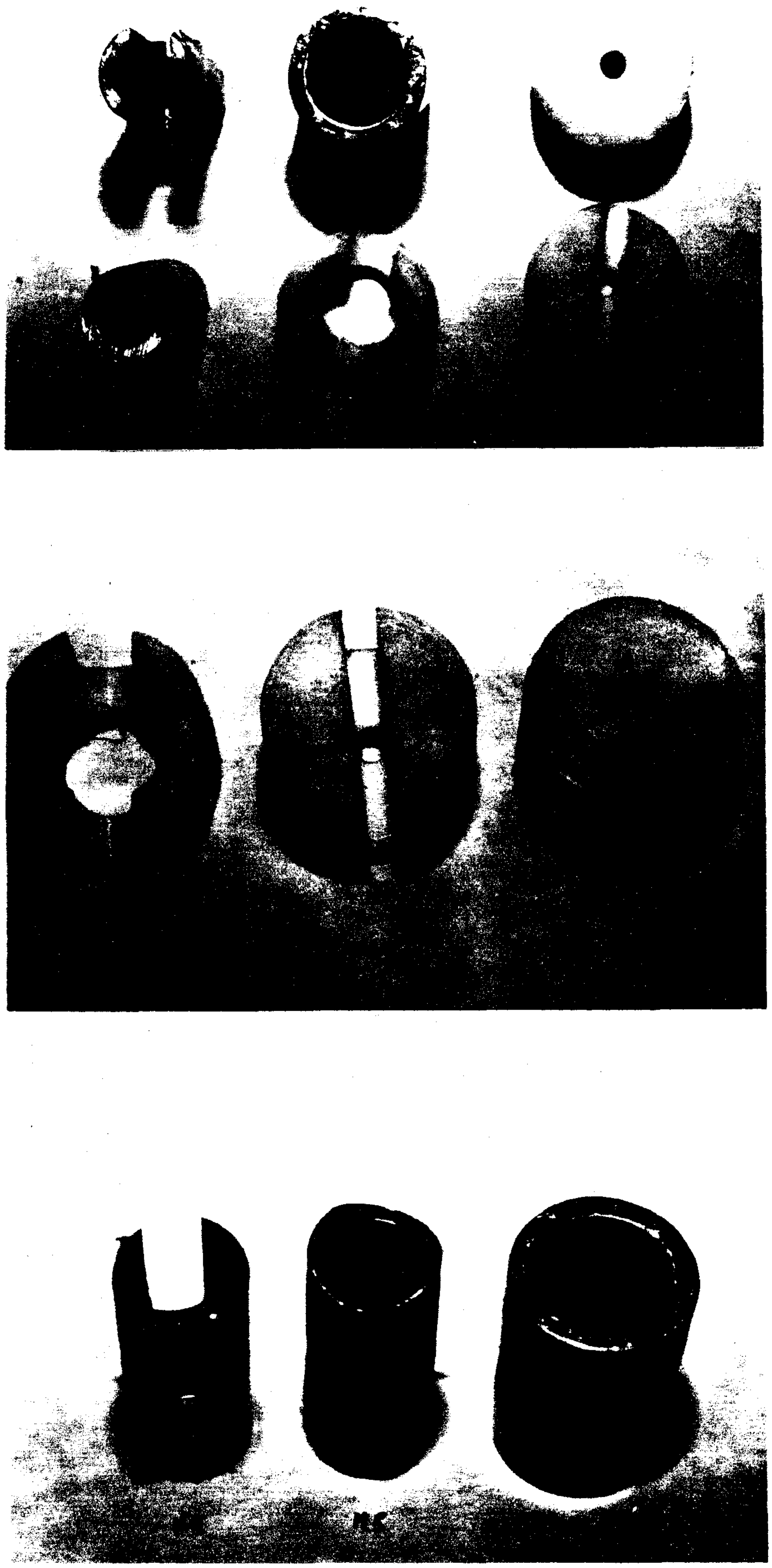

Fig. 2-3

geometrical configurations and materials. These two characteristics are discussed in the following sections of this chapter. The ultrasonic wave propagation through the diffuser will be studied in chapter 3.

2-2 DIFFUSER GEOMETRY:

In high-intensity ultrasound applications, wave energy is transferred from the transducer to the medium. The transmission lines of various configurations have a considerable effect on the wave propagation. The amplitude of an echo signal at the face of the transducer depends upon the geometry and material of the transmission line, energy losses, the amplitude of incident wave at the mouth, the incident angle, and reflected waves.

A tapered transmission line or diffuser component produces displacement amplification. Therefore, they are called mechanical amplifiers. In general, it can spread the concentrated waves emitting from the face of the transducer over a large area (mouth) so that they can continue with negligible reflection. Another important purpose of the diffuser is to concentrate the sound into a directed beam, so that most of the radiated energy is sent out in one direction. Note that the diffuser should not flare too rapidly, because the ultrasonic wave will not cling completely onto the inner walls of the diffuser.

2-3 THE MATERIAL EFFECTS:

Based on the theory of electromagnetic waves, an important characteristic of a material is its impedance, or more accurately its characteristic acoustic impedance, $Z = \rho c$. The percentage of incident wave reflected from the walls of the diffuser depends upon the ratio Z_1/Z_2 and also the angle of incidence. The characteristic acoustic impedance of coolant (volume fraction 4% Bestcut-Interlub with respect to tap water at 20^0C) is Z_1=(995 kg/m^3)(1516 m/s)=1.51E06 kg/m^2s, and Z_2 is 45.5E06 kg/m^2s for stainless-steel 302, 17.3E06 kg/m^2s for aluminum-2So, and 3.E06 kg/m^2s for teflon. The coefficient of reflection is defined as the ratio of the reflected to incident ultrasonic pressures

$$R=\frac{P_r}{P_i}=(\frac{z_2-z_1}{z_2+z_1}) \qquad (2\text{-}1)$$

$$1+R=T$$

The values of R are 0.936, 0.840, and 0.336 for stainless-steel-302, aluminum, and teflon respectively. The intensity reflection coefficient is also defined as the ratio of the reflected to incident energy fluxes (Watt/m^2). Thus, $R_I=R^2$.

The transmission and reflection coefficients for the walls of the diffusers are related by R=1-T, since the total acoustic energy is conserved. The amount of acoustic energy transmitted from the walls of three types of diffusers may be defined as, $T_{st\text{-}st}<T_{Al}<T_{tef}$. Therefore, the conical stainless-steel dominates the other types. But it should be noted that the manufacturing of an aluminum diffuser is easier and cheaper than for stainless-steel.

In the treatment of high frequency wave propagation through liquids confined within nozzles and diffusers, absorption of the ultrasound energy within the liquids (particularly two phases flow) increases more rapidly than absorption at the walls of these components. The quality of the flow pattern and the wave propagation are mostly dependant upon the configuration and material of the diffuser. The mouth of the diffuser is open to the environment, therefore the conditions of fluid flow and ultrasound propagation and reflection can be controlled by the diffuser. Hence, information about the quality of the flow pattern in the diffuser would be helpful in analyzing the wave phenomena.

2-4 THE FLOW PATTERN INSIDE THE DIFFUSER:

The fluid pattern in the diffuser is of paramount importance because it exhibits several physical phenomena.

First, the separation of fluid flow from the diffuser walls is considered. If this condition occurs, a portion of the echo wave is attenuated. Second, the signal is not stable and has some fluctuations, therefore analyzing the signal and its measurement cannot be performed accurately.

In fluid dynamics, the primary objective of a diffuser is to recover static pressure from a fluid stream while reducing the flow velocity. The fluid slows as it passes through a diffuser, and a portion of the kinetic energy of the fluid is converted into the potential energy of pressure.

In the diffuser, the pressure gradient opposes the flow. Consequently, the boundary layer in a diffuser decelerates and thickens rapidly and it can separate from the diffuser walls to form large unsteady eddies that block the diffuser flow. The separation of flow from the diffuser walls is called diffuser stall, and it always degrades the diffuser pressure recovery. Thus the limit of diffuser performance is largely governed by boundary layer growth and the start of stall.

Theoretical aspects of diffuser performance can be studied by considering a control volume, the dotted lines in Fig. (2-4), which is bounded by the interior walls of the diffuser. The following assumptions are made for the fluid flow:

- Homogenous and isotropic fluid flow.
- Incompressible flow.
- The friction is negligible.

- Steady flow, the fluid is pumped in the system with constant discharge pressure.
- Irrotational flow.

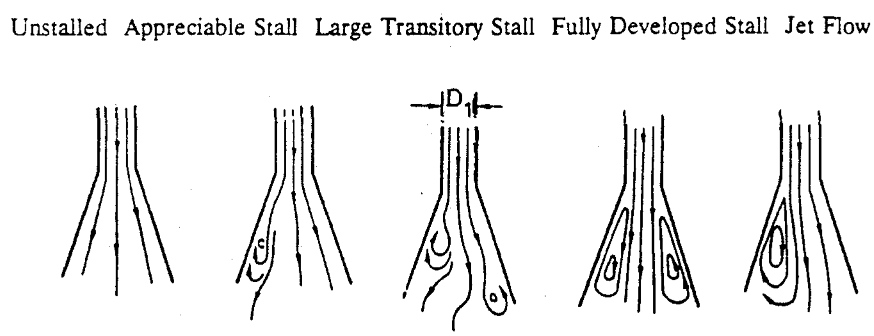

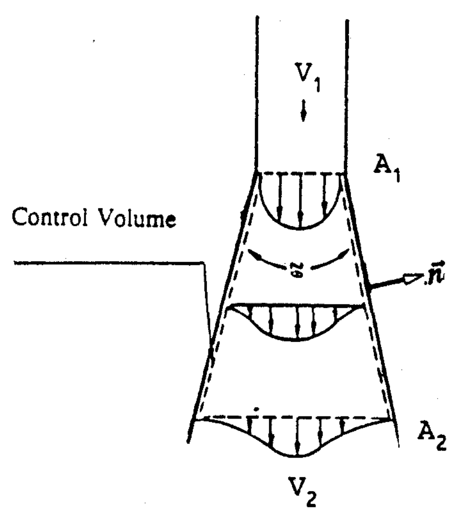

FIG. (2-4)

Applying experimental data yields the following boundary values for our conical diffuser.

The flow-rate: $q^{\bullet}=q/sec= V_1 * A_1=V_2 * A_2$ (2-1)

Table 2-1:

Diffuser cross-section	Diameter (D) ($m*10^{-3}$)	Velocity (V) (m/s)	Flow-rate(q^{*}) lit/s
Throat (inlet)	D_1=3.1750	V_1=2.5160	1./51
Mouth (outlet)	D_2=11.1125	V_2=0.2054	1./51

By using the Bernoulli's equation, we are able to analyze the characteristics of the fluid along a stream line through a control volume inside the diffuser as;

$$\frac{P_2-P_1}{\rho}=\frac{V_1^2-V_2^2}{2}+\Delta z \qquad (2\text{-}2)$$

$$\rho_{4\%coolant}=[0.96*998+0.04*924]\approx 995\frac{kg}{m^3} \qquad (2\text{-}3)$$

where:

$\Delta(z)=15.5956$ mm

P_1(static press.)=9839 pa=98.390 kpa

P_2(static press.)=Atm. press.=101.33 kpa

Conservation of energy can be described as

$$\rho\int_{A_1}(u+\frac{P}{\rho}+\frac{V^2}{2}-gz)\vec{V}.\vec{n}=\rho\int_{A_2}(u+\frac{P}{\rho}+\frac{V^2}{2}-gz)\vec{V}.\vec{n} \qquad (2\text{-}4)$$

Where, vector V is the local velocity and n is the unit vector outward normal from the control surface of the diffuser. The fluid is incompressible, therefore, its density is constant.

It should be noted that there is no heat generation source and shaft work across the control volume.

If we assume, first, the changes in internal energy (u) are negligible (the viscous dissipation is neglected), second, the static pressure is uniform over each cross section of the area of the diffuser, and third, the energy attenuation is restricted to the components of flow parallel to the center-line of the diffuser (where the fluid velocity is maximum). Then the equation (2-4) may be simplified as;

$$P_1\int_{A_1} vdA + \frac{\rho}{2}\int_{A_1} v^3 dA - \rho\int_{A_1} zvdA = P_2\int_{A_2} vdA + \frac{\rho}{2}\int_{A_2} v^3 dA - \rho\int_{A_2} zvdA \qquad (2\text{-}5)$$

The axial flow velocity (v) varies from zero at the diffuser walls to a peak value along the center-line of the diffuser. The velocity distribution is characterized by a kinetic energy flux profile factor as:

$$\alpha = \frac{1}{A}\int_A \left(\frac{v^3}{V_{av.}}\right) dA \qquad (2\text{-}6)$$

Where:

$$V_{av.} = \frac{1}{A}\int_A vdA$$

The velocity profile factor generally varies along the diffuser axis. It is the ratio of fluid kinetic energy passing through the cross-section of diffuser area (A) to minimum possible transport of fluid kinetic energy at the same mass flow. The a minimum value of the kinetic energy flux profile factor is $\alpha = 1$, which corresponds to the uniform flow. If this factor at the mouth of the diffuser is minimized, the exiting kinetic energy of the diffuser is minimized and the exiting potential energy is also decreased (since the diffuser is in a vertical position, the elevation decreases), Therefore, the pressure recovery is maximized to satisfy the conservation of energy. Thus, a uniform flow at the exit produces the best pressure recovery in the diffuser. Hence, the performance of a diffuser can be defined by the diffuser pressure recovery coefficient.

$$C_p=\frac{P_2-P_1}{\frac{1}{2}\rho V_1^2}=\alpha_1-\alpha_2(\frac{A_1}{A_2})^2 \qquad (2\text{-}7)$$

The value of C_p is strongly influenced by the flow profile at the entrance and the exit through the factor α. For uniform flow $v=V_{av.}$ and $\alpha_1=\alpha_2=1$. Therefore, equation (2-7) changes to;

$$C_p=\frac{P_2-P_1}{\frac{1}{2}\rho V_1^2}=1-(\frac{A_1}{A_2})^2 \qquad (2\text{-}8)$$

Therefore, we can compute the pressure recovery coefficient for both the general condition and ideal flow by equations (2-7) and (2-8) respectively. Substituting the experimental values into equation (2-7) yields:

$$C_p=(101330 \text{ pa}-98390 \text{ pa})/[0.5*(995 \text{ kg/m}^3)(2.516 \text{ m/s})^2]=0.9335$$

And for the uniform flow:

$$C_p = 1 - 0.0816 = 0.9184$$

Where: $(D_1 / D_2)^2 = 0.0816$

A total pressure loss coefficient, K, for a diffuser can be defined as

$$K=1-\left(\frac{A_1}{A_2}\right)^2-C_p \qquad (2\text{-}9)$$

The value of K for a perfect diffuser with excellent performance is very close to zero . Equation (2-9) for a diffuser with a free discharge, A_2 = infinity, can be written as;

$K = 1-C_p = 1- 0.9335 = 0.0665$

which is a good value. Therefore, our diffuser design predicts a good performance. It should be noted that the excellent theoretical diffuser has C_p close to one.

Blockage Factor: This factor is defined as

$$B_t=\frac{A_{BL}}{A_1}$$

where A_{BL} is the wall blocked, or displaced, by the retarded boundary layer flow at the inlet.

According to the fluid dynamics tables, for our experimental data, $B_t<0.01$ is lower than the standard range ($.03< B_t <.12$).

2-5 DIFFUSER STALL:

The phenomenon of the flow separation from the diffuser walls and the formation of unsteady separated or eddies flow within the diffuser is known as *stall*. Diffuser stall has been illustrated in Figure (2-5) for two dimensional diffusers.

The diffuser stall is due to:

1) The difusser inlet conditions.

2) The diffuser exit conditions.

3) Inlet Reynolds number (Re #).

4) Inlet Mack number Ma = V_1/a, for our experimental data, Ma=(2.516 m/s)/(340 m/s) = 0.0074 << 0.3 for an incompressible fluid.

5) Geometry, which is the most important property of a diffuser.

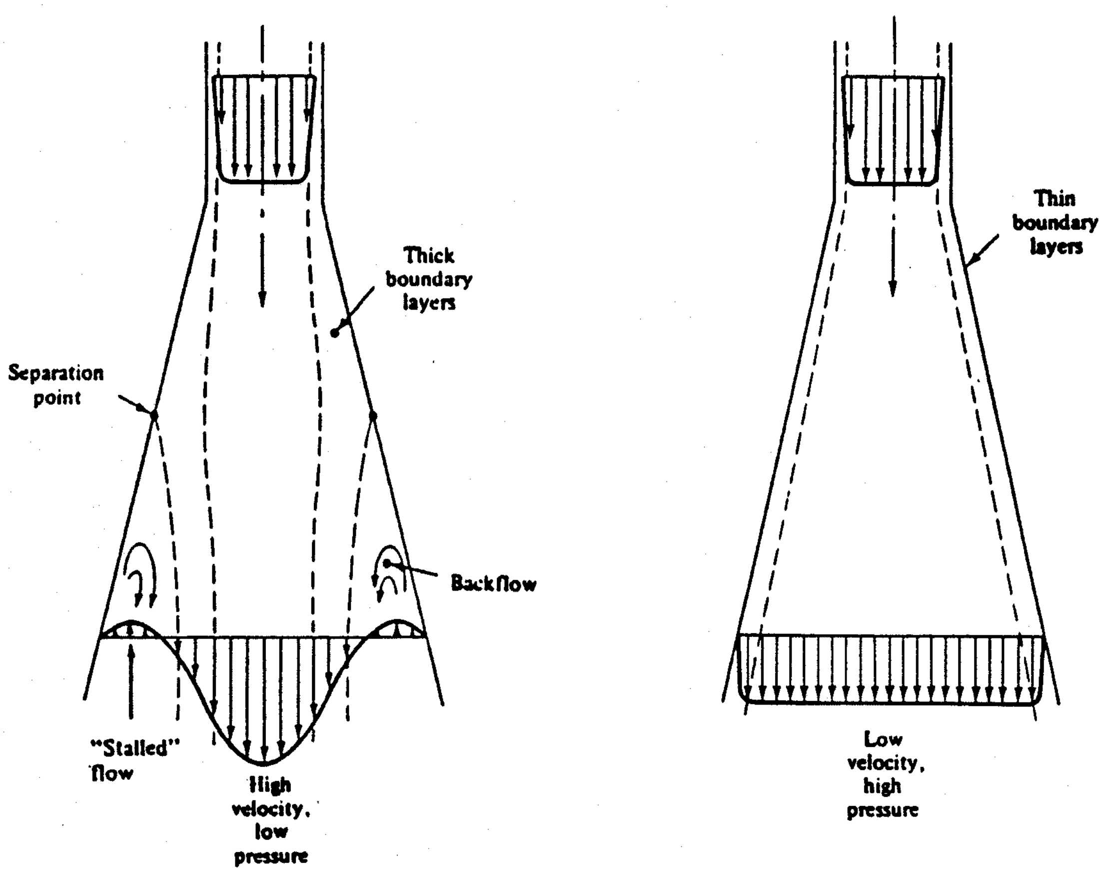

Actual measured pattern with boundary layer separation and resultant poor performance

Ideal pattern with good performance

FIG. (2-5)

In general, stall often occurs initially in the corners of two dimensional diffusers. Since the conical diffusers are free from corners, they are somewhat more resistant to stall, [3,4].

A complete stability map of diffuser flow patterns was published in 1962 by Fox and Kline, as shown in Figure (2-6). The stall regimes for different geometries of diffusers may be investigated from this stability map, [8].

Application of the experimental data yields:

The aspect ratio = depth/D_1 = (15.5956 mm)/(3.175 mm) = 4.912

which is approximately 5.0. By geometry dimensions of our diffuser, the divergence angle (2θ) is almost 28.6 degree. Therefore, the diffuser works in appreciable stall regime which is not a stall condition. It means the flow generally follows the diffuser walls. For a conical diffuser (such as our experimental diffuser) the regions of separation and erratic flow are not seen in the corners. Therefore, the separation of flow from the diffuser walls is almost negligible.

During the experiment the quality and the stability of the signals on the oscilloscope screen was the best evidence for a flow free from any separation, bubbling, and turbulence. It should be noted that manufacturing the diffuser with very small dimensions and with a divergence angle, 2θ, of about 10 degree is very difficult and expensive.

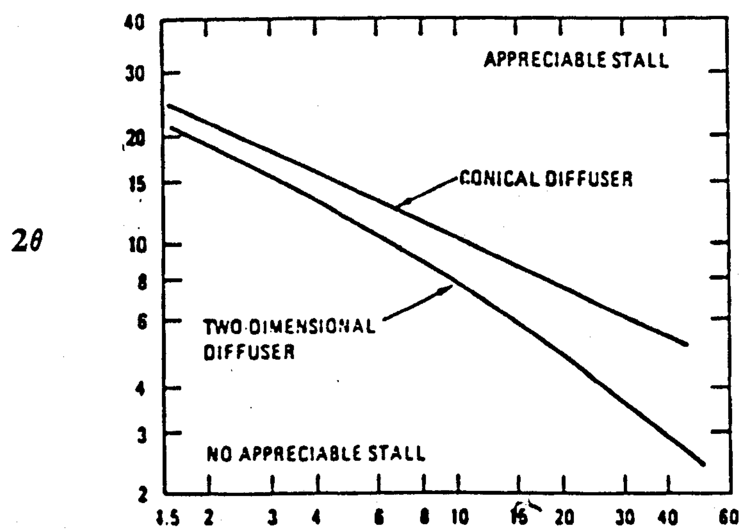

Aspect Ratio

FIG. (2-6)

2-6 EFFECTIVENESS OF A DIFFUSER:

Diffuser effectiveness can be defined to measure the actual diffuser performance against the theoretical ideal, or

$$\eta = \frac{\text{Actual Static Pressure Recovery}}{\text{Ideal Static Pressure Recovery}} = \frac{C_p}{1-(\frac{A_1}{A_2})^2} \qquad (2\text{-}10)$$

In practice, C_p will gradually fall below the theoretical ideal and η will be less than 1.0. The pressure recovery of a diffuser is reduced by the viscous dissipation and velocity or kinetic energy reduction at the outlet stream .

Substitution of our experimental values in equation (2-10) yields:

$$\eta=(0.9184)/(1.0)=0.9184$$

This value which is very close to one verifies the effectiveness and the high performance of the diffuser.

2-7 THE PERFORMANCE OF A DIFFUSER WITH FREE DISCHARGE:

Free discharge is the actual condition for the diffuser in this experiment. The free space can be assumed to be a very large reservoir. The pressure recovery gradually decreases with increasing inlet boundary layer thickness. Similarly, the diffuser performance generally decreases with decreasing Reynolds number, which corresponds to increasing boundary layer thickness. Where μ = [0.96 (11.3)+0.04(260)]10^{-4}=21.25.0 * 10^{-4} N.s/m^2

$$R_e=\frac{(D*v)_{throat}}{\nu}=(995\frac{kg}{m^3})(3.175*10^{-3}m)\frac{(2.516\frac{m}{s})}{(21.25*10^{-4}N.\frac{s}{m^2})}=3740.$$

If Re > 7 * 10^4, then the inlet boundary layer is fully turbulent and the performance of the diffuser is independent of Reynols number (Re#). This implies that the flow pattern in our experiment was certainly laminar.

2-8 BOUNDARY LAYER THICKNESS IN A DIFFUSER:

Diffuser performance usually decreases with increased boundary layer thickness. This phenomenon causes an increase in the blockage coefficient and a decrease in the fluid velocity and Reynolds number (Re#).

The ratio of boundary layer thickness to the throat diameter of a diffuser $2\delta/D_1 \approx$ 0.1 corresponds to a fully developed boundary layer. The value of δ can be computed by using

$$\delta = \int_0^{\frac{D_1}{2}} (1 - \frac{v}{v_c}) dr \qquad (2\text{-}11)$$

where

$$v = \frac{v_c}{1 + \frac{(2r\tan\theta)}{D_1}}$$

Hence, v_c is the center-line velocity and v is the local velocity at distance r from the diffuser inlet walls. Now the analysis of the boundary layer thickness at a distance $D_1/2$ from the throat of the diffuser is presented.

For $r = D_1/2 = 3.175/2$ mm, $v = v_c = 2.516$ m/s, and $\theta = 14.3$ degree, the value of v= 2.0 m/s, and

$$\delta = \int_0^{D_1} (1 - \frac{2.516}{2.}) dr = .326 * 10^{-3} m$$

Then $2\delta/D_1 \approx .41*10^{-3}$. The value of $2\delta/D_1$ from our experiment is found to be much less than 0.1, therefore the boundary layer thickness is very thin or the flow pattern through the diffuser is a laminar flow.

2-9 THE FLOW PATTERN CONCLUSIONS:

Based on our analyses the following results are concluded.

1) Incompressible fluid

2) Thin boundary layer, almost no separation.

3) Laminar flow, free of bubbling.

REFERENCES:

1- Schlichting H., Boundary-layer Theory. 6th E., MacGraw-Hill, 1968.

2- Sovron G., and E.D. Klomp, Experimentally Determined Optimum Geometries for Rectilinear Diffusers with Rectangular, Conical or Annular Cross-sections, in Fluid Mechanics of Internal Flow, Elsevier Publisher Co. New York, 1967.

3- McDonald A.T. and R.W. Fox, An Experimental Investigation of Incompressible Flow in Conical Diffuser, Int. J. Mech. Sci. 8, 125-135, 1966.

4- Waitman B.A., Effects of Inlet Conditions on Performance of the Two- Dimensional Subsonic Diffusers, J. Basic Eng. 83, 349-360, 1961.

5- Wolf, S., and J.P. Johnston, Effects of Nonuniform Inlet Velocity Profile on Flow Regimes and Performance in 2-Dim. Diffusers, J. Basic Eng. 91, 462-474.

6- Reneau, L.R., Performance and design of straight, 2-Dim. Diffuser, J. Basic Eng. 89, 141-150, 1967.

7- Frank M. White, Fluid Mechanics, 2nd E., MacGraw Hill, 345-351, 1986.

8- Ensminger, Ultrasonics, Marcel Dekker, INC, 113-138, 1988.

9- Javanaud. P. Sound Absorption in emulsions, Ultrasonic J., V.24, 138-142, 1986.

CHAPTER 3

ULTRASONIC WAVE PROPAGATION MODELING THROUGH THE COOLANT PATH:

3-1 INTRODUCTION:

Ultrasonic wave propagation through the moving fluids is the main topic of discussion in this chapter. Most of the available research work studied either the propagation of sonic wave through compressible fluids and/or static fluids. An analysis will be presented for wave propagation in moving incompressible fluids through different geometries.

3-2 DERIVATION OF THE ULTRASONIC WAVE EQUATION:

The ultrasonic wave equation is derived based on the flow pattern specifications obtained in chapter 2 and the following additional assumptions:

1) Flow pattern specifications:

   1-1) Incompressible fluid

   1-2) Thin boundary layer

   1-3) Laminar flow

   1-4) Flow free from bubbling

2) Assumptions:

   2-1) Homogenous fluid.

   2-2) Isotropic fluid.

   2-3) Frictionless flow ($\tau_{ij}=0$) or inviscid flow. Since the coolant is incompressible and inviscid, it can be considered as an ideal fluid.

   2-4) Exchanges of heat conduction and convection with the environment are negligible.

Entropy may be considered constant for this process or the process is reversible adiabatic and the adiabatic equations for instantaneous acoustic pressure and density can be used which are written as

$$P_{inst} = P_o + P'(r,t) \qquad (3\text{-}1)$$

$$\rho_{inst} = \rho_o + \rho'(r,t) \qquad (3\text{-}2)$$

Where:

P_0: The mean pressure of medium.

P': The pressure perturbation caused by acoustic wave propagation, or acoustic pressure.

ρ_o: The undisturbed density of medium.

ρ': The density variation due to ultrasonic wave radiation.

Based on these points, we are now able to write the primary equations which are required for derivation of the ultrasonic wave equation.

The infinitesimal change of the medium pressure is written as

$$dP' = \left(\frac{\partial P_{inst}}{\partial \rho_{inst}}\right)_s d\rho' + \left(\frac{\partial P_{inst}}{\partial s}\right)_\rho ds \qquad (3\text{-}3)$$

and the dynamic fluid equation (3-3) can be changed to.

$$\frac{DP_{inst}}{Dt} = \left(\frac{\partial P_{inst}}{\partial \rho_{inst}}\right)_s \left(\frac{DP_{inst}}{Dt}\right) + \left(\frac{\partial P_{inst}}{\partial s}\right)_\rho ds \qquad (3\text{-}4)$$

Then, for an adiabatic process, equation (3-4) is written as

$$\frac{DP_{inst}}{Dt} = c^2 \frac{D\rho_{inst}}{Dt} \qquad (3\text{-}5)$$

Where:

$$\frac{D}{Dt} = \frac{\partial}{\partial t} + \vec{V} \cdot \nabla$$

$$\textit{local speed of sound } c^2 = \left(\frac{\partial P_{inst}}{\partial \rho_{inst}}\right)_{s=s_o}$$

The values of P'& ρ'are very small compared with P_o & ρ_o.

$$\frac{dP_{inst}}{dt} = c^2 \frac{d\rho_{inst}}{dt} \qquad (3\text{-}6)$$

[1]

The equation (3-6) contains total derivatives and it is satisfied for a given particle of the medium (the Lagrangian description). But, for our purpose, the Eulerian description (flow field motion) is more appropriate. Since the fluid is assumed to be homogeneous, isotropic, and incompressible ($\nabla v = o$, or ρ=constant), and the coordinate system for the

---

[1] The departures from equilibrium density (ρ_0) are very small, we can expand $(\partial P/\partial \rho)s_o$ in Taylor series about ρ_o. Thus,

$$c^2 = \left(\frac{\partial P}{\partial \rho}\right)_{s_o} = \left[\left(\frac{\partial P}{\partial \rho}\right)_{s_o}\right]_{\rho=\rho_o} + \left[\left(\frac{\partial^2 P}{\partial \rho^2}\right)_{s_o}\right](\rho - \rho_o) + \cdots = c_o^2(r) + d_o(r)\rho' + \cdots$$

But ρ' is very small, then

$$c^2 = c_o^2 + c'^2$$

coolant at a given time. Converting the Lagrangian description to a Eulerian description invokes the following discusions:

Based on homogeneous and isentropic assumptions, the equation of state can be expressed as, P = P(ρ,s).

$$\left(\frac{1}{c^2}\right)\frac{\partial P'}{\partial t}=\frac{\partial \rho'}{\partial t}+\vec{V}.\nabla\rho \qquad (3\text{-}7)$$

Where V is the local velocity of the medium.

The pressure, density, and local velocity of the fluid must satisfy the hydrodynamic theory. Hence

1) Dynamic equation of fluid when the ultrasonic wave generates a perturbation in the fluid flow (Euler equation for an incompressible and inviscid flow).

$$\rho_{inst}\frac{dv_{inst}}{dt}=-\nabla P_{inst} \qquad (3\text{-}8)$$

2) Continuity equation:

$$\frac{\partial \rho_{inst}}{\partial t}=-\nabla.(\rho_{inst}v) \qquad (3\text{-}9)$$

3) Substituting the equations (3-1) and (3-2) in the two last equations respectively and discarding higher order terms yields

$$\rho\frac{\partial v}{\partial t}=-\nabla P' \qquad (3\text{-}10)$$

and

$$\frac{\partial \rho'}{\partial t}=-\rho_o\nabla\cdot(v) \qquad (3\text{-}11)$$

Differentiating equation (3-11) with respect to time yields

$$\frac{\partial^2 \rho'}{\partial t^2}=\rho_o\nabla.(\frac{\partial v}{\partial t})$$

Then, substituting equation (3-10) in this equation gives

$$\frac{\partial^2 P'}{\partial t^2}=-\nabla\cdot(-\nabla P')=\nabla^2 P' \qquad (3\text{-}12)$$

Then differentiating equation (3-7) with respect to time yields.

$$\frac{1}{c^2}\frac{\partial^2 P'}{\partial t^2}=\frac{\partial^2 \rho'}{\partial t^2}+\frac{\partial v}{\partial t}.\nabla\rho_o \qquad (3\text{-}13)$$

First we assume that $c = c_o + c' = c_o + \Delta c$, and $\rho(r)=\rho_o + \Delta\rho(r)$, then, substituting the equations (3-10) and (3-12) in equation (3-13) gives.

$$\nabla^2 P'-(\frac{1}{c_o^2}-\frac{2\Delta c}{c_o^3})\frac{\partial^2 P'}{\partial t^2}=[\frac{1}{\rho_o}\nabla(\Delta\rho)-\frac{\Delta\rho}{\rho_o^2}\nabla(\Delta\rho)]\cdot\nabla P'$$

It should be noted that in the derivation of this equation, small quantities of second order have been ignored and, also, it is assumed that $1/(1-\Delta) \approx 1-\Delta$. By neglecting the second order term $(\Delta\rho/\rho_o^2)\nabla(\Delta\rho)\cdot\nabla P$, we finally get the wave equation as:

$$\nabla^2 P' - \frac{1}{c_o^2}\frac{\partial^2 P'}{\partial t^2} = -\frac{2\Delta c}{c_o^3}\frac{\partial^2 P'}{\partial t^2} + \frac{1}{\rho_o}\nabla(\Delta\rho)\cdot\nabla P' \qquad (3\text{-}14)$$

This is a general form of the wave equation which works even for nonhomogeneous media. The right side of this equation includes the scattering terms that vanish for a homogeneous medium (such as our coolant). Thus, the wave propagation model for this experiment is

$$\nabla^2 P' = \frac{1}{c_o^2}\frac{\partial^2 P'}{\partial t^2} \qquad (3\text{-}15)$$

The incident field can be studied by considering the following assumptions, [1,3,4,5]:

1) No other sources exist in the measurement system.
2) The properties of the fluid at any cross section area of the flow path are the same, or the ultrasonic wave spreads out uniformly over the cross section area of the path.
3) The part surface has inconsistent surface finish which causes wave scattering.
4) The direction of incident wave is normal to the part surface.
5) The interface is the part surface with various degree of roughness.

The field of ultrasonic wave propagation can be verified by employing the velocity potential $\varphi(r,t)$ and linear version of Euler's equation and plane wave condition as follows.

$$P'(r,t) = -\rho_o \frac{\partial \varphi(r,t)}{\partial t} \qquad (3\text{-}16)$$

Where:

$$V(r,t) = \nabla \varphi(r,t) \qquad (3\text{-}17)$$

V(r,t) is the actual fluid velocity when there is perturbation due to wave propagation.

The field is conveniently studied by applying the velocity potential φ(r,t). A model of wave equation may be written in term of the velocity potential for homogeneous medium (coolant) as.

$$\frac{\partial^2 \varphi}{\partial t^2} = c_o^2 \nabla \varphi \qquad (3\text{-}18)$$

Note that the sub (o) is omitted from this point to the end of the text.

Detail of equation derivations and calculation procedures can be found in references 1,3,4, and 5 of this chapter.

3-2 THE WAVE PROPAGATION PATH:

The ultrasonic waves are propagated through the coolant flow. The coolant system is fabricated from two main parts, a squirter and a diffuser. The squirter itself has different tube shape passages, therefore, the coolant path can mainly be categorized in two geometric configurations, a tube and a diffuser. The coolant flows through a short distance which is a free space between the diffuser mouth and the surface of the part (interface surface), The flow path geometry can be considered to have a conical shape with the same angle as the diffuser. A fraction of the incident energy might be reflected from the surfaces of the coolant system due to the variation in cross section area . Therefore, it is necessary to analyze this phenomenon during derivation of the wave propagation equation. In general, the propagation in such a case is not related to the longitudinal plane wave mode only, but we have to consider the effects of the lateral propagation and reflection phenomena. When the diffuser does not flare too rapidly or the cross-sectional area changes very slightly and gradually (such as our experimental diffuser), we can assume that the lateral waves are negligibly small provided that their frequencies are below the cut-off frequency inside the diffuser. It should be noted that the lateral waves have negligible effects inside the tube sections of the flow path if their frequencies are below the cut-off frequency. In these cases, there may be only the longitudinal plane wave propagation.

3-2-1 The Ultrasound Propagation Through the Tube Shape Section of the Fluid Flow Path:

When a sonic wave is transmitted in a moving fluid, the fluid motion is predominantly parallel to the tube axis, It is possible to analyze the wave propagation with a one-dimensional wave equation (in terms of z, and t), provided that the sonic wave length is much larger than the diameter of the tube. But from the experimental design data for air coolant system, the ultrasonic wavelength is much less than the tube diameter (contrary to the last condition), so the application of one-dimensional wave equation will not be a proper approach for analyzing our problem, therefore, a two dimensional wave equation must be tried for this problem at the second step. The characteristics of the flow path are as follows:

- Two ends of the tube.
- Rigid walls.
- Only one wave generation source (transducer) exists in the system (either 10 MHZ, 20 MHZ or 30 MHZ).

- The transducer is located along z-axis and the transducer, tube and diffuser center line are located on the z-axis. Therefore, the problem can be analyzed as a 2-dimensional problem in cylindrical coordinates (due to symmetric condition the effects of angular parameter is negligible).
- The tube diameter, D_{tube}=3.175 mm. The wavelengths of sources or transducers are; λ_{10MHZ}=0.1516 mm, λ_{20MHZ}=0.0758 mm, and λ_{30MHZ}=0.0505.

The field equation (Helmholtz equations) is used to study the wave propagation through the tube, if either ultrasonic pressure or velocity potential behave as:

$$\varphi = Re\{\tilde{\Phi} e^{-i\omega t}\}, \quad P' = Re\{\tilde{P} e^{-i\omega t}\}$$

The wave equations (3-15) or (3-18) can be written in the Helmholtz forms

$$\nabla^2 P' + k^2 P' = 0, \quad \nabla^2 \tilde{\phi} + k^2 \tilde{\phi} = 0 \qquad (3\text{-}19)$$

Noting that our problem is 2-dimensional in cylindrical coordinates (r,z) because wave propagation in radial directions of any cross-section area is consistent (symmetric condition), therefore, equation (3-19) will be changed to.

$$\frac{\partial^2 P'}{\partial r^2} + \frac{1}{r}\frac{\partial P'}{\partial r} + \frac{\partial^2 P'}{\partial z^2} + k^2 P' = 0 \qquad (3\text{-}20)$$

where:

$k = \omega / c$ is called wave number.

$P'(r,z,t) = \rho[\partial \varphi(r,z,t)/\partial t]$ is called acoustic pressure.

It is assumed that the pulses generated by the fixed transducer inside the coolant system are plane waves.

The following solution procedure can be applied for both equations (3-19).

1) Separation of variables:

$$\tilde{\phi}(r,z)=R(r)Z(z) \qquad (3\text{-}21)$$

substituting (3-21) in (3-19), velocity potential form, gives.

$$\frac{\ddot{R}(r)+\frac{1}{r}\dot{R}(r)}{R(r)}=-\frac{\ddot{Z}(z)}{Z(z)}-k^2=-\alpha^2$$

Let $\xi=\alpha r$, then

$$\frac{d^2R(r)}{d\xi^2}+\frac{1}{\xi}\frac{dR(\xi)}{d\xi}+R(\xi)=0 \qquad (3\text{-}22)$$

R(ξ) may be written as

$$R(\xi)=\xi^m f(\xi) \qquad (3\text{-}23)$$

substituting R(ξ) in equation (3-22) gives

$$\ddot{f}(\xi)+\frac{2m+1}{\xi}\dot{f}(\xi)+(1+\frac{m^2}{\xi^2})f(\xi)=0 \qquad (3\text{-}24)$$

The second order differential equation (3-24) may be rearranged in the standard Bessel's differential equation, [1,5,13].

$$\xi^2\ddot{f}(\xi)+\xi\dot{f}(\xi)+(\xi^2-\nu^2)f(\xi)=0 \qquad (3\text{-}24')$$

Then, comparing (3-24) with Bessel's equation, gives 2m+1=1, and m=0. So, the general solution of (3-24) for lateral propagation can be written in terms of the first and the second kinds of zero order Bessel's functions (m=υ=0) or J_0 and Y_0 Bessel's functions.

$$\therefore R(\alpha r)=(\alpha r)^m[AJ_\upsilon(\alpha r)+BY_\upsilon(\alpha r)]=[aJ_0(\alpha r)+BY_0(\alpha r)]_{m=0} \quad (3\text{-}25)$$

The second differential equation that is obtained from the separation of variables is

$$-\frac{\ddot{Z}(z)}{Z(z)}=-\alpha^2+k^2=K_z^2 \qquad (3\text{-}26)$$

Then, the cut-off frequency can be determined by discussing different conditions of the following equation:

$$K_{nz}^2=k^2-\alpha_n^{\ 2}=k^2\sqrt{1-\frac{\alpha_n^2}{k^2}}=k^2\sqrt{1-\frac{c\alpha_n^2}{\omega^2}} \qquad (3\text{-}27)$$

Where k=ω/c is the wave number. The general solution of this second order differential equation (3-26) for longitudinal propagation is written as:

$$Z(z)=C\sin K_z+D\cos K_z \qquad (3\text{-}28)$$

The general solution of (3-19), velocity potential can be expressed as.

$$\tilde{\phi}(r,z)=[AJ_0(\alpha r)+BY_0(\alpha r)](C\sin K_z z+D\cos K_z z) \quad (3\text{-}29)$$

Since the ultrasonic pressure and velocity potential are always finite while Y_0 becomes infinite as $\xi=\alpha r$ approaches zero, we cannot use Y_0 and must choose B=0.

Definitely "A" is not equal zero since otherwise $R(\alpha r)$ will be equal zero. So, the Bessel's equation has only a finite solution $R(\alpha_n r)=AJ_0(\alpha_n r)$ as ξ approaches zero. The constant value "A" should be calculated by applying the boundary or initial conditions.

At r=a (tube walls), the boundary condition is dR/dr=0 because the walls of the tube are rigid bodies. The values of α_n must be such that $dR/dr=\alpha_n dJ_0/dr=0$. The discrete set of the values of $j_{mn}=(\alpha_{mn}a)$ will satisfy the equation:

$$j_{mn}/a \, dJ_0(\alpha_n a)/dj_{0n}=0, \text{ (for m=0, and n=1,2,3,,4,...)} \qquad (3\text{-}30)$$

Then the zeros or roots of these first kind Bessel's functions are computed and plotted for finite number of modes (α_n, eigenvalues) by Matlab software package. The results are also presented in the following table:

Table (3-1):

Zeros of $dJ_0/dj_{0n}=0$.

m n	1	2	3	4	5
$j_{0n}=\alpha_n r$	0	3.83	7.02	10.17	13.32
J_0	1.00	- 0.4026	0.3001	- 0.2497	0.2184
J'_0	0	0	0	0	0
α_n (m^{-1})	0	$2.41*10^3$	$4.41*10^3$	$6.40*10^3$	$8.38*10^3$

where the tube radius , $a=3.175mm/2=1.5875*10^{-3}$ m$\approx 1.59*10^{-3}$ m.

Then, solution (3-25) will be changed to

$$R_{0n}(\alpha_n r)=A_{on}J_0(\alpha_n r)=A_n J_0(\frac{j_{0n}}{a}r) \qquad (3\text{-}31)$$

$R_{0n}=R_n$ are eigenfunctions for lateral propagation modes.

Before being involved in this solution procedure, it would be better to find the revised general solution (3-28) by applying the second boundary condition as follows: At z=0, the transducer face or piezoelectric crystal face is in equilibrium position (origin of coordinates located at the center of face surface area), hence

$$\frac{d\tilde{\phi}(r,z)}{dz}=0, \quad \frac{dZ}{dz}=\dot{Z}=[C\ \cos K_z z-D\ \sin K_z z]_{z=0}=0, \qquad \therefore\ C=0 \qquad (3\text{-}32)$$

Therefore, the solution for Z associated with R_n is;

$$Z_n(z)=D_n\cos K_z z, \qquad Z(z)=\sum_{n=1}^{\infty} D_n\cos K_n z \qquad (3\text{-}33)$$

The general solutions of the velocity potential and ultrasonic pressure equations (3-19) for tube section of the wave propagation path is obtained for m=0;

$$\varphi(r,z,t)=\sum_{n=1}^{\infty} E_n J_0(\alpha_n r)\cos(K_{nz} z)\exp(-i\omega t) \qquad (3\text{-}34)$$

Then, for ultrasonic pressure general solution is

$$P'=-\rho_o\frac{\partial\varphi}{\partial t}$$

$$P'=\sum_{n=1}^{\infty} E_n\rho_o\omega J_0(\alpha_n r)\cos(K_{nz})\exp(-i\omega t) \qquad (3\text{-}35)$$

The constant values E_n can be determined by contribution of a Bessel's theory in conjunction with acquired information from the two previous boundary conditions. The theory is stated as follows:

For each fixed "n" value (positive and integer) the Bessel's functions $J_m(\alpha_{m1}r), J_m(\alpha_{m2}r), \ldots\ldots, J_m(\alpha_{mn}r)$ form an orthogonal set on the interval $0 \le r \le a$ (a is the tube radius) with respect to weight function $P(r)=r$, that is, [10], for m=0

$$\int_0^a r J_0(\alpha_{0n}r) J_0(\alpha_{0k}r) = \begin{cases} 0 & when \quad n \neq k, \\ \frac{1}{2} J_1^2(\alpha_n) & when \quad n=k \end{cases}$$

If, at initial condition, a function f(r) has an eigenfunction expansion in terms of one of those orthogonal set elements, the expansion may be written as, [3,8,10,13]

$$f(r) = a_1 J_0(\alpha_{01}r) + a_2 J_0(\alpha_{02}r) + \ldots\ldots + a_5 J_0(\alpha_{05}r)$$

Also, we state f(r) in a Fourier series;

$$f(r) = \sum_{n=1}^{\infty} \frac{1}{2} \sin \omega_n t \qquad (3\text{-}36)$$

Now this form of f(r) will be used in following general solution procedure. The arbitrary coefficient "1/2" has been optimized by trial and error. Then, using the Fourier-Bessel series technique yields

$$|J_m(\alpha_{mn}r)|^2=\int_0^a rJ_m^2(\alpha_{mn}r)dr=\frac{a^2}{2}J_{m+1}^2(\alpha_{mn}r)$$

Finally, the constant coefficients A_n can be computed by the following formula:

$$A_n=\frac{2}{a^2J_{m+1}^2(\alpha_{mn}r)}\int_0^a rf(r)J_m(\alpha_{mn}r)dr \qquad (3\text{-}37)$$

The values of first five constant coefficients (A_1 to A_5) can be determined by this method when only the lateral modes are considered.

The response of ultrasonic wave can also analyzed by considering the case in which the piezoelectric crystal surface (transducer face) changes instantaneously from its initial condition, z=0 (equilibrium) at time t=0, to a new or final value, z=maximum face deflection for t⟩0. We may apply these initial conditions to find the initial solution form of (3-34) as

$$P'(0,r,0)=\sum_{n=1}^{\infty} E_n J_0(\alpha_n r)$$

substituting (3-36) for f(r) in (3-37), gives the following expression for the coefficients A_n.

$$A_n=\frac{2}{a^2J_1^2(\alpha_n)}\int_0^a \frac{1}{2}r(\sin\alpha_n r)J_0(\alpha_n r)dr \qquad (3\text{-}38)$$

Integration of equation (3-38) must be carried out "integration by parts" where :

$$\int u\,dv = uv - \int v\,du, \quad where \quad v=\sin(\alpha_n r), \quad du = rJ_0(\alpha_n r)dr,$$

$$then \quad u=\int_o^a rJ_0(\alpha_n r)dr = \frac{1}{\alpha_n} rJ_{+1}(\alpha_n r), \quad dv=\alpha_n \cos(\alpha_n r)dr$$

Approximate amplitudes of the first five modes, A_1, to A_5 can be computed from the expanded form of (3-38), [10]. The values of α_nr are recalled from Table (3-1), and a≈1.59E-03m (tube radius).

$$A_n = \frac{1}{a^2 J_1(\alpha_n)^2}\{\frac{r}{\alpha_n}[(J_1(\alpha_n r)+J_3(\alpha_n r)+J_5(\alpha_n r)+J_7(\alpha_n r)+\ldots) \\ \sin(\alpha_n r)-(J_2(\alpha_n r)+J_4(\alpha_n r)+J_6(\alpha_n r)+\ldots)\cos(\alpha_n r)]_0^a\} \tag{3-39}$$

Bessel functions J_0 to J_6 are plotted in Fig.(3-1)

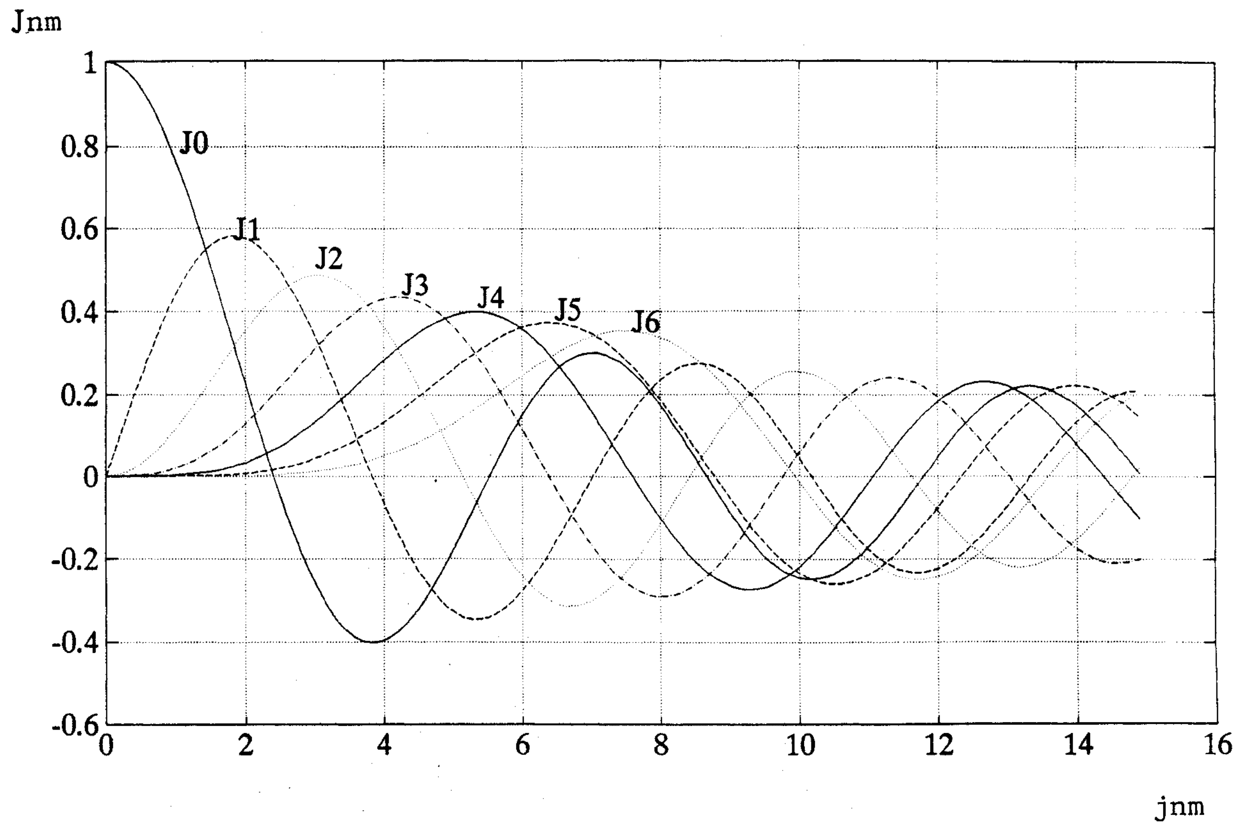

Fig. 3-1

Table (3-2):

The amplitudes of lateral propagating waves in term of the eigenvalues α_n along the tube radius:

α_n (L. eigenvalues)	$\xi=\alpha_n r$	A_n
$\alpha_1=0$	0	$A_1=1.9155*10^4$
$\alpha_2=2.41$	3.83	$A_2=5.355*10^{-3}$
$\alpha_3=4.41$	7.02	$A_3=6.213*10^{-3}$
$\alpha_4=6.40$	10.17	$A_4=1.157*10^{-1}$
$\alpha_5=8.83$	13.32	$A_5=7.676*10^{-2}$

Note-1: The amplitude oscillation is due to the periodic characteristic of the Bessel's functions.

Note-2: the fundamental mode for $\alpha_1=0$ is dominant to the other four lateral modes. Therefore, at initial conditions the lateral modes are negligible compared with the fundamental mode.

The following analytical discussions in conjunction with experimental data analysis gives sufficient information for studying the incident wave modes through the tube section of the waveguide assembly.

Discussion: The transmission of longitudinal and lateral propagation modes can be studied by the ultrasonic pressure, Eq. (3-34) in the form of a series and the equation of wave number (3-27).

The data have been acquired from Table (3-1) for $n=1$ and $\alpha_1=0$, $K_{1z}=k=\omega/c, J_0=0$, in conjunction with general solution (3-34) will help us to analyze the first five propagation modes in the 2-dimensional coolant system. Therefore, the first term of the series (3-34), $E_1\cos(K_{1z}z)EXP(-i\omega t)$ represents a purely one-dimensional, plane wave propagation along the z-axis of the tube or coolant system. This mode is denoted a longitudinal mode to differentiate from the other modes of the series (3-34). The other modes (series terms) which have the lateral term function (Bessel's functions) are called transverse modes because they may travel in lateral direction too. The domination of the longitudinal mode to lateral mode can be investigated by using the values of K_{nz} in term of α_n. Thus, in view of wave number equation (3-27), we have the following possibilities.

The expression under the square root of equation (3-27) is analyzed in three different conditions:

1) $K_{zn}=k[1-(c\alpha_n)^2/\omega^2)]^{1/2}>0$, or $\omega>\omega_n$, $(n=2,3,4,..)$. Where $\omega_n=c\alpha_n$ is called the nth characteristic frequency for lateral oscillations.In this case, K_{zn} is real and positive in equation (3-27), so that the ultrasonic transverse mode is progressing in time toward increasing values of z, and eigenfunction P_n is called propagating mode. It should be noted that the amplitude of this mode is decreasing in +z direction, also cos $K_{zn}z$ term.
2) $K_{zn}=0$, or $\omega=\omega_{cn}$. This case is known as the cut-off condition and ω_{cn} is named cut-off frequency. When $K_{nz}=0$, there is a purely transverse wave oscillation, independent of "z". There is a resonance in this case; that is, the transducer frequency matches exactly with one of the characteristic frequencies of the lateral oscillations or cut-off frequency in the region between the tube walls.
3) $K_{zn}<0$, or $\omega<\omega_{cn}$. In this case the input frequency (transducer frequency) is lower than

the cut-off frequency and the nth mode decays exponentially very sharp with an increase in the +z direction, so that its amplitude is negligible. In this case, the eigenfunction is called evanescent mode. In general, if the input wave frequency is less than the cut-off frequency, that wave cannot travel in the tube.

Based on the foregoing discussion, the variation of E_n, or propagation amplitudes, in term of radius parameter, is plotted in Figs.(3-2,3). It is clear that the amplitude of the first mode (fundamental mode) is very large compared with the other four modes and this trend is similar for the second mode compared with the third one, and so on. Therefore, the fundamental mode is much more dominant than the other lateral modes in the tube section of coolant system. The experimental results for the first five modes are tabulated in tables (3-3,4).

In general, since all the values of K_{zn} are greater than zero, problem is in case one. Therefore, amplitudes of first five ultrasonic propagation modes in the tube section of the coolant system can be analyzed by the amplitudes E_n which are computed by application of the experimental data in the theoretical results. The detail of the code is presented in Appendix-C, also its description in Chapter 7.

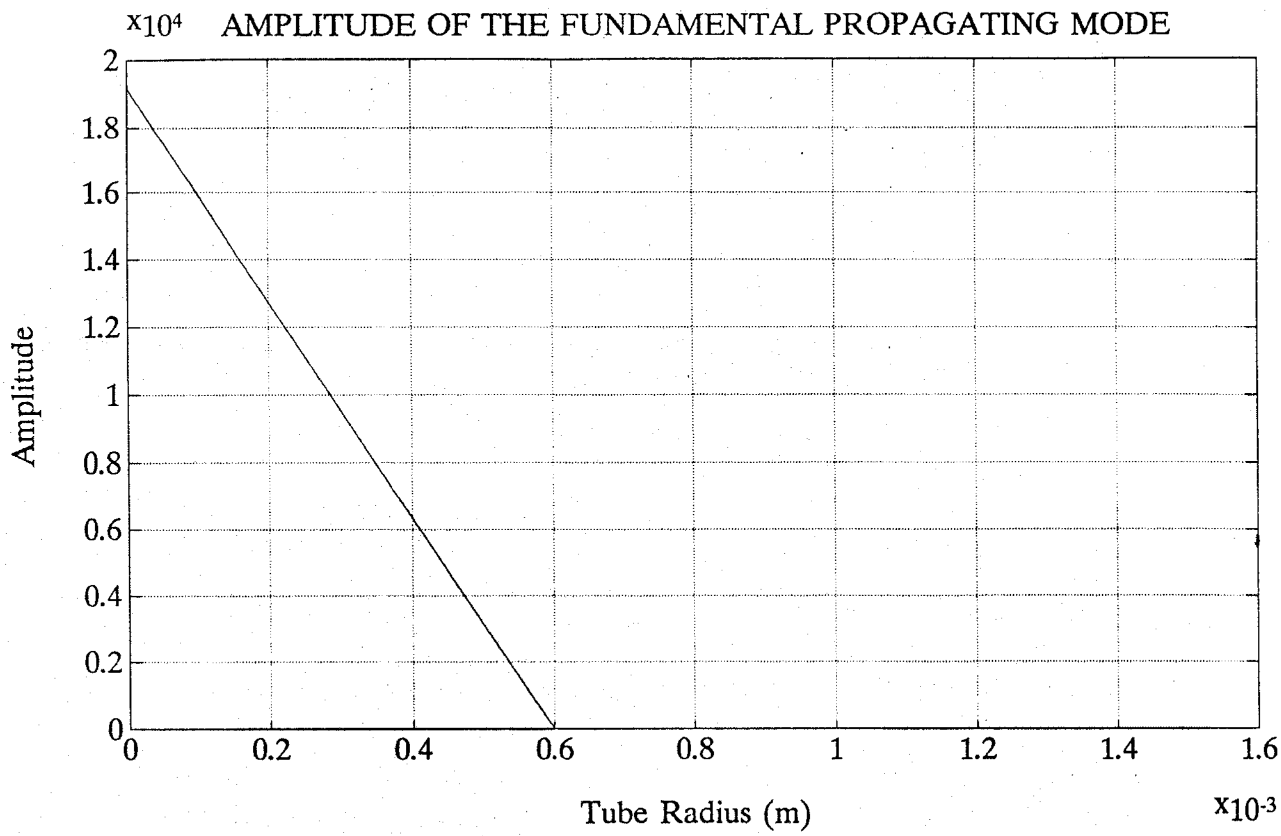
x10^4 AMPLITUDE OF THE FUNDAMENTAL PROPAGATING MODE
Amplitude
2
1.8
1.6
1.4
1.2
1
0.8
0.6
0.4
0.2
0
0
0.2
0.4
0.6
0.8
1
1.2
1.4
1.6
Tube Radius (m)
x10-3

Fig. 3-2

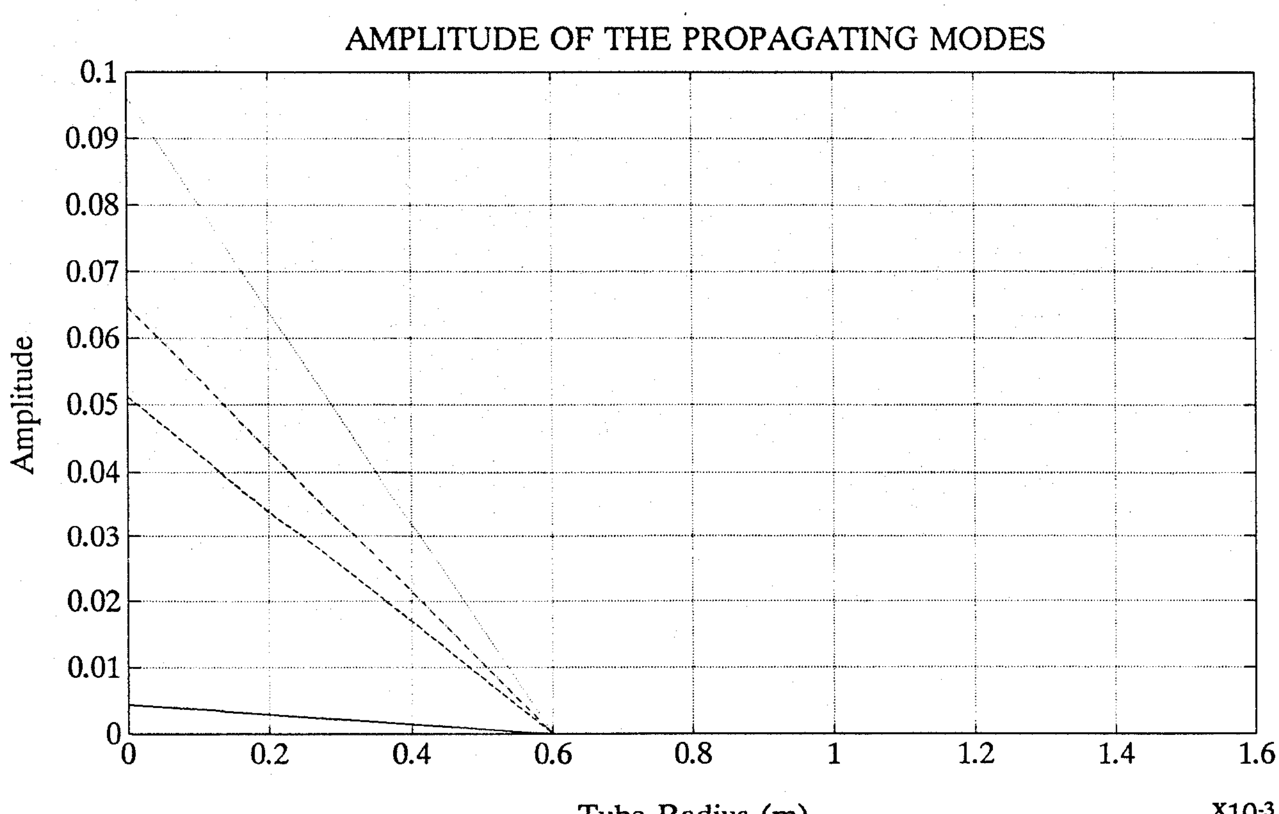
AMPLITUDE OF THE PROPAGATING MODES
Amplitude
0.1
0.09
0.08
0.07
0.06
0.05
0.04
0.03
0.02
0.01
0
0
0.2
0.4
0.6
0.8
1
1.2
1.4
1.6
Tube Radius (m)
x10-3

Fig. 3-3

Table (3-3):

α_n	K_{zn}	f_{zn}	source freq.
$\alpha_1=0$	$K_{z1}=41.446*10^3$	$f_{z1}=10$ MHZ	10 MHZ
$\alpha_2=2.41*10^3$	$K_{z2}=41.305*10^3$	$f_{z2}=9.966$ MHZ	10 MHZ
$\alpha_3=4.41*10^3$	$K_{z3}=41.211*10^3$	$f_{z3}=9.943$ MHZ	10 MHZ
$\alpha_4=6.40*10^3$	$K_{z4}=40.949*10^3$	$f_{z4}=9.880$ MHZ	10 MHz
$\alpha_5=8.38*10^3$	$K_{z5}=40.590*10^3$	$f_{z5}=9.793$ MHZ	10 MHZ

Here, the mean velocity of ultrasonic wave propagation through the coolant is approximately c=1516 m/sec.

The amplitudes of first five ultrasonic propagation modes (E_n) are tabulated in Table (3-4).

Table (3-4):

The E_n values for first five modes.

α_n	f_{zn}	E_n (amplitude)
$\alpha_1=0$	$f_{z1}=10$ MHZ	$E_1=2.137*10^4$
$\alpha_2=2.41*10^3$	$f_{z2}=9.966$ MHZ	$E_2=0.0044$
$\alpha_3=4.41*10^3$	$f_{z3}=9.943$ MHZ	$E_3=0.0512$
$\alpha_4=6.40*10^3$	$f_{z4}=9.880$ MHZ	$E_4=0.0963$
$\alpha_5=8.38*10^3$	$f_{z5}=9.793$ MHZ	$E_5=0.0648$

Tube section results analysis: Based on the acoustic theory, when the input frequency becomes less than the cut-off frequency the mode is evanescent mode which transport no sonic energy, because the power transports in radial directions is represented by integral of the average intensity ($\int I_{r,av.}$) over the entire cross-sectional area, which is equal to zero (energy cannot transport through tube). Using the experimental data shows that, the frequencies of first five modes are larger than the cut-off frequency. Consequently, all these modes can be propagated in time in +z direction. Amplitude of the first mode (fundamental mode) is so much larger than the other modes in order of magnitude. Therefore, we can continue our computation for the entire cooling system only by applying the fundamental mode and ignore the other modes. It is also shown from a certain mode the input frequency is less than the cut-off frequency and those modes will be evanescent modes (continuation of Table (3-3)).

Additionally, the general solution (3-34) can be truncated to its first term of the series

$$\underline{\varphi_1=(1.9155*10^4)\cos(kz)\exp(-i\omega t)} \qquad (3\text{-}40)$$

where $K_{z1}=k=\omega/c$,and eigenvalue $\alpha_1=0$, Thus $J_0(\alpha_1 r)=J_0(0)=1$.

3-3-2 The Ultrasonic Propagation through the Diffuser Section of the Path:

When the ultrasonic wave travels through a diffuser whose cross-sectional area varies slightly in axial (+z) direction, or the change of the cross-section area along the diffuser height compare to the smallest length scale (throat diameter/diffuser length) is small, it can be assumed that the wave properties on any cross-section of the tube are uniform, or the propagation is one-dimensional in time. If propagation originates from the narrow section (throat), we can consider a small portion of the diffuser as a straight tube and compute for it a cut-off frequency based on the lateral dimension there. If the frequency of the source (transducer) is greater than the computed cut-off frequency, then only the fundamental plane-wave mode travels along this portion of the diffuser or, in general, along the entire diffuser. According to the diffuser specifications, we can apply both assumptions: 1) the diffuser does not flare too rapidly, and 2) the propagation is plane wave.

The experimental diffuser specifications:

$$length\ scale = \frac{average\ lateral\ dimensions}{wavelength} =$$

$$\frac{\frac{(3.1750+11.1125)}{2}}{0.1516} = 47.122$$

$$change\ of\ area = \frac{S_{mouth} - S_{throat}}{S_{av.}} = 1.70$$

Thus, the length scale is much greater than 1.7 and propagation can be considered one-dimensional plane wave which travels from diffuser throat towards the diffuser mouth in "+z" direction. So, the lateral reflection from the diffuser walls are negligible. However, since the diffuser cross-sectional area varies from point to point, the propagation equation should be derived by applying the integral form of the continuity equation.

The continuity equation may be derived for a control volume of the diffuser as follows.

• The Gauss theorem:

$$\frac{d}{dt}\int_{V=vol} \rho(z,t) = -\int_{s} \rho\vec{v}.\vec{n}ds$$

where dV=s(z)dz, v.n=0, ∇P.n=0 on the side wall of the diffuser, and v & P are the local velocity and the pressure of the coolant respectively. For some intermediate location z_1, we can write $s(z+\Delta z)-s(z) << s(z_1)$, and in limit the integral form of the continuity equation is changed to

$$s(z)\frac{\partial\rho}{\partial t}+\frac{\partial(\rho vs)}{\partial z}=0$$

This is the field form of the continuity equation for a diffuser and in general condition. we require only the approximate expresion for small density changes due to perturbation caused by the ultrasonic pressure. Thus, as before in the case of the tube section, we let $\rho=\rho_o+\rho'$ and using linearization approximation or retaining only the first order terms, we obtain

$$s\frac{\partial\rho'}{\partial t}+\rho_o\frac{\partial(vs)}{\partial z}=0$$

This is an approximation expresion of continuity equation when the media density changes slightly. The second equation that we need is the linearized momentum equation

$$\rho_o\frac{\partial v}{\partial t}+\frac{\partial P'}{\partial z}=0 \qquad (3\text{-}41)$$

Then, the linearized isentropic relation gives

$$P' = (\frac{\partial P}{\partial \rho})_o \rho' + \frac{1}{2}(\frac{\partial^2 P}{\partial \rho^2})_o (\rho')^2 + ...$$

for incompressible flow $\rho = constant$ (3-42)

$$\therefore P' = c^2 \rho'$$

Therefore, the continuity equation (3-41) becomes

$$\frac{\partial P'}{\partial t} + \rho_o c_o^2 [\frac{\partial v}{\partial z} + v\frac{\partial (\ln s)}{\partial z}] = 0 \qquad (3\text{-}42)$$

We can use the momentum equation to eliminate P'or v from (3-42). Since the flow of the coolant is incompressible and also assumed irrotational, then $v = \partial\varphi/\partial x$. Further, $P' = -\rho_o(\partial\varphi/\partial t)$, so that

$$\frac{\partial^2 \varphi}{\partial t^2} = c_o^2 [\frac{d(\ln s)}{dz}\frac{\partial \varphi}{\partial z} + \frac{\partial^2 \varphi}{\partial z^2}] \qquad (3\text{-}43)$$

This is a one-dimensional plane wave equation in transient form for diffuser in terms of a velocity potential. One of the advantages of this term may be seen by considering the monochromatic form of the diffuse equation. It is more convenient to use the following notation for one-dimensional velocity potential.

$$\varphi(z,t) = Re\{\tilde{\phi}(z)\exp(-i\omega t)\}$$

where Re{ }is used to remind us that the velocity potential is given by the real part of the quantity in brackets only. This is a Helmholtz wave equation and is independent of time, [1,3,5].

$$\frac{d^2\varphi}{\partial z^2}=\frac{d(\ln s)}{dz}\frac{d\varphi}{dz}+k^2\frac{d^2\varphi}{dz^2}=0$$

$$\text{where} \quad k=\frac{\omega}{c_o} \qquad (3\text{-}44)$$

The exact solution for (3-43) can be obtained by expressing cross-sectional area variation in +z direction as

$$s(z)=s_0(z/z_0)^n$$

where for positive n diffuser configuration (divergence), and for negative n the nozzle configuration (convergence) is obtained from this expression. Then, let w=kz, so that equation (3-44) becomes

$$\frac{d^2\tilde{\phi}(w)}{dz^2}+\frac{n}{w}\frac{d\tilde{\phi}(w)}{dz}+\tilde{\phi}(w)=0 \qquad (3\text{-}45)$$

We may transform equation (3-45) to Bessel's differential equation (3-24') by considering the notation, $\phi=w^m f(w)$ as

$$w^2\ddot{f}(w)+w(2m+n)\dot{f}(w)[w^2+m(m-1)+nm]f(w)=0 \qquad (3\text{-}46)$$

comparing this equation with (3-24') gives the value of s as m=(1-n)/2, and m(m-1)+nm =-$[(n-1)/2]^2$. Therefore, $\nu=\pm(n-1)/2$ and the general solution of (3-46) for conical diffuser (n=2) may be expressed as

$$f(w)=AJ_\nu(w)+BJ_\nu(w)=AJ_{1/2}(w)+BJ_{-1/2}(w)$$

But $J_{1/2}(w)=$ sqrt($2/\pi w$)cos(w), and $J_{-1/2}(w)=$sqrt($2/\pi w$)sin(w). Thus

$$\tilde{\phi}(w)=\sqrt{2/\pi}\frac{1}{kz}[A\sin(kz)+B\cos(kz)] \qquad (3\text{-}47)$$

and for one-dimensional plane wave, it becomes

$$\varphi = \frac{1}{kz}[A\exp^{i(kz-\omega t)} + B\exp^{-i(kz+\omega t)}] \qquad (3\text{-}48)$$

This is the useful solution form for studying the ultrasonic propagation in the cone type diffuser. Because the reflection from the diffuser walls is negligible, then B=0.

This solution model shows that, ultrasonic propagation in a straight conical diffuser is So

$$\varphi = \frac{A}{kz}\exp i(kz-\omega t) \qquad (3\text{-}49)$$

that ultrasonic waves of all frequencies are transmitted with the same velocity. In addition, the experimental data provide

$$k(r_{mouth}) = (\omega/c_o)(r_{mouth}) = 460 > 3$$

It means the amplitudes of the reflected modes are small compared with the fundamental incident mode and they can be ignored .

The ultrasonic pressure can be defined as

$$P' = -\rho_o\frac{\partial\varphi}{\partial t} = +i\rho_o\omega\frac{A}{kz}\exp i(kz-\omega t) \qquad (3\text{-}50)$$

The coefficient A is calculated by applying the boundary conditions.

Boundary conditions:

At diffuser throat (z=16.1544 mm) equations (3-40) and (3-49) give

1-*Tube solution at diff. throat,*

$$\varphi = 1.9155 * 10^4 \cos(kz) \exp -i(\omega t) =$$

$$1.9155 * 10^4 (-.931234) \exp -i(\omega t), \qquad (3\text{-}51)$$

2-*Diffuser solution at throat,*

$$\varphi = \frac{A}{kz} \exp i(kz - \omega t) = \frac{A}{669.5} \exp i(669.5) \exp -i(\omega t)$$

equating equations (1) and (2) yields the coefficient A as

$$A = 1.0725309 * 10^7 + i\, 7.914079 * 10^6 \text{, and } |A| \approx 1.33E07$$

Therefore the general solution of (3-49) or diffuser equation becomes

$$\varphi = \frac{1.2055E07}{kz} \exp i(kz - \omega t)$$

$$P' = \frac{7.400E17}{kz} \exp i(kz - \omega t) \qquad (3\text{-}52)$$

The approximate cut-off frequency for the conical diffuser is $mz_0 = \ln(1/z_0)/(1/z_o - 1)$. The cut-off frequency $f_{cutoff} = mc_o$. Substituting the experimental data gives $f_{cutoff} = 146{,}850$ HZ, which is much less than the fundamental or transducer frequency.

We can conclud the most dominant one-dimensional plane wave which travels toward the increasing z-axis in time is fundamental mode with source or transducer frequency (10 MHZ, 20 MHZ, 30 MHZ) because this frequency is much greater than the cut-off frequency of the experimental diffuser. Therefore, the ultrasonic propagation through the diffuser is analyzed by one-dimensional transient equation in terms of z and t.

3-3-3 *The Ultrasonic Propagation in the Free Space Section of the path:*

The wave propagation analysis in the coolant column is simplified by considering the following assumptions:

- The velocity does not become zero, as was the case with the tube and the diffuser.
- The boundary conditions that must be satisfied for all time at all points of the interface are the ultrasonic pressure (P') and normal velocity (v) of the coolant, and these boundary conditions should be continuous across the interface along the conical coolant column. Continuity of pressure means that there is no net force on the interface, and continuity of normal velocity requires that the coolant remains in contact with air. Based on these boundary conditions, we can assume the hypothetical straight conical coolant column between the diffuser mouth and part surface has a constant conical configuration having the same diffuser angle ($2\theta = 28.6°$).
- Assume the fundamental frequency is larger than the cut-off frequency in this hypothetical straight cone. Therefore, the fundamental mode dominates to the other modes. Thus, the intensity transmission and reflection coefficients that depend on the characteristics of the two media, coolant ($\rho_1 c_1 =$ 1508420 kg/m^{2}s) and air ($\rho_2 c_2 = 483$ kg/m^{2}s), can be written as

$$1+R=T$$

$$R_I=\left(\frac{\rho_2 c_2-\rho_1 c_1}{\rho_2 c_2+\rho_1 c_1}\right)^2 \qquad (3\text{-}53)$$

$$T_I=\frac{4(\rho_1 c_1)(\rho_2 c_2)}{(\rho_1 c_1+\rho_2 c_2)^2}$$

$$at \quad x=0$$

Substituting the experimental data in the equations (3-53) provides $R_I=(0.99935)^2=0.99872$ and $T_I=0.00128$. Therefore, the amount of sonic energy transmission is negligible and almost all the energy reflects toward the center of conical coolant column. Therefore, due to low transmission coefficient, a high frequency ultrasonic wave (such as 10 MHZ) cannot be transmited through the interface in air. Hence, the propagation equation for this section of the path with reactive wall to the pressure is the product of models (3-52) for the diffuser by a coefficient β. Hence, we can ascribe to the interface between coolant and air an acoustic admittance (β). Then the boundary condition, to be satisfy everywhere on the perimeter, is

$$\frac{\partial\varphi}{\partial n}=ik\beta\varphi$$

$$where \quad k=\frac{\omega}{c}$$

Where the vector n is normal to the interface between coolant and air, toward outside. The interface is purely reactive, thus, β can be calculated for free space path by using the velocity potential model of diffuser, Eq. (3-52) and the boundary conditions and as follows:

$$\frac{\partial\varphi}{\partial n}=\frac{\partial\varphi}{\partial r}\frac{\partial r}{\partial n}+\frac{\partial\varphi}{\partial z}\frac{\partial z}{\partial n}$$

where: $\vec{n}=(\cos(\theta)\vec{r}+(-\sin(\theta))\vec{z}$

and $\vec{z}=(\cos(\theta)\vec{t}+(\sin(\theta)\vec{n}$

θ: Interface wall angle with respect to z-axis. $\vec{r}$, $\vec{t}$, $\vec{z}$ and $\vec{n}$ are unit vectors in radial, interface wall, z-axis and normal to interface directions (toward outside) respectively. The magnitude of β becomes equal to 5.96 $*10^{-6}$. The velocity potential and ultrasonic pressure models can be expressed as

$$\varphi=\frac{1.2055E07}{kz}\exp i(kz-\omega t)$$
$$P'=\frac{7.4E17}{kz}\exp i(kz-\omega t) \qquad (3\text{-}54)$$

These instantaneuos experimental models can be applied for studying the normal incidence waves propagation (such as this experimental work).

3-3-4 Oblique Incidence:

A one-dimensional plane wave propagates inside the coolant at incident angle θ_1 with z-axis. According to the previous results, an experimental model for oblique incident wave can be derived by a proper modification in (3-54) as, [1].

$$\varphi=\frac{1.2055E07}{kz}\exp i\omega(\frac{z}{c_1}\sin\theta_1+\frac{z}{c_1}\cos\theta_1-t)$$
$$P'=\frac{7.4E17}{kz}\exp i\omega(\frac{z}{c_1}\sin\theta_1+\frac{z}{c_1}\cos\theta_1-t) \qquad (3\text{-}55)$$

Blocking the empirical data (1°,2°,3°,4°,and 5°) into (3-35) gives the approximate model for this range of data as

$$\varphi = \frac{1.2055E07}{kz} \exp i\omega \left(\frac{z}{1516} \cos\theta_1 - t \right)$$
$$P' = \frac{7.4E17}{kz} \exp + i\omega \left(\frac{z}{1516} \cos\theta_1 - t \right) \qquad (3\text{-}56)$$

Where ultrasound velocity in the medium one is equal to 1516 m/s. In mathematical point of view, these models are being decayed by increasing time, distance from transducer to ground part, and θ_1.

REFERENCES:

1- Temkin S., "Element of Acoustic", Wiley, 1981.

2- Jensen J.A, " A model for propagation and scattering of ultrasound in tissue", Journal of Acoustic, 1991.

3- Morse and Ingard, " Theoretical Acoustic", MacGraw-hill, 1954.

4- Lindsay, "Concepts and Methods of Theoretical physics.

5- Prience A., "Acoustics ", MacGraw-Hill, 1981.

6- Chernov, "Wave Propagation in a random Medium", MacGraw-Hill, 1960.

7- Kinsler F., "Fundamental of Acoustics", 3th Ed., Wiley, 1981.

8- Hilderbrand, "Advanced Calculus for Applications", 2nd Ed., Prentice Hall, 1976.

9- Wylie, Barrett, "Advanced Engineering Mathematics", 5th Ed., MacGraw-Hill, 1976.

10- Waston G.N., "Treatise on Theory of Bessel functions", 2nd Ed., Cambridge University Press, 1944.

11- Ultrasonic Journals, page 128- 132, May 1985.

12- Acoustic Journal, page 550-558, Feb. 91.

13- Kreyszing E., "Advanced Engineering Mathematics", 3th Ed., Tower Press, 1973.

14-Malecki I., "Physical Foundations of Technical Acoustics", Pergamon Press, 1969.

CHAPTER 4

MATHEMATICAL MODELING OF SURFACE FINISH:

4-1 INTRODUCTION:

Surface finish measurements are accomplished by measuring the amount of ultrasonic reflection from the surface roughness of a machined part. Due to this discontinuity of the part surface some of the incident energy will be scattered in undesired directions. In order to analyze this phenomenon, it is better to consider the characteristic impedance of the part surface instead of the behavior of wave propagation into it. Therefore, the interface between two media (coolant and the solid part) can be considered as the surface of the machined part. Then, based on the specifications of the grinding process, we can model the surface finish. This model will be applied to determine the rate of scattering and ultimately the attenuation caused by this phenomenon. The methods for surface finish measurement and the required instruments or devices will be studied in the last section of this chapter.

4-2 SURFACE PROFILE CHARACTERIZATION:

We consider a two-dimensional (x,z) scattering from a one-dimensional surface profile, z(x), of a real 3-dimensional machined part.

In this research, ultrasonic waves have been recognized as an effective approach in precision grinding technology (due to presence of the coolant). Therefore, the problem of ultrasound scattering must be considered carefully.

The reflection phenomena from the surface roughness may be analyzed through different incident waveguide positions, such as in the normal direction to the grinding part or in oblique positions.

The experimental results proved that the normal incident direction (parallel to z-axis) is the most effective position for surface finish measurement. Also, a set of experiments for oblique positions 1, 2, 3, 4, and 5 degrees were performed and the rate of attenuation for higher oblique angle was increased considerably. It means an increase in oblique or tilt angle of the incident wave (θ_1) causes a reduction in reflected energy onto the transducer face. The more commonly used surface parameters are usually defined in term of one-dimensional surface profile, z(x). The average mean of expected value of z(x) over a certain length of the part, L, is denoted by z_{mean} and defined as

$$z_{mean}=\lim_{L\to x}\frac{1}{L}\int_0^L z(x)dx \qquad (4\text{-}1)$$

The surface finish $z(x)=z_{mean}$ would be considered perfectly smooth. Roughness is defined in terms of deviations from the mean value. Thus, the arithmetic average roughness, σ_a or R_a, can be expressed as

$$\sigma_a=\lim_{L\to x}\frac{1}{L}\int_0^L |z(x)-z_{mean}|dx \qquad (4\text{-}2)$$

This is a standard definition of roughness in the machine tool industry because it is obtained from stylus measurement naturally. The result is almost accurate for a sinusoidal surface roughness.

Another surface-height average is the root-mean-square roughness σ, RMS or R_q. The RMS roughness can be obtained directly from the reflection measurements of electromagnetic waves (such as ultrasonic waves). There is a convenient relationship between σ and total integrated scatter (TIS), including reflected energy on the transducer face. The RMS roughness is also defined in terms of surface-height deviations from z_{mean}.

$$\sigma = \{\lim_{x \to L} \frac{1}{L} \int_0^L [z(x) - z_{mean}]^2 dx\}^{\frac{1}{2}} \qquad (4\text{-}3)$$

Note that, for most physically realizable ground surfaces, these two measurement criteria, σ_a and σ, have usually close or identical values.

The surface profile produced by precision grinding machines are usually periodic, FIG.(4-1).

$$(z-R)^2 + x^2 = R^2 \qquad (4\text{-}4)$$

$z \approx x^2/2R$ for $-d/2 \le x \le d/2$

when $R >> d$

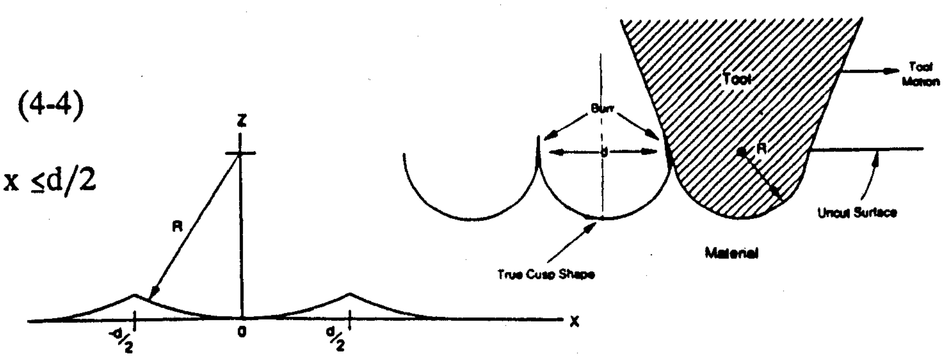

FIG. (4-1)

Where R is the cutting depth radius (average grids radii distributed on the wheel surface) and d is the feedrate.

An easy approach is to use the Fourier theorem to express the cusp shape as

$$z(x)=\frac{a_0}{2}+\sum_{n=1}^{\infty}a_n\cos(\frac{2n\pi x}{d}) \qquad (4\text{-}5)$$

Where $a_0=d^2/12R$ and $a_n=(-1)^n d^2/2(n\pi)^2R$ are obtained from Fourier transform. The z_{mean} or mean surface height of the dc term in the expansion ($a_0/2$) and it can be dropped out from the integral (4-3). Therefore, the RMS roughness or σ can be expressed by Fourier series as

$$\sigma=(\sum_{n=1}^{\infty}\frac{a_n}{2})^{\frac{1}{2}}=(\frac{1}{8\pi^4}\sum_{n=1}^{\infty}\frac{1}{n^4})^{\frac{1}{2}}\frac{d^2}{R}=0.0373\frac{d^2}{R} \qquad (4\text{-}6)$$

The RMS roughness is determined by d and R and ultrasonic scattering is analyzed by the surface profile or values of d and R.

In real measurement z(x) is not known in an arithmetic form, but it can be sampled at discrete points. When z(x) is specified as a string of N samples, given by $z_n=z(x_n)$ instead of a continuous function, the expression used to provide numerical values at these locations are called " estimators" and indicated by (^) sign. The estimator used for RMS roughness is

$$\sigma\approx\hat{\sigma}=[\frac{1}{N}\sum_{n=0}^{N-1}(z_n-z_{n|mean})^2]^{\frac{1}{2}} \qquad (4\text{-}7)$$

where

$$z_{n|mean}=\frac{1}{N}\sum_{n=0}^{N-1} z_n \ , \quad n=0,1,2,\ldots,N-1$$

If the RMS roughness depends only on the height of surface discontinuity, the two models (a) and (b), Fig. (4-2) have the same roughness and the thumbnail test shows the surface (b) is smoother than surface (a). Therefore some sort of transverse quantity needs to be added to the height definitions in order to improve roughness characterization. The surface slope (m) seems a logical choice and can be defined for RMS roughness as

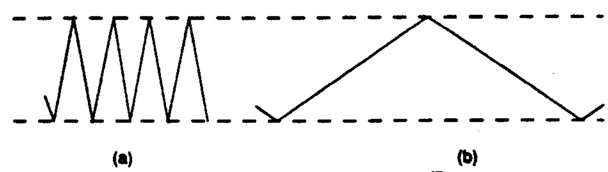

Fig. (4-2)

$$m=[\lim_{L\to\infty}\frac{1}{L}\int_0^L(\frac{dz}{dx}-z_{mean})^2dx]^{\frac{1}{2}} \qquad (4\text{-}8)$$

For the case of N discrete data points the results are represented as estimators.

$$m\approx\hat{m}=[\frac{1}{N-1}\sum_{n=1}^{N-1}(\frac{z_n-z_{n-1}}{x_n-x_{n-1}}-z'_{n|mean})^2]^{\frac{1}{2}} \qquad (4\text{-}9)$$

where

$$z_{n|mean}=\frac{1}{N-1}\sum_{n=0}^{N-1}(\frac{z_n-z_{n-1}}{x_n-x_{n-1}})$$

$$z'_{n|mean}=\lim_{L\to x}\frac{1}{L}\int\frac{dz_n}{dx}dx$$

The surface RMS height and slope may be combined to form transverse surface length parameter or average surface wavelength "λ", Where:

$$\lambda=2\pi\sigma/m \qquad (4\text{-}10)$$

The values of height, slope, and average wavelength are evaluated from these definitions and for sinusoidal grating.

$$z(x)=\xi=a\cos(2\pi f)=a\cos(hx) \qquad (4\text{-}11)$$

The correlation between these parameters and surface discontinuity properties (frequency and amplitude) are presented in the following table.

Table 4-1:

Sinusoidal surface grating parameters.

Parameters	RMS
σ (height)	$a/\surd 2$
m (slope)	$\surd(2\pi fa)$
λ (wavelength)	1/f

Comparison of RMS roughness for various surface profiles are shown in Table (4-2). All of the profiles are defined with peak to valley height of 2a and zero mean and evaluation is over an integer number of wavelengths, [4] .

Table 4-2:

Roughness waveform	Arithmetic (σ_a)	RMS (σ)
Triangle	0.5a	$a/\sqrt{3}$
Sinusoid	$2a/\pi$	$a/\sqrt{2}$
Square Wave	a	a
Circular Cusp	0.51a	0.60a

It should be noted that the resulted surface model and other equations of this chapter will be used in the following chapters.

REFERENCES:

1- Kinsler, " Fundamental of acoustic", 3th Ed., Wiley, 1980.

2- Pierce A., " Acoustics", MacGraw-Hill, 1981.

3- Born & Wolf, " Principles of Optics", 4th Ed., Oxford, 1970.

4- Stover J., "Optical Scattering measurement and analysis", MacGraw-Hill,1990.

5- Kachoyan & Macaskill, "Acoustic Scattering From An Arbitrary Rough Surface", J. of Acoust. Soc. of Am., 85(5), Nov. 1987.

6- Waston & keller, " Rough-Surface Scattering Via The Smoothing Method", J. of Acoust. Soc. of Am., 75(6), June 1984.

7- Spivack.M. "A Numerical Approach To Rough-Surface Scattering By The Parabolic Equation Method",J. of Acoust. Soc. of Am., 87(5), May 1990.

CHAPTER 5

REFLECTION AND TRANSMISSION PHENOMENA:

5-1 INTRODUCTION:

The reflection of ultrasonic waves from a rough surface is usually weaker than the reflection from a smooth or plane surface. The term *smooth* implies that height variations of the surface roughness are small compared to the wavelength of the wave. The scattering phenomenon can be analyzed by a mathematical model of the interface or boundary between two media (coolant and solid part). The surface roughness profile may be assumed as a sinusoidal function (as described in chapter 4) which is expandable as a Fourier series.

The geometric characteristics of the prototype, particularly the diffuser part is very important in the determination of the reflection rate to the transducer face. Optimization of the reflection angle will provide sufficient information about the quality of the prototype design.

The losses due to the boundary surface discontinuities can be computed by the velocity potential or pressure of the reflection wave.

5-2 VERIFICATION OF THE WAVE STATUS AT THE PART SURFACE:

In general, the reflection and transmission phenomena will occur at the interface or boundary of two media . We can analyze these phenomena for a plane wave at the interface by the characteristic impedances. The ratio of the pressure amplitudes or intensities of the reflected and transmitted waves to those of the incident waves depend on the characteristic acoustic impedances, wave speeds in two media and incident angle.

Characteristic impedance (ρc) of a medium is defined as the product of the medium density (ρ) and the wave speed (c) inside the medium. Then, the continuity equation for ultrasonic pressure and density at interface can be written as

$$P'_i + P'_r = P'_t$$

$$\rho_i + \rho_r = \rho_t$$

Where

$$P'_i = P_{oi} \text{Exp } i(\omega t - k_1 z)$$

$$P'_r = P_{or} \text{Exp } i(\omega t + k_1 z)$$

$$P'_t = P_{ot} \text{Exp } i(\omega t - k_2 z)$$

It should be noted that $k_1 = \omega / c_1$ and $k_2 = \omega / c_2$ have different values because the wave speed is not the same in various media. Finally, the coefficients of reflection (R) and transmission (T), for a two-dimensional (x,z) scattering from a one-dimensional surface profile (z(x)) can be obtained by some mathematical manipulations

For ultrasonic pressure:

$$R = \frac{(\rho_2 c_2 - \rho_1 c_1) + ix_n}{\rho_2 c_2 + \rho_1 c_1 + ix_n}$$

$$T = \frac{2r_2 + ix_n}{\rho_2 c_2 + \rho_1 c_1 + ix_n}$$

where, the characteristic impedance for this case is a complex value equal to "$\rho_{\underline{n}} c_{\underline{n}} + ix_{\underline{n}}$", and it is also called normal specific sonic impedance. This expression comes from the ratio and it is also called normal specific sonic impedance. This expression comes from the ratio of ultrasonic pressure to dot product of local velocity of fluid by normal vector to interface surface ($P'/(\vec{v}.\vec{n})$).

For ultrasonic intensity:

$$R=\frac{(\rho_2 c_2-\rho_1 c_1)^2+x^2}{(\rho_2 c_2+\rho_1 c_1)^2+x^2}$$

$$T=\frac{4\rho_1 c_1 \rho_2 c_2}{(\rho_2 c_2+\rho_1 c_1)^2+x^2}$$

Notice that the sonic pressure amplitude, P'_r, is complex and consequently the reflected wave at interface may either lead or lag the incident wave by angles ranging from 0 to 180 degrees (except for the positions where impedance is a real value).

Characteristic impedance is an important sonic parameter for indication of the wave status at interface of two media, because we can identify which one, reflection or transmission, controls the process by its order of magnitude. Therefore, the derivations of related equations can be limited to those having that predominant phenomenon.

5-3 SCATTERING FROM THE SURFACE ROUGHNESS OF A SOLID PART:

In chapter 4, we studied a two dimensional scattering problem from a one-dimensional surface. The mathematical model of the interface or scattering surface was defined as

$$z_s(x)=\xi=a\cos(2\pi f_s x)=a\cos(hx) \quad (5\text{-}1)$$

The x,z coordinates and the positions of transducer and part are shown in Fig.(5-1).

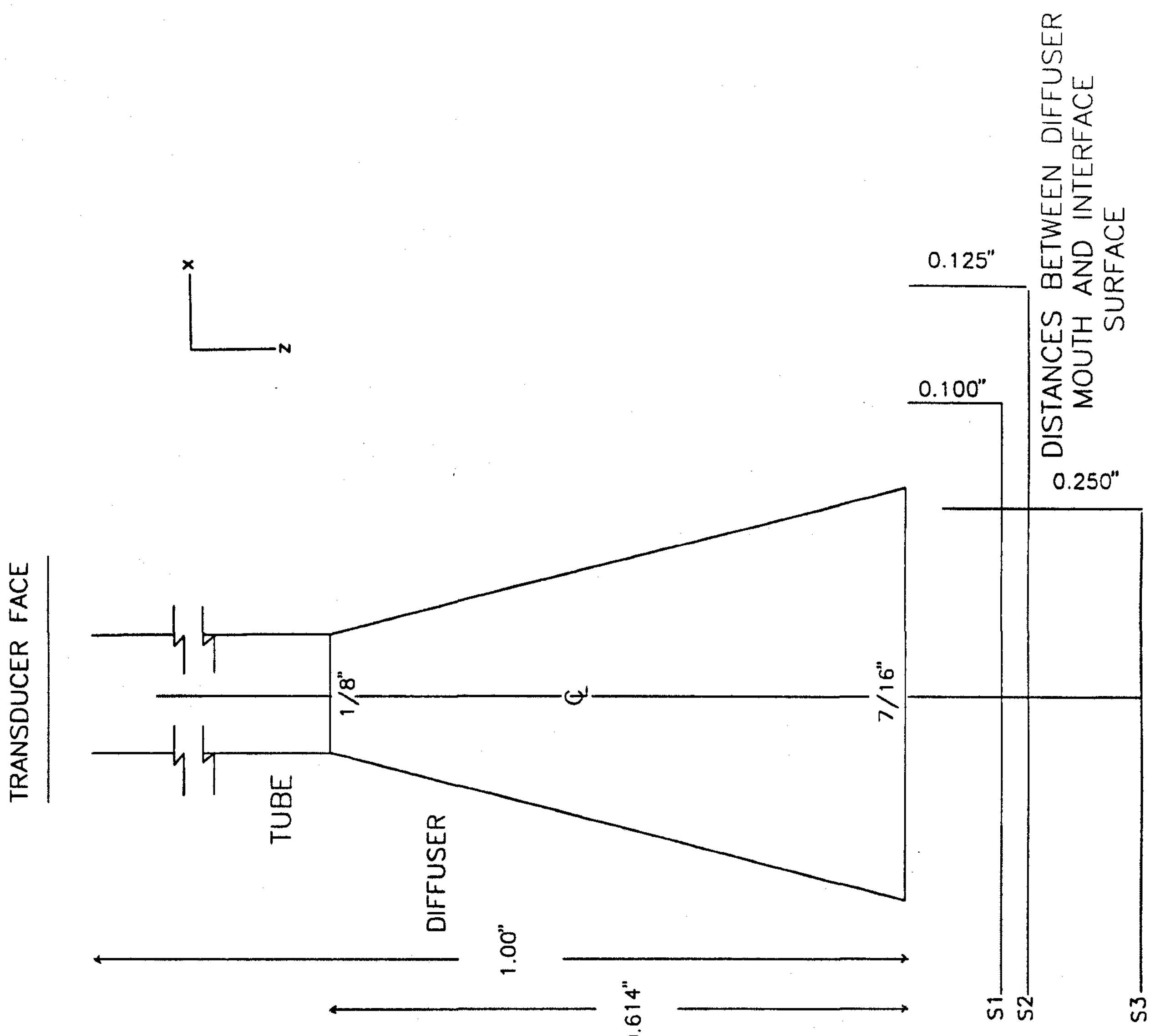

TRANSDUCER FACE
TUBE
DIFFUSER
x
z
1/8"
℄
7/16"
1.00"
0.614"
0.125"
0.100"
0.250"
DISTANCES BETWEEN DIFFUSER MOUTH AND INTERFACE SURFACE
S1
S2
S3

Fig. 5-1

reflected from a smooth surface. The analytical verification of this fact and the effects produced by surface roughness are very important from both ultrasonic and optical view points. The optimization must be done for the geometry of the prototype components and boundary or interface surface . In order to generalize this analysis, we need to consider the following assumptions:

1) The surface of grinding part is considered as the interface of two media (coolant and solid part).
2) Instead of the wave propagation study inside a solid part, the wave behavior can be analyzed in terms of the characteristic impedance of that part.
3) The type of surface grinding by CNC machine is sinusoidal.
4) The incident and reflection waves are plane waves.
5) The problem is limited to the normal incident condition.
6) The boundary of rough surface is defined by model (5-1).
7) Assume the multi-reflections inside the surface corrugations is negligible. Therefore, the corrugation configuration may be shallow.

Based on these assumptions, we are able to derive the scattering equations in general and then optimize the range of reflection.

In order to analyze the scattering problem, we need to specify the geometric configurations of the waveguide assembly components versus the interface surface conditions, Fig. (5-2).

According to geometric specifications of the diffuser and the tube components, the incident wave propagates parallel to z-axis toward the boundary (irrigular surface) in x-z plane. The scattered waves are reflected at different angles which are dependent on the

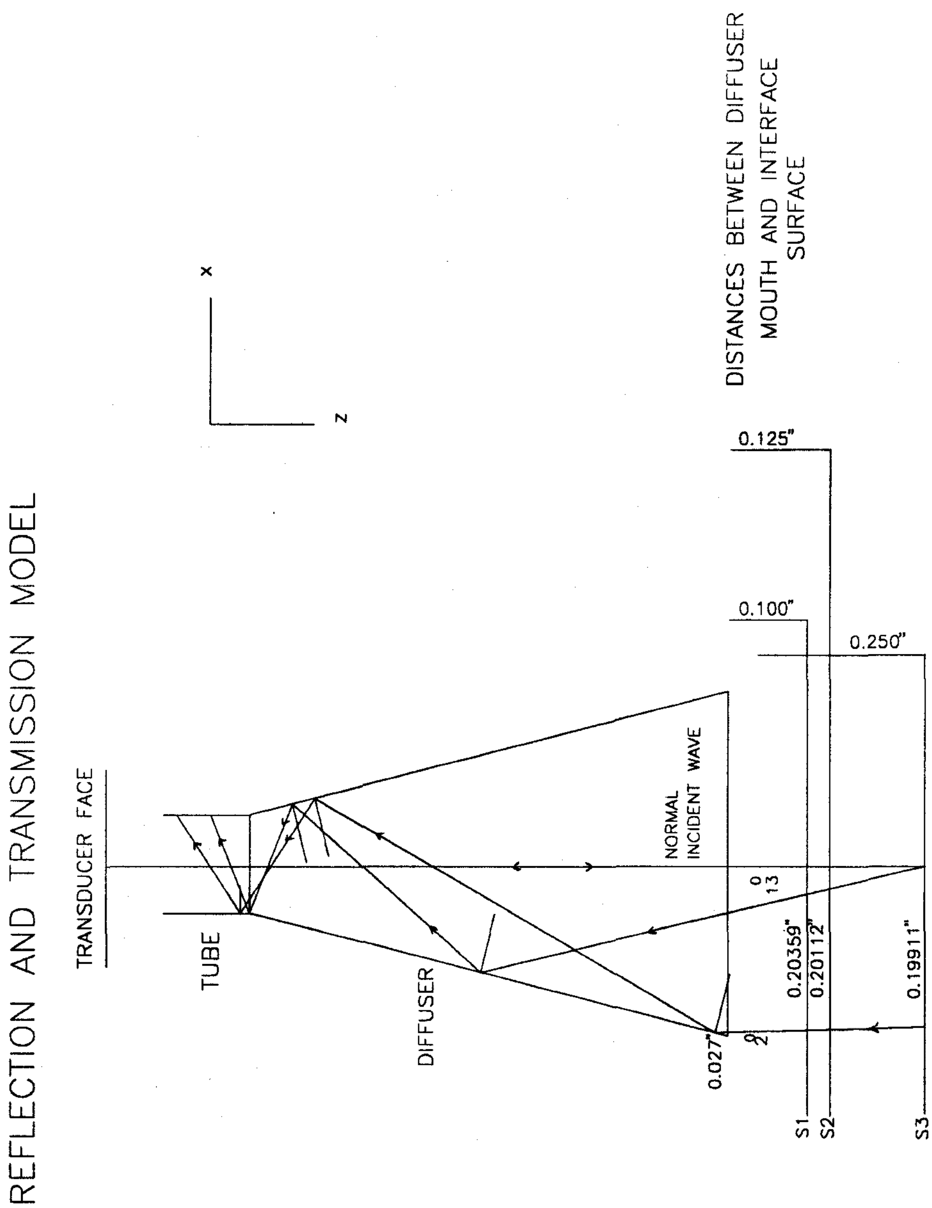
REFLECTION AND TRANSMISSION MODEL
TRANSDUCER FACE
TUBE
DIFFUSER
NORMAL INCIDENT WAVE
x
z
DISTANCES BETWEEN DIFFUSER MOUTH AND INTERFACE SURFACE
0.125"
0.100"
0.250"
0.027"
0.20359"
0.20112"
0.19911"
S1
S2
S3

Fig. 5-2

surface condition at the impact point. According to the geometry of the surface roughness , we are able to obtain a general expression for the resultant scattered wave, by using the Fourier series

$$z_s(x) = \sum_{n=1}^{\infty} a_n \cos(h_n x)$$

$$\tilde{\Phi}_r = A_0 \exp(-ik_z) + A_1 \exp(-i\mu_1)\cos hx + A_2 \exp(-i\mu_2)\cos(2hx) + \ldots\ldots \qquad (5\text{-}2)$$

Where the wave number of reflected modes are defined as

$$\mu^2_m = k^2 - (mh)^2, \qquad m = 1, 2, 3, \ldots.. \qquad (5\text{-}3)$$

The coefficients cos(mhx) represent the phase shifts caused by the differences in the paths of the incident wave to the points of reflection. The component A_0 also corresponds to the reflection from the plane boundary surface, i.e. to the wave propagating at the angle $\theta = 0$ (with respect to the normal to the interface surface) is called principal reflected wave, but the remaining components have various physical meanings depending on whether their wave numbers are real or imaginary.

Discussions: we can verify the conditions of scattered waves by analyzing their wave numbers as follows:

1) h>k: in this case, μ_1, μ_2,....,μ_m are imaginary numbers. Therefore, the reflected waves will be decayed soon and series (5-2) reduced to its first term. In other words the ordinary reflected wave is close to the fundamental propagation mode at initial condition.

2) h=k: this is the cut-off condition and there is no reflection.

3) h<k: in this case, μ_1, μ_2,....,μ_m are real numbers, the corresponding component waves are

the ordinary homogeneous reflected waves. The velocity potential of the resultant scattered waves (5-2) is defined as (chapter 3)

$$\varphi = Re\{\tilde{\phi}\exp(-i\omega t)\}$$

The direction of scattering of any component can be determined by

$$\tan\theta_s = \pm\frac{mk}{[k^2-(mh)^2]^{\frac{1}{2}}} \qquad (5\text{-}4)$$

where , θ_s is the angle between the normal (parallel to z-axis) to surface and reflection direction. There are two symmetric reflections with respect to normal line. Note that for k>>h, we can assume $\mu_s \approx k$.

Boundary conditions: The following boundary conditions should hold on the boundary or interface

$$\rho_1\varphi(r) = \rho_2\varphi_1(r)$$
$$\frac{\partial\varphi(r)}{\partial z} = \frac{\partial\varphi_1(r)}{\partial z} \qquad (5\text{-}5)$$

where, r=r(x,z), $\varphi(r)$ and $\varphi_1(r)$ are defined as resultant field in media one and two (coolant and solid part) respectively.

Substituting the experimental data in first boundary condition gives

$$\varphi_1 = (\rho_1/\rho_2)\varphi = (0.983/8.03)\varphi$$

Therefore, the resultant field inside the second media is negligible compared to that of the first media. Thus, the resultant field on the boundary surface becomes

$$\varphi(r,t) = \varphi_{inc.}(r,t) + \varphi_{ref.}(r,t); \qquad (5\text{-}6)$$

The constant coefficient "A" of the reflection equation (5-2) may be computed by substituting the velocity potential of unity amplitude incident wave (the actual amplitude will be considered in the final solution) and reflection series (5-2) into (5-6). We can get the following relations for z corresponding to the boundary surface $z_s = \xi = a[\cos(hx)]$, (chapter 4).

$$\frac{d\varphi}{dz} = ik[\exp(+ik\xi) - A_0\exp(-ik\xi) - A_1\exp(-ik\xi)\cos(hx) - ....];$$

$$so \quad \frac{d\varphi}{dz} = ik\varphi, \; then \; \frac{d\varphi_1}{dz} = ik_1\varphi_1 = ik_1\frac{\rho}{\rho_1}\varphi \qquad (5\text{-}7)$$

The following points are to be noted: 1) The time factor, (exp(-iωt)), is dropped out in equation (5-7) for simplicity in calculations. 2) The origin of coordinates x-z_s which defines the interface surface is located at a smooth surface interface 3) In the second boundary condition, the differentiation velocity potential with respect to z, various terms of the resultant reflected wave in media one and two will be multiplied by their reflected wave numbers (μ_1, μ_2,.... and μ'_1, μ'_2,...). When h^2 is very small or negligible compared to k and k_1, the values of μ_m and μ'_m can be substituted by k and k_1 respectively. Eqn (5-7) and the following equations are derived based on these notations.

By applying the boundary conditions, φ_1 is eliminated and the following relation can be obtained, [4, 5, 10].

$$k_1\rho[\exp(+ik\xi)+A_0\exp(-ik\xi)+A_1\exp(-ik\xi)\cos(hx)+......]=$$
$$k\rho_1[\exp(+ik\xi)-A_0\exp(-ik\xi)-A_1\exp(-ik\xi)\cos(hx)-......] \quad (5\text{-}8)$$

or we can rewrite (5-8) as

$$A_0+\frac{k_1\rho-k\rho_1}{k_1\rho+k\rho_1}\exp(+2ik\xi)+$$
$$A_1\cos(hx)+A_2\cos(2hx)+.....=0 \quad (5\text{-}9)$$

For the smooth or plane interface (reflector surface), $z_s=\xi=0$, equation (5-9) is changed to

$$A_0=\frac{k\rho_1-k_1\rho}{k\rho_1+k_1\rho}=\frac{Z_2-Z_1}{Z_2-Z_1}=R=\textit{The reflecton index} \quad (5\text{-}10)$$

where, Z_1 is the characteristic impedance of coolant is equal to $1.51*10^6$ kg/(m^2.sec) and Z_2 is the characteristic impedance of stainless steel 302 is equal to $45.5*10^6$ kg/(m^2.sec). But, in general case, the determination of A_0, A_1,... requires the expansion of $\exp(2ik\xi)$ in Fourier's series as

$$\exp(2ik\xi)= \exp[2ik(a\,coshx)]=J_0(2ka)-2J_2(2ka)\cos(2hx)$$
$$+2j_4(2ka)\cos(4hx)+...+i[2J_1(2ka)coshx-2J_3(2ka)cos3hx+...] \quad (5\text{-}11)$$

Where, J_0, J_1, J_2,....are Bessel's functions of various orders. A condition for identically satisfying equation (5-8) is the equality of the coefficients of the harmonic functions cos(mhx). Thus, the general expressions for the coefficients "A" are $A_0=RJ_0(2ka)$,

$A_1=2iRJ_1(2ka)$,......, $A_m=2(-i)^mRJ_m(2ka)$ (5-12)

Where m represents only positive integer numbers. Thus, the coefficients of even order are real values, and those of odd order are pure imaginary values. Ultimately, the complete solution of the reflection problem is obtained by blocking these constant coefficients in equation of reflection (5-2). The revised equation can be used to calculate the field of reflected ultrasonic waves with sufficient accuracy for engineering applications. The revised equation or scattered waves model becomes

$$\varphi_r = R[J_0(2ka)\exp i(-ikz) + 2iJ_1(2ka)\exp(-i\mu_1 z)\cos(hx) \\ -2J_2(2ka)\exp(-i\mu_2 z)\cos(2hx) + ...] \qquad (5\text{-}13)$$

5-4 EXPERIMENTAL DATA ANALYSIS:

The "ka" value and Bessel's functions of equation (5-13) can be calculated by using the experimental data and assuming that the RMS value of surface roughness heights is almost equal to the amplitude, a, of the surface mathematical model in equation (5-1). As a typical test parameter, we can choose a 10 MHZ ultrasonic transducer and a 10 μin (0.254 μm) surface finish sample, then.

$$2ka = 2(\omega/c)a = 2[(2\pi * 10\ \text{MHZ})/(1513\ \text{m/sec})](0.254\ \mu\text{m})$$

$$\therefore \qquad 2ka = 0.00211$$

The following plot of Bessel's functions (Fig. 5-8) shows that for 2ka values, the constant coefficients A_1, A_2, ... are negligible compared to the coefficient A_0 of the velocity potential for reflected wave in equation (5-2). Therefore, the principal reflected wave controls the reflection process and the resultant field in first medium (coolant) at the interface (Eq. (5-6)) can be written in term of the incident wave model (see Chapter 3, Eq.(3-54)) as

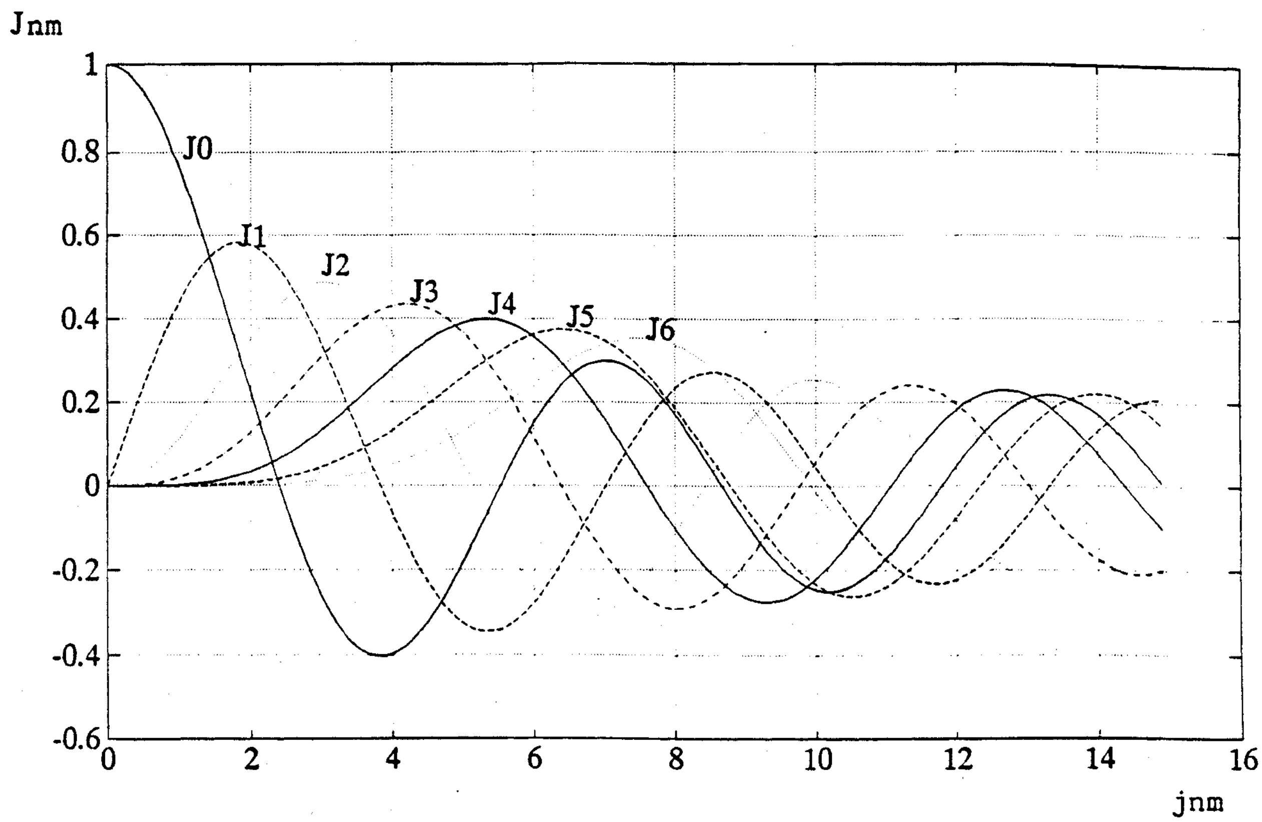

Fig. 5-3

$$\varphi = \frac{141.62}{kz}\exp i(kz-\omega t) + RJ_0(2ka)\exp[-i(kz+\omega t)] \qquad (5\text{-}14)$$

Where: $J_0(0.00211) \approx 1$.

$$R = (Z_2 - Z_1)/(Z_2 + Z_1) = (45.5 - 1.51)10^6/(45.5 + 1.51)10^6;$$

$$R = 0.936$$

Thus, equation (5-14) becomes

$$\begin{aligned} \varphi &= \frac{1.2055E07}{kz}\exp i(kz-\omega t) + \frac{.936}{kz}\exp[-i(kz+\omega t)] \\ P' &= \frac{7.4E17}{kz}\exp i(kz-\omega t) + \frac{5.785E10}{kz}\exp[-i(kz+\omega t)] \end{aligned} \qquad (5\text{-}15)$$

These are the instantaneous velocity potential and ultrasonic pressure models for field. In these models the absorption and attenuation phenomena are not considered, therefore, they will be re-analyzed for these parameters in Chapters 6,7.

It is possible to assume a number of values for the interface scattering surface amplitude, a, (Eq 5-1) which are almost in the range of the RMS value of the surface finish. Hence, we can generalize the test procedure for the "ka" values of the experimental surface finish range . Therefore, from a certain range of surface finish the other terms of equation (5-13) may have influence in reflection or scattering phenomenon. The Bessel's functions for our reflection problem are computed and tabulated in Table (5-1). The experimental surface finish range of 4 to 75 μin or 0.1016 to 2.032 μm respectively, are considered in this research. The wave number for 10 MHZ transducer and inside the first medium (coolant) is

$$k=\omega/c=(2\pi*10^7\ MHZ)/(1516\ m/s)=41446\ m^{-1}$$

The approximate values for amplitudes "a" are:

a_1=4 μin=.1016 μm, a_2=10 μin=.254 μm, a_3=20 μin=.508 μm,

a_4=30 μin=.762 μm, a_5=40 μin=1.016 μm, a_6=50 μin=1.27 μm,

a_7=60 μin=1.524 μm, a_8=70 μin=1.778 μm, and a_9=80 μin=2.032 μm.

Table 5-1:

computation of Bessel's Functions J_0 to J_5.

$2ka_1$= .0084	$2ka_2$= .0211	$2ka_3$= .0422	$2ka_4$= .0632	$2ka_5$= .0842	$2ka_6$= .1053	$2ka_7$= .1263	$2ka_8$= .1474	$2ka_9$= .1684
$J_0\approx1.$	$\approx1.$	$\approx1.$	$\approx1.$	$\approx1.$	$\approx1.$	$\approx1.$	$\approx1.$	$\approx1.$
$J_1\approx0.$	0.01	0.02	0.03	0.04	0.05	0.06	0.07	0.08
$J_2\approx0.$	0.0	2E-4	4E-4	0.001	12E-4	2E-3	3E-3	4E-3
$J_3\approx0.$	0.0	0.0	0.0	1E-4	0.0	0.0	0.0	1E-4
$J_4\approx0.$	0.0	0.0	0.0	0.0	0.0	0.0	0.0	0.0
$J_5\approx0.$	0.0	0.0	0.0	0.0	0.0	0.0	0.0	0.0

Table 5-2:

The corresponding constant coefficients, A.

	A_0	A_1	A_2	A_3	A_4	A_5
$2ka_1=.0084$	≈0.9360	0.0047	0.0000	0.0000	0.0000	0.0000
$2ka_2=.0211$	≈0.9360	0.0094	0.0000	0.0000	0.0000	0.0000
$2ka_3=.0422$	≈0.9360	0.0187	0.0002	0.0000	0.0000	0.0000
$2ka_4=.0632$	≈0.9360	0.0281	0.0004	0.0000	0.0000	0.0000
$2ka_5=.0842$	≈0.9360	0.0375	0.0009	0.0000	0.0000	0.0000
$2ka_6=.1053$	≈0.9360	0.0468	0.0011	0.0000	0.0000	0.0000
$2ka_7=.1263$	≈0.9360	0.0562	0.0019	0.0000	0.0000	0.0000
$2ka_8=.1474$	≈0.9360	0.0656	0.0028	0.0000	0.0000	0.0000
$2ka_9=.1684$	≈0.9366	0.0749	0.0037	0.0001	0.0000	0.0000

Results Analysis: The values of amplitudes (A) presented in Table (5-2) and also the decreasing coefficients of cos(mhx) versus increasing m and x values , show that the other terms of the reflected wave equation (5-13) will be decayed very fast. Therefore, approximation theory confirms that the principal reflected mode controls the reflection process in the experimental precision grinding at the range of 4 to 75 μin . It means, in order of magnitude the other terms of reflection series, equation (5-13) do not have a considerable influence in the reflection model, equation (5-15).

The field equation in medium one (coolant), equation (5-15) contains two individual terms. The first term defines only the incident wave model and the second term is representative of the reflected wave in z-axis direction. Hence, in the field, the scattered wave reflected from the interface surface in opposite direction of the incident wave propagation, it may either oppose to incident wave or reinforce this wave when it is reflected from the diffuser walls toward the interface surface.

To consider the effect of the diffuser geometry, we have to multiply the second term of the model, equation (5-15) by a proper coefficient. This coefficient will be found and optimized for this experimental work in Chapter 6, this would be the final model of reflection term of equation (5-15). The boundary condition for this model will also be discussed in detail in Chapter 6 , where we are going to find and formulate the final solution for the problem.

The interesting result concluded so far is that at the precision grinding range (4 to 75 μ in), the mathematical model of the surface finish does not have an important role in derivation of the field equation (5-15).

Additionally, the effects of the other parameters such as oblique incident, coolant temperature, grinding machine RPM, distance, and transducer frequency were analyzed in this research. The influence of these parameters will be studied in Chapters 6 & 8.

REFERENCE:

1- Kinsler, " Fundamental of Acoustic ", 3rd Ed., Wiley, 1980.

2- Pierce A., " Acoustics ", MacGraw-Hill, 1981.

3- Brown & Wolf, " Principles of Optics ", 4th Ed., 1970.

4- Stover J., " Optical Scattering Measurement and Analysis ", MacGraw-Hill, 1990.

5- J.W.S. Rayleigh, "The theory of sound", Vol.2, Dover, 1945.

6- Kachoyan & Macaskill, " Acoustic scattering from an arbitrary rough surface ", J. Ac.Soc. Am. 85 (5) Nov. 1987.

7- Watson & Keller, Rough surface scattering via the smoothing method ", J. Ac. Soc. Am. 75 (6). June 1984.

8- Spivack M., " A numerical approach to rough-surface scattering by the parabolic equation method ", J. AC. Soc. Am. 87 (5), May 1990.

9- Temkin, " Elements of Acoustics ", Wiley, 1981.

10- Malecki, " Physical Foundations of Technical Acoustics ", PWN, 1969.

CHAPTER 6:

ULTRASONIC WAVE ATTENUATION:

6-1 INTRODUCTION:

In chapter 2, the fluid pattern in the diffuser (a component of the waveguide assembly) was studied. The fluid (coolant) used in this system was a two phase flow (emulsion). The emulsion characteristics cause attenuation of the ultrasonic energy, the attenuation increases with increasing oil volume fraction in the coolant composition (2-phase flow). A common cause of the ultrasonic energy attenuation is wave scattering from the interface surface roughness. The geometrical configuration of the waveguide components and the part surface are investigated for attenuation purposes in this chapter. Analysis of three high frequency transducers (10 MHZ, 20 MHZ, and 30 MHZ) and three approved distances from the transducer face to the interface surface are also a part of this chapter. Eccentric and oblique orientation of the waveguide assembly cause considerable ultrasonic energy attenuation and were investigated in this experimental research (results will be presented in Chapter 8). The other parameters such as grinder rpm variation (from 0 up to 500 rpm) and temperature variation (from 60 to 87 °F) which did not have considerable effects in surface finish measurement were verified in the experimental work (see the experimental in Chapter 8).

6-2 ULTRASONIC ATTENUATION IN EMULSIONS:

The attenuation of ultrasound in *emulsions* (oil and water or any two phase flow) can be regarded as the sum of three terms. These terms are differences between the two phases in density, ρ, compressibility $(\rho c^2)^{-1}$ (where c is the velocity of sound in emulsion) and $\beta/(\rho c_p)$ (where β is the coefficient of volume expansion and c_p is specific heat). The values of these terms are listed in Table (6-1). Based on the physical properties of Interlub and tap water, the compressibilities of the two liquids are almost identical, therefore, the thermal term contributes to the ultrasonic attenuation more than the other terms over the frequency range 10-30 MHZ.

TABLE 6-1:

Physical constants for Interlub and tap water at 20°C

PARAMETERS	BESTCUT-INTERLUB (SUB I)	WATER (SUB 2)
Density, ρ kg/m^3	924	998
Vel. of sound, c m/s	1650	1482
Coef, of viscos., μ N.s/m^2	$61.0*10^{-4}$	0.001
Specific heat, c_p J/kg.°C	1874	4179
Thermal cond.,k W/m.°C	0.148	0.598
Expansion coef., β °K^{-1}	$0.68*10^{-3}$	$0.2068*10^{-3}$

Under the following limited conditions, the theoretical predictions of the attenuation of ultrasound have a simple analytic expression:

1) The distance between emulsion droplets is much greater than the droplet radius, a (0.1 μm<a<1.0 μm).

2) The incident wavelength (λ_{10MHZ}=1.516E-04 m, λ_{20MHZ}=0.758E-04 m and λ_{30MHZ}= .505*10^{-4} m) is much greater than the radius of the droplet, a=0.7 μm, for the volume fraction Interlub in tap water of 3% to 5%, at 20^{0}C in our experiment.

$$\alpha_T=\phi\frac{\sqrt{\omega}}{a}c_2T_O\rho_2(\frac{\beta_1}{\rho_1C_{p1}}-\frac{\beta_2}{\rho_2c_{p2}})^2\frac{\sqrt{(\rho_1C_{p1}K_1\rho_2C_{p2}K_2)}}{\sqrt{(\rho_1C_{p1}k_1)}+\sqrt{(\rho_2C_{p2}k_2)}} \quad (6\text{-}1)$$

where the angular frequency (ω) is in MHZ scale in this equation.

The percentage of ultrasound attenuation in terms of volume fraction of Interlub in coolant (ϕ %) are listed in Table (6-2) and the results are also plotted in Fig. (6-2).

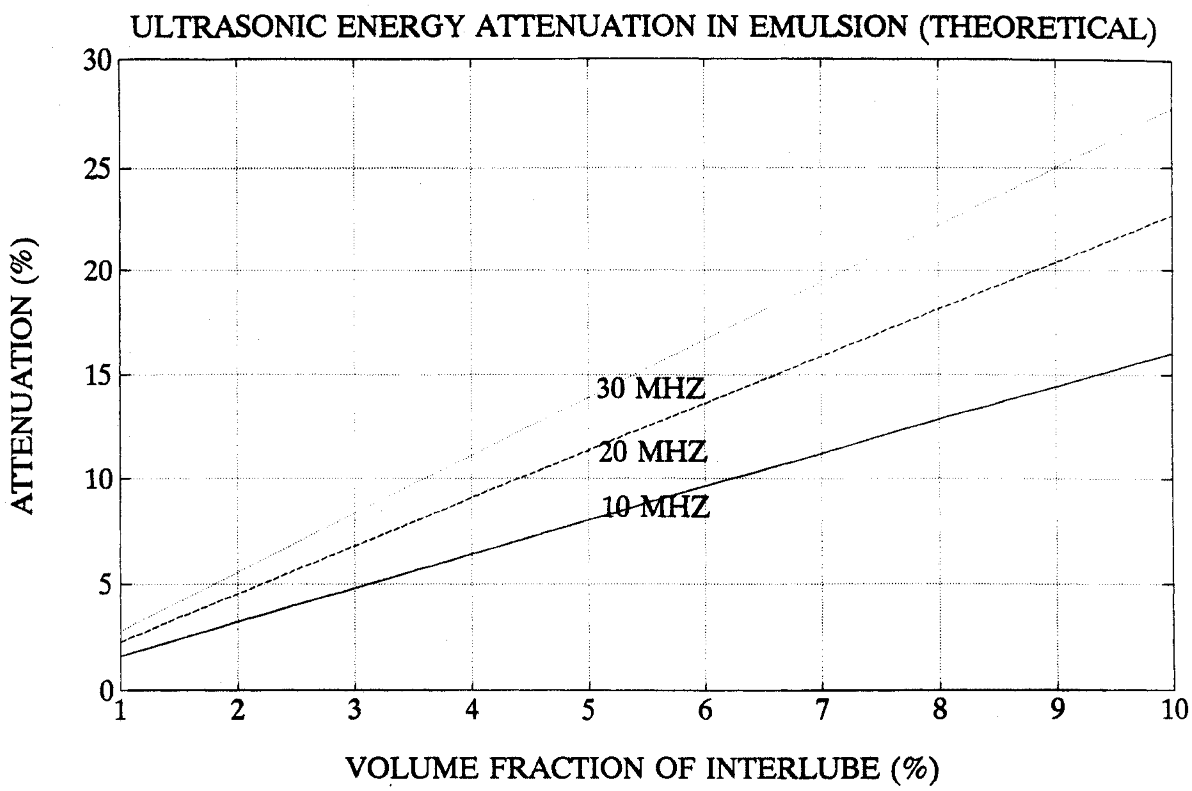
ULTRASONIC ENERGY ATTENUATION IN EMULSION (THEORETICAL)
ATTENUATION (%)
0
5
10
15
20
25
30
1
2
3
4
5
6
7
8
9
10
30 MHZ
20 MHZ
10 MHZ
VOLUME FRACTION OF INTERLUBE (%)

Fig. 6-1

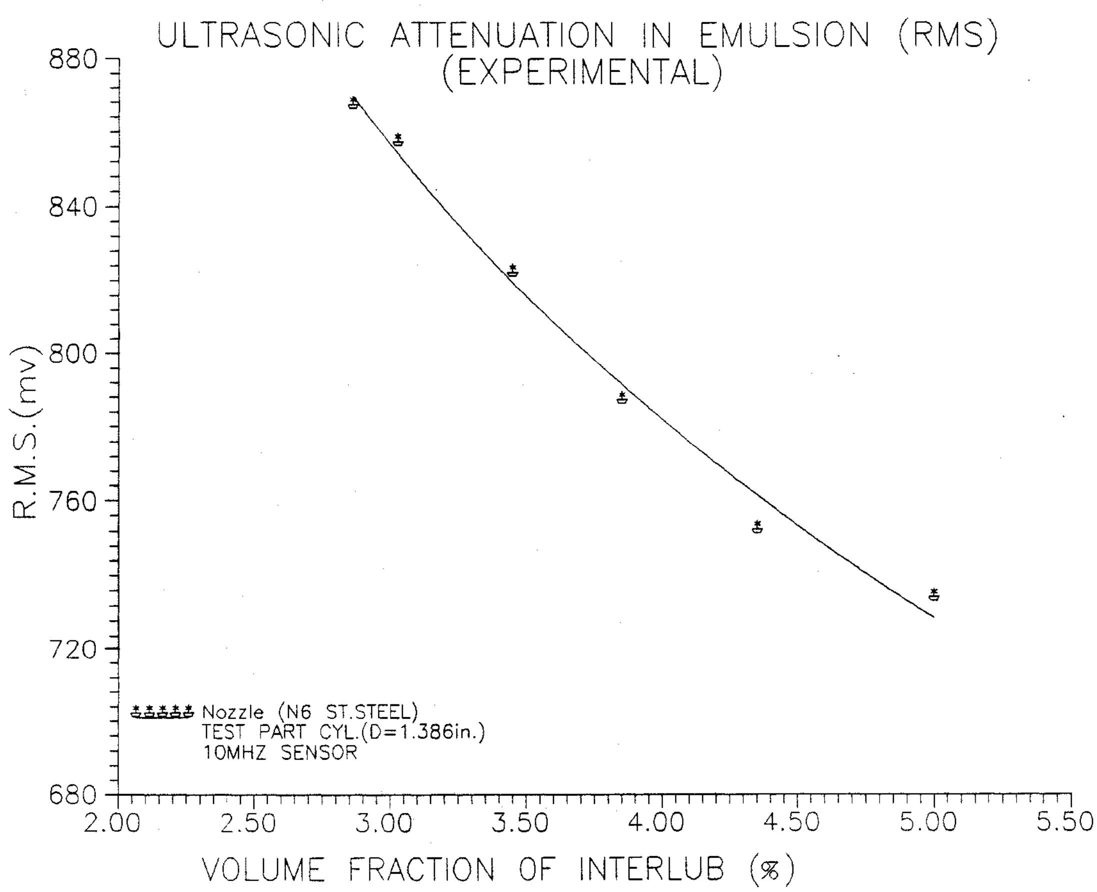
ULTRASONIC ATTENUATION IN EMULSION (RMS)
(EXPERIMENTAL)
R.M.S.(mv)
880
840
800
760
720
680
2.00
2.50
3.00
3.50
4.00
4.50
5.00
5.50
Nozzle (N6 ST.STEEL)
TEST PART CYL.(D=1.386in.)
10MHZ SENSOR
VOLUME FRACTION OF INTERLUB (%)

Fig. 6-2

TABLE 6-2:

Ultrasonic attenuations in emulsion.

VOLUME FRACTION OF INTERLUB (ϕ %)	ATTENUATION $(\alpha_T)_{10MHZ}$	$(\alpha_T)_{20MHZ}$	$(\alpha_T)_{30MHZ}$
1%	1.6037	2.2680	2.7777
2%	3.2074	4.5359	5.5553
3%	4.8111	6.8039	8.3330
4%	6.4147	9.0718	11.1107
5%	8.0184	11.3398	13.8883
6%	9.6221	13.6077	16.6660
7%	11.2258	15.8757	19.4436
8%	12.8295	18.1436	22.2213
9%	14.4332	20.4116	24.9990
10%	16.0368	22.6795	27.7766

6-2-1 REMARKS ON EMULSIONS RESULTS:

The attenuation of ultrasound in emulsions depends upon absorption of acoustic energy within the coolant. The rate of increase in attenuation is associated mainly with an increase in the volume fraction of the oil (Bestcut-Interlub) and water.

During the experimental tests, we observed that an increase of the volume fraction (oil/water) had immense influence on the amplitude reduction. The experimental results are shown in Fig. (6-2) which were obtained using a 10 MHZ transducer. The trend of the experimental and theoretical plots in Figs. (6-1 and 6-2) do confirm each other fundamentally. Deviation of the experimental plot from the theoretical one (exponential to linear) is due to the assumptions in theoretical analysis, and some possible errors such as environmental effects and measurement errors. In reality, the compressibility term in higher range of volume fraction causes a kind of nonlinearity effect, therefore it cannot be ignored. Fortunately, the volume fraction worked without any corrosive problem for grinders and parts, and also offered a sufficiently high amplitude for measurements in the range of 3% to 5% volume fraction of concentration oil in tap water. In this range the experimental and theoretical results are consistent.

6-3 ATTENUATION DUE TO WAVEGUDE GEOMETRY AND SURFACE ROUGHNESS:

Before analyzing this problem, we need to consider some assumptions as follows:

- The incident and reflected waves are plane waves.
- The incident and reflected waves are coplanar (x-z plane).
- The interface between the coolant and solid part is the part surface.
- The amount of the incident wave which penetrates inside the solid part (refraction) is negligible.

The reflection phenomenon from a solid part surface is the main purpose of this section. Due to surface discontinuity, a normal incident wave scatters at the interface. Sonic energy attenuation at the interface surface may happen in two ways:

1) In single scattering case, the wave reflects in a path different from the normal incident

wave direction. Therefore, the reflected wave energy will be attenuated proportional to deflected angle. For reflection angle equal or less than a certain amount, the reflected wave is able to travel through the waveguide system and impact the transducer face. The attenuation of this reflected wave is due to the difference in path lengths which is traveled by normal incident and reflected waves.

2) In multiple scattering case, a reflected wave may be scattered many times through successive incidence and reflection either at interface surface or inside the waveguide system. If the reflected wave is able to pass through this system and exited the transducer, part of its energy will be lost (similar to first condition), otherwise, the scattered wave cannot reach the transducer face and will be scattered. In this case, all of the scattered wave energy will be dissipated.

Based on the geometrical configuration of the experimental waveguide system and the surface finish quality, we have to optimize; 1) the capability of waveguide assembly for capturing and transmitting the scattered waves to the transducer face, 2) scattering angle versus a certain length of the cylindrical part, in x-axis direction scanned by the ultrasonic wave. It should be noted that the ultrasonic transducer position is always fixed during each experiment, see Figs (6-3 to 6-5). Therefore, the correlation of attenuation phenomena due to both surface condition and the waveguide geometry should be studied at this point.

The field velocity potential at the boundary surface was studied for surface finish range from 4 to 75 μin 3), Chapter 5. The result presented in equation (5-15) verifies that the principal reflected mode control the reflection process. We also found that, for rougher part surfaces more terms of the series, Eq. (5-13), participate in the calculation of the velocity potential of the reflected wave. The field equation which was derived in

Chapter 5 is presented here for further interpretation and calculations.

$$\varphi = \frac{1.2055E07}{kz}\exp i(kz - \omega t) + .\frac{936}{kz}\exp - i(kz + \omega t)$$
$$P' = \frac{7.4E17}{kz}\exp i(kz - \omega t) + \frac{5.785E10}{kz}\exp - i(kz + \omega t) \qquad (6\text{-}2)$$

In general case, the normal incident plane waves are scattered at the interface surface discontinuity in various directions. The portion of scattered waves captured by the diffuser can be either conducted up to the transducer face or reflected back from the diffuser walls to outside environment, Figs.(5-1,2). Both the waveguide geometry and its position mainly control the rate of reflected waves which are captured by the diffuser. The reflected waves travel from the normal incidence which is located along the center line of diffuser (point C) to a position (D) along the part surface which coincides with reflected waves impinging point at almost the diffuser mouth edge (demonstrated in Figs. 6-3 to 6-5). The waveguide system position for all cases are perpendicular to the interface surface. In each case the diffuser mouth is fixed for a certain distance or height (experimental values) to the part surface. Thus, the distance between the transducer face and the boundary surface is always constant for each position s_1, s_2, or s_3. Optimization of attenuated wave for hypothetical model of the experiment was done by computing accurate reflected angles and the locations for some sampling points along the part surface selected from the z-axis, for about 0.2" traveling length (x-axis). These distances were measured with up to 10^{-5} accuracy by computer graphic. The graphical analysis shows a scattered waves at point C can be captured and transmitted to the transducer face by waveguide assembly if its reflection angle

(θ_s) is equal to or less than 16, 14 or 13 degrees (for part positions s_1, s_2 and s_3 respectively). If the scattered wave travels along the grinding part (x-axis), the reflected angle decreases to almost 2 degrees for all The three grinding part positions. It means any scattered wave whose reflection angle is zero (along z-axis) or two degrees with respect to normal can fed back to the thransducer without any loss due to waveguide geometry. The measurement results were curve fitted for 200 sampling points resolution. The theory of estimation can predict proper estimated coefficient to express the percentage of attenuation for each position of the ground part, Figs.(6-3 to 6-5). The exponential expression forms can be used to study the variations in the reflection angle versus ratios of sampling lengths along the ground part (x_s) as an independant variable computed in x-z plane. The computational exponential expressions are experessed in terms of aspect ratio (x/z), where $z=s_n$ for three different fixed and known positions ($z=s_1=0.100"$, $s_2=0.125,"$ and $s_3=0.250"$). These non-dimensional expressions provide integration in term of independent variable (x) and measure the reflection angles in degree. The results are presented in three empirical relations as follows:

CASE a) For part position $s_1=.100"$, length of sampling points x_s:0 to CD=0.20539", AB=0.35318", 10 MHZ transducer.

$$\theta_s=15.8079[\exp-(10.451297x)]\ \textit{degree}. \qquad (6\text{-}3)$$

CASE b) For part position $s_2=.125"$, length of sampling points x_s:0 to CD=0.20112", AB=0.33859", 10 MHZ transducer.

$$\theta_s = 14.2136[\exp -(10.5200112x)] \textit{ degree.} \qquad (6\text{-}4)$$

CASE c) For part position s_3=,250", length of sampling points x_s: 0 to CD=0.19911", AB=0.32811", 10 MHZ transducer.

$$\theta_s = 13.1005[\exp -(10.5290332x)] \textit{ degree.} \qquad (6\text{-}5)$$

It should be noted that information about the scattering angle range for various sampling point locations (along the x-axis), Figs.(6-3 to 6-5) give us a precious knowledge about capability of the waveguide system for capturing and conducting the scattered waves. The geometrical modeling is studied only for waveguide assembly wave conductivity, regardless how rough is the part surface.

Note that the model is analyzed for the three distances 0.100", 0.125" and 0.25" between the waveguide outlet (diffuser mouth) and the grinding part surface were recommended by grinder manufacturers through inquiring.

6-4 THE WAVEGUIDE GEOMETRICAL ATTENUATION RESULTS ANALYSIS:

The estimated results are obtained by applying empirical equations (6-3 to 6-5) for three different workpiece positions.

Reference case is defined for the condition where the diffuser mouth contacts exactly on the surface of a 10 μin surface finish standard flat plate. It is assumed that all the reflected waves from the flat surface which enter the diffuser can be conducted to the

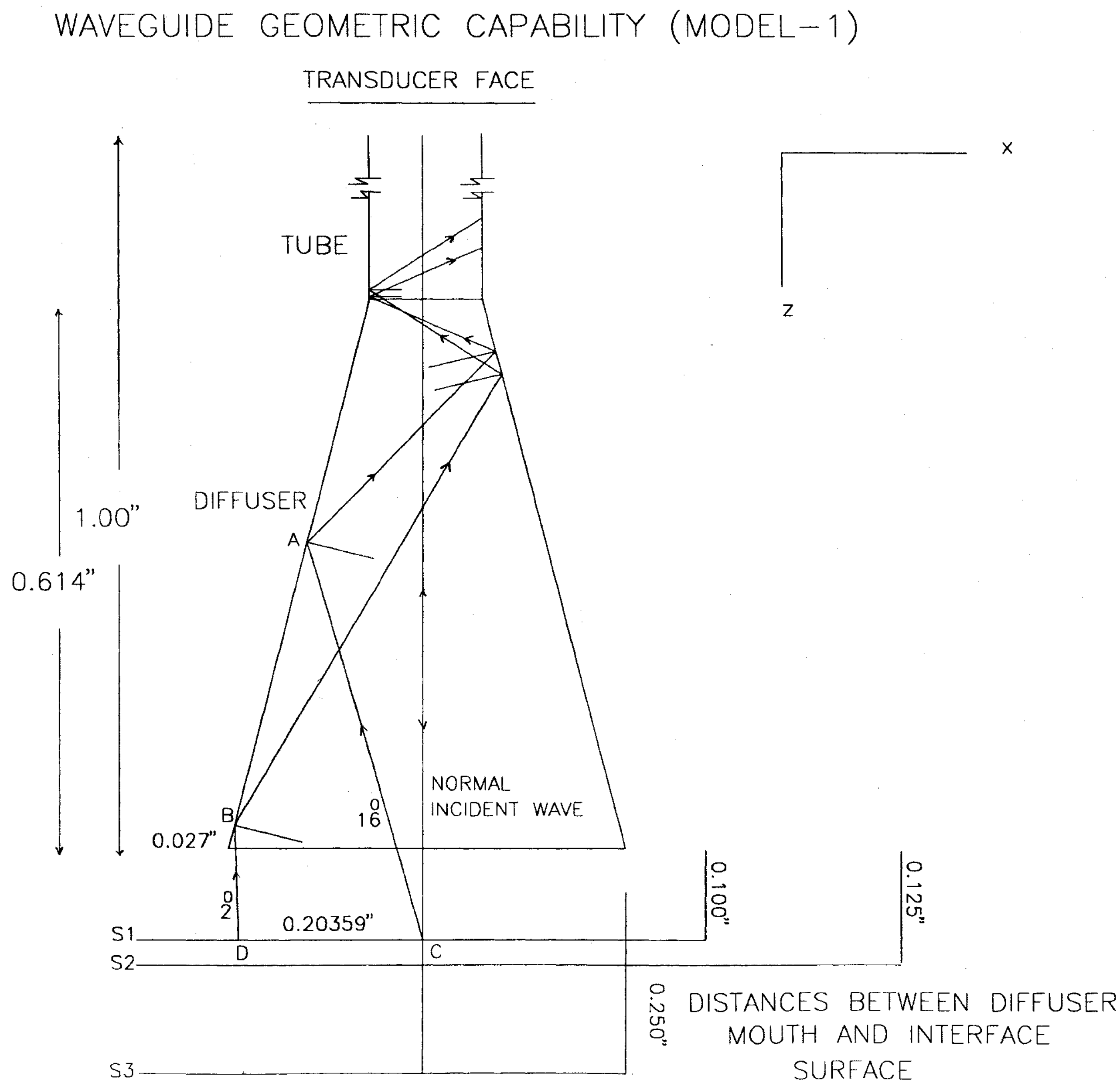
WAVEGUIDE GEOMETRIC CAPABILITY (MODEL-1)
TRANSDUCER FACE
X
Z
TUBE
DIFFUSER
1.00"
0.614"
A
B
0.027"
16°
2°
NORMAL INCIDENT WAVE
0.20359"
S1
S2
S3
D
C
0.100"
0.125"
0.250"
DISTANCES BETWEEN DIFFUSER MOUTH AND INTERFACE SURFACE

Fig. 6-3

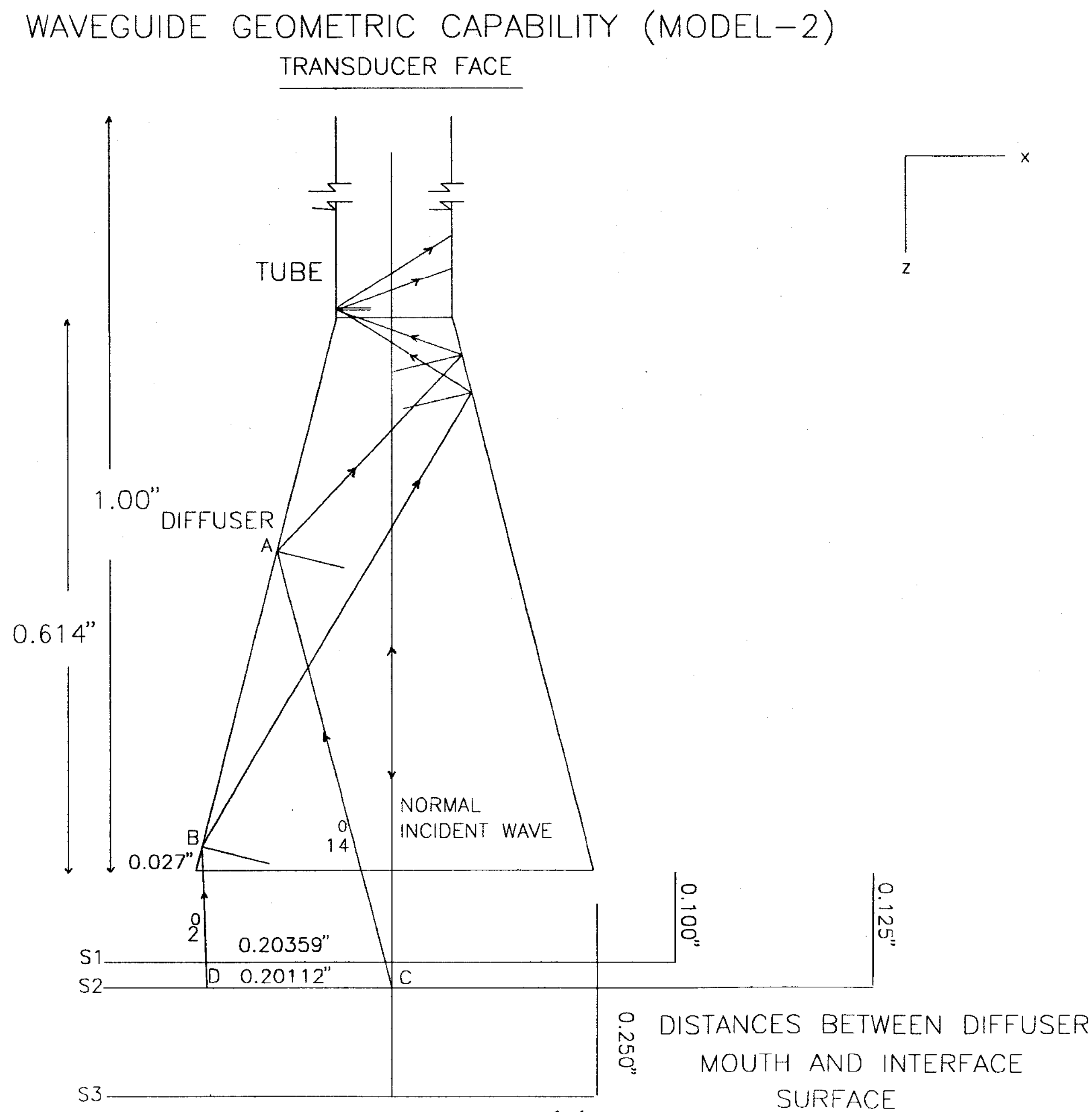
WAVEGUIDE GEOMETRIC CAPABILITY (MODEL-2)
TRANSDUCER FACE
x
z
TUBE
1.00"
DIFFUSER
A
0.614"
B
0.027"
0
14
NORMAL
INCIDENT WAVE
0
2
0.20359"
S1
D 0.20112"
C
S2
S3
0.100"
0.125"
0.250"
DISTANCES BETWEEN DIFFUSER
MOUTH AND INTERFACE
SURFACE

Fig. 6-4

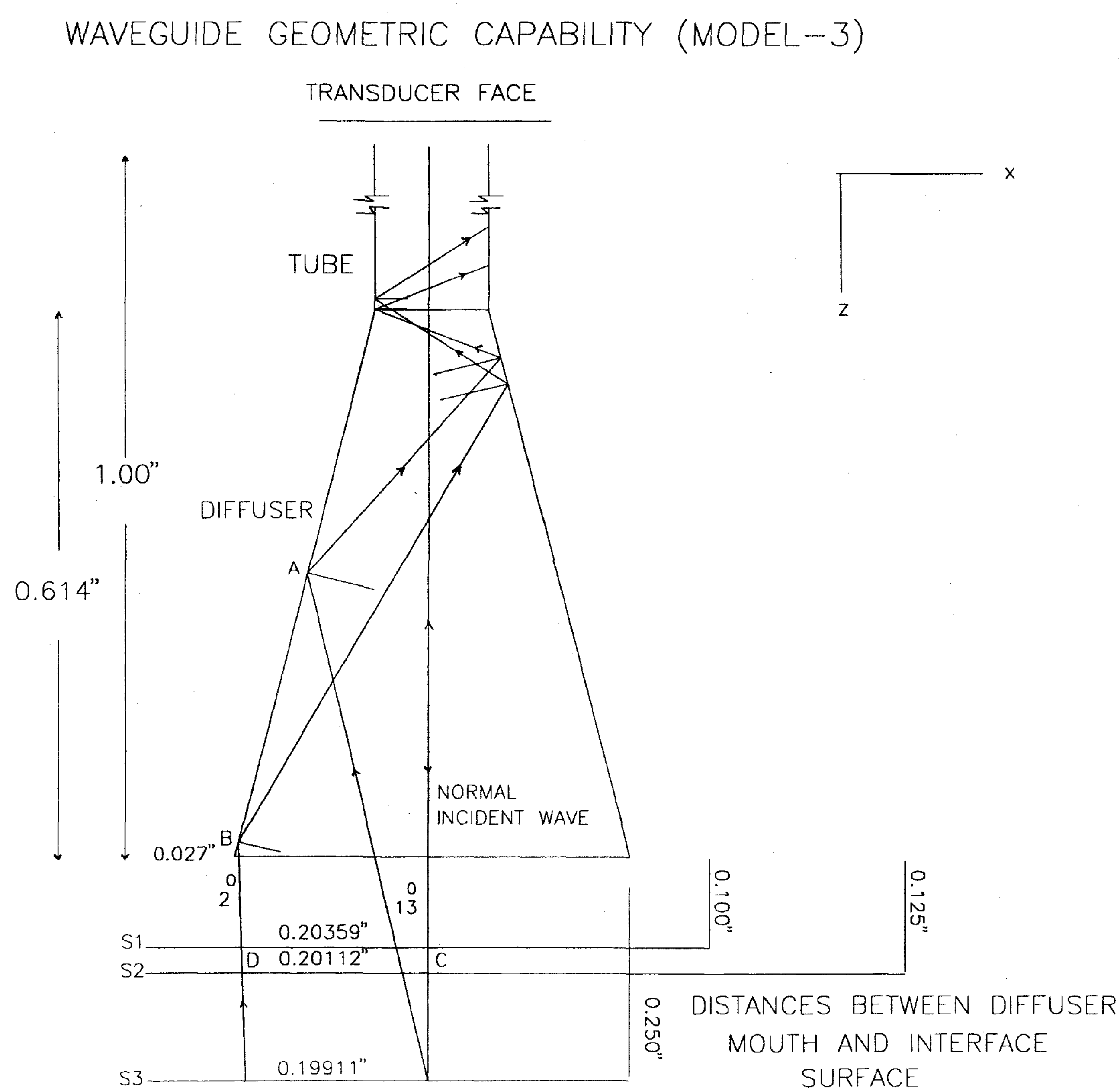

WAVEGUIDE GEOMETRIC CAPABILITY (MODEL-3)
TRANSDUCER FACE
TUBE
DIFFUSER
1.00"
0.614"
A
B
0.027"
NORMAL
INCIDENT WAVE
x
z
0
2
0
13
S1
S2
S3
D
C
0.20359"
0.20112"
0.19911"
0.100"
0.125"
0.250"
DISTANCES BETWEEN DIFFUSER
MOUTH AND INTERFACE
SURFACE

Fig. 6-5

transducer face either with a single reflection or multi-reflections.

So far total attenuation in ultrasonic energy may be caused by the part position with respect to the diffuser mouth and its surface roughness, waveguide geometry, volume fraction of Interlub coolant can be determined by using the Table (6-2) for the experimental research.

Scattering problem will be investigated in next chapter by using a computer code. The range of scattering angle from a precision part surface (4 to 75 μin.) can be estimated by using the related code.

6-5 THE ULTRASONIC ENERGY ABSORPTION:

In Chapter 2, attenuation of the ultrasonic energy was studied versus only oil volume fraction of the coolant. In reality, the sonic energy dissipation takes place in the medium due to the fluid characteristics or at the boundary or interface. The interface is considered as waveguide walls (rigid), interface with the environment or air (reactive) and the grinding part interface surface (rigid). The losses are mainly heat conduction loss, molecular exchange of energy (kinetic energy to potential energy of molecules). A absorption process is usually characterized by a relaxation time (τ). Therefore, the wave number $k=\omega/c$ of the Helmholtz equation (3-19), Chapter 3, is changed a new expression

$$K=\omega/c(1+j\omega\tau)^{-.5}=k-j\alpha \qquad (6\text{-}6)$$

where
$$\alpha=(\omega/c)*1/\surd 2*\{[(1+(\omega\tau)^2)^{.5}-1]/[1+(\omega\tau)^2]\}^{.5} \qquad (6\text{-}7)$$

For 10 MHZ transducer, ultrasonic velocity in coolant (1516 m/s) and τ equals to 3.059*10E-08 sec. Substituting these values in Eq. (6-7) yields $\alpha=395.2\ sec^2.m^{-1}$.

Therefore, the general solution of the problem for a plane wave ultrasonic becomes, [4]

$$A = \exp -395.2 * 0.3429$$

$$P' = \frac{7.4*E17}{kz} \exp i(kz - \omega t) * A + \frac{5.785E10}{kx} \exp -i(kz + \omega t) * A \qquad (6\text{-}8)$$

This is the final solution of this research work which is used for computer coding. The empirical solution (6-8) is obtained under the experimental condition and prototype specifications. We can write a general solution form for similar problems as

$$P' = \exp -(\alpha z)[\frac{A}{kz} \exp i(kz - \omega t) + \frac{B}{kz} \exp -i(kz + \omega t)] \qquad (6\text{-}9)$$

It should be reminded that this model can be used for any waveguide assembly with the same configuration as this research but different geometries. The model coefficients should be computed for any wave guide assembly and coolant.

REFERENCES:

1- Kachoyan and Macaskill, " Acoustic Scattering for an arbitrarily rough surface, J. Acoust. Soc., 82(5), nov. 1987.

2- Watson and Keller, " Rough surface scattering via the smoothing method ", J. Acoust. Soc. Am. 75 (6), June 1984.

3- Rayleigh J.W.S., "The Theory of Sound", vol. 2, Dover, 1945.

4- Kinsler, "Fundamentals of Acoustics", 3rd Ed.,Wiley, 1976.

CHAPTER 7

CODE DEVELOPMENT AND PARAMETERS ANALYSIS:

7-1 INTRODUCTION:

In order to analyze the variation of several parameters, a computer code is developed. This chapter discusses the main features of this code. The analysis is pursued with the following conditions for which the experiments were performed:

- Normal incident ultrasonic wave strikes the top center of grinding part. In reality, there are no oblique and eccentric impingement wave conditions in this research.
- Volume oil fraction mixed with tap water varies between 3.45% to 5%. The oil used in this experiment has the commercial name Bestcut-Interlub (see Table 6-1, Chapter 2 for oil specifications).
- Grinding part rotates about its horizontal axis (x-axis). The coolant pressure is regulated at 1 psig. The coolant temperature is varied from 65°F≈18.33°C to 90°F≈32.22°C.
- The axis of the waveguide assembly is normal to the part center line (z-axis direction).
- Measurement is mostly carried out in SI units.

Some of the parameters such as tilted incident wave, eccentric normal incidence and flat plat are analyzed in the experimental portion of this research. The analysis of these parameters is undertaken just for an investigation of the ultrasonic wave process in the coolant system and finally, measurement of the surface finish by energy feedback to the transducer.

7-2 CODE OBJECTIVES:

Main topics such as the wave propagation model analysis, attenuation of the ultrasonic energy with increasing distance (between interface surface and transducer face), volume oil fraction and surface roughness are investigated by using the related codes which are written based on PC-MATLAB and Fortran-77. The details of these computer programs are presented in Appendix-C.

At this point a description of the energy in a transducer and its operation is warranted. Then, we will develop several codes to investigate the energy attenuation under various conditions of either coolant flow properties or waveguide assembly specifications.

7-2-1 Ultrasonic Transducer Specifications and Operation:

The transducers used in this research work are Videoscan immersion type with various frequencies (10 MHZ, 20MHZ and 30 MHZ). The crystal material for all of them is piezoelectric, but the type of piezoelectric product is not known. In general, lead titanate zirconate is the dominant transducer material for the MHZ range employed by transducers in various ultrasonic applications.

The effect of any magnetic field is ignored when dealing with piezoelectric materials and only the influences of an electrical field is considered. The vibrating piezoelectric crystal also occurs in adiabatic conditions .

Fundamentals of Piezoelectricity: The piezoectric operation can be defined by four linear equations, the form depending on the choice of electrical field or charge density on the one hand or mechanical stress or strain (caused by ultrasonic wave) on the other as the independent variables, details of these equations are on pages 64-65 of [1]. In the pulse-echo technique used in the experimental research work, the electrical field and the mechanical vibrational stress work as independent variables.

The coupling factors are among the most important properties of piezoelectric materials. It is defined as the square root of the ratio of electrical (mechanical) work which can be done under ideal conditions to the total energy stored from a mechanical (electrical) source. Thus, the coupling factor defines the relation between these energies as follows:

$$k^2 = W_1/(W_1 + W_2)$$

where W_1 is the amount of the electrical input energy and W_2 defines the amount of mechanical energy (ultrasonic energy) at transducer output.

In the experimental work, the input energy to the transducer was set at $94*10^{-6}$ Joules. Therefore, the intensity inputs to the crystal cross section area (Diam.0.250"=0.00635m) of the 10 MHZ transducer is equal to 2.968 watt/m^2. A fraction of this energy is converted to an ultrasonic compressional wave (mechanical energy). This energy will be considered in the problem.

7-2-2 Propagation Model Analysis:

This code is capable of analyzing both fundamental and lateral modes of the wave propagation inside the tube part of the waveguide assembly. The first five transient propagating modes are only considered in this code.

Code Description: The code can compute the amplitudes of the fundamental and lateral modes at five different points along the radius (from tube center line to the tube wall) and toward increasing z-axis of tube part of the waveguide assembly and based on either velocity potential equation (3-54) or ultrasonic pressure. Application of the theory of approximation shows that the amplitude (E_1) of the fundamental mode dominates those of lateral modes. Therefore, the amplitude of propagation mode amplitude can be calculated based on order of magnitude. The Code-1 and 2 were written and developed as a part of Chapter 3. The value of amplitudes were tabulated in Tables (3-2 and 3-4), Chapter 3. The code was run for 10 MHZ transducer as a particular computation. It should be noted, however, that the program works for other frequencies just by changing the value of omega. The codes for A and E computations are titled under Codes-1 and 2 in Appendix-C. The plotted results were shown in the Figs.(7-1 and 7-2).

7-2-3 Energy attenuation versus oil volume fraction: The code predicts the ultrasonic energy attenuation in term of the oil volume fraction in the coolant.

Code Description: Relative attenuation value can be computed using this code. The program is also able to investigate this phenomena when different transducers are used in the same coolant and experimental set up conditions. The tap water is chosen as reference, because it has higher wave transmission capability (compared with coolant). The program was written for a two phase fluid flow (emulsion) with different properties, Chapter 2.

The obtained results by using this code have been tabulated in Table (6-2) of Chapter 6. Data are plotted in Fig. (7-3). The code is presented in Appendix-C under Codes-3 and 3a title.

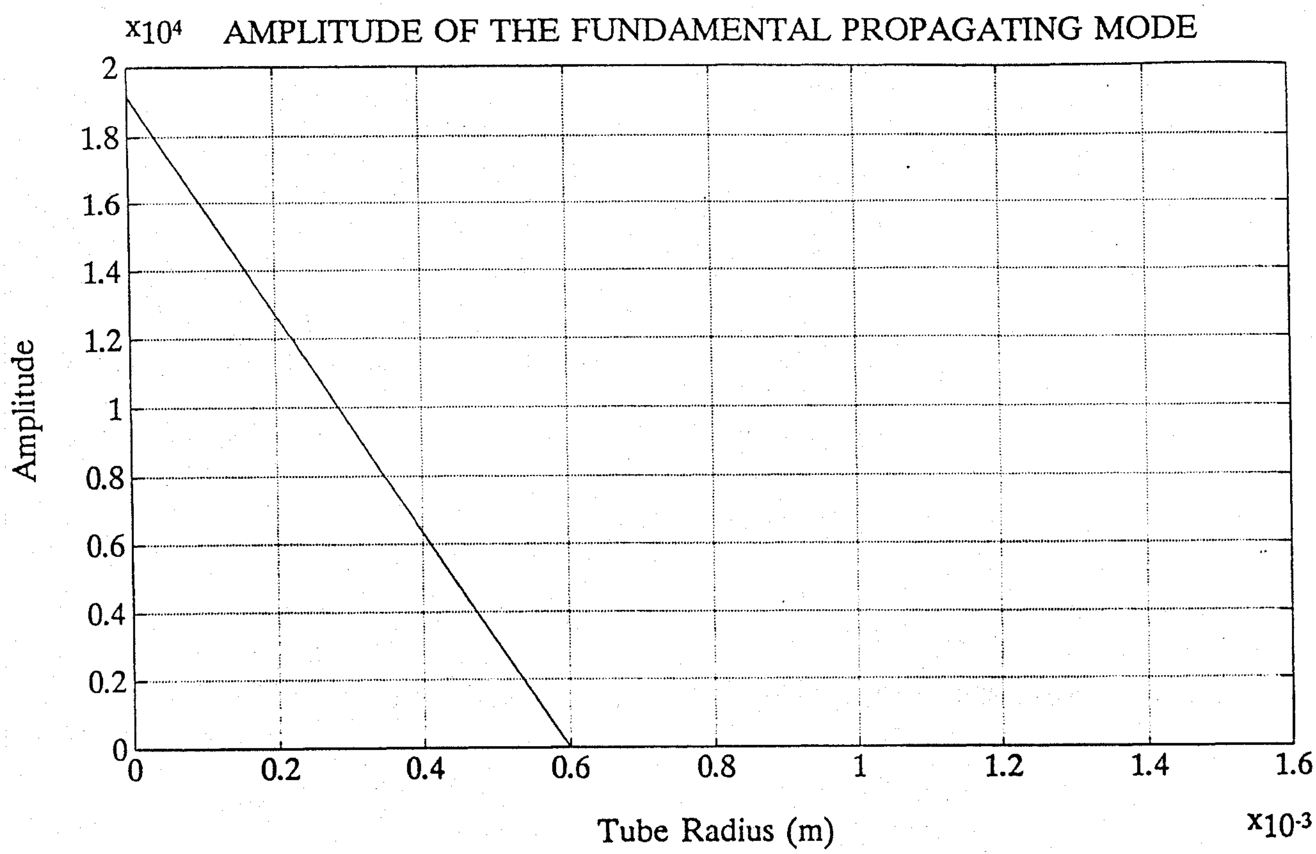
x10^4 AMPLITUDE OF THE FUNDAMENTAL PROPAGATING MODE
Amplitude
2
1.8
1.6
1.4
1.2
1
0.8
0.6
0.4
0.2
0
0
0.2
0.4
0.6
0.8
1
1.2
1.4
1.6
Tube Radius (m)
x10-3

FIG. 7-1

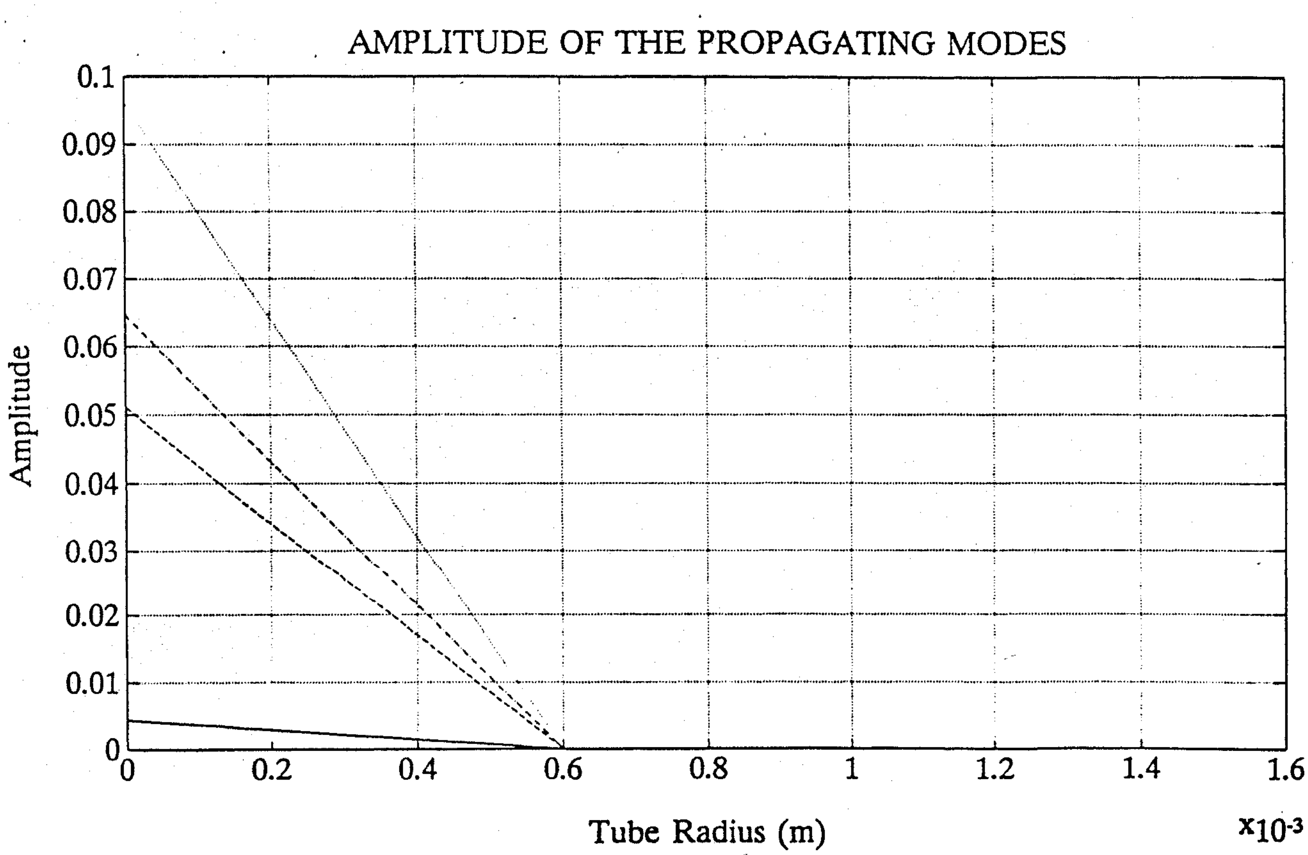
AMPLITUDE OF THE PROPAGATING MODES
Amplitude
0.1
0.09
0.08
0.07
0.06
0.05
0.04
0.03
0.02
0.01
0
0
0.2
0.4
0.6
0.8
1
1.2
1.4
1.6
Tube Radius (m)
x10-3

FIG. 7-2

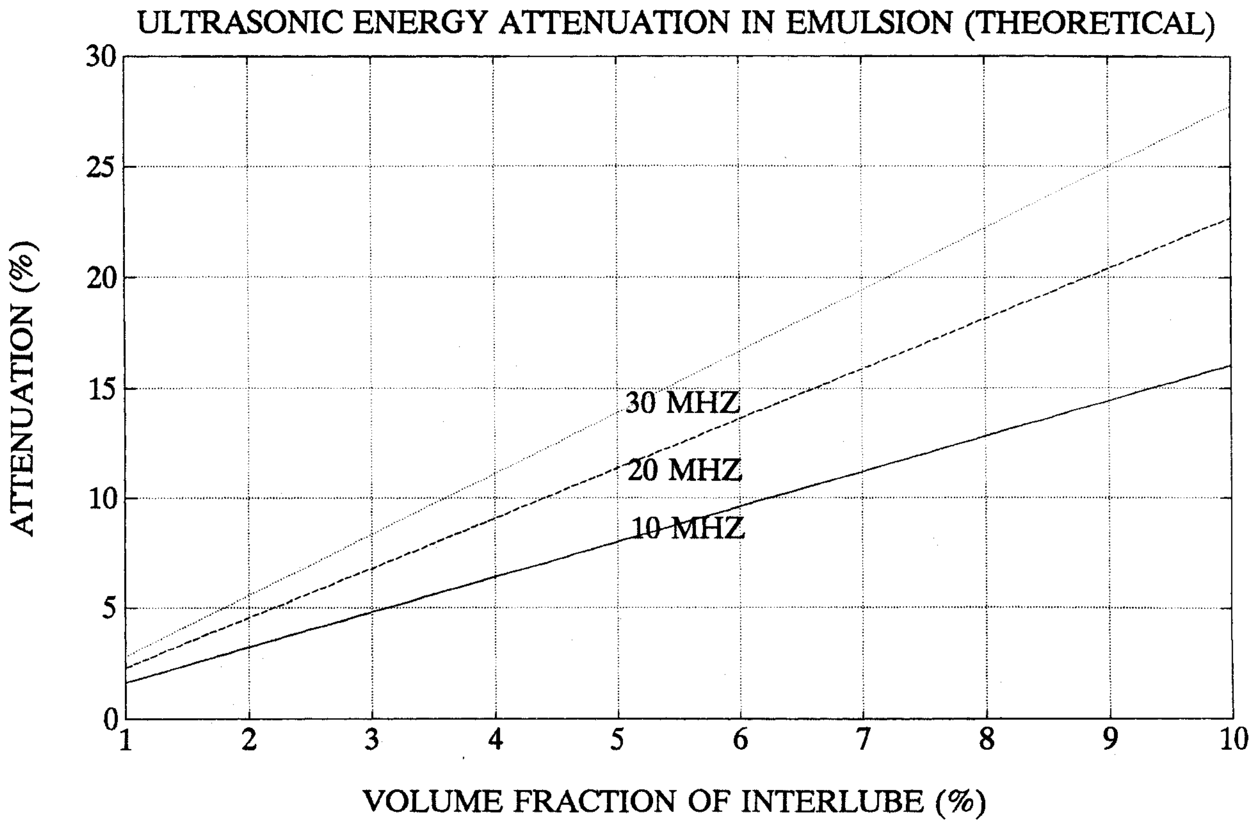

ULTRASONIC ENERGY ATTENUATION IN EMULSION (THEORETICAL)
ATTENUATION (%)
30
25
20
15
10
5
0
1
2
3
4
5
6
7
8
9
10
30 MHZ
20 MHZ
10 MHZ
VOLUME FRACTION OF INTERLUBE (%)

Fig. 7-3

7-2-4 Ultrasonic Scattering at Interface Surface:

The scattering rate increases when the interface surface becomes rougher. The ground surfaces manufactured by precision grinder (CNC-machines) are assumed to have a sinusoidal surface finish, see Eq. (4-11). The grinding specifications of the CNC machine (Milacron) and the use of Eq. (4-4) for surface finish (RMS values) enable us to study the scattering angle from the surface roughness for some different finish specimen which have the same diameter and length. Three codes are written to analyze the scattering in terms of: 1) for fixed cutting depth or grit size (R) and variable feedrate (d), 2) for fixed feedrate but variable grit size (cutting depth), and 3) different grid size or radius and feedrate are variable.

The normal incident waves scatter from the part interface surface with angles (θ_s) after impinging the interface surface in x-z plane, Fig. (7-4). A relation indicating the variation of θ_s can be derived from triangle OBC.

It is clear that rougher surface or higher RMS value which is proportional to the square of the feedrate and inverse propotional to the cutting radius (grit size) or cutting depth causes wider θ_s and also higher slope value, Figs(7-5 to 7-7).

Parameters	RMS
$\sigma = 0.037d^2/R$	$a/\sqrt{2}$
m (slope)	$\sqrt{(2\pi fa)}$
λ (wavelength)	1/f

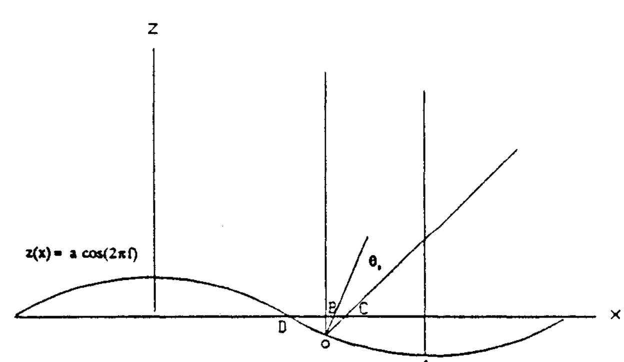

Fig. (7-4)

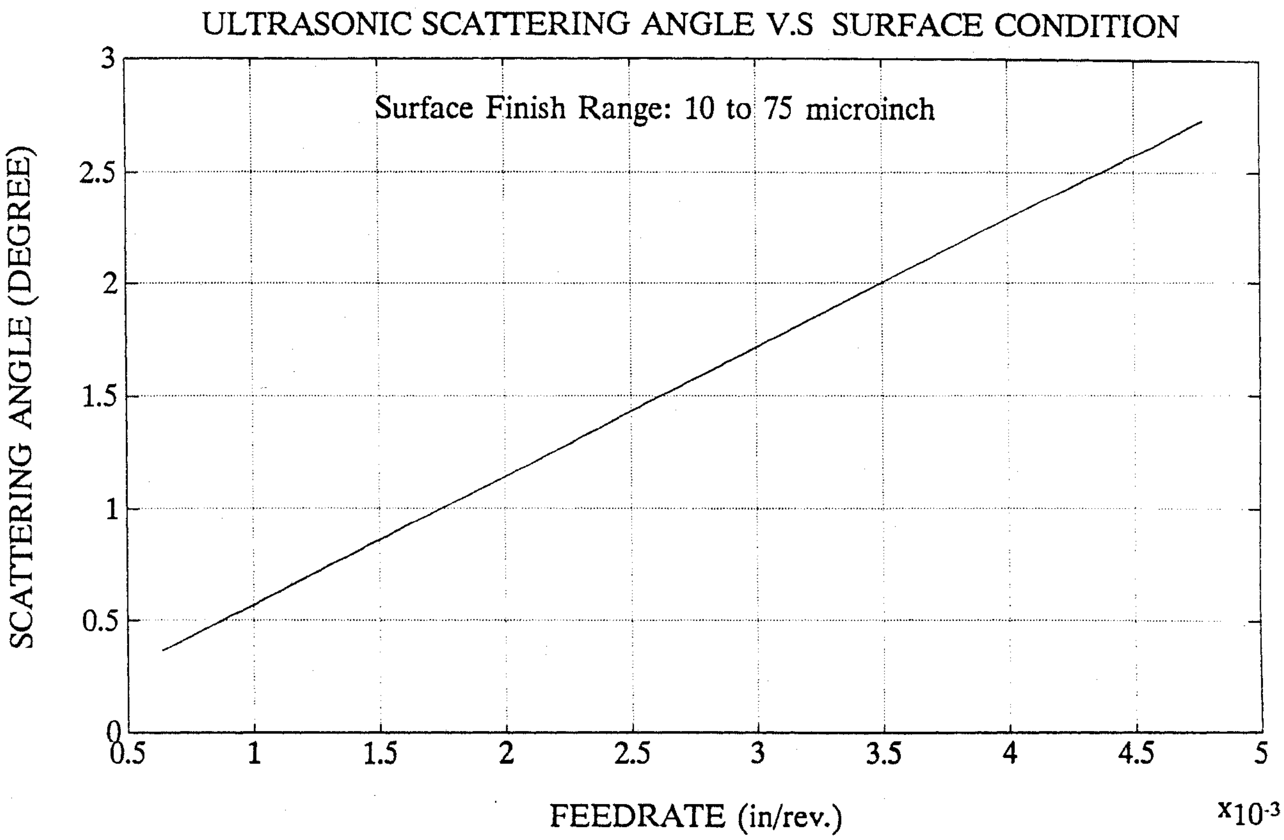
ULTRASONIC SCATTERING ANGLE V.S SURFACE CONDITION
Surface Finish Range: 10 to 75 microinch
SCATTERING ANGLE (DEGREE)
0
0.5
1
1.5
2
2.5
3
0.5
1
1.5
2
2.5
3
3.5
4
4.5
5
FEEDRATE (in/rev.)
x10-3

Fig. 7-5

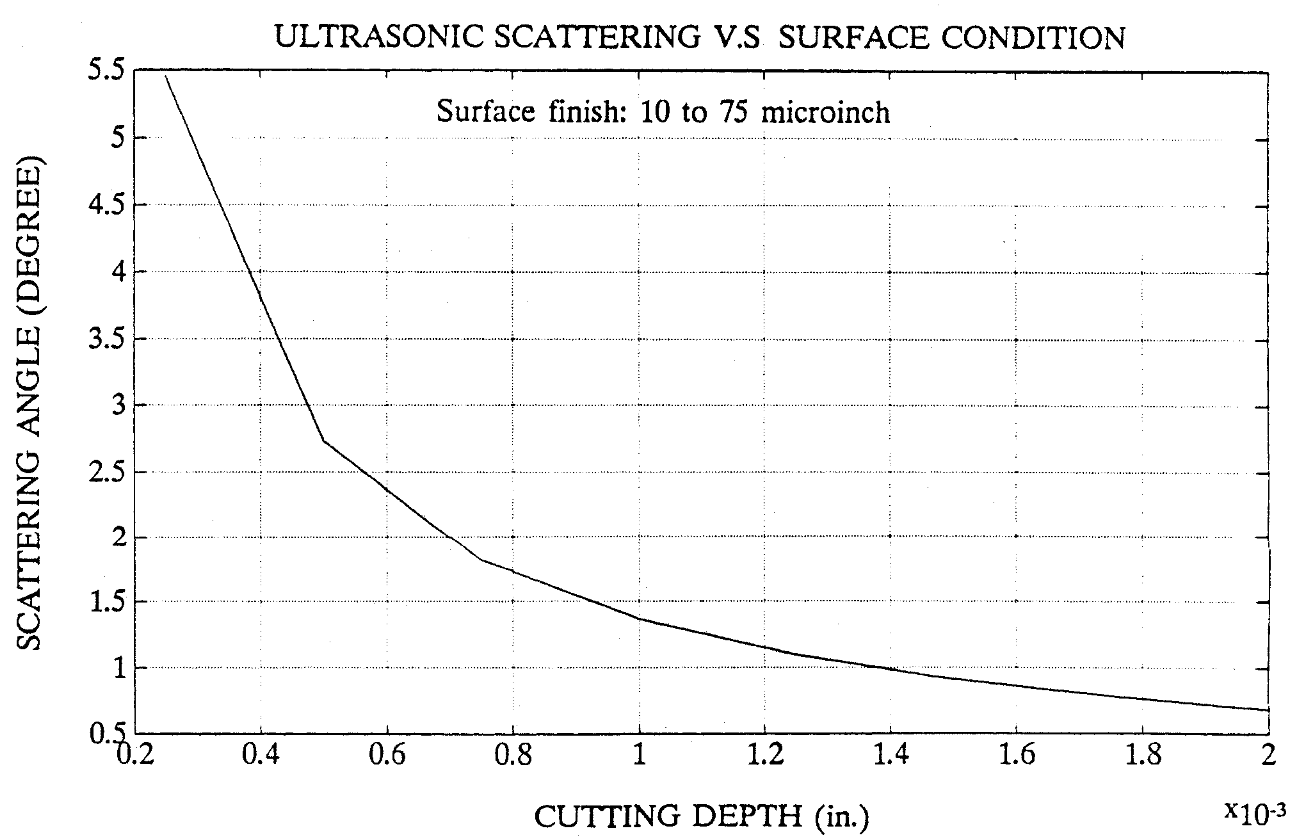
ULTRASONIC SCATTERING V.S SURFACE CONDITION
Surface finish: 10 to 75 microinch
SCATTERING ANGLE (DEGREE)
0.5
1
1.5
2
2.5
3
3.5
4
4.5
5
5.5
0.2
0.4
0.6
0.8
1
1.2
1.4
1.6
1.8
2
CUTTING DEPTH (in.)
x10-3

Fig. 7-6

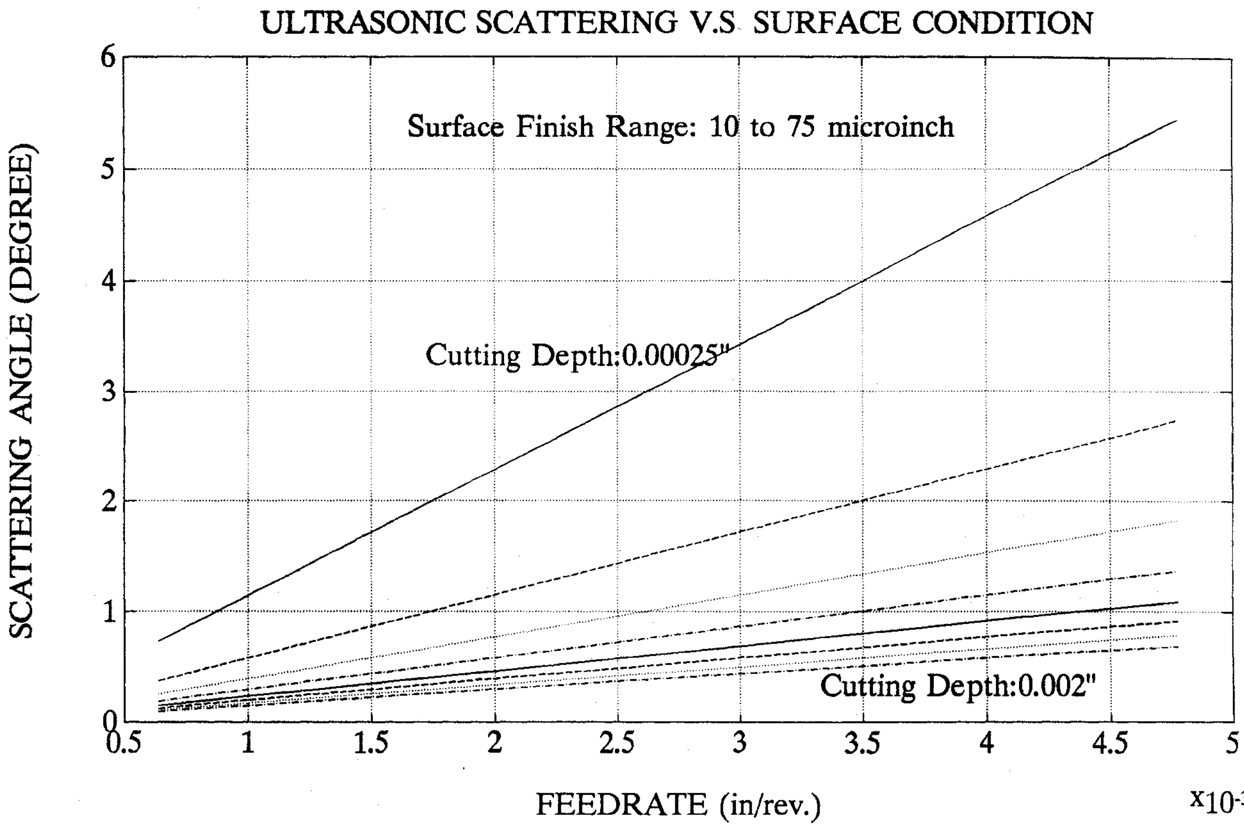

ULTRASONIC SCATTERING V.S SURFACE CONDITION
Surface Finish Range: 10 to 75 microinch
Cutting Depth:0.00025"
Cutting Depth:0.002"
SCATTERING ANGLE (DEGREE)
FEEDRATE (in/rev.)
x10-3
0
1
2
3
4
5
6
0.5
1
1.5
2
2.5
3
3.5
4
4.5
5

Fig. 7-7

The results of some related researches performed by Olsen and Karmakar are shown in Fig. (7-8) as references.

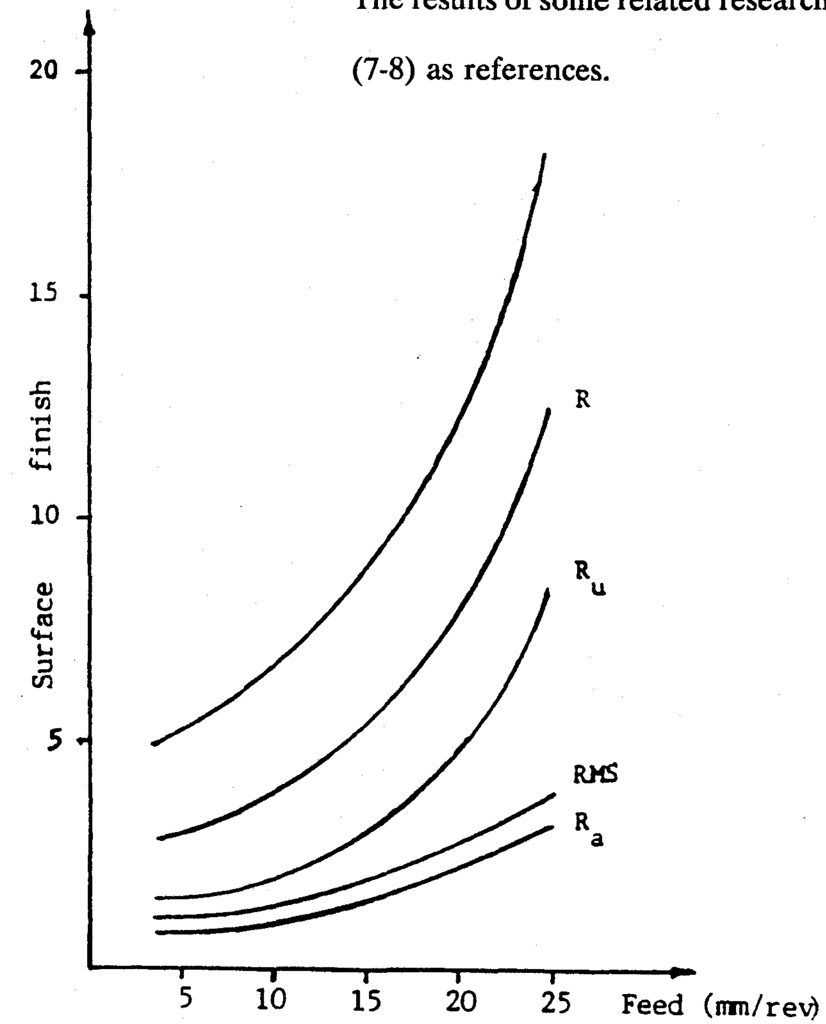

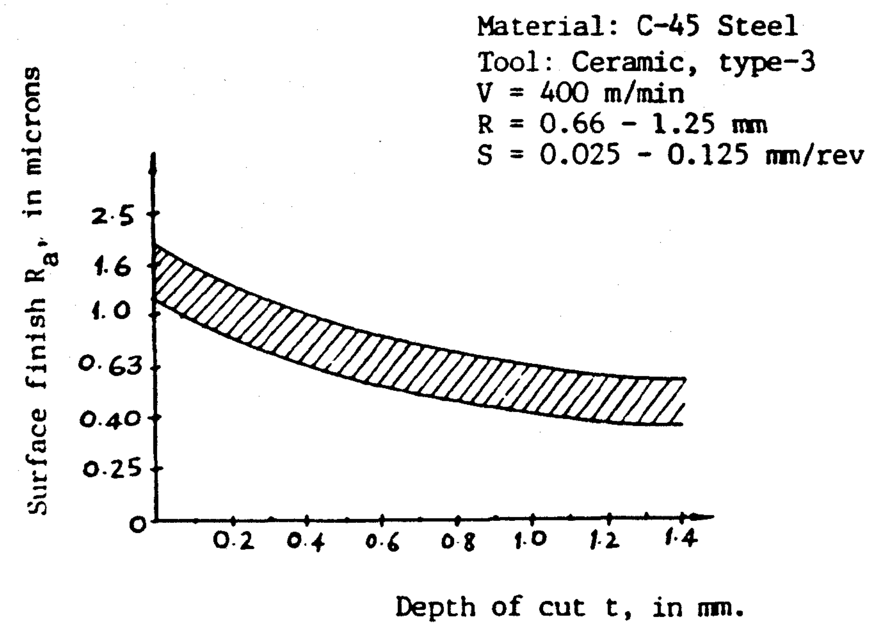

(adapted from Karmakar 1970 [43])

(adapted from Olsen 1964 [13])

Fig. (7-8)

The variation of θ_s can be shown by following equations

$$\tan\theta_s = \frac{\Delta(x)}{z(x)} \qquad (7\text{-}1)$$

$$\tan^{-1}\theta_s \frac{\Delta(x)}{a\cos(2\pi f x)}$$

The values of Δ(x), a and f are defined in related codes,

Appendix-C, see Codes 4, 5 and 6.

It is assumed that all the ultrasonic waves are plane waves which are propagated in normal direction locally parallel to z-axis. A quarter of a grating wavelength can be chosen for the scattering analysis. If the first normal plane wave impinges on the sinusoidal interface surface at point A, and the second one at point O, then the scattered wave at point A (peak point of grating wave) is reflected back on the same direction line (perpendicular to tangent at point A) and the second one is scattered in a direction line which makes an angle, θ_s, with the normal direction. Δ(x) value increases if the impinging point, O, moves towards point D, along a quarter of grating wavelength.

Code Description: The surface quality is changed in terms of either cutting radius (grit size) or feedrate, Eq.(4-4)

$$\sigma = \text{roughness(RMS)} = 0.037\ d^2/R$$

The feedrate values are changed for surface finish ranging from 4 to 75 μin. (see Code 4 in Appendix-C). In the first two investigations, the code predicts variation of θ_s for a fixed cutting radius (0.0015" and .0002") and nine various feedrates(see Code 4 and 5, Appendix-C). In the other surveys both feedrate and cutting radius are made variable. The variation of these two parameter are shown in Code-6 of Appendix-C.

Fig. (7-5) shows that the scattering angle expands as feedrate increases. It means that the rate of scattering angle promotion is directly proportional to the roughness increase.

Results Analysis: The feedrate is a very powerful parameter in the grinding process control because the surface finish process is controlled by square of this parameter. Therefore, this parameter is more significant than the cutting radius (grit radius). Comparing Figs. (7-5) and (7-6) shows that the quality control of surface finish by using this parameter as independent variable is better than when cutting radius is chosen as independent variable.

It is noted that the wheel dressing can also control the grinding process for a required range of finishing. The wheel condition (grit size, grit distribution and sharpness or dullness) is investigated by the power wheel signal communication.

Therefore, the scattering analysis for ultrasonic intensity measurement can be scanned from the normal incident wave at point A to O along a quarter wavelength of each specimen surface finish and by $\Delta(x)=BC$ increments. This analysis gives us useful information to generate a procedure which can be applied in the other parts of this problem. The concluded data from Figs. (7-5) to (7-6), also confirm the results obtained from Fourier-Bessel series expansion, Eq.(5-13), in Chapter 5, where it was shown that the principal reflection dominates to the other modes. Therefore, this reflected mode in almost normal direction can be conducted through the waveguide assembly to the transducer face, without any scattering losses.

The conclusions are true provided that, 1) wheel is fresh dressed or at least sharp enough and grits are distributed on the wheel surface homogeneously, 2) the surface finish process is done consistent (grinder protected from undesired environmental signals), 3) surface discontinuity has sinusoidal configuration and 4) precision surface finish, range (up to 75 μin).

It should be noted that the surface topography is not within the scope of this research. Hence, a hypothetical sinusoidal surface roughness is analyzed here only for the estimation purposes of wave scattering.

7-2-5 Ultrasonic Energy Attenuation for Distances Variation and Different Transducers:

The ultrasonic intensity analyzed for different normal distances between waveguide assembly and interface surface are recommended by the grinding machine manufacturers. The intensity is also studied in terms of different transducer frequencies.

The case is analyzed by Code-7 which is shown in Appendix-C

Code Description: The propagated ultrasonic wave intensity is attenuated during proceeding toward the interface surface in time (transient wave). Therefore, a fraction of the energy attenuation is due to an increasing distance. The code is written utilizing the ultrasonic wave propagation model, the first expression of Eq. (6-6) in Chapter 6 and for three recommended distances 0.100", 0.125" and 0.25 " (from transducer face to part surface). The program also investigates the phenomenon for three transducers 10 MHZ, 20 MHZ and 30 MHZ. The maximum electrical energy per pulse delivered to the transducer (piezoelectric crystal) and parallel damping resistance (4Ω) is $94*10^{-6}$ Joules. A portion of this energy is transformed to mechanical energy (sonic wave) which is used in this experimental works.

Results Analysis: The ultrasonic intensity decreases as the wave propagates towards the grinding part interface surface (distances increases). The output intensity of 10 MHZ transducer is about 1.2 watt/m^2 which is dissipated down to the interface surface (part at position s_1 of Chapter 6). The distance attenuation is equal to 0.2616 watt/m^2, α_d, Fig. (7-9). The energy attenuation for 10, 20 and 30 MHZ transducers are analyzed and the resulting data presented in Fig. (7-10). The results shows that 10 MHZ transducer has much better performance and signal quality. These two codes are called Codes-7 and 8 in Appendix-C.

7-2-6 The Ultrasonic Intensity Feedback to the Transducer:

The problem analysis for this part is very complicated due to the interface surface geometry (round shape), therefore, a fraction of incident wave can easily follow the coolant flow path which slides down around the part surface to the coolant tank. Estimation of this portion of energy attenuation is not possible except by using the energy continuity at interface. The scattering results, section 7-2-3 show that the reflection angle cannot be more than 5 degrees for surface finish range of the 10 to 75 μin. In the worst case ($\theta_s = 5^0$), the attenuation can be estimated by using Fig. (7-11) and a simple geometric relation

$$\alpha_g = (2A_1)/A = (0.00036\ in^2)/(0.1919\ in^2)100 = 0.19\%$$

where A_1 is small area in the bottom of Fig.(7-11),left side, and A is the diffuser longitudinal cross section area minus the longitudinal cross section of a hypothetical tube section in the center of the diffuser, For distance z=1.35 in or 34.29 mm (transducer face to workpiece surface).

Fig. (7-12) shows that the intensity drops 0.1128 or 0.1450-0.0322 watt/m^2 in reflection from interface to almost the transducer (α_r). The energy difference at the interface surface, Figs. (7-9 and 7-12) is equal 0.1166 (0.2616-0.1450) watt/m^2 which is mostly defined as the energy dissipation due to sliding motion of the wave around the part surface or α_s. This type of attenuation is called sliding attenuation in the research. It should

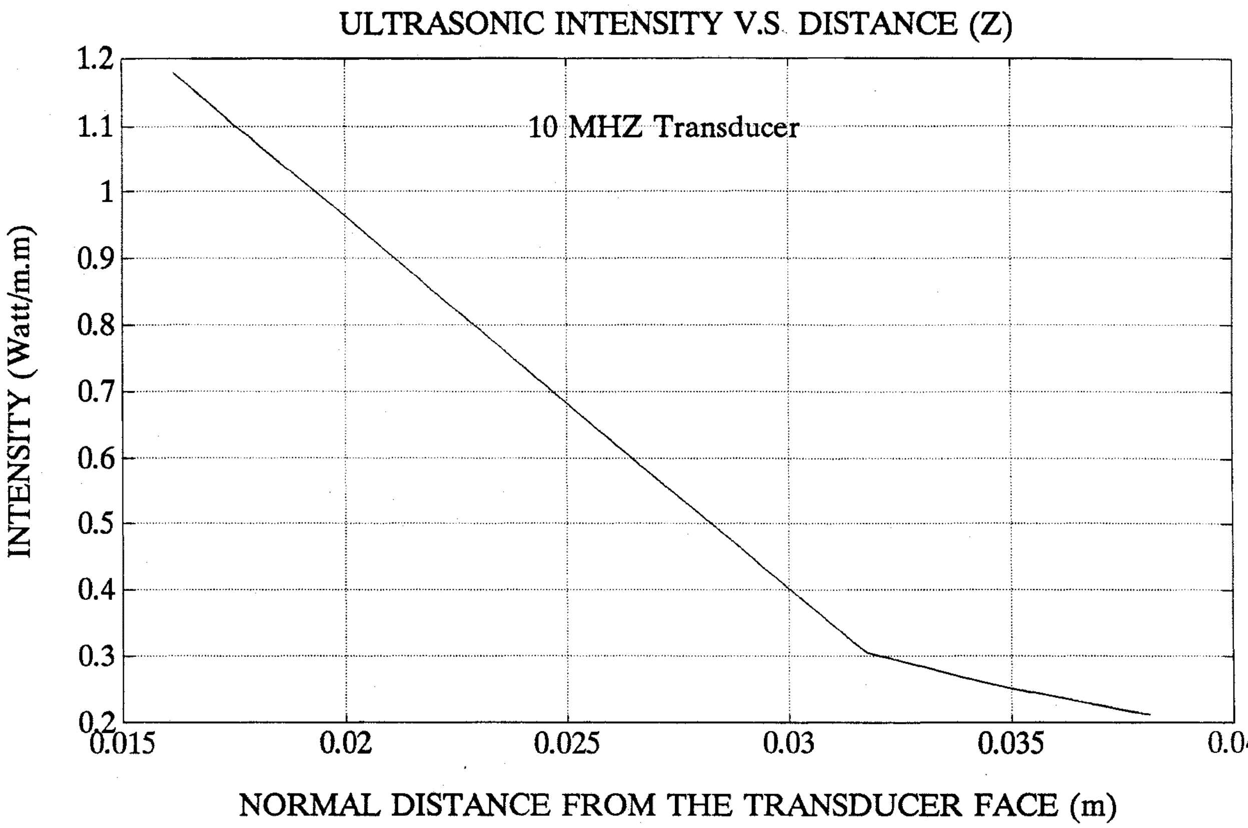
ULTRASONIC INTENSITY V.S. DISTANCE (Z)
10 MHZ Transducer
INTENSITY (Watt/m.m)
1.2
1.1
1
0.9
0.8
0.7
0.6
0.5
0.4
0.3
0.2
0.015
0.02
0.025
0.03
0.035
0.04
NORMAL DISTANCE FROM THE TRANSDUCER FACE (m)

FIG. 7-9

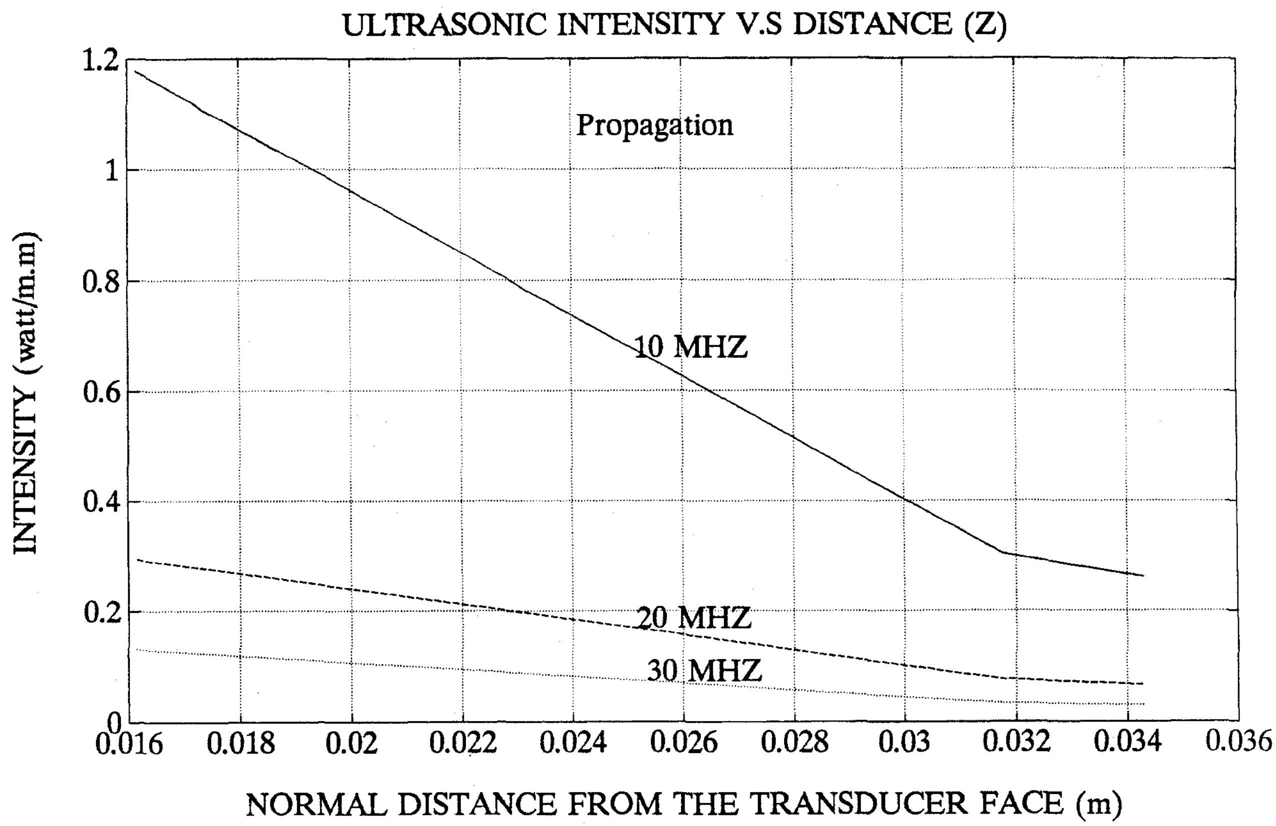
ULTRASONIC INTENSITY V.S DISTANCE (Z)
Propagation
10 MHZ
20 MHZ
30 MHZ
INTENSITY (watt/m.m)
1.2
1
0.8
0.6
0.4
0.2
0
0.016
0.018
0.02
0.022
0.024
0.026
0.028
0.03
0.032
0.034
0.036
NORMAL DISTANCE FROM THE TRANSDUCER FACE (m)

FIG-7-10

WAVEGUIDE ASSEMBLY OPTIMIZATION

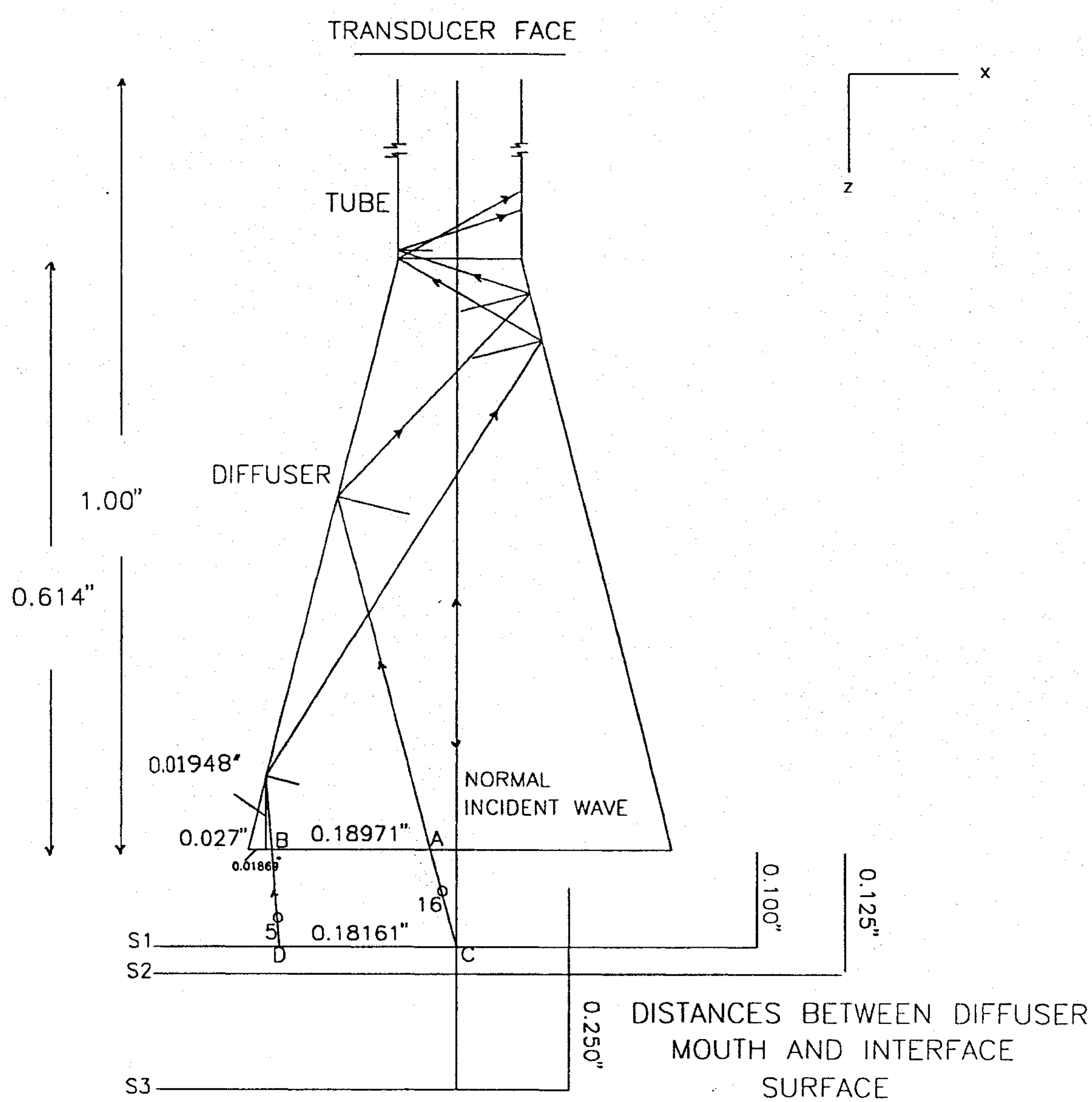

Fig. 7-11

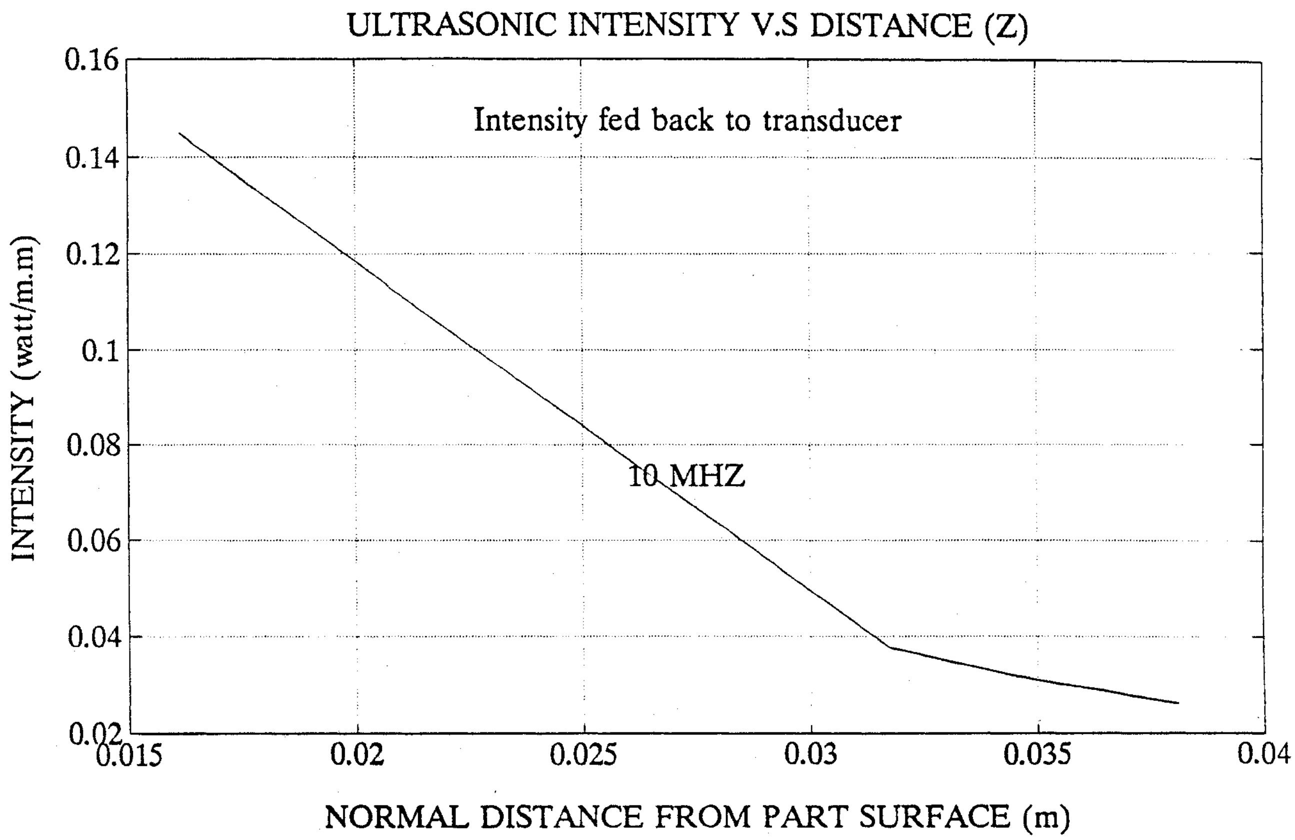

Fig. 7-12

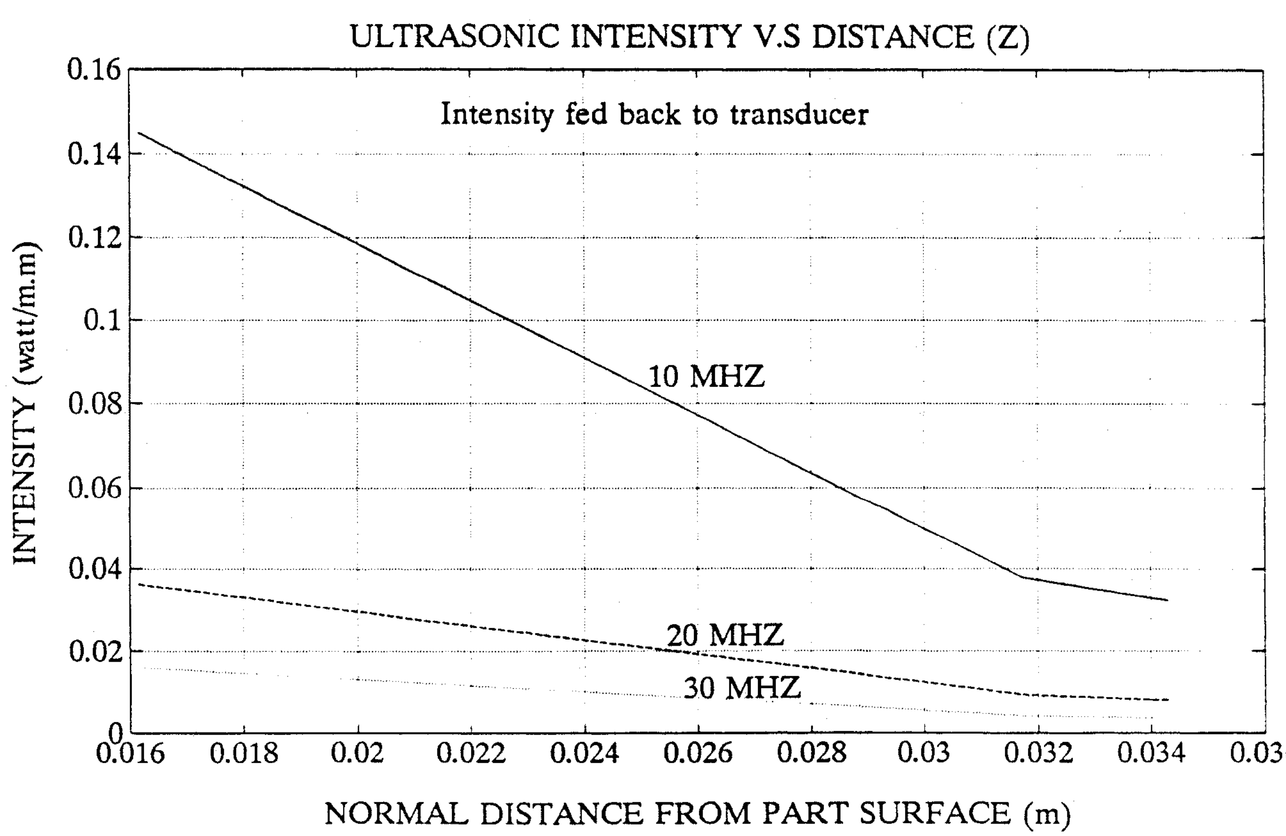

Fig. 7-13

be noted that the α_s value is inversely proportional to the cylindrical part diameter.

The total energy attenuation in ultrasonic wave transmission, for a round trip (2(1.35)in) is equal 1.1466 (1.1788 -.0322) watt/m^2. This total attenuation in percentage rate which is included the attenuation due to 3% to 5% volume oil fraction (α_t) is

$$\alpha=\alpha_t+\alpha_d+\alpha_g+\alpha_r+\alpha_s=6.415\%+23.420\%+0.19\%+11.280\%+11.387\%=53.186\%$$

Therefore, the energy balance for 10 MHZ transducer can be written as the rest of ultrasonic energy available which is equal to product (0.468141)(0.1788)=0.518 watt/m^2. A portion of this amount of energy fed back to the transducer (0.1450 watt/m^2) and rest of it which is almost 0.373 watt/m^2 is attenuated due to kinetic to potential energy conversion loss, heat conduction, molecular exchange of energy and viscous losses [1]. The last part of attenuation is named as attenuation due to ultrasonic energy absorption in the research.

This code is written based upon the negligible transmission waves through the grinding part. Therefore, the reflection wave energy is determined by coefficient of reflection at interface surface. The reflection coefficient (R) was calculated equal to 0.936 in Chapter 5.

7-3 CONCLUSIONS:

The analysis of the results of ultrasonic energy attenuation shows that some parameters such as distance, oil volume fraction, absorption, scattering angle, waveguide geometry and its orientation, interface geometry (cylindrical surface) and surface condition participate in ultrasonic energy attenuation. Total of the uncontrolled energy dissipation parameters (sliding and absorption) values is a significant intensity attenuation. The sliding attenuation value increases when the cylindrical part is thinner. Therefore, they almost control the energy attenuation in wave transmission process.

The concluded results show that the designed waveguide assembly in this research was an efficient and satisfactory device. The advantages of this diffuser component are: 1) better wave transmission property, 2) minimum lateral reflection (flared slowly), 3)wave capturing capability. Note that these advantages are not generalized for any waveguide assembly with the same configuration but various dimension and sizes.

REFERENCES:

1- Kinsler, " Fundamental of Acoustics " 3rd Ed., Wiley, 1976.

2- Ensminger, " Ultrasonics " 2nd Ed., Marcel Dekker, Inc. 1988.

CHAPTER 8

THE EXPERIMENTAL RESULTS ANALYSIS:

8-1 INTRODUCTION:

Surface finish measurement during the precision grinding process addresses a need for high-precision grinding technique in the manufacturing of very sophisticated parts. Realization and detection of the surface finish quality during the grinding process is dependent upon the development and integration of the grinding process feedback control signals. The signals are generated from five sensors: accelerometer for sensing vibration, acoustic emission sensor, grinding wheel power sensor, normal force, and ultrasonic sensor for surface finish measurement. The first four signals protect a grinding process from undesired signals. Thus, utilizing a grinding machine with integration of these five signals provides an accurate condition for surface finish measurement during the process.

The purpose of this experimental research was to select a commercially available non-contact surface finish measurement device and develop technology for this type of measurement during the grinding process. The device could be particularly used to measure the surface finish of cylindrical workpiece during manufacture, a task that cannot be performed with existing techniques. The potential benefit of this product is increased reliability by meeting the surface finish requirements on machined parts. A master program plan was prepared, included; extensive tests, data analysis, measurement improvement and finally the needed technology was developed and performed.

8-2 SURVEY/SELECT A COMMERCIAL DEVICE:

Several commercially available devices based upon laser, ultrasonic and fiber optics were investigated in the research work. All the devices except ultrasonic device need dry surfaces for proper measurement. Thus, they are not appropriate approaches for surface finish measurement during the grinding process. The ultrasonic device could be used with the machine coolant as a couplant medium for ultrasonic wave propagation.

Since the ultrasonic device has more potential for in-process use on a grinder, it was selected for continuation of the research work. An in-depth study was conducted to understand the applications of ultrasonics in this research work.

8-3 TEST PROTOTYPE:

The prototype, Fig. (8-1), was designed to perform the planned tests on the grinding machines. The squirter assembly was also capable of use for flat surface finish measurement. The test plan (prototype) was approved by National Institute of standards technology (NIST) with some comments (sept. 26, 1988). All of their recommendations were incorporated in the test plan. The main components of this design are transducer and waveguide assembly (squirter, diffuser or nozzles). The system consists of a transducer which works as both ultrasonic wave emitter and receiver. Three transducer frequencies of 10, 20 and 30 MHZ were recommended by NIST. An analyzer (pulser, receiver) and a 100 MHZ bandwidth digital oscilloscope are used for surface finish analysis.

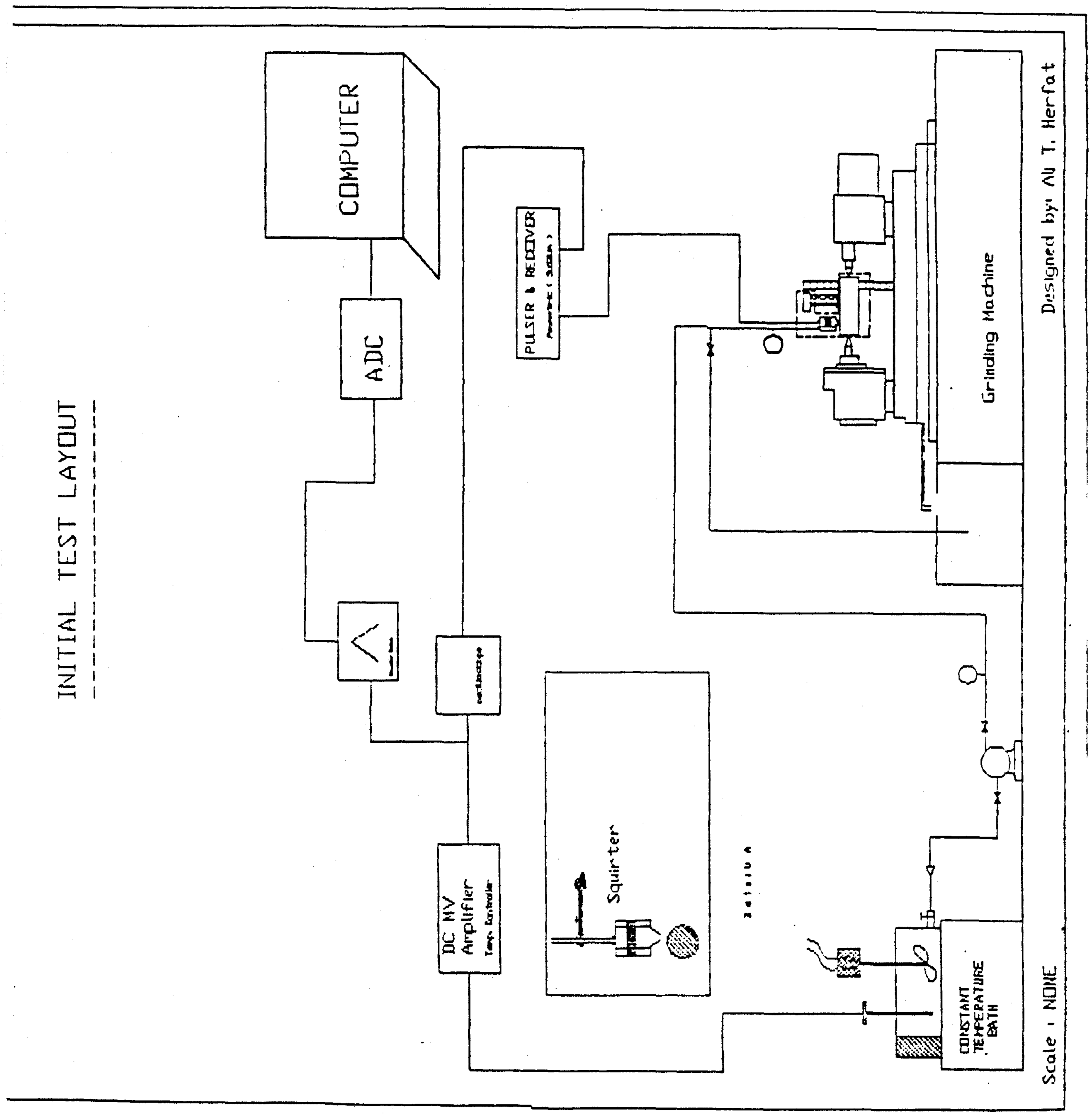

INITIAL TEST LAYOUT
COMPUTER
ADC
PULSER & RECEIVER
DC MV
Amplifier
Squirter
Grinding Machine
CONSTANT
TEMPERATURE
BATH
Scale : NONE
Designed by: Ali T. Herfat

Fig, 8-1

8-4 PRELIMINARY TESTS:

The purpose of this task was to conduct preliminary tests and develop concepts of design. The measurement system should have capability, reliability and repeatability of the produced signals by the transducers.

The tests were completed on a bench with a control temperature container. Flat test workpieces and water as ultrasonic wave couplant were used in the preliminary tests. Through the preliminary tests, all of the variables were varied one at a time, and their specific effects on the surface roughness measurement were recorded. The transducer (10, 20 or 30 MHZ) was placed in its position inside the squirter, Fig. (8-2).

The instrumentation settings and test part specifications used in the performance of the research tests either for flat part or cylindrical are presented in Appendix-B.

Only the flat plate test specimens were used in the preliminary tests for two purposes: 1) the results of some similar tests performed in the past were available. Thus, we could compare the acquired results of the preliminary texts with them. Comparison of the results proved a sufficient capability and reliability of the measurement system. 2) The preliminary tests were accomplished by using tap water. It should be noted that tap water is not a proper coolant for grinder (corrosion and no lubrication characteristics). Additionally, in the former researches for flat plate surface finish measurement, water was used as a couplant for ultrasonic wave propagation. Therefore, we had to establish the same conditions for the preliminary tests.

8-4-1 Test Variables :

The variables that participated in the ultrasonic energy dissipation were studied in the preliminary tests. The test variables were as follows:

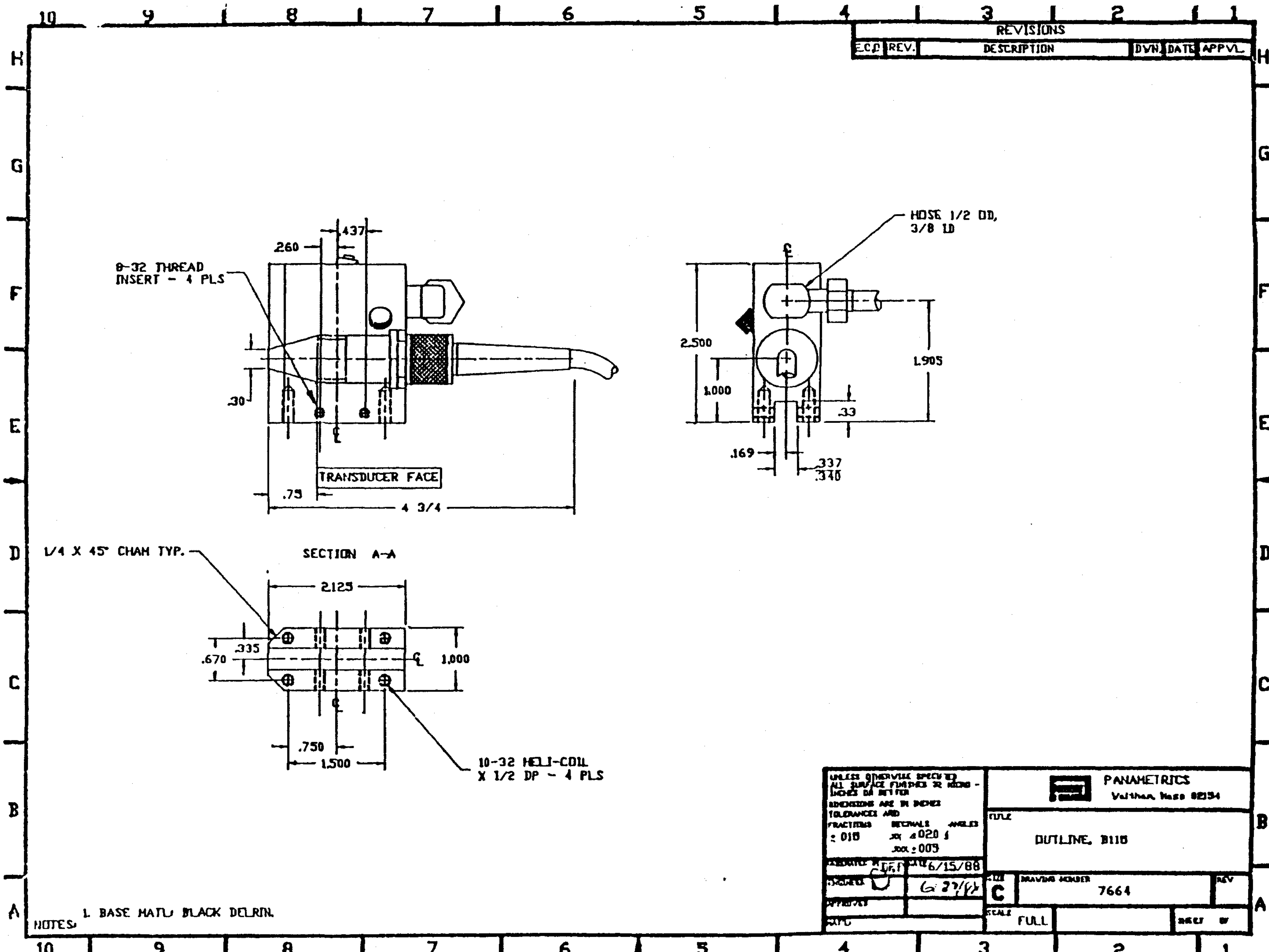

Fig. 9.2 A squirter assembly

- Transducer (ultrasonic source) frequency.
- Waveguide (squirter) outlet from the test part surface.
- Oblique angle of the waveguide with respect to normal to the test parpart surface.
- Fluid flow rate.
- Fluid temperature.

In the first set of tests, tap water was selected as ultrasonic couplant. During the tests performance, each variable was varied one at a time while the other variables were held at constant values.

8-4-2 Test Results:

For each test, the RMS value (mv) of the first echoed ultrasonic wave, representing a reflected signal from the test part's surface, was recorded. Each recorded RMS value was repeated at least in three individual tests. If there was a slight difference between them, then mean value of the RMS values was recorded for the test. All tests were conducted on flat test parts.

The obtained results for the test variables are as follows:

8-4-2-I) Distance Variable:

The tests were conducted at three specific distances. Each distance was measured from the top of the test part surface to the bottom surface of the squirter assembly. These distances were 0.25", 0.375" and 0.500".

The resulting data showed that when the distance increases, the RMS (mv) value or signal amplitude , decreases. The test results were plotted in Fig. (8-3 to 8-5) for 10 MHZ, 20 MHZ and 30 MHZ transducers, respectively. The decaying rate of RMS values is also different for the three transducers. The 10 MHZ echo amplitude is higher than those of the

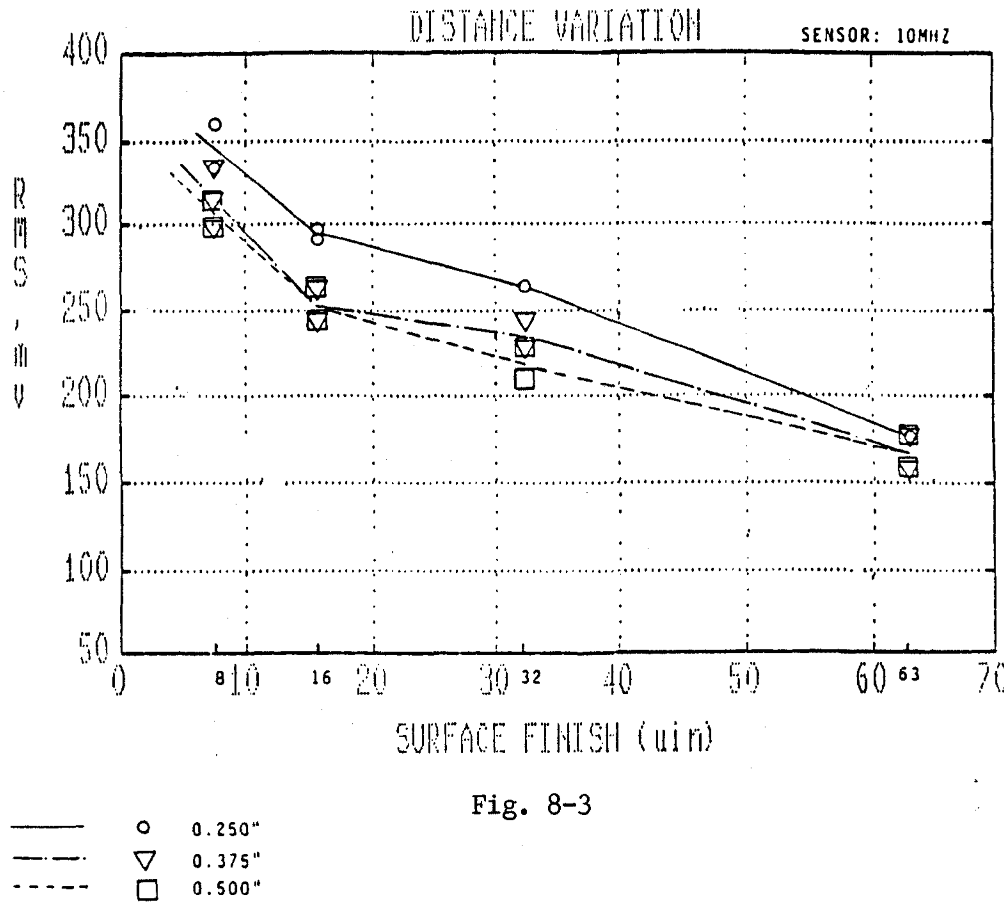
DISTANCE VARIATION
SENSOR: 10MHZ
RMS, mV
SURFACE FINISH (uin)
0.250"
0.375"
0.500"

Fig. 8-3

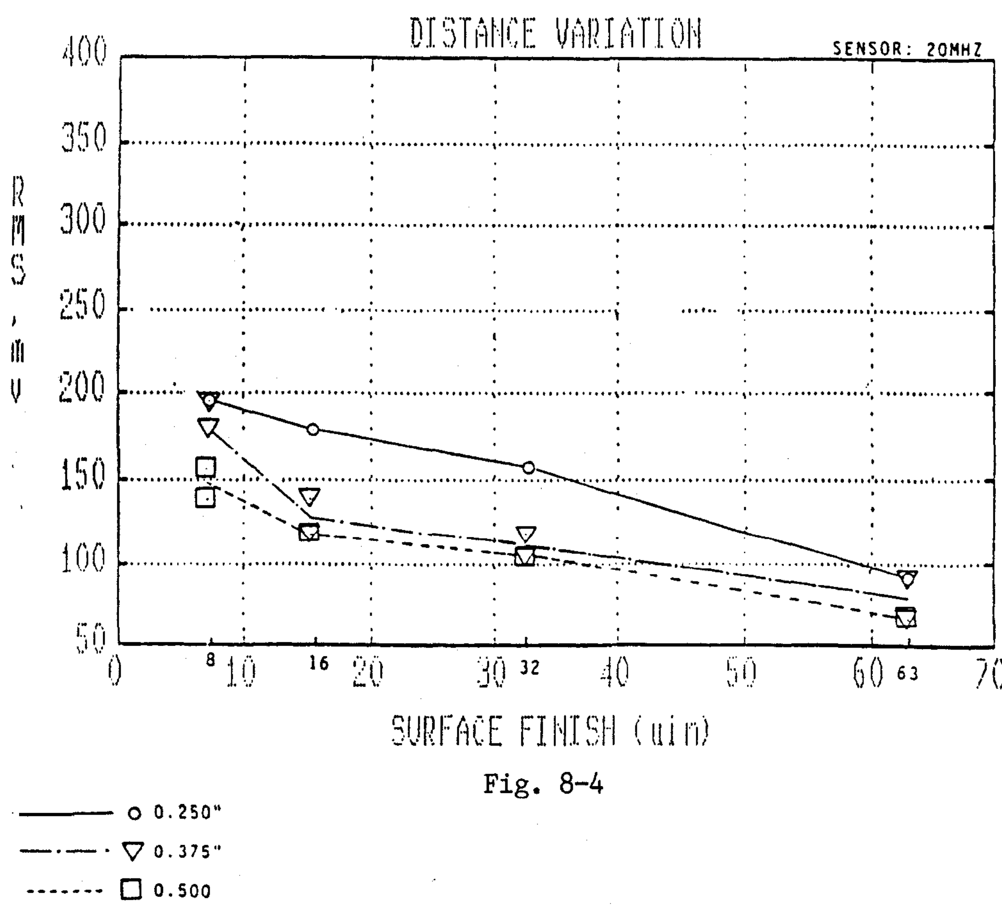
DISTANCE VARIATION
SENSOR: 20MHZ
RMS, mV
SURFACE FINISH (uin)
0.250"
0.375"
0.500

Fig. 8-4

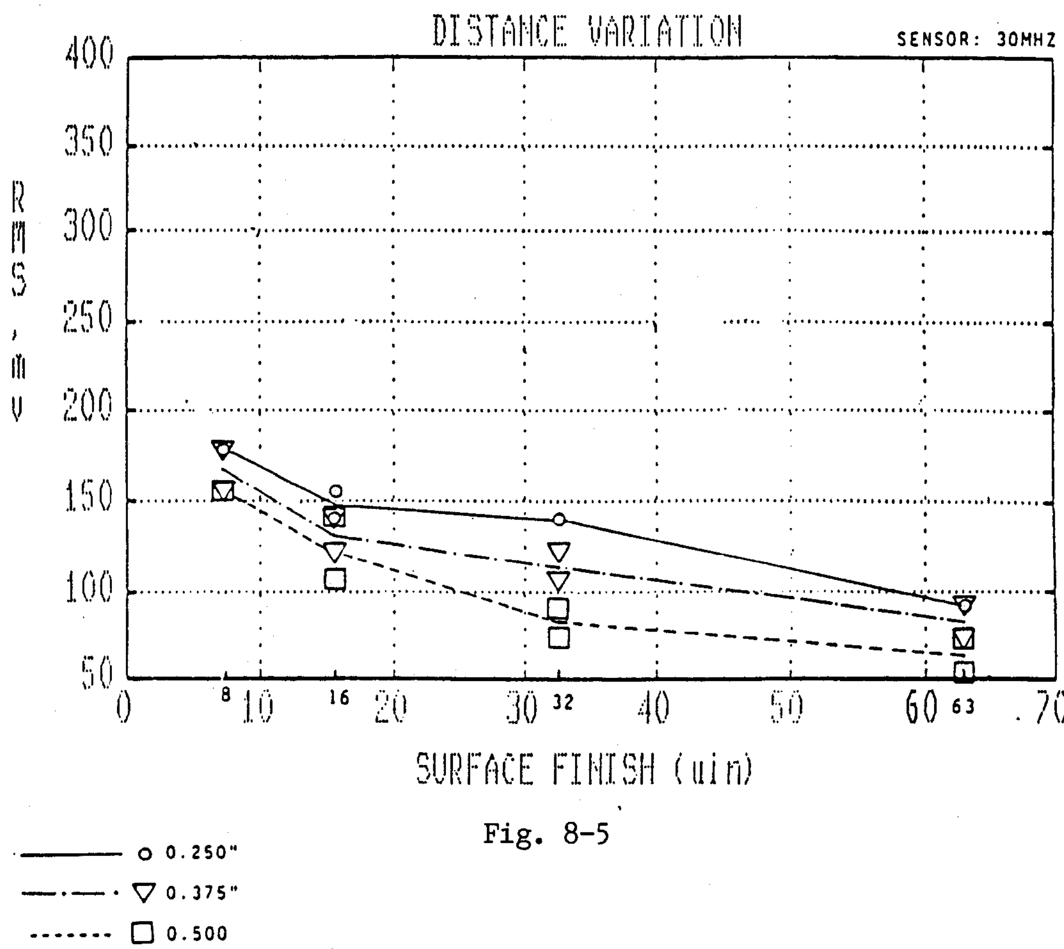
DISTANCE VARIATION
SENSOR: 30MHZ
RMS, mV
400
350
300
250
200
150
100
50
0
8
10
16
20
30
32
40
50
60
63
70
SURFACE FINISH (uin)
o 0.250"
▽ 0.375"
□ 0.500

Fig. 8-5

other two transducers (comparing the plotted results in Figs. (8-3 to 8-5)).

8-4-2-II) Temperature Variation:

The test results show no significant change in the echo signal amplitude with the water temperature variations from 65^{0}F to 90°F. The test data are plotted in Figs. (8-6 to 8-8) for 10 MHZ, 20 MHZ and 30 MHZ.

8-4-2-III) Tilt (Oblique) Angle Variation:

The tilt angle was varied from normal to the test part surface (zero angle) to 5 degrees from the normal line. The test data are plotted in Figs. (8-9 to 8-11) for 10 MHZ, 20 MHZ and 30 MHZ transducers. The test results show that a slight tilt angle greatly deteriorates the signal.

8-4-2-IV) Water Flow Rate:

The flow rate variations were 1/54 liter/sec, 1/44 liter/sec, 1/37 liter/sec, 1/32 liter/sec, and 1/29 liter/sec. The following observations were recorded:

- When the flow rate changed from 1/51 lit/sec to 1/44, it produced a sudden drop and fluctuation in the echo signal, but as the flow rate stabilized, the echo signal repeated at the original value. For the rest of flow rates, the same conditions happened but the signal amplitudes were lower than those for the first two flow rates.
- The best flow rate for most stable echo signal was obtained at the two first water flow rate.

The test results are shown in Figs. (8-12 to 8-14).

8-4-3) Conclusions:

The following conclusions were drawn from the test results analysis:

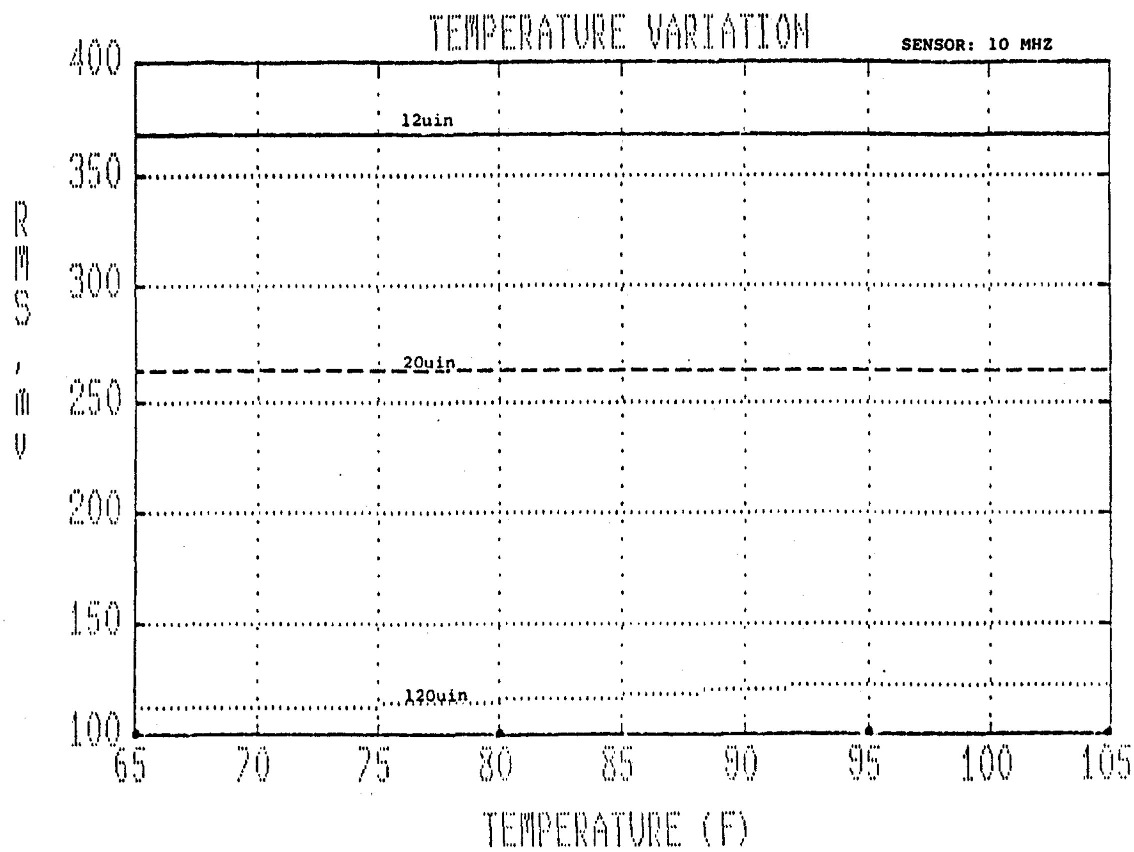

TEMPERATURE VARIATION
SENSOR: 10 MHZ
400
350
300
250
200
150
100
RMS, mV
12uin
20uin
120uin
65
70
75
80
85
90
95
100
105
TEMPERATURE (F)

Fig. 8-6

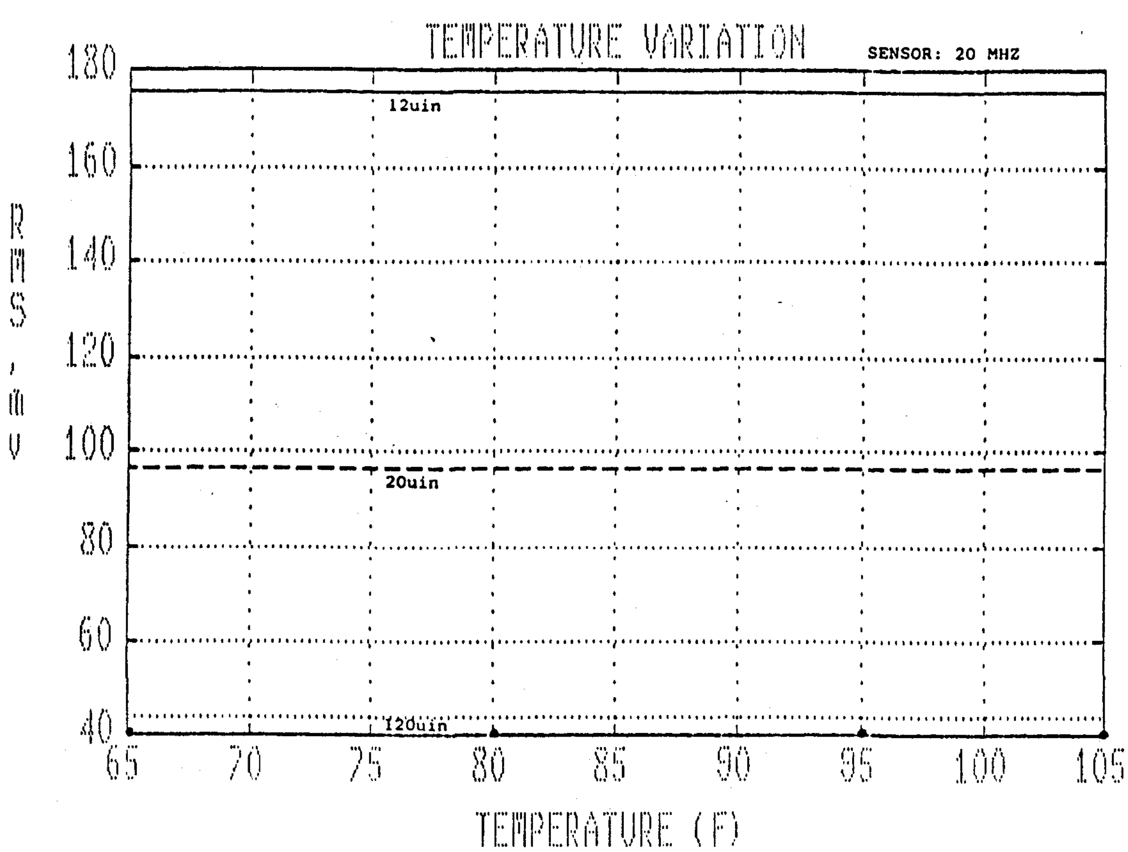

TEMPERATURE VARIATION
SENSOR: 20 MHZ
180
160
140
120
100
80
60
40
RMS, mV
12uin
20uin
120uin
65
70
75
80
85
90
95
100
105
TEMPERATURE (F)

Fig. 8-7

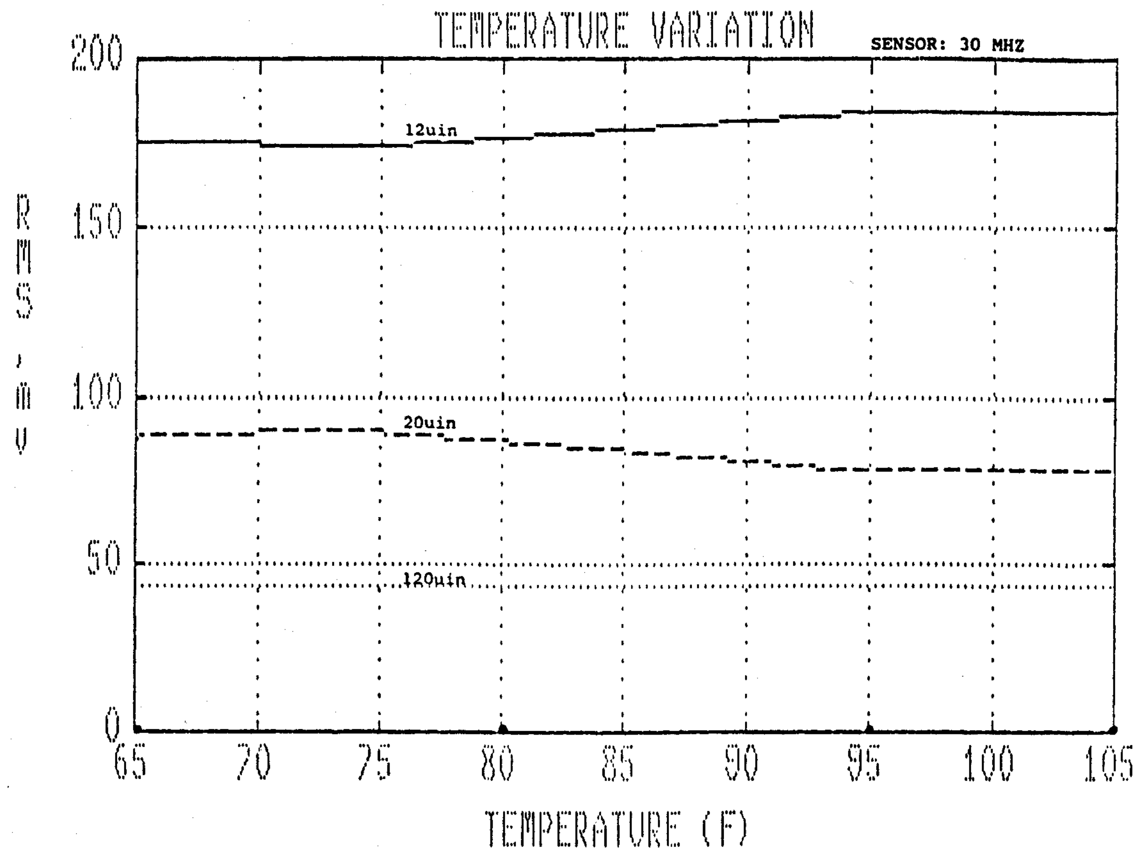

TEMPERATURE VARIATION
SENSOR: 30 MHZ
200
150
100
50
0
R M S , m V
12uin
20uin
120uin
65
70
75
80
85
90
95
100
105
TEMPERATURE (F)

Fig. 8-8

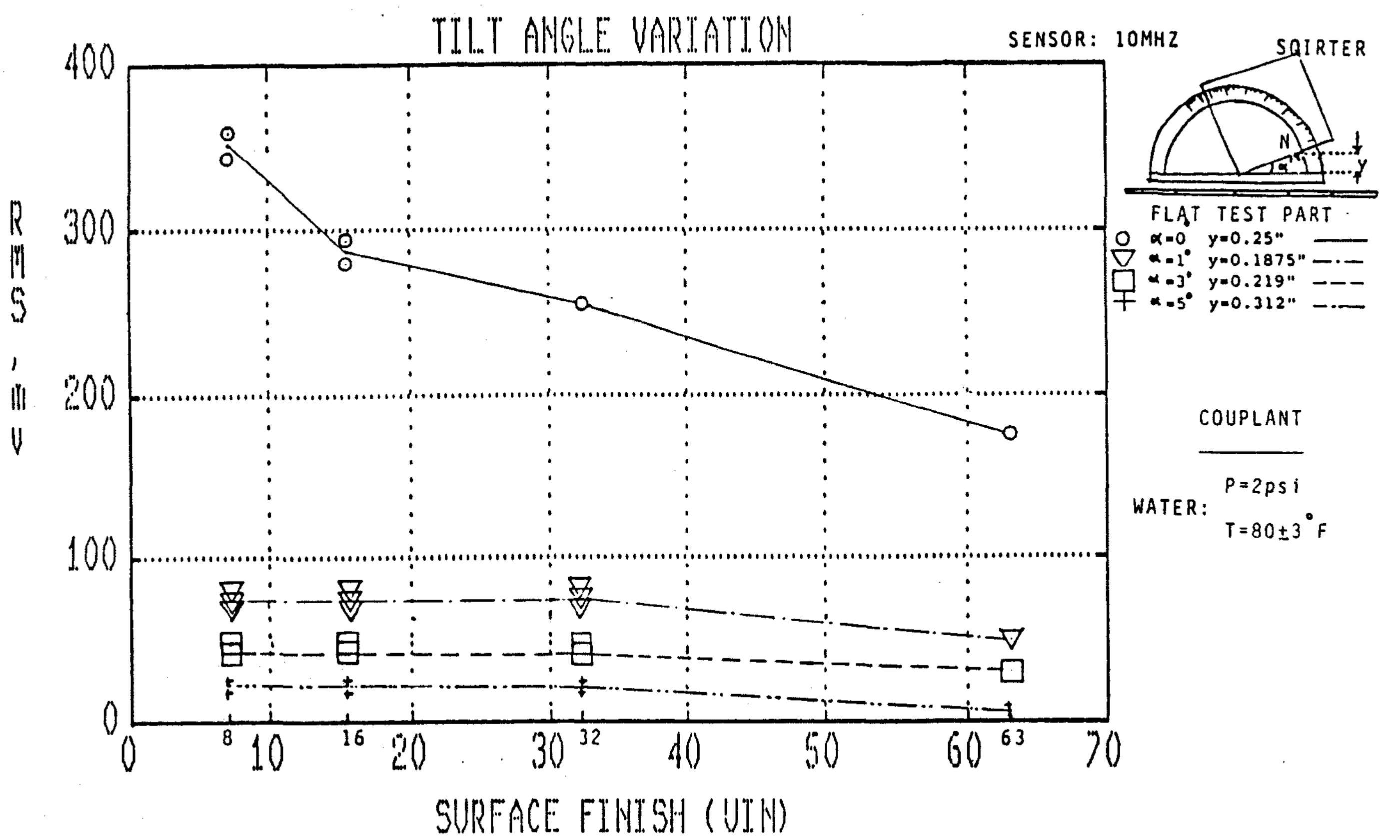

Fig. 8-9

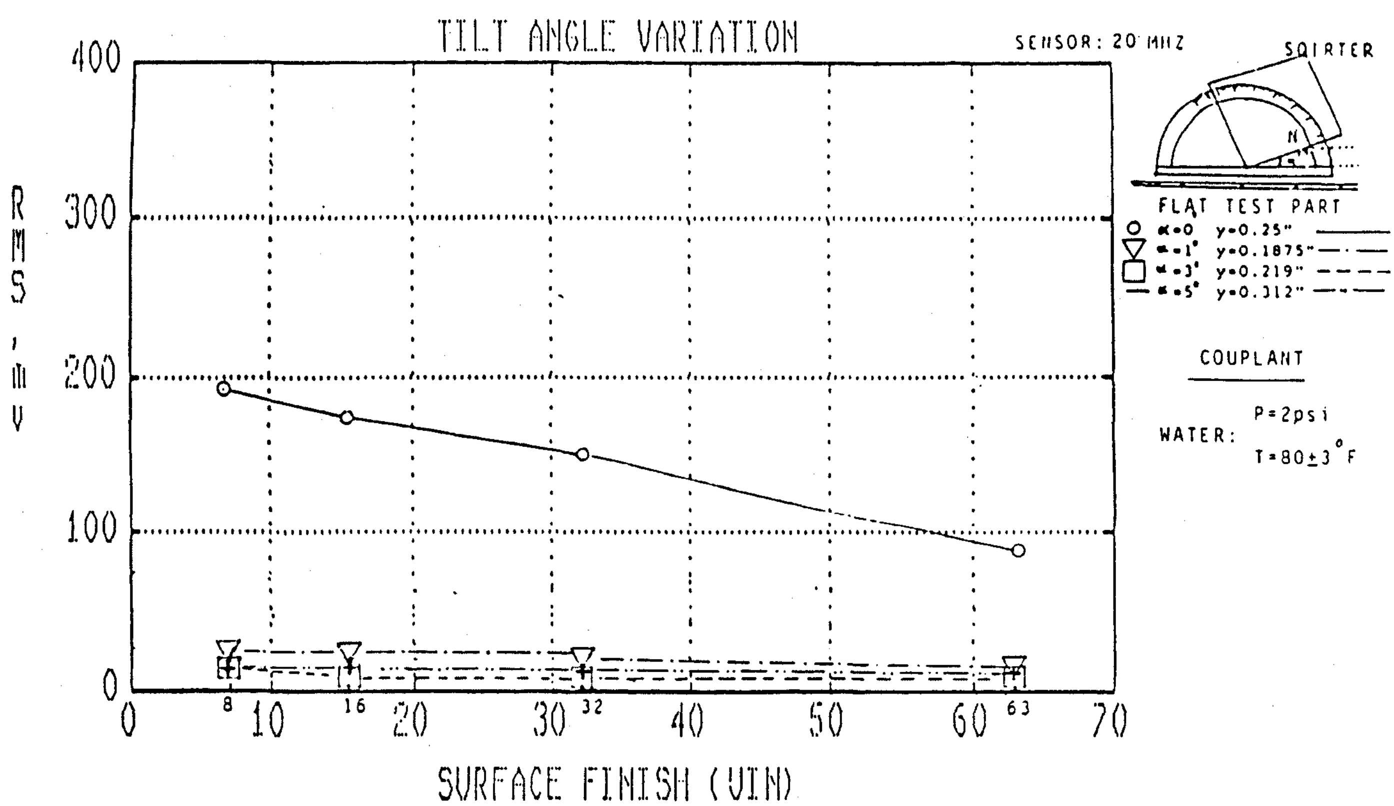

Fig. 8-10

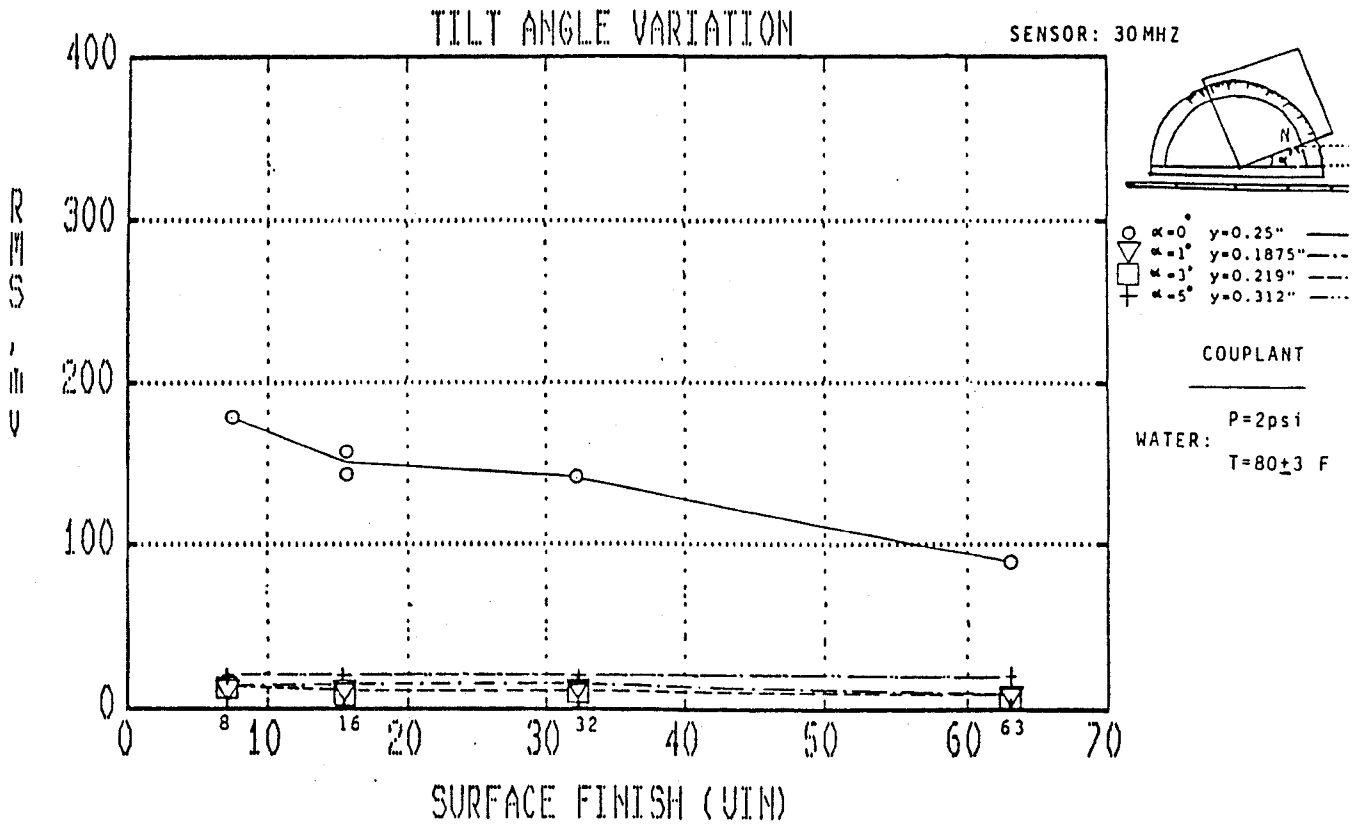

TILT ANGLE VARIATION
SENSOR: 30MHZ
RMS, mV
400
300
200
100
0
0
10
20
30
40
50
60
70
8
16
32
63
SURFACE FINISH (UIN)
α=0° y=0.25"
α=1° y=0.1875"
α=3° y=0.219"
α=5° y=0.312"
COUPLANT
WATER:
P=2psi
T=80±3 F

Fig. 8-11

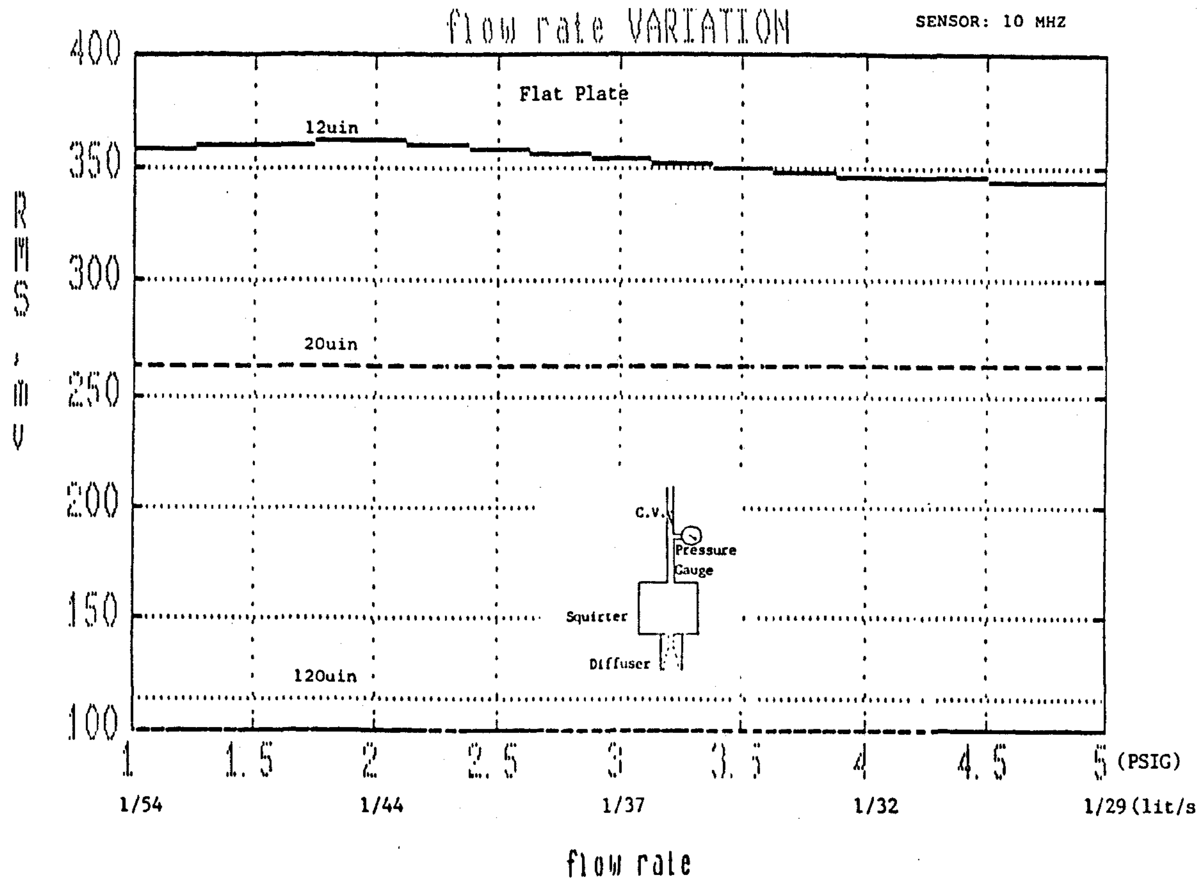

Fig. 8-12

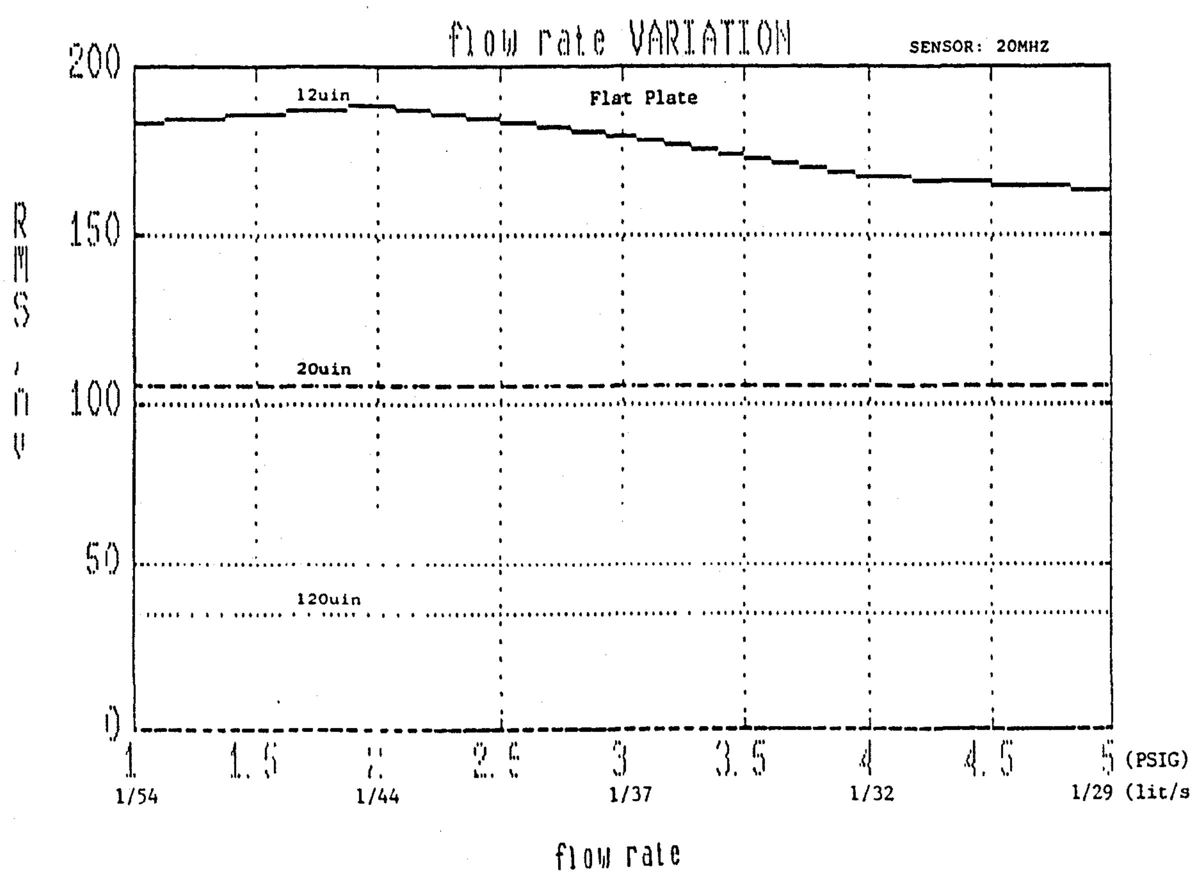

Fig, 8-13

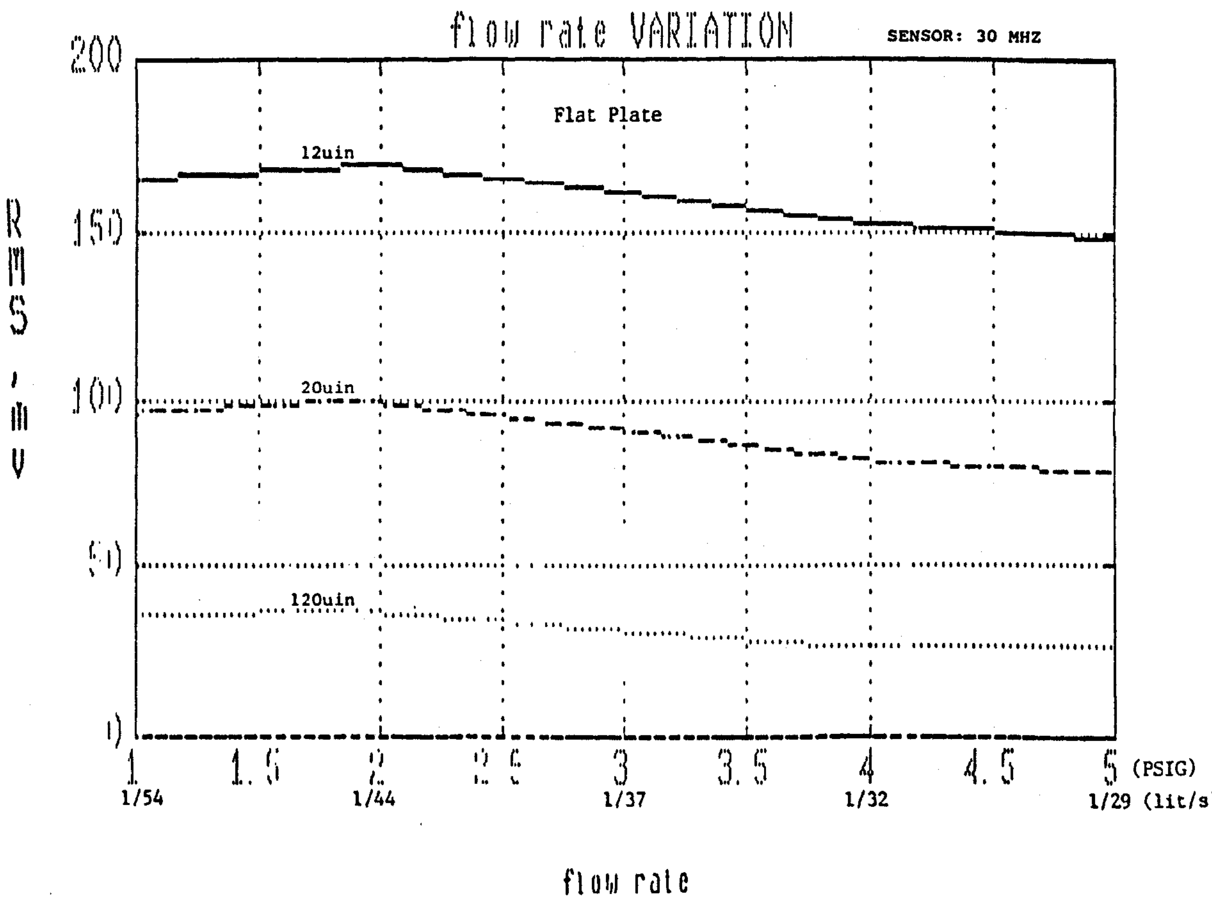

flow rate VARIATION
SENSOR: 30 MHZ
Flat Plate
12uin
20uin
120uin
RMS, mV
200
150
100
50
0
1
1.5
2
2.5
3
3.5
4
4.5
5 (PSIG)
1/54
1/44
1/37
1/32
1/29 (lit/s)
flow rate

Fig, 8-14

- The signal amplitude (RMS) values of the transducer would change with change in the surface roughness values. The higher the surface roughness value the lower would be the measured RMS (mv) value of the echo signal.
- The echo signals from the 10 MHZ transducer are higher than with either the 20 MHZ or the 30 MHZ transducers. Also, the 10 MHZ transducer provides a better resolution with changes in surface finish values, Figs. (8-3 to 8-5).
- The transducer distance from the test part surface is a critical parameter which influences the ultrasonic energy dissipation. The distance should be kept at a minimum practical value.
- The water temperature variations from 65°F to 90°F produce a negligible effect on the echo signal measurements.
- The tilt (oblique) angle is very critical. The squirter assembly must be kept perpendicular to the test part surface. A slight tilt of even one degree of squirter assembly reduced the measured signal amplitude to less than 25% of that was recorded at the perpendicular position (no tilt).
- The best water flow rate for this preliminary test plan was from 1/51 lit/sec to 1/44 lit/sec.

The concluded results agreed with those obtained by other researchers.

8-5 SURFACE FINISH MEASUREMENT ON THE CYLINDRICAL PARTS:

The tests were conducted to determine sensitivity of the measured transducer signal with the various selected process parameters, for an outside diameter cylindrical grinding machine. The cylindrical test parts were manufactured by a Cincinnati Milacron series # 210

CNC controlled center-type grinder at Metcut Research. The machine tool used for conducting most of these tests was a small and precise engine lathe, located at the mechanical engineering machine shop, University of Cincinnati. This lathe provided the workpiece rotation capability similar to a cylindrical grinding machine. The specifications of the selected coolant (Bestcut 105, Interlube Corporation) were tabulated in Table (6-1). The Ultrasonic analyzer, Panametrics-Model 5052 UA, was selected for the research work. The ultrasonic analyzer and osciloscope settings are presented in Appendix-B.

Test Part: Four test parts with various dimensions but the same material were designed for the research work, see their specification in Figs. (8-15 to 8-18).

8-5-1 Process Variable:

The following process variables were selected to analyze this part of the research:

- Transducer frequency (10 MHZ, 20 MHZ and 30 MHZ).
- Oil volume fraction in the tap water, coolant composition.
- Coolant temperature variations.
- Diffuser or nozzle component geometry and materials.
- Distance variations, from waveguide assembly to the cylindrical part surface.
- The tilt (oblique) incidence.
- Eccentric incidence.
- Cylindrical test part rotation (rev/min).
- Coolant flow rate.

Tests were conducted with parameters changing one at the time with others remaining constant.

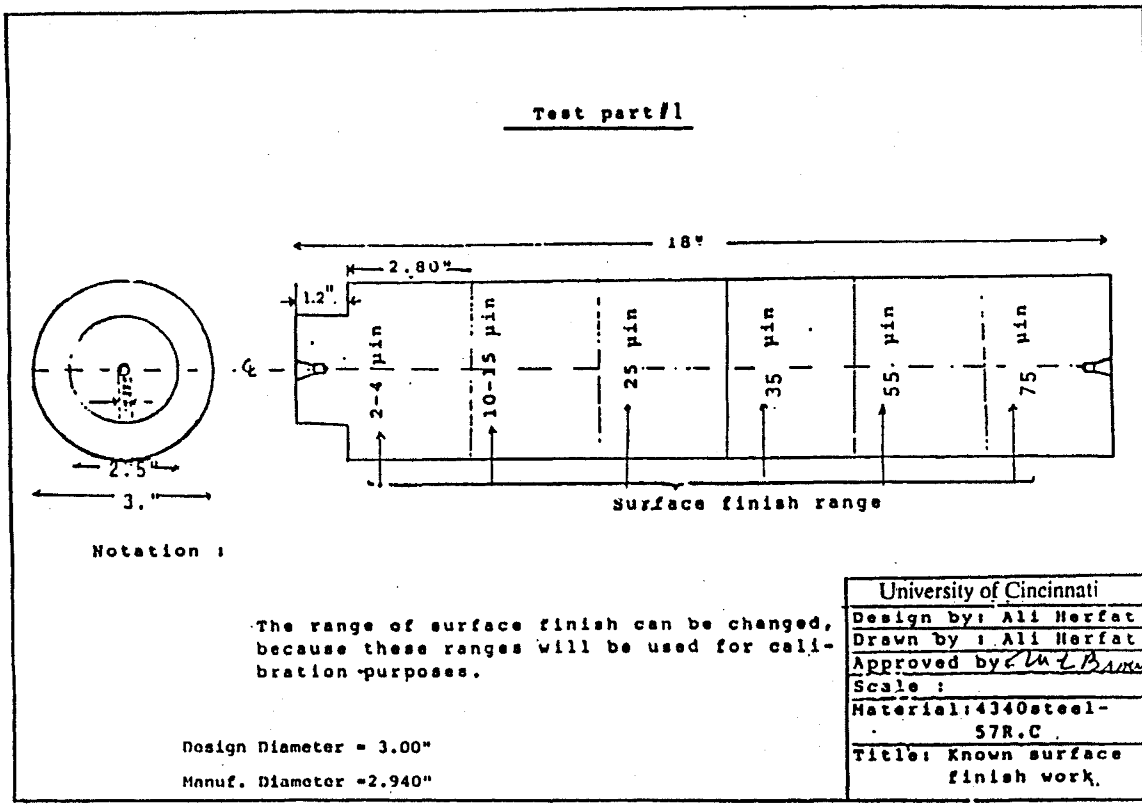

Fig. 8-15

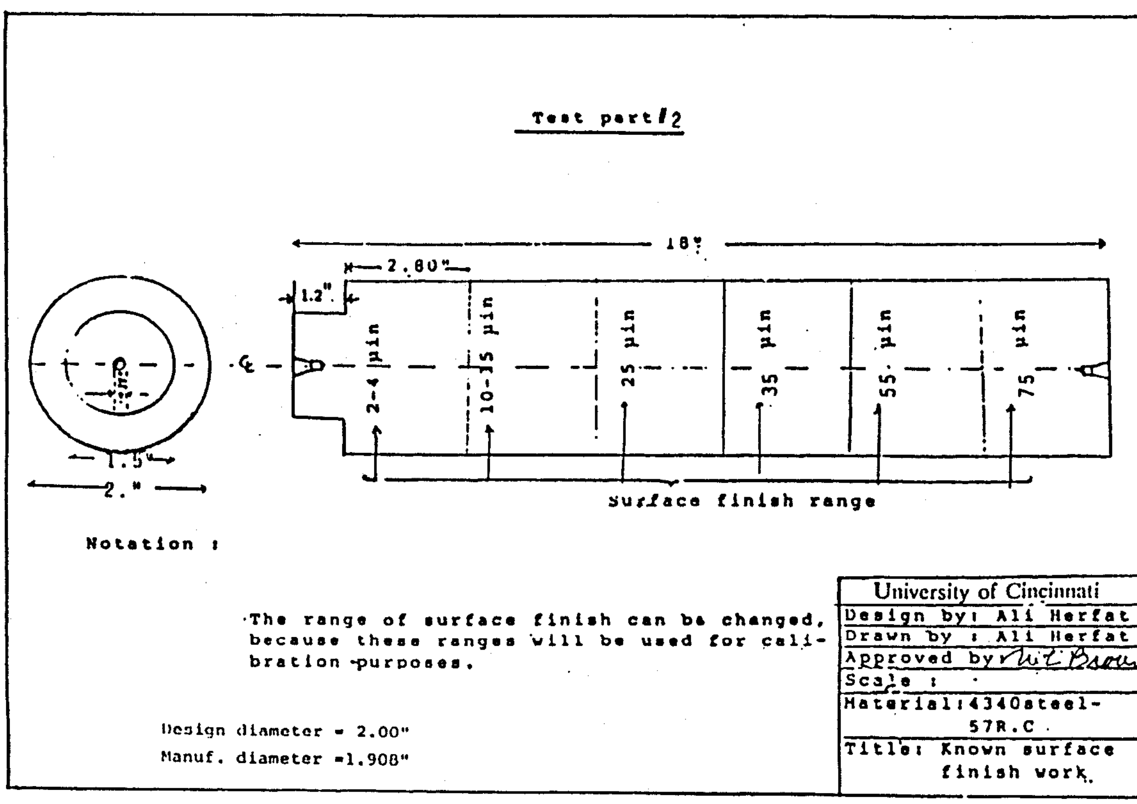

Fig. 8-16

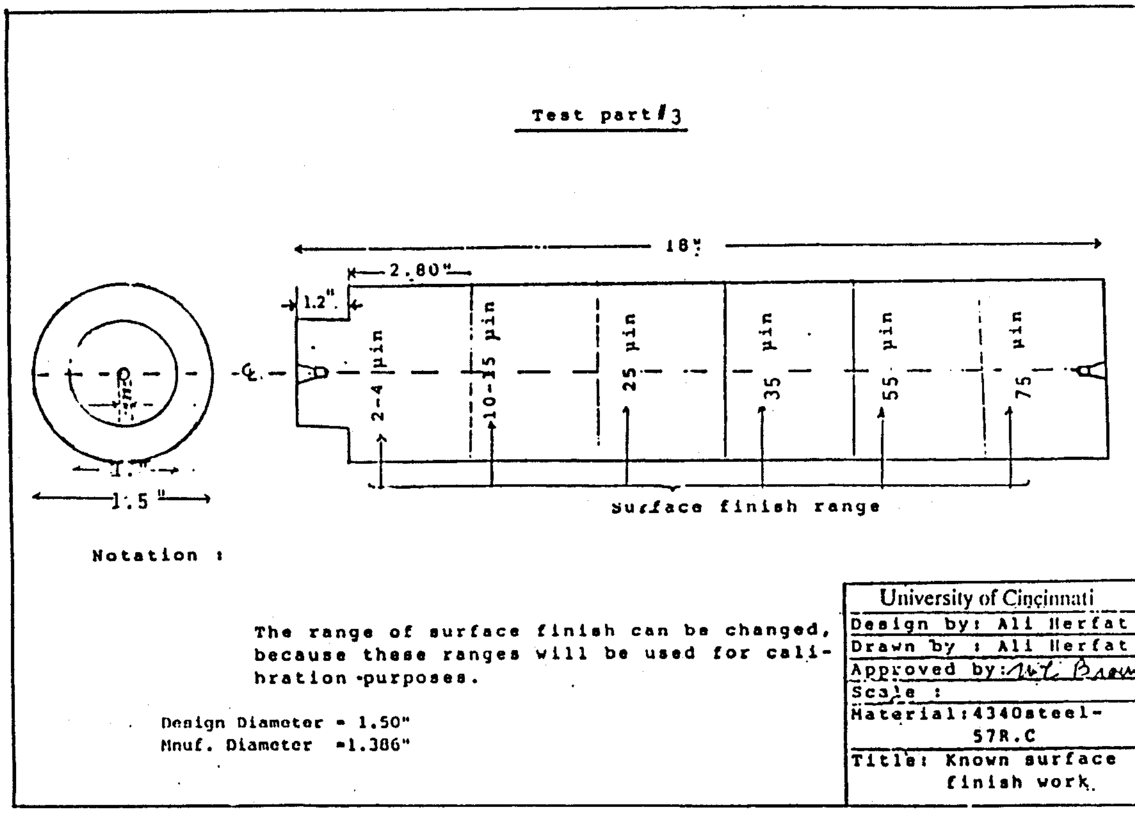

Fig. 8-17

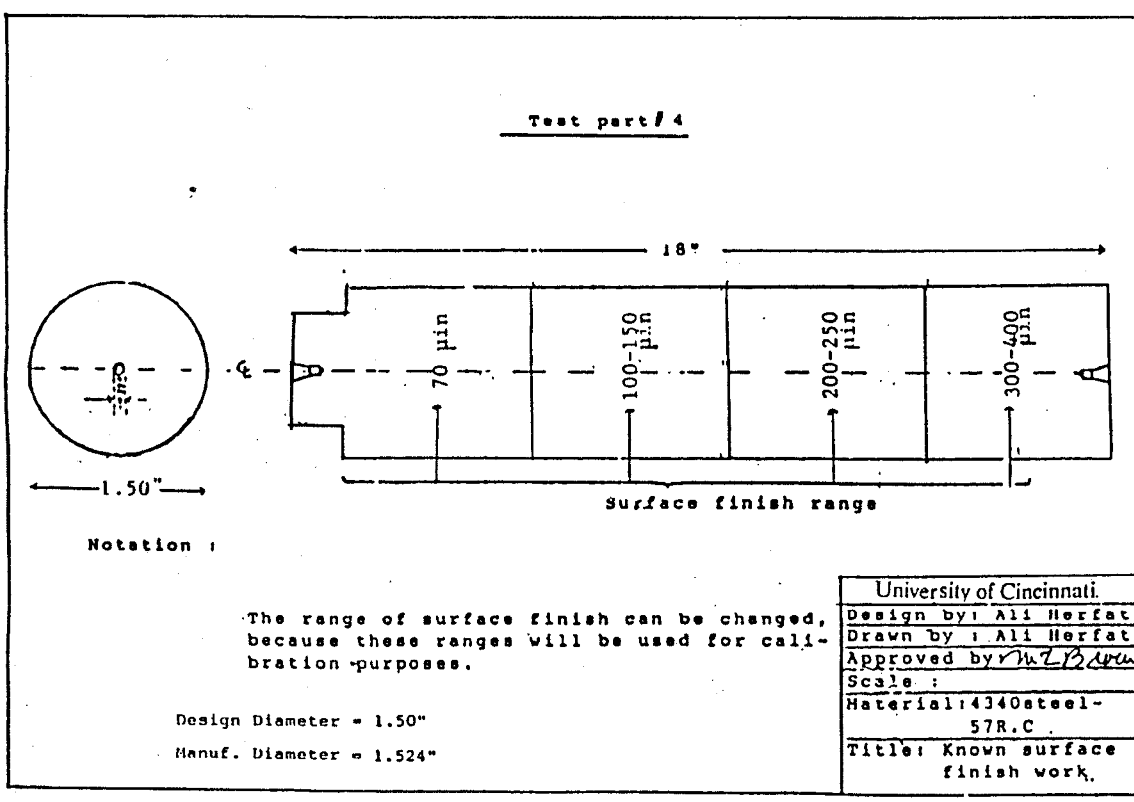

Fig. 8-18

8-5-2 Test Results:

The RMS (mv) values of the first ultrasonic wave echo was recorded for each test. Each recorded RMS value was repeated at least in three consecutive tests. If there was a slight difference between the obtained data, then the mean value of the RMS values was recorded for the test.

8-5-2-I) Transducer Frequency:

Three transducers were recommended by National Institute of Standards Technology (NIST), 10 MHZ, 20 MHZ, 30 MHZ. These transducers were used in the research work. The surface finish measurement test expanded to a range of surface finish from 4 μin to 380 μin by using two test parts. Note that the second test part (manufactured at Machine Shop of Mechanical Engineering Department, University of Cincinnati) with the surface finish range from 45 μin to 380 μin, Ra, was also used in this test. The spuirter bottom face just touched the test surface along its center line. The coolant was a mixture of 1/30 Bestcut-Interlube volume fraction with tap water. The test data was plotted in Fig. (8-19). The data showed that the 10 MHZ transducer provided the stronger RMS (mv) signal amplitude than 20 MHZ and 30 MHZ transducers. It also provided more sensitivity than the other two transducers for surface finish measurement, particularly for precision finish range (4 to 75 μin). Therefore, 10 MHZ transducer was selected for all of the following tests.

8-5-2-II) Oil Concentration:

The tests conducted by starting with the coolant having one volume of oil (Bestcut-Interlube) in 20 volumes of tap water. The oil concentration was reduced by adding more water into the coolant. The data plotted in Fig. (8-20) showed that the amplitude

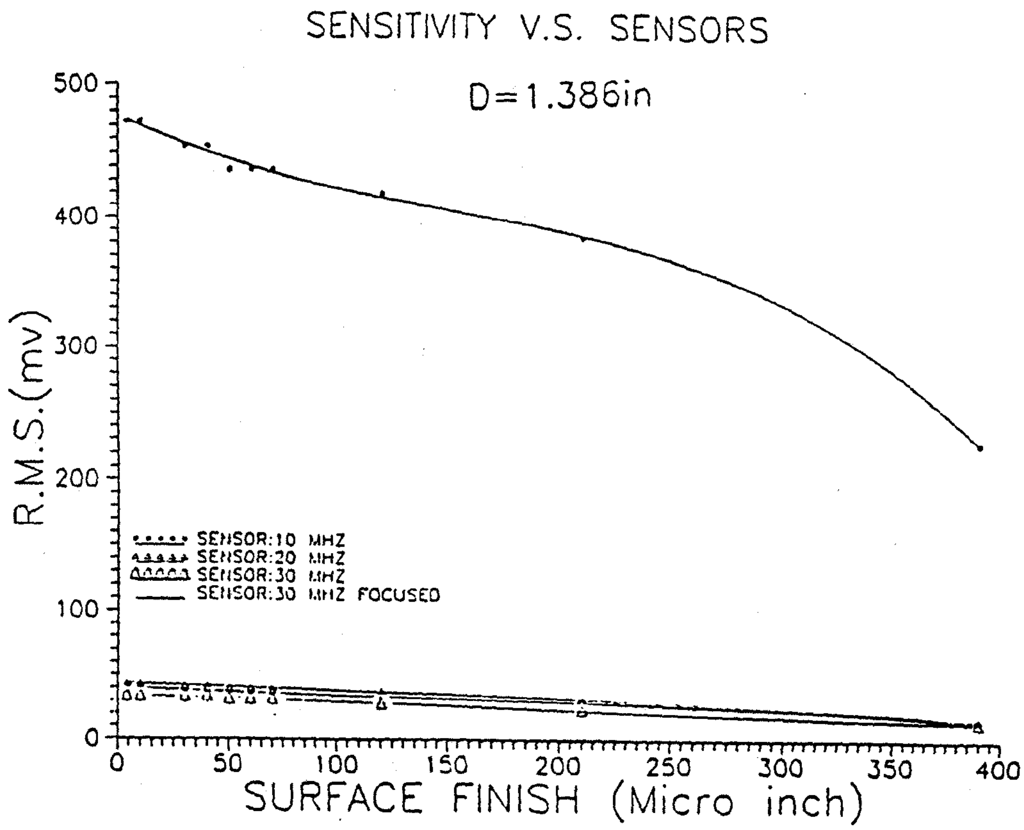

Fig. 8-19

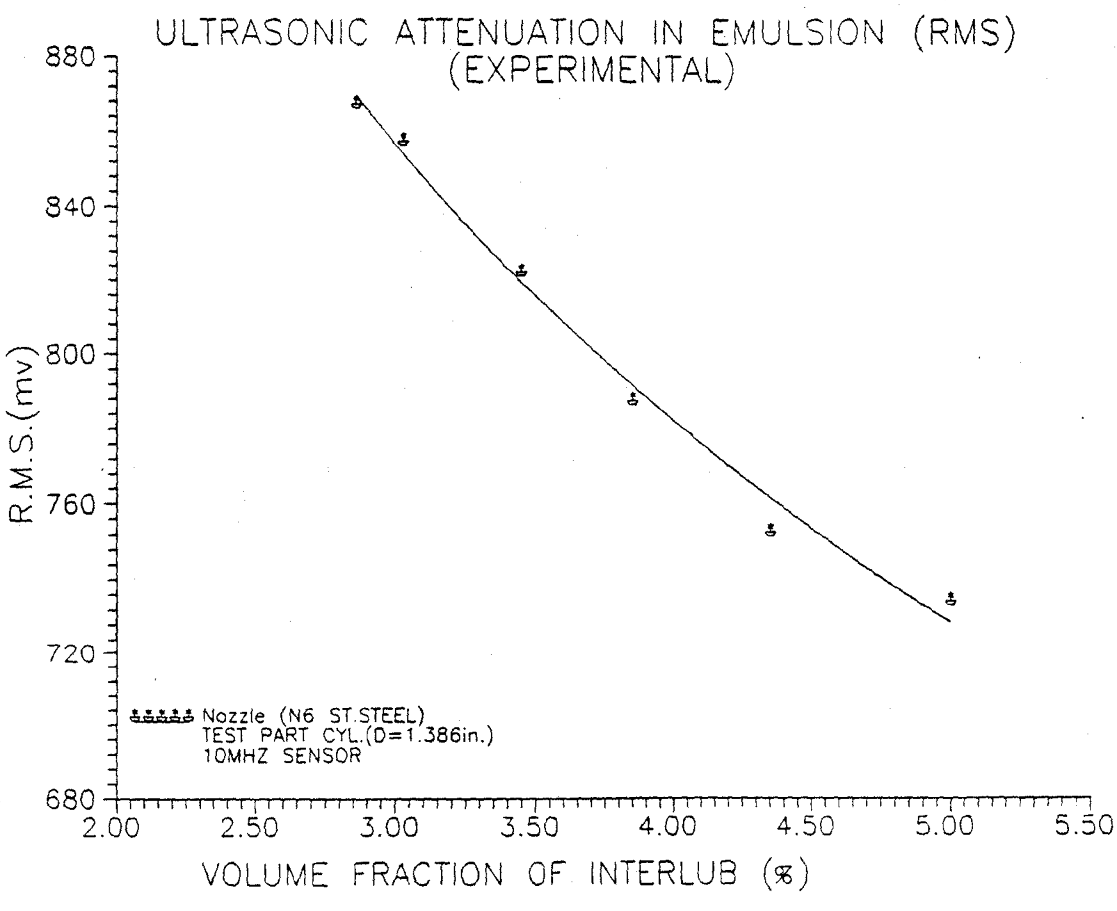

Fig. 8-20

of ultrasonic signal was sensitive to oil concentration volume.

The oil concentration in the range of 1/29 to 1/32 was used for all the other tests. This concentration range was tested as a non-corrosion characteristic and lubrication capability of this solution (coolant). The results shows high reliability and capability of the coolant with this range of oil concentration.

8-5-2-III) Coolant Temperature Variation:

The coolant temperature was varied from 70°F≈21.11°C to 87°F≈30.56°C for three hours coolant circulation, in the summer time. The acquired data was plotted in Fig. (8-21). The data showed that for this temperature range, there was no significant difference in the transducer signal amplitude.

8-5-2-IV) Nozzles and Diffuser Components:

The short and narrow tube shape pieces are called nozzles in this research work. One of the purposes of this research work was to improve the sensitivity of sensor signal measurements in the precision surface finish range (4 μin to 75 μin). In order to achieve this goal, five nozzles and one diffuser pieces were designed, built and tested, Fig. (8-22a). Signal sensitivity and quality was analyzed with diameter variations of the nozzles and tube shape section of N1. The experimental results showed a better resolution and distinguishable signals, when a smaller diameter nozzle or tube shape section of diffuser was used in the signal measurement (see each nozzles and diffuser drawings, Fig. 8-22a). A 1/8 " diameter tube shape section of the waveguide assembly was the lowest size passsage diameter that was possible to build at Mechnical Engineering Machine Shop, University of Cincinnati. A new squirter assembly was also designed and built for this purpose, Fig.(8-22). Each nozzle or diffuser was epoxied to the new squirter assembly, leaving no leakage or build-up through

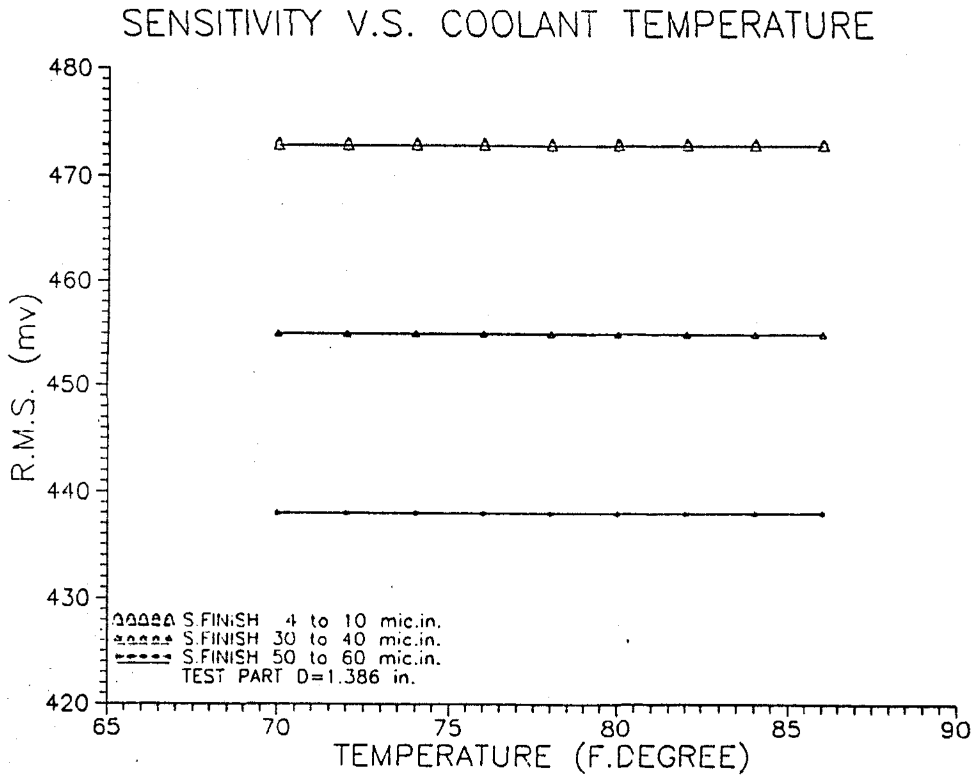

A6-3H

Fig. 8-21

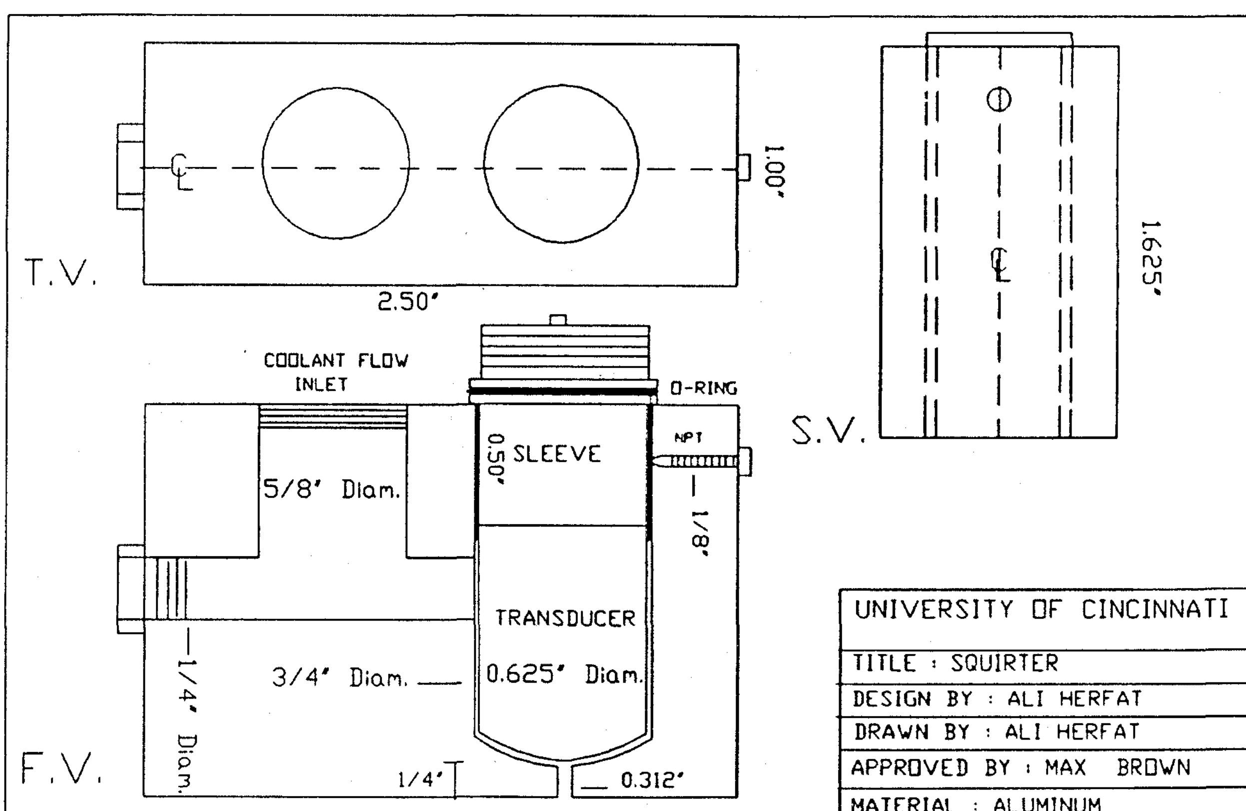

Fig.8-22

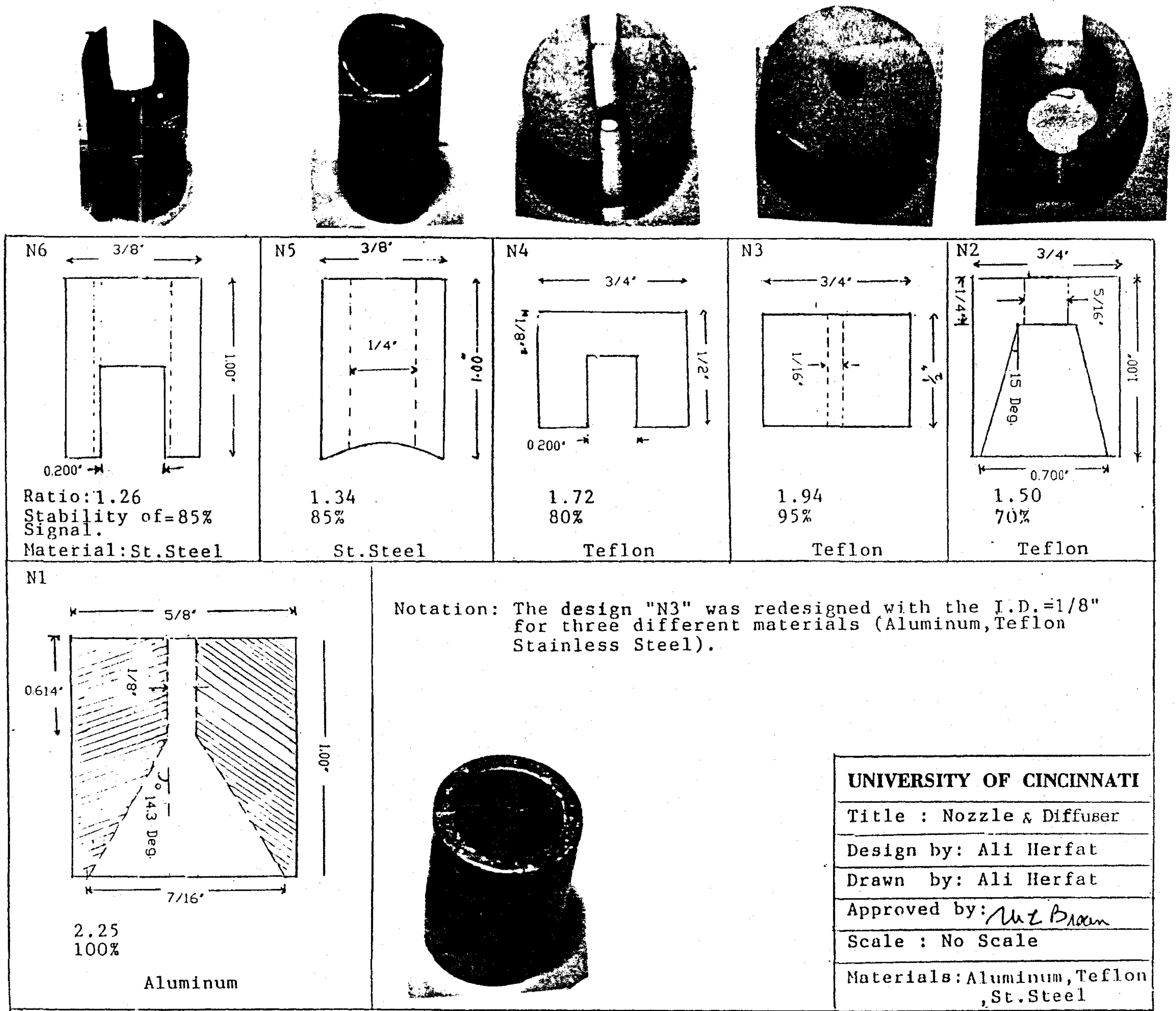
N6
3/8"
1.00"
0.200"
Ratio: 1.26
Stability of = 85%
Signal.
Material: St.Steel
N5
3/8"
1/4"
1.00"
1.34
85%
St.Steel
N4
3/4"
1/8"
1/2"
0.200"
1.72
80%
Teflon
N3
3/4"
1/16"
1.94
95%
Teflon
N2
3/4"
1/4"
5/16"
15 Deg.
1.00"
0.700"
1.50
70%
Teflon
N1
5/8"
0.614"
1/8"
14.3 Deg.
1.00"
7/16"
2.25
100%
Aluminum
Notation: The design "N3" was redesigned with the I.D.=1/8" for three different materials (Aluminum, Teflon Stainless Steel).
UNIVERSITY OF CINCINNATI
Title : Nozzle & Diffuser
Design by: Ali Herfat
Drawn by: Ali Herfat
Approved by: M L Brown
Scale : No Scale
Materials: Aluminum, Teflon ,St.Steel

Fig. 8-22a

the fluid passage hole. The lower surface (outlet) of the waveguide assembly was fixed at 0.250" distance from the top center of the cylindrical test part. The test data were plotted in Fig. (8-23). The aluminum diffuser (No 6) seemed to provide a signal with the highest sensitivity in the selected range of precision surface finish. The signal stability was excellent, being 100% compared to less than 100% for other nozzle designs. The diffuser is a straight cone type diffuser. It should be noted that the new waveguide assembly (diffuser and squirter) has the same material (aluminum). Thus, it has the same characteristic impedance. It means there is no reflection and/or transmission problem which is caused due to variety in the material of this assembly.

8-5-2-V) Distance Variations :

The distance from the diffuser output (mouth) to the part surface was varied 0.100" to 0.250."

The data was plotted in Fig. (8-24). The results showed that the intensity of the transducer signal varied considerably with the distance parameter. Therefore, for a proper accuracy of measurements and obtaining higher echo intensity the waveguide assembly must be kept in the normal position with respect to the grinding part (lower wave transmission path length) and also as close as possible to the part surface. Note that the distance parameter also gave us a normal distance information between the transducer and the cylindrical test part, at the top center.

8-5-2-VI) Waveguide Assembly Tilt (Oblique) Position:

The diffuser longitudinal axis (center line) was tilted along and across the center line axis of cylindrical part. The test data were plotted in Fig (8-25). The test data showed that

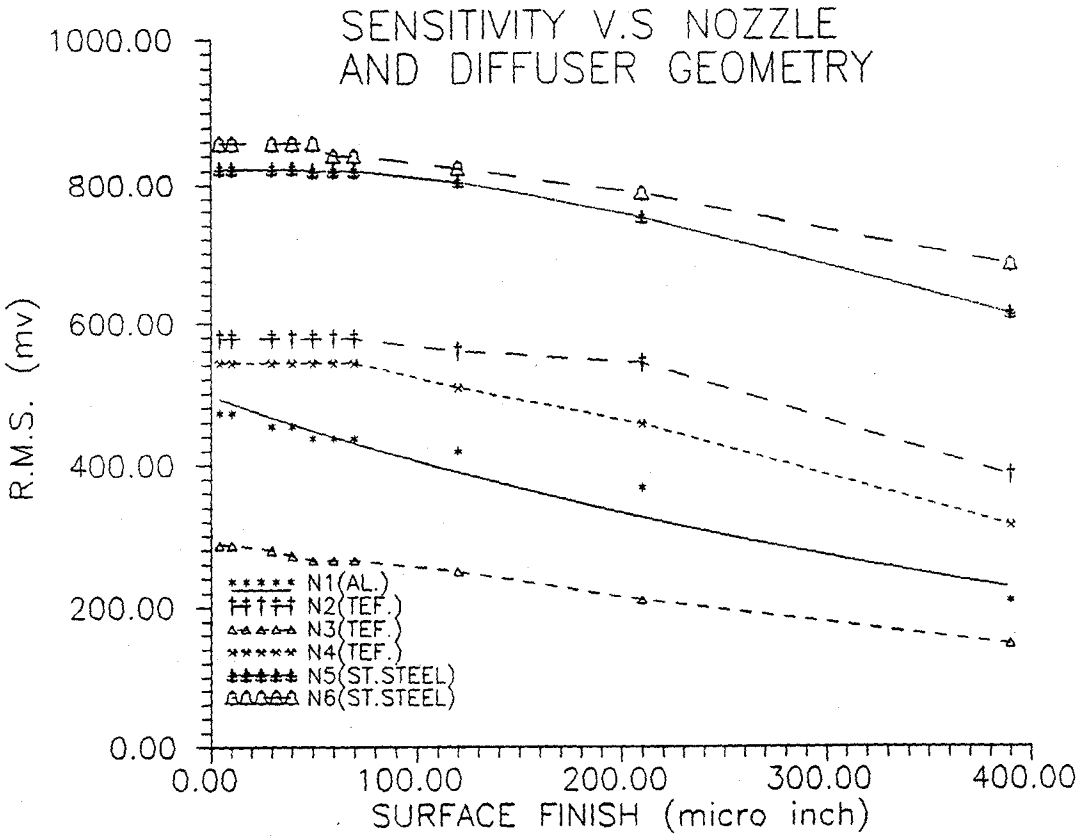

Fig. 8-23

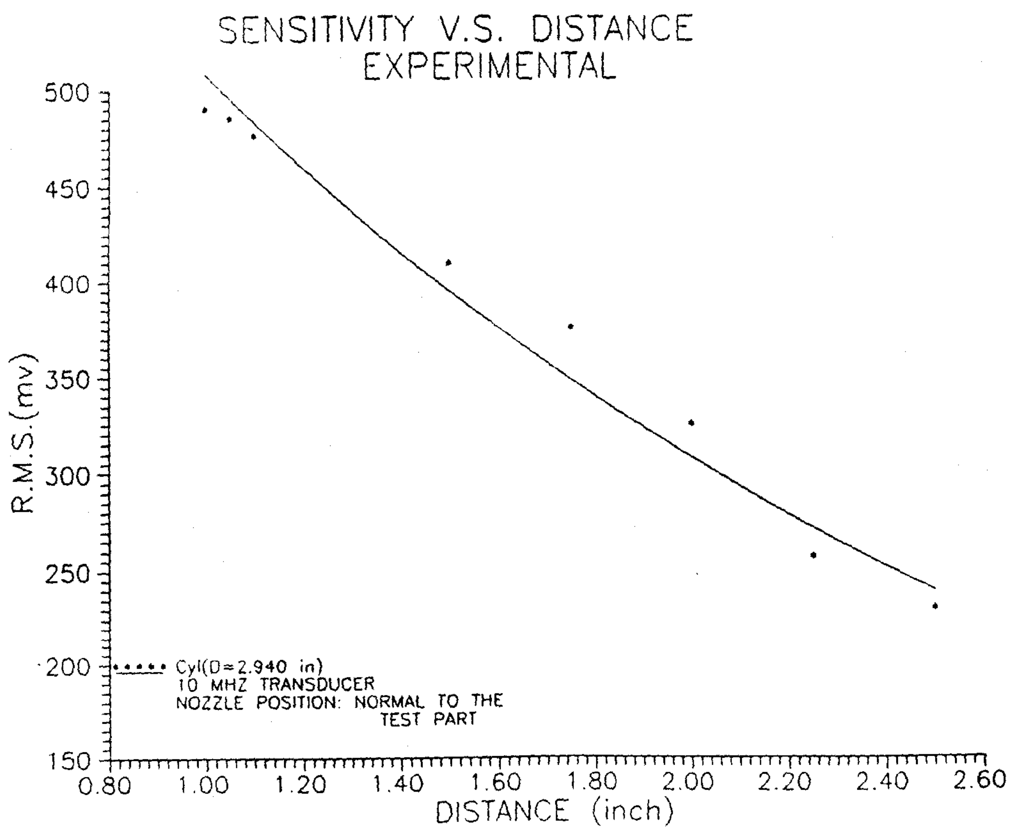

Fig.8-24

a slight angle of tilt, in order of one to two degrees, deteriorates the signal amplitude. The influence of this parameter was more crucial for cylindrical than flat plate (in the preliminary test) because in the cylindrical part a great amount of incident waves propagates in the environment without striking part interface surface. It means the rate of energy reduction is also dependent on the part diameter, a part with a larger diameter causes lower wave energy attenuation (flat part radius is very large or infinity value) in the tilt condition. This effect is shown in Figs. (8-25) for various parts of different diameters.

8-5-2-VII) Eccentricity:

When the position of the waveguide assembly's nozzle or diffuser longitudinal axis is varied, making it eccentric to the part center line. The test data was plotted in Fig. (8-26). Three cylindrical test parts with different diameters were used in this experiment. The measured data showed that the eccentricity of the waveguide assembly outlet, from the test part surface, had large attenuation effects on the transducer signal. Therefore, the diffuser or nozzle center line must be kept exactly perpendicular to the center line of the cylindrical part. Note that the eccentricity effects are due to increasing the distance between transducer and the part interface surface.

8-5-2-VIII) Grinding Part Rotational Speed:

Tests were conducted by varying the work rotational speed from stationary position to 500 rpm (sufficient range for grinding part rotation on grinders). The plotted data in Fig. (8-27) showed that the test part rotational speed had negligible effects on the signal measurements.

8-5-2-IX) Coolant Flow Rate:

The coolant flow rate was varied from 1/54 liter/sec to 1/29 liter/sec. The resulting

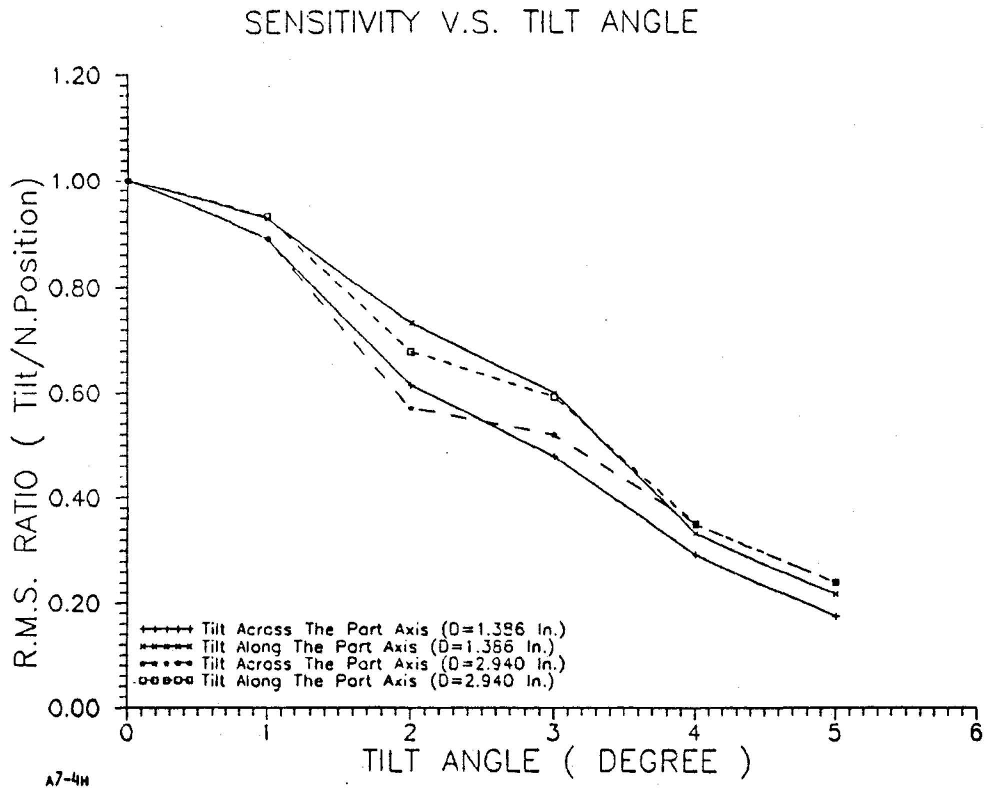

Fig. 8-25

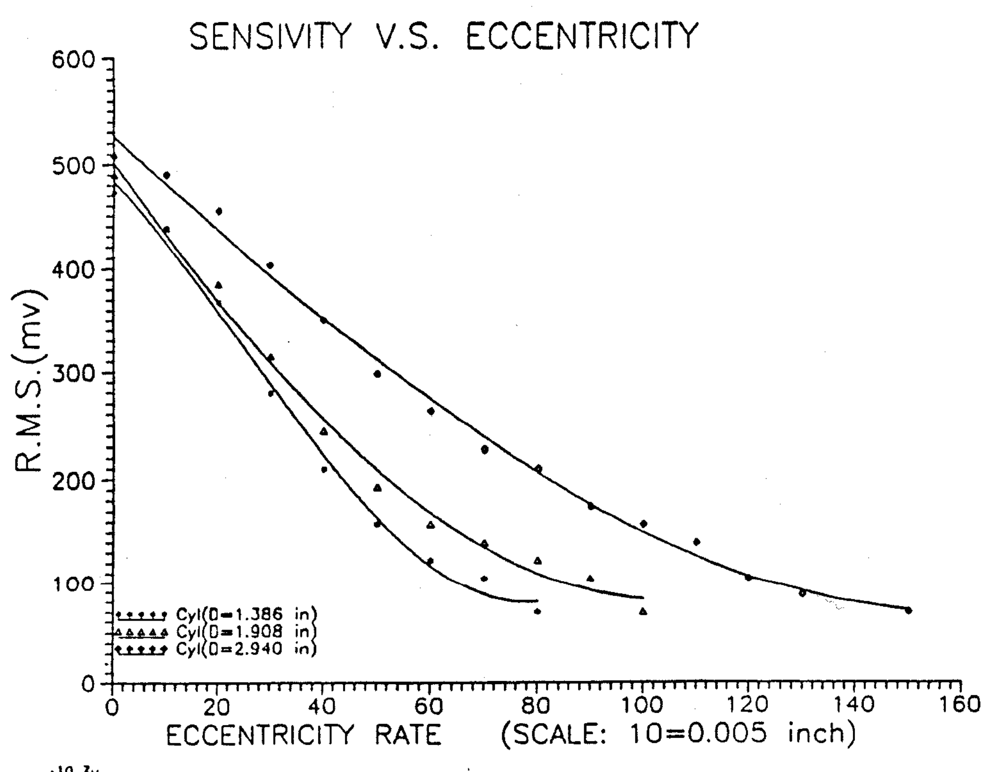

Fig. 8-26

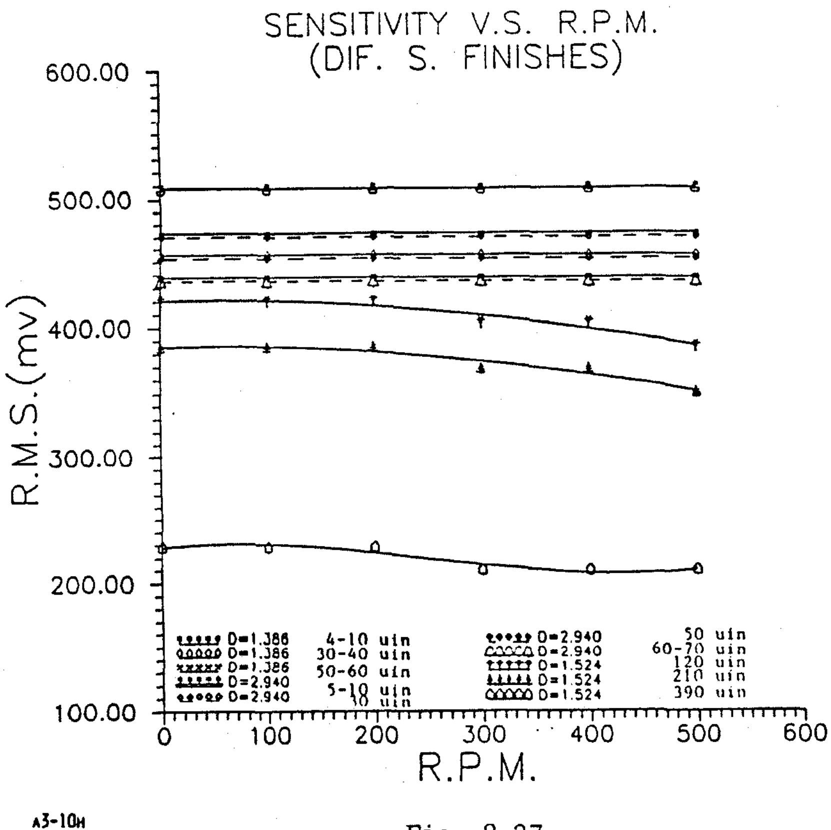

Fig. 8-27

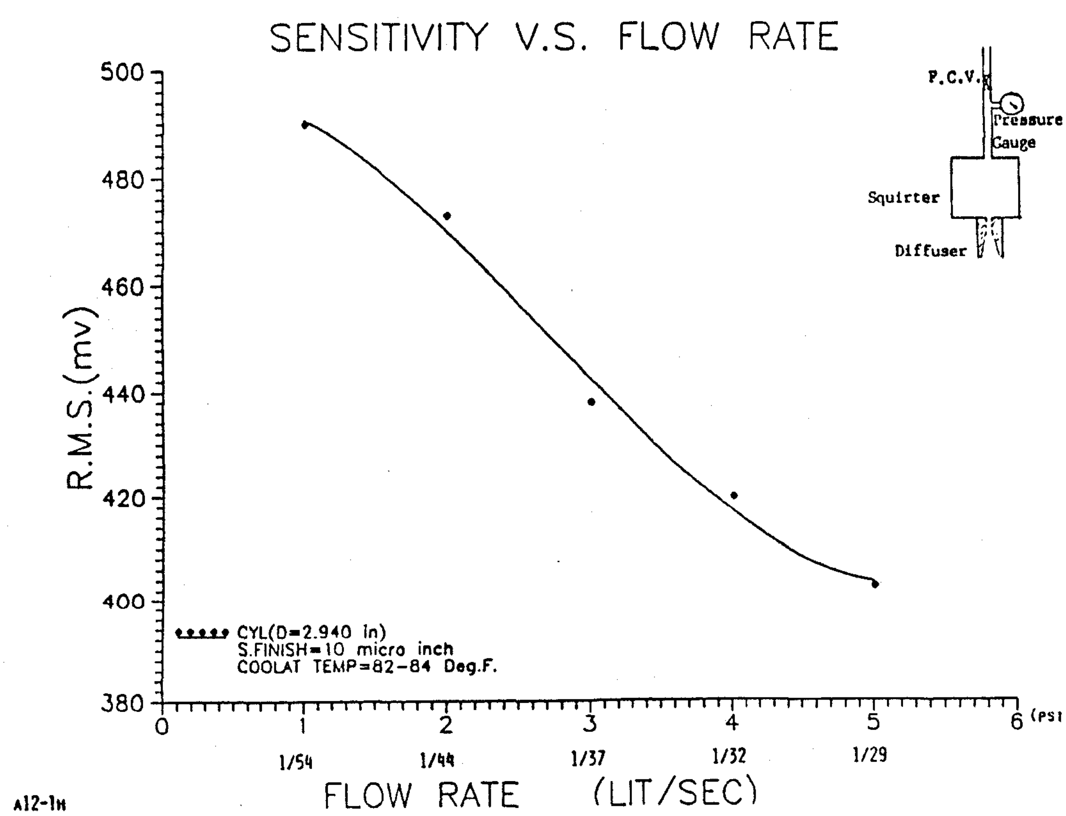

Fig. 8-28

data are plotted in Fig. (8-28). The measured data showed that the coolant flow rate should be kept to a minimum for higher diffuser performance and no possibility for turbulence and separation problems.

8-5-2-X) Test Part Diameter:

Tests were conducted on three test parts, D=1.386", 1.908", 2.940". The data were plotted in Fig. (8-29) and showed that the larger diameter part provides a higher echo signal amplitute for measurement.

8-5-3) Cylendrical Part Tests Conclusions:

The resulting data analysis gave us the following conclusions:

- The 10 MHZ transducer provided the higher signal intensity and more sensitivity to measure the surface finish value.
- The Bestcut-Interlube with oil/water concentration 1/29 to 1/32 oil volume / tap water volume provided high signal intensity and non-corrosion condition.
- The coolant temperature variations had negligible effects on the signal intensity.
- The Nozzle or diffuser geometry showed very important influence for signal measurement. The straight conical diffuser with diffuser angle $2\theta=28.6$ degree and aluminum material, provided the higher sensitivity for measuring the precision surface finish values for 4 μin to 75 μin.
- Waveguide outlet distance should be kept as short as possible.
- The diffuser or nozzle longitudinal axis must be perpendicular to center line of the cylindrical part, in all experimental works. This geometric orientation provides highest signal intensity for surface finish measurement.
- For cylindrical part surface finish measurements the diffuser or nozzle longitudinal axis

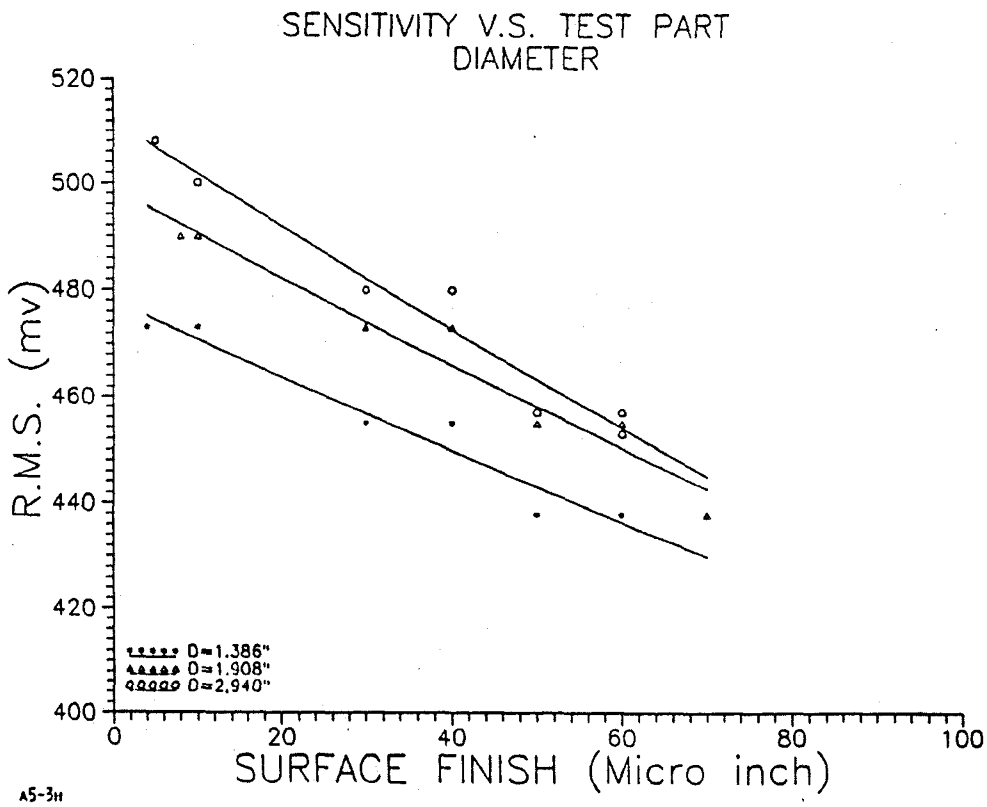
SENSITIVITY V.S. TEST PART DIAMETER
520
500
480
460
440
420
400
R.M.S. (mv)
D=1.386"
D=1.908"
D=2.940"
0
20
40
60
80
100
SURFACE FINISH (Micro inch)
A5-3H

Fig. 8-29

was perpendicular to the part center line.

- The selected grinding part rotational speed variations had negligible effects on the signal intensity.
- The coolant flow rate was kept as low as possible, for no fluid flow separation, no turbulence flow and high diffuser performance.

The above conclusions were obtained through the experimental part of this research work and with the research prototype specifications and coolant properties. It is obvious that any change in the design specifications of waveguide assembly components (squirter or diffuser), geometry and/or materia, and coolant properties provides a deviation in the resulted data.

CHAPTER 9

THEORETICAL AND EXPERIMENTAL RESULTS ANALYSIS:

9-1 INTRODUCTION:

Correlation between experimental and analytical results and scientific proofs for them are the main purposes of this chapter. The research is proposed to develop the basic science for the development of a product. This product would measure the surface roughness values of cylindrical parts while they were being ground on an outside diameter. The final data analysis and revised empirical equations in conjunction with recommendations in this chapter, will be conducted to a product with such specifications that are able to fulfill the research purpose.

Optimization of the effective parameters and the process conditions for a commercial product are the main goal of this research work.

9-2 PARAMETERS ANALYSIS:

Based on the experimental and theoretical results (Chapters 7 and 8), the research parameters can be categorized to effective and ineffective parameters in the precision surface finish measurement during the process.

The ineffective parameters were coolant temperature in the machining range (65°F to 90°F) and work piece rpm. The effective parameters are divided into two sub-categories, controllable and uncontrolled parameters. The uncontrollable parameters are those parameters whose influence are considerable in the surface finish measurement process but they cannot be controlled or chosen by machine tools engineer for a grinding process, such as cylindrical part diameter (design parameter which is demanded for manufacturing of the part) and work piece material which is chosen for a specific purpose by designer (various materials have different characteristic impedance).

The most important controllable parameters are as follows:

9-2-1 Frequency Parameter:

The frequency variation parameter was studied in terms of distance variation and surface roughness. In both cases the sensitivity and signal amplitude of 10 MHZ transducer was much better and stronger than those of 20 MHZ and 30 MHZ transducers. The 10 MHZ ultrasonic wave superiority can be due to matching between this ultrasonic wave length and the precision surface integrity wavelength and also more capability of the 100 MHZ bandwidth oscilloscope for analyzing a 10 MHZ ultrasonic wave rather than 20 MHZ and 30 MHZ. The ultrasonic energy attenuation with distance and increasing of the frequency can be investigated from the research general solution, Eq. (6-6) in Chapter 6 and Figs. (7-9 and 7-12). The amplitude of both terms of Eq. (6-6) are changed in inverse proportion to angular frequency and distance (z). The experimental results, Fig. (8-19), showed that the ultrasonic energy or amplitude of the echo signal decreases when the surface roughness increases. This result is also concluded from the scattering angle variation in term of surface roughness increasing, Fig. (7-6) and Eq. (4-4). It means when the scattering angle increases, a fraction of the ultrasonic wave is diverted to the environment, thus, that fraction of scattered waves will not be captured and conducted by the waveguide assembly. Therefore the amplitude of the measurement signal decreases and also drops with increasing the surface roughness value.

The reason for using a high frequency transducer (10 MHZ, 20 MHZ and 30 MHZ) for precision surface finish measurement is their very small wavelength which enable the wave to scan the microinch range surface discontinuity.

9-2-2 Oil Concentration: The experimental results, Fig. (8-20), proved that the ultrasonic intensity decreases with increasing the concentration oil volume fraction in the coolant, this result is also confirmed by theoretical results, Fig. (7-3), which stated the ultrasonic energy attenuation increases when the concentration oil volume fraction increases. Therefore, increasing the oil volume fraction causes a drop in the measurement signal amplitude.

9-2-3 Nozzle or Diffuser Geometry:

The straight conical diffuser with diffuser angle $2\theta = 28.6^{\circ}$ (slightly flared) which were used in this experimental work has two following advantages for this research prototype and also for precision surface finish measurement range (4 μin to 75 μin):

- The incident waves can propagate out of the diffuser mouth with very little reflection back to the diffuser throat.
- The diffuser cross-sectional area changes with distance slowly (not flared fast), thus, we can assume ultrasonic wave is a plane wave.
- The diffuser has more capability than nozzles to capture more scattered waves.
- The parameters such as angle, length and material of the diffuser have considerable influence in a measurement signal amplitude. The lower diffuser angle gives better diffuser performance, but manufacturing of a diffuser with e.g. $2\theta = 10^{0}$ and available machine tools require a longer diffuser length. A longer diffuser causes an increase in distance, thus, the measurement system efficiency decreases. Hence, the correlation between these two diffuser parameters must be considered when a diffuser is designed.

The ultrasound reflection and transmission values also vary in term of the characteristic impedance (ρc), where ρ is density of the diffuser material and c is ultrasound velocity in a medium. Therefore, lower transmission through the diffuser walls or higher reflection from those walls needs a high characteristic impedance material.

9-2-4 The Tilt (Oblique) Incidence and Eccentricity: These parameters are only analyzed in the experimental part of the research. These parameters had considerable influence in the ultrasound energy attenuation. Therefore, the problem was analyzed for the condition when the center line of the wave guide assembly is perpendicular to the test part surface (normal position). Note that in the case of cylindrical part grinding, the diffuser center line must be aligned perpendicular to the part center line.

9-2-5 The Coolant Temperature Parameter: This parameter is negligible in the ordinary range (65° F to 90°F) for surface finish measurements. Thus, this parameter is not a considerable parameter for a coolant with similar properties.

9-2-6 The Grinding Part RPM: The workpiece rpm is not usually above 200 rpm. In this research, we studied the effects of part rpm parameter up to 500 on the measurement signal. The test results showed there is no significant effect of this parameter in surface finish measurement. Thus, this parameter does not participate in the measurement. It should be noted that the wheel is usually rotated in several thousand rpm or much higher than the workpiece rpm.

9-2-7 The Cylindrical Test Part Diameter: The higher grinding part diameter yields the lower sliding attenuation value (α_s) and smaller scattering angle (lower α_r), see Chapter 7. Note that this parameter is a design demand factor and cannot be changed or optimized for surface finish measurement purposes.

9-3 RECOMMENDATIONS FOR A COMMERCIAL PRODUCT:

The following recommendations are included both for surface finish measurement process and the commercial product components.

9-3-1 Process Conditions:

The experimental and analytical results analysis and their correlations, either for flat plate or cylindrical parts, provide the following optimized conditions to generalize some conventions for a product development which will be used in surface finish measurement during the precision grinding process.

The problem parameters (such as transducer frequency, coolant oil concentration, distance, diffuser or nozzle geometry and characteristic impedance) should be optimized in terms of the process conditions and coolant specifications. A clear and strong signal for surface finish measurement can be obtained under the following conditions:

- Waveguide assembly must be fixed in normal position with respect to grinding part.
- The concentration oil volume fraction must be kept at minimum safe (no corrosion and good lubrication) value.
- The transducer signal must be protected against undesired environment effects, if it is possible.
- The grinding machine must work without off center (tolerance) rotation for precision surface finish measurement. Any misalignment rotation causes distance, eccentric and oblique problems.

9-3-2 Commercial Product and Auxiliary Instrumentations: Based upon the data acquired in the experimental and the theoretical parts of this research and development of these data in the previous chapters, a commercial product (prototype unit) can be built for precision surface finish measurement during the grinding process. The prototype unit consists of the following components and axillary devices:

1) An ultrasonic transducer is located in the squirter component of the waveguide assembly. The squirter component of waveguide assembly must be positioned in the cooling system. The waveguide assembly must be fixed as close as possible to the grinding workpiece, but the distance must be adjustable (automatic adjustment is preferable). The waveguide assembly must also be able to maneuver along or across the workpiece and its motion should be controllable from the grinder control panel. It is recommended to equip the grinder with a robot for both motion and distance variation purposes. Trying a 5 MHZ transducer is also recommended.

2) Manufacturing a diffuser with smaller length and angle by using a high technology should be investigated in the future. Ultrasonic propagation through a diffuser with smaller angle and length will decrease the energy attenuation due the fluid flow stall condition and distance parameter. Building the diffuser from various material is another recommendation for the research continuation. Check the material with higher impedance such as stainless-steel.

3) The coolant flow rate should be maintained as low as possible particularly when a diffuser component is used in the waveguide assembly. The fluid velocity or flow rate have significant effects in the fluid separation from the diffuser walls and also turbulence condition. In this research work it was usually controlled on 1/54 liter/sec.

4) Pulse generator, for pulse-echo technique application or in general a signal generator. This unit provides excitation energy to the ultrasonic transducer

5) A detector or receiver which consists a variable attenuator unit, amplifier unit, filter unit and gated radio frequency output, Fig. (9-1).

6) The surface finish measurement signal should be sent to grinder control panel which is intermediator between the grinder and a computer which is programmed to control the whole grinding process. The computer can be programmed for any function (such as RMS, Peak to peak and etc) for surface finish measurement signal.

7) A meter showing a range of RMS values and their relationships with the surface roughness values (microinch preferred) should be installed on the grinder control panel.

8) A high bandwidth oscilloscope can be used for displaying the echo signal quality.

These items may require some modifications for a specific grinder or under a certain condition. In general a prototype unit with above mentioned specifications can work for a precision surface finish measurement and a CNC controlled grinder.

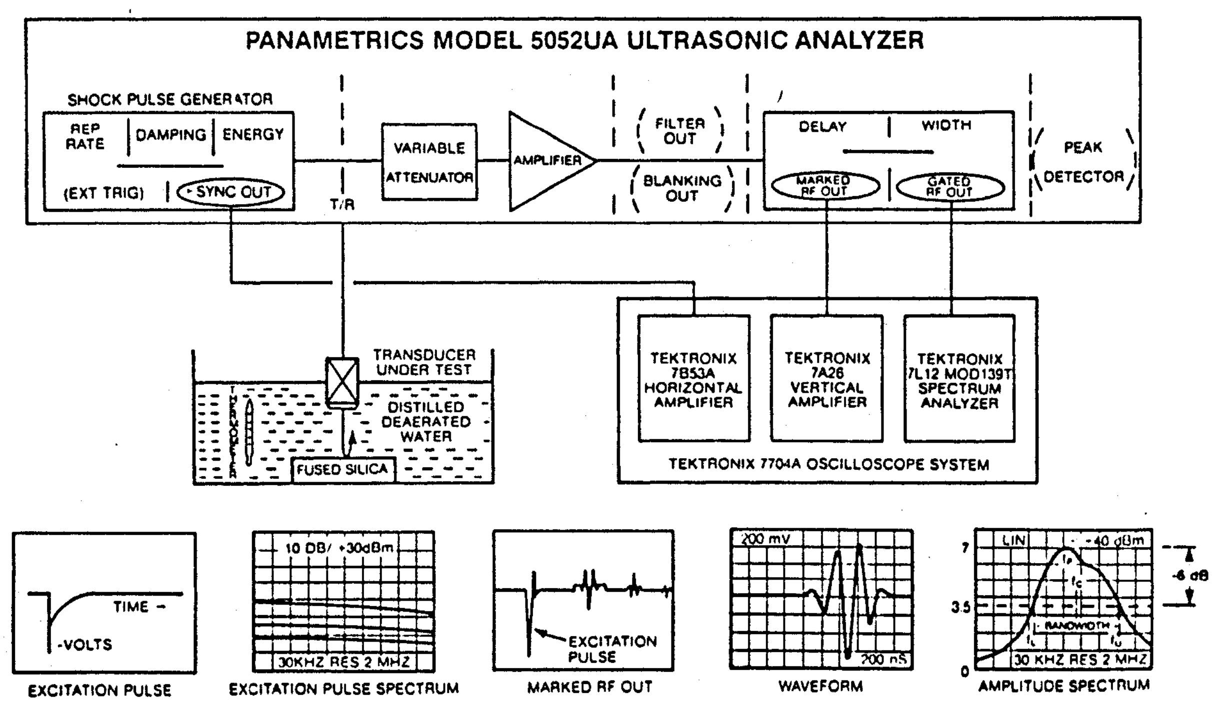

Fig. 9-1

APPENDIX-A:

A-1 TEST SETUP AND LIST OF MATERIALS:

The initial test layout is shown in Fig. A-1 . Series 210 CNC cylindrical grinding machine can be used as a test bed.

A constant temperature bath can be used in preliminary tests, for flat plat surface finish measurement processes. A centrifugal pump can feed both the grinder coolant system and the constant temperature bath fluid flow. Water or grinder coolant is used as ultrasonic couplant. The squirter is connected to a 12" long copper or galvanized pipe. Other end of the pipe is joined to the pump discharge by a plastic tube. The copper or galvanized pipe is held by a clamp which assists in adjusting the distance between the part surface and the transducer. An electrical heater and a mixer are installed in the bath to maintain a desired test temperature and a homogenous fluid, if concentration oil is added to tap water. This assembly is loaded to a device which is capable of moving along and across the grinding part with adjustable distance (height) between transducer and cylindrical part surface. This device can be a small robot. Note that the waveguide assembly was fixed on the feedrate system of a precise lathe machine with a magnetic piece, at Mechanical engineering machine shop, University of cincinnati.

The pulser/receiver and the temperature controller are wired to an oscilloscope and through an analog to digital convertor (ADC) board to a pc-computer, based upon data acquisition system. A list of material is presented in Table (A-1).

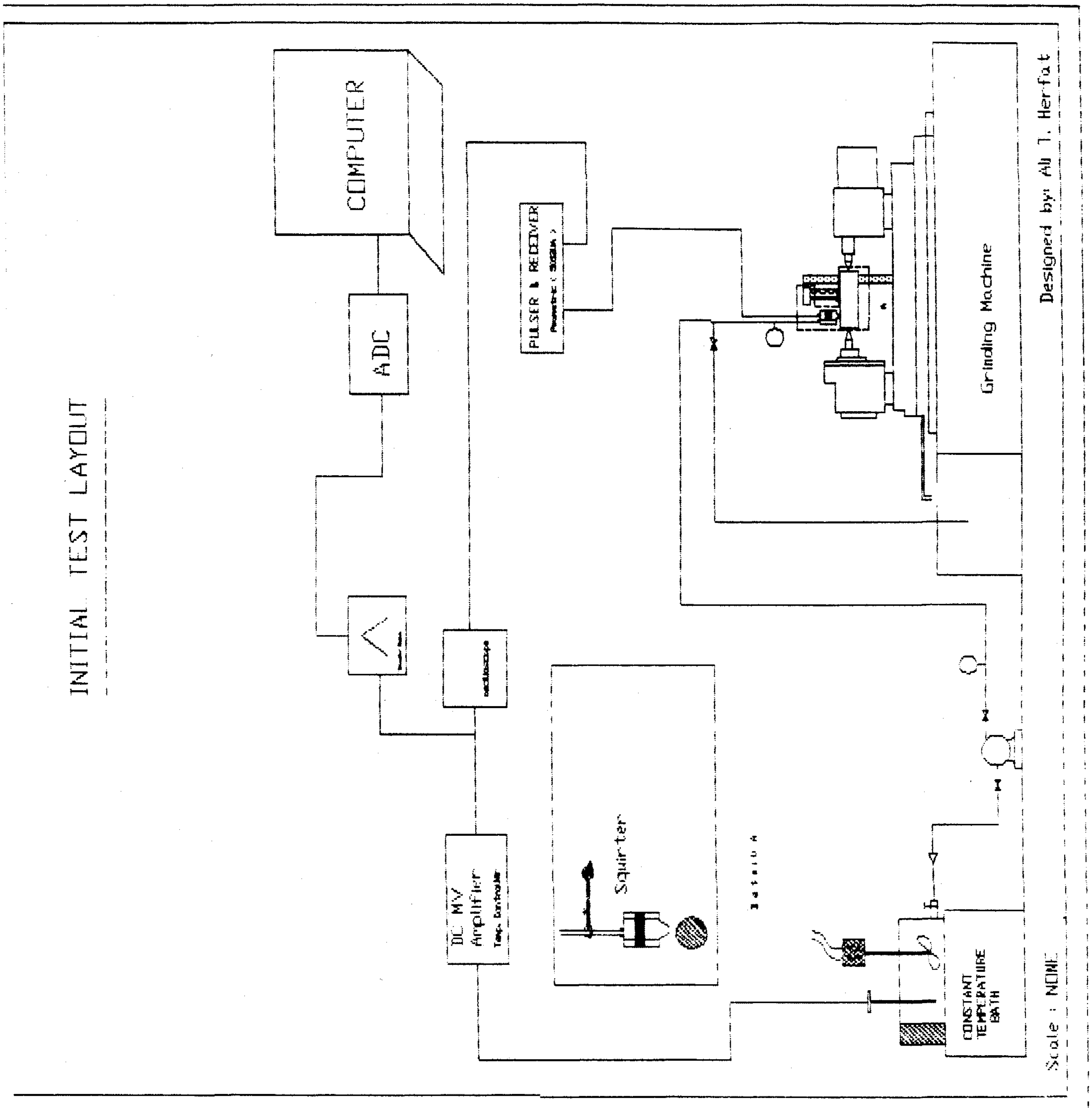
INITIAL TEST LAYOUT
COMPUTER
ADC
PULSER & RECEIVER
Grinding Machine
Designed by: Ali T. Herfat
Squirter
DC MV Amplifier
CONSTANT TEMPERATURE BATH
Scale : NONE

Fig. A-1

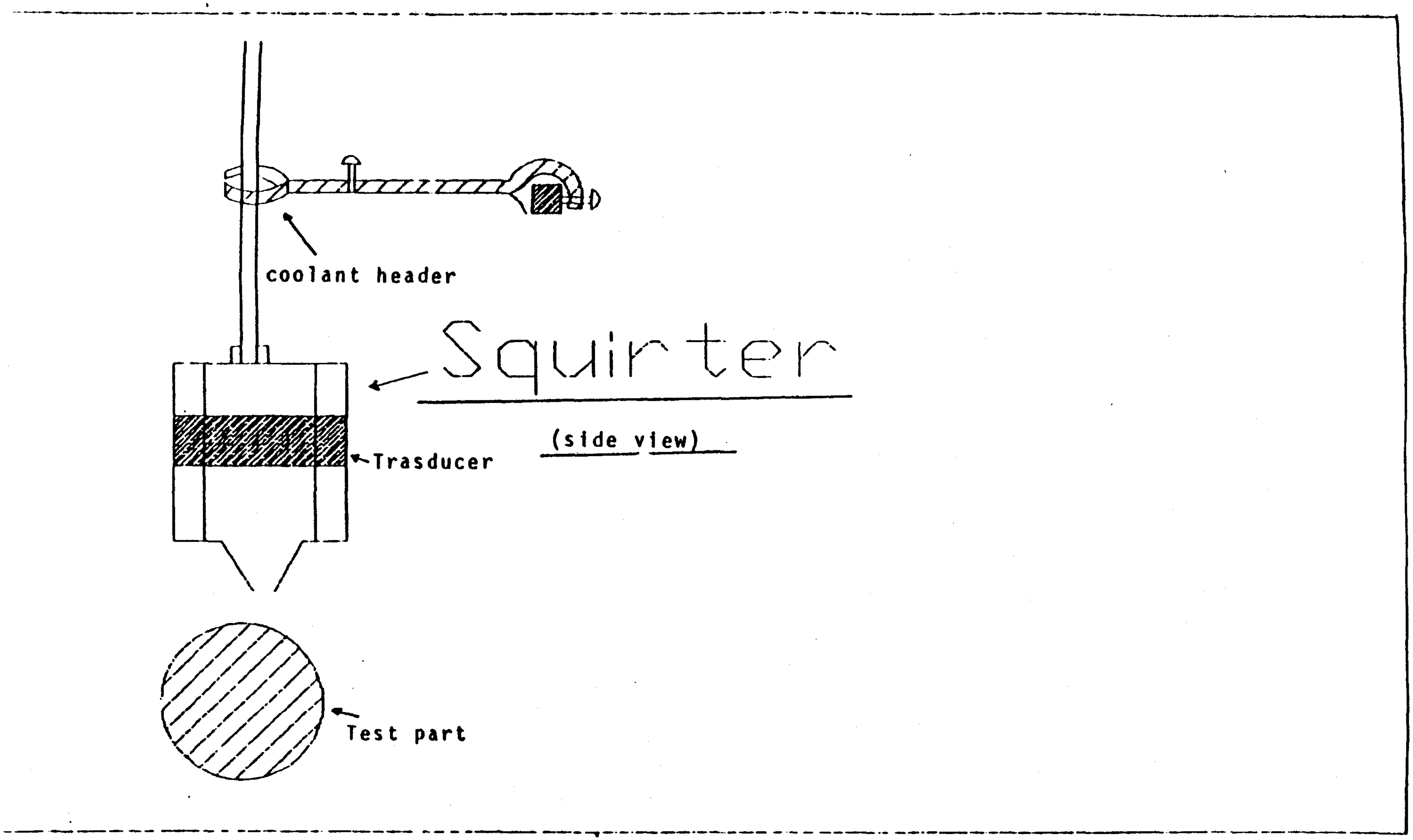

Detail: A

LIST OF MATERIALS

Item	No.	Name of Material	Specifications	Estimated Price
1	1	1" ball valve	bronze-low pressure for use with water, oil, class 150	
2	1	3/4" ball valve	" " " " " " "	
3	1	1/2" ball valve	" " " " " " "	
4	1	thermocouple	stem length = 12", copper-constantan - T	
5	1	D.C. millivolt amplifier	thermocouple D.C.millivolt amplifier with cold function compensation	
6	1	temperature controller	miniature microprocessor temperature controller	
7	2	press gauge	range 0-30 or 0-50 or 0-100 PSI	
8	1	mixer	variable speed utility stirrer (225 to 1600 rpm)	
9	1	pump	centrifugal pump pressure boosting = ISPSI, 14 GPMat's head	
10	1	heat element	specification of fig. 1 of catalog (immersion type)	
11	1	tank	5 gallon capacity (*)	
12		piping	1" = 5' , 3/4" = 5' , 1/2" = 15'	
13		fitting	nipple, coupling, clamps, elbow, tee, union, etc.,	
14		squirter clamp	For changing the clearance between nozzle & workpiece surface (medium utility clamp round jaws port #67618	
15		electrical wire	wire and subsidiary elements	
16		miscellaneous	focusing lens, etc.	
17	1	focusing lens	focusing lens for imersion transducers, and focal length equals 1.25"	

A-2 TEST PROCEDURE:

The following general procedure is used to perform the surface finish measurements in this research work:

- Calibration: 1) Complete the initial test layout as shown in Fig. (A-1), 2) Install a transducer inside the squirter and use water as first couplant, 3) Put the ultrasonic analyzer (pulser/receiver) in service. Connect transducer to this instrument, according to the analyzer operational manual, 4) Choose the pulse echo position of analyzer,

  5) Select a spot on each surface finish specimen of a test part and measure its surface finish by using a portable stylus type surface finish measurement device. Repeat same measurement procedure for the other specimens of the test part (each test part should have several surface finish specimens), 6) The ultrasonic back-scattered energy will be received by the same transducer and measured with the analyzer.
- Data Recording Process: The acquired data should be tabulated in different matrices as shown at the end of this appendix.
- Data analysis: The obtained data should be analyzed through the parameters variations. All of the data are analyzed to determine a feasible prototype design with respective optimized operating parameters.

APPENDIX-B

B-1 THE SETTING AND SPECIFICATIONS OF INSTRUMENTATIONS:

Ordinarily, a device for measuring surface roughness is a stylus device that operates like a phonograph needle on a record. As the stylus moves across the surface, its vertical motion is converted to an electrical signal which can be plotted to give an indication of surface profile.

Advanced technologies that enable us to measure fine surface finish are: ultrasound, laser, and fiber optic approaches. The superiority of ultrasound is due to its propagation inside the coolant liquid for measuring the surface finish during the grinding process.

The ultrasonic scattering from the surface discontinuity is analyzed by considering the case of perpendicular incidence, similar to our experimental situation. The amount of reflected acoustic energy in conjunction with the incident energy (field energy) at the sensitive surface (peizoelectic) of the transducer is converted to an electrical signal which is analyzed in either time domain or frequency domain. Ultrasonic wave generation and reflection measurement require a certain instrument and device with sufficient capability, and speed.

B-1-1 THE ULTRASONIC WAVE GENERATION AND MEASUREMENT PROCEDURES:

The analyzers that utilize pulse and echo technique are broadly classified as monostatic (one transducer as transmitter and receiver) and bistatic (two transducers, one as a transmitter and another as a receiver).

In our prototype pulse-echo ultrasonic experiment, only one ultrasonic transducer was located perpendicular to the ground part at a certain distance (monostatic). The pulser section of the analyzer (Panametrics Analyzer Model 5052UA) generates short, large-amplitude electrical pulses of controlled energy which are applied to the ultrasonic transducer (piezoelectric crystal). The ultrasonic transducer converts the electrical pulses to the vibrational or sonic pulses that are sent out to the media. At time zero the transducer sends out a pulse of duration, τ, where 20 ns $< \tau <$ 250 ns. Therefore, $\tau / T = (\tau)(f) =$ (250 ns)(10 MHZ) = 2.5 pulses. The distance from the transducer face surface to the test part surface, $z = 31.75*10^{-3}$ m which is greater than $(\tau)(c)/2$ = (250 ns)(1516 m/s)/2 = $18.95*10^{-5}$ m, therefore, the reflection or scattering from the surface roughness of the aimed part is received in the transducer's far field.

By applying the appropriate boundary and initial conditions, we are able to solve the wave equation (3-18) and compute the velocity potential for the incident field. Then the acoustic pressure can be computed by equation(3-16). This final solution will give us the information about the wave propagation in term of the our parameters variation.

Application of mathematical modeling of surface finish, the reflection and scattering enables us to study the geometrical and the mathematical behavior of ultrasonic reflected or echoed waves available to the transducer surface.

The ultrasonic transducer converts the received ultrasonic pulses to the electrical signals. The transducer electrical signals are amplified by the receiver section of the analyzer and sent to the stepless gate section through the high-pass filter.

The stepless gate feature provides capability of selecting the part of the signal train to be analyzed. The stepless nature of the gate is derived from a double-balanced mixer

(DBM) circuit which permits a small segment from the time-domain signal train to be passed by the DBM during the time the gate pulse is on.

The A-scan or time-domain presentation of the oscilloscope is taken from the marked output connector of the analyzer (Panametric 5052UA). This signal is the radio-frequency (R.F.) output from the pulser-receiver with a pedestal superimposed on the signal that corresponds to the position and the width of the gate pulse. This enable us to find out the position of the gate from the time-domain wave.

The A-scan signals were analyzed by a sophisticated digital programmable oscilloscope (Gould Model 4072) equipped with color digital plotter interface with the following important specifications:

1) Bandwidth
   DC: 0 - 100 MHZ (-3dB), and AC: 4 HZ - 100 MHZ (-3dB). The input coupling DC was chosen in our measurements, because the input signal is directly coupled to the oscilloscope. In this way, all frequency components of the input signal can be displayed since the bandwidth is normally from DC (0) to 100 MHZ.
2) Sensitivity
   2 mV/div to 5 V/div, we programmed on 500 mv/div
3) Accuracy
   ± 3 % of full scale
4) Acquisition System
   Maximum signal event useful storage bandwidth is 100 MHZ
5) Maximum Sample Rate
   400 M samples/sec when operating in a single channel mode at 250 ns/div or 200 M samples/sec with both input channels(first rate was programmed in our experiment)
6) Post-Storage Analysis functions
   6-1) filter: There are six selectable low-pass filtering per timebase range.
      Cut-off frequency = $(15.92/t_d)\ln(1+1/2^n)$
      where t_d = timebase range in sec/div, it was adjusted on 20 ns/div (maximum delay 0.4sec).
      n = selected filter step, n=6 was used in our tests
      Therefore, cut-off frequency = 12.34 MHZ
      Note: Timebase sample accuracy is ±0.01 %.
   6-2) Restore: It displays trace as if the most recent post-storage function selected is removed .
   6-3) Trace magnification/attenuation: It magnifies the trace from 0.06 to 4.00 times in 63 steps selectable by increment/decrement controls.

6-4) Integration: the oscilloscope can calculate the indefinite integral with respect to the voltage datum and displays the resultant waveform on its screen. The trace is auto-scaled.

6-5) Area: the oscilloscope can calculate the area under a curve with limits defined by the cursor and datum. The integration and area functions are useful tools for comparing the received signals from the different surface finishes.

Post-Storage Measurements

This oscilloscope is able to measure rise/fall Time, Overshoot, duty cycle, pulse width, max. min., peak-peak Of a maveform, and RMS (root mean square) voltage of a waveform bracketed between the cursor and datum.The RMS values are calculated with respect to both the voltage datum and the mean of the waveform, excluding some cases when the measurements were done in term of Peak-Peak,we usually measured the received or echoed signals in term of the RMS values during our experiments.

B-2 INSTRUMENTATION SETTING IN THE RESEARCH WORK:

The instrumentation used in the research were first calibrated, then set according to the tests requirements and conditions. The following instrumentation settings are listed for flat part and cylidrical part surface finish measurement.

B-2-1 Flat Plate:

Pulser: Pulse Repetition Rate=100 HZ
Electrical Energy Input to Transducer Piezoelectric Crystal=$94*10^{-6}$ joules
Exit Pulser= Pulse Echo.

Receiver: Attenuation rate=10 db
H.P. Filter=1. MHZ
Receiver Gain= 40 dB at 1 MHZ.

Oscilloscope: Trigger=500 mv: 250 ns
Function: RMS (mv)

Test Part: Four gauge flat plat specimens were purchased from microfinish Comparator, catalog No. s-22, the respective surface finishes were 8,16, 32, 63 μin, Ra. Another gauge flat plat was manufactured at Metcut Research Associates Inc. It had three surfaces with respective surface finishes 12, 20 and 120 μin ,Ra.

B-2-2Cylindrical Part:

Pulser: Repeating Rate=100 Hz
Electrical Energy Input to Transducer Piezoelectric Crystal=$94*10^{-6}$ joules.

Exit Pulser=Pulse Echo

Receiver: Attenuation Rate=10 db
H.P. Filter=1.0 MHZ
Receiver Gain=40 db at 1 MHZ

Oscilloscope: Trigger=500 mv: 250 ns
Function: RMS (mv) value

TEST PART: The specifications of four cylindrical parts are presented in Chapter 8.

ULTRASONIC ANALYZERS

(MODEL 5052UA)

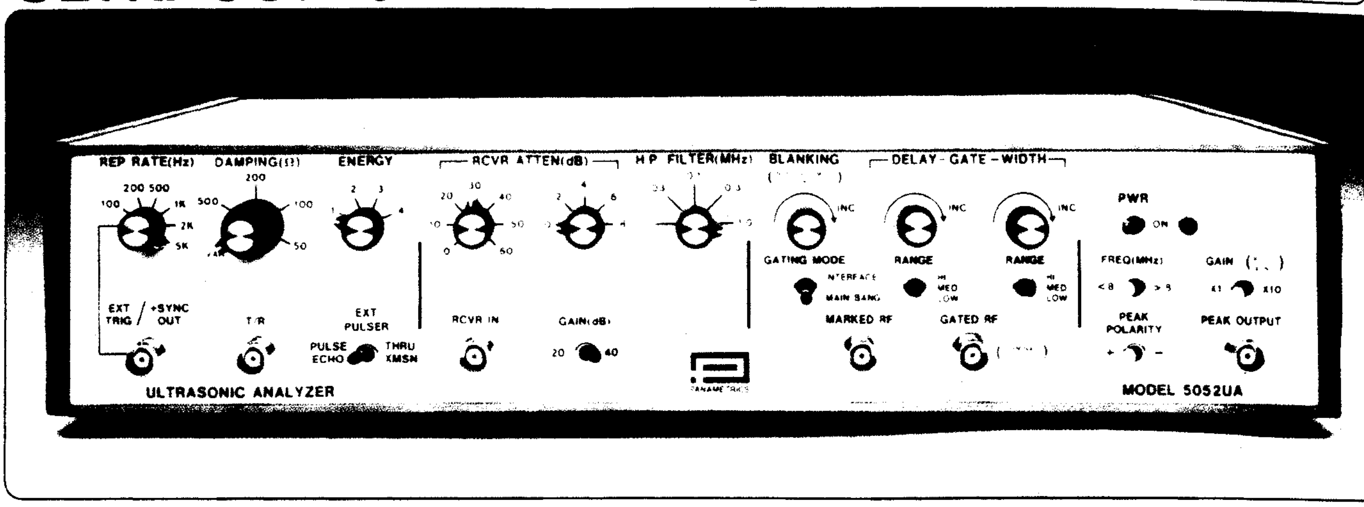

The Model 5052UA Ultrasonic Analyzer is a flexible ultrasonic instrument that incorporates a broadband Pulser/Receiver, Stepless Gate and Gated Peak Detector in a single convenient stand-alone package. It has earned a worldwide reputation for performance and reliability in an extremely broad range of applications.

The Pulser/Receiver section has all of the performance and versatility of our Model 5052PR, with controls that offer both discrete calibrated settings for easy and accurate reproduction of test conditions, and continuous adjustment capability.

The 5052UA's Stepless Gate section allows the user to select a specific portion of an ultrasonic signal for further analysis. The gate may be triggered from the main bang or a selected interface echo; the gate window's position and width are continuously variable from 100 nsec to > 200 μsec in three overlapping ranges, permitting isolation of virtually any part of a signal for analysis.

The Gated Peak Detector section generates a DC voltage proportional to the peak amplitude of either an RF positive or negative ultrasonic waveform within the gate window, which may be used as an output for analog or gray scale recording. It features an extremely fast response time to a minimum number of pulses.

When combined with an oscilloscope and appropriate transducers, the 5052UA can be used for such applications as flaw detection, thickness gaging and sound velocity measurements. With the addition of a spectrum analyzer, it has been widely used for ultrasonic transducer characterization and spectrum analysis.

SPECIFICATIONS

PULSER RECEIVER SECTION	
MAXIMUM PULSER VOLTAGE:	-220V into 50Ω -300V into 500Ω
AVAILABLE ENERGY CONTROL:	Switch selectable: 14, 36, 58 and 94 microjoules
RISE TIME:	<10nS (50Ω damping, #1 energy position)
DAMPING:	Switch selectable: 50, 100, 200 and 500Ω (Pulse echo mode) Variable: 10 to 400Ω ± 10%
REPETITION RATE:	Internal: 0.1, 0.2, 0.5, 1, 2 and 5KHz switch selectable External: 0 to >10KHz
VOLTAGE GAIN:	Switch selectable 20dB (×10) or 40dB (×100)
BANDWIDTH (-3dB):	0.001 - 35MHz
NOISE (Referred to the input):	<80μV pk-pk (BW = 35MHz)
ATTENUATION:	0 to 68dB (2dB Steps)
HIGH PASS FILTERS:	Switch selectable: 1, 30, 100, 300 and 1000KHz
STEPLESS GATE SECTION	
GATE DELAY RANGE:	0.1 to >200μS
DELAY MODE:	Main Bang or selected interface echo
GATE WIDTH RANGE:	50nS to >200μS
BLANKING DELAY:	3 to 100μS
GATE BANDWIDTH:	0.05 - 50MHz
GATED RF LEVEL:	±0.6V pk max. into external 50Ω
MARKED RF OUTPUT LEVEL:	Gate Pedestal Level: ≈ +40mV RF Output Level: equal to input (±1dB up to 1V pk) Z_0 = 50Ω

STEPLESS GATE SECTION CONTINUED	
SWITCHING TRANSIENTS:	<15mV
ISOLATION:	Typically 46dB @ 30MHz for signals less than ±0.6V pk
PEAK DETECTOR SECTION	
OUTPUT LINEAR DYNAMIC RANGE:	+20mV to >1.0V (>34dB)
CONVERSION GAIN: Peak Detector Output / Gated RF Peak Amplitude	Selectable 1.0 or 10.0 ±5%
OUTPUT DRIVE IMPEDANCE:	20Ω
PEAK LEVEL ACCURACY:	±5% of full scale (0.1-20MHz) Useable to 40MHz
TYPICAL RESPONSE TIME:	1 pulse < 3.0MHz 8 pulses < 10MHz 20 pulses < 30MHz (repetitions required for output to settle within 5% of final value)
POLARITY OF DETECTED RF:	Selectable positive or negative
OUTPUT RESET:	Completed within 4μS following every tenth or fifth sync pulse
DECAY RATE:	Internally selectable: SLOW: <0.1V/sec FAST: 20μS
MISCELLANEOUS	
OPERATING TEMPERATURE:	0° to 50°C
SIZE:	17" W × 3½" H × 13" D, (432mm × 89mm × 330mm)
POWER:	115/230VAC, 50-60Hz, 20W
WEIGHT:	8.5 lbs. (3.8 Kg)

All specifications subject to change without notice.

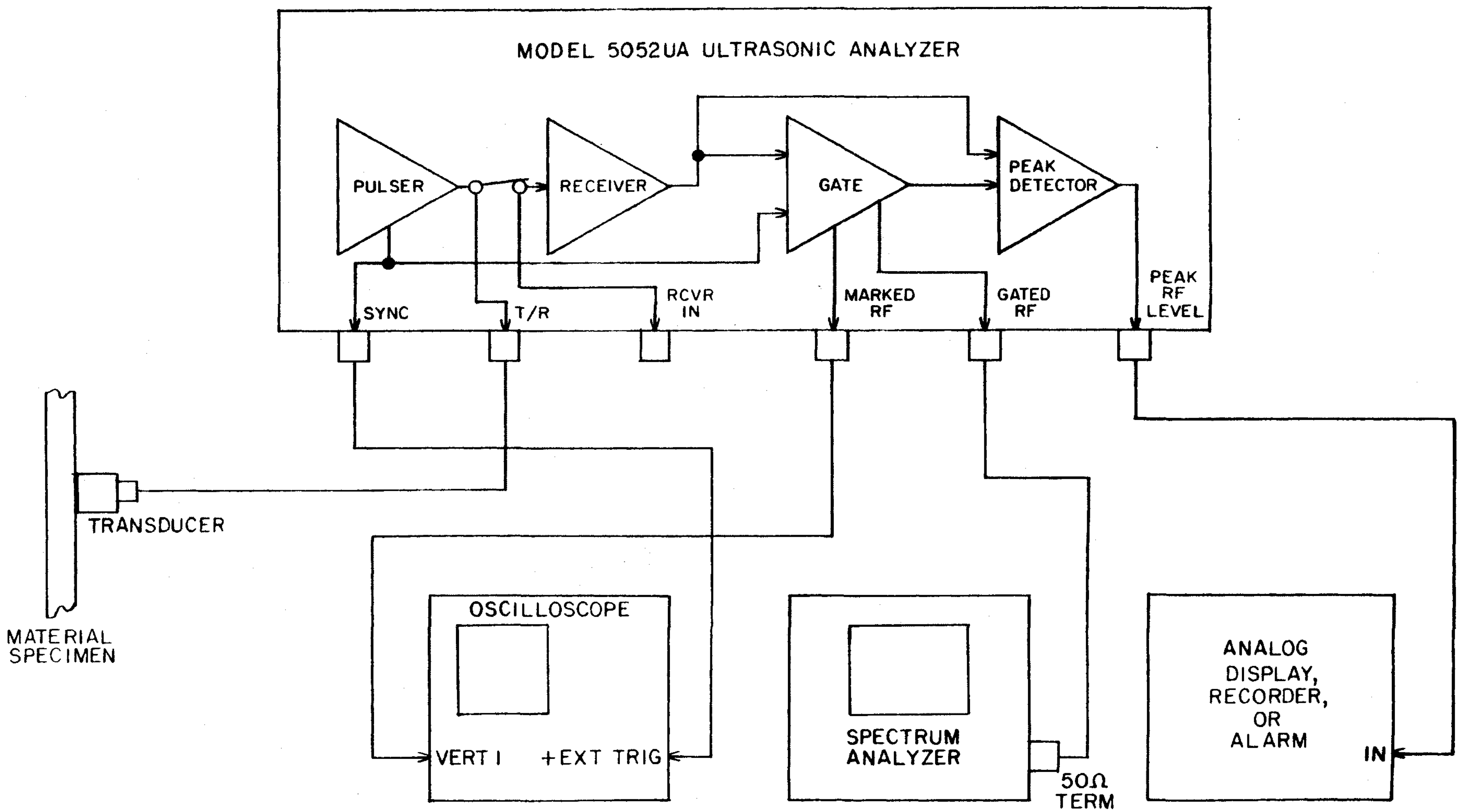

BASIC CONNECTION DIAGRAM FOR ULTRASONIC ANALYZER MODEL 5052UA

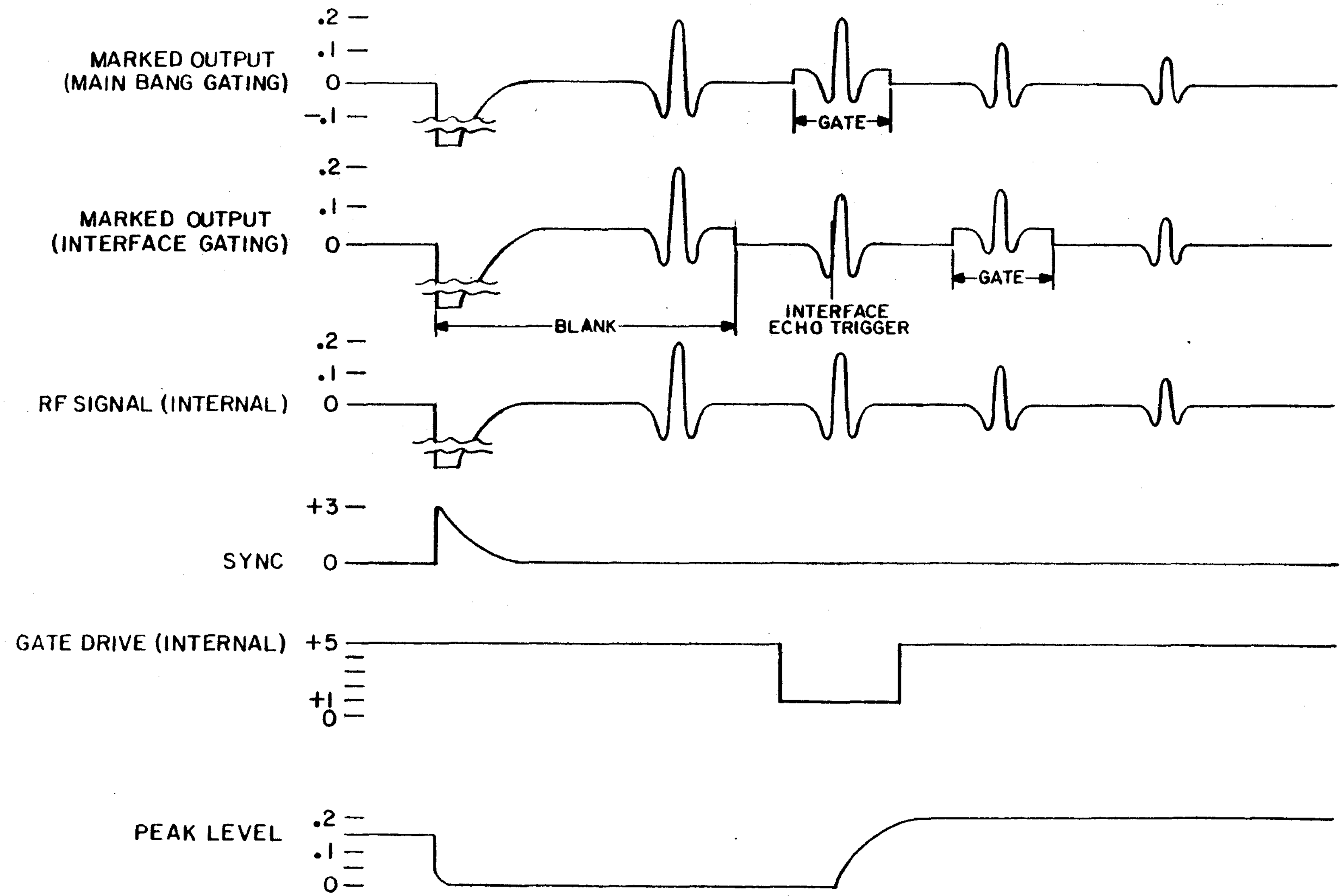

TYPICAL WAVEFORMS SHOWING GATING AND SINGLE SHOT PEAK DETECTION.

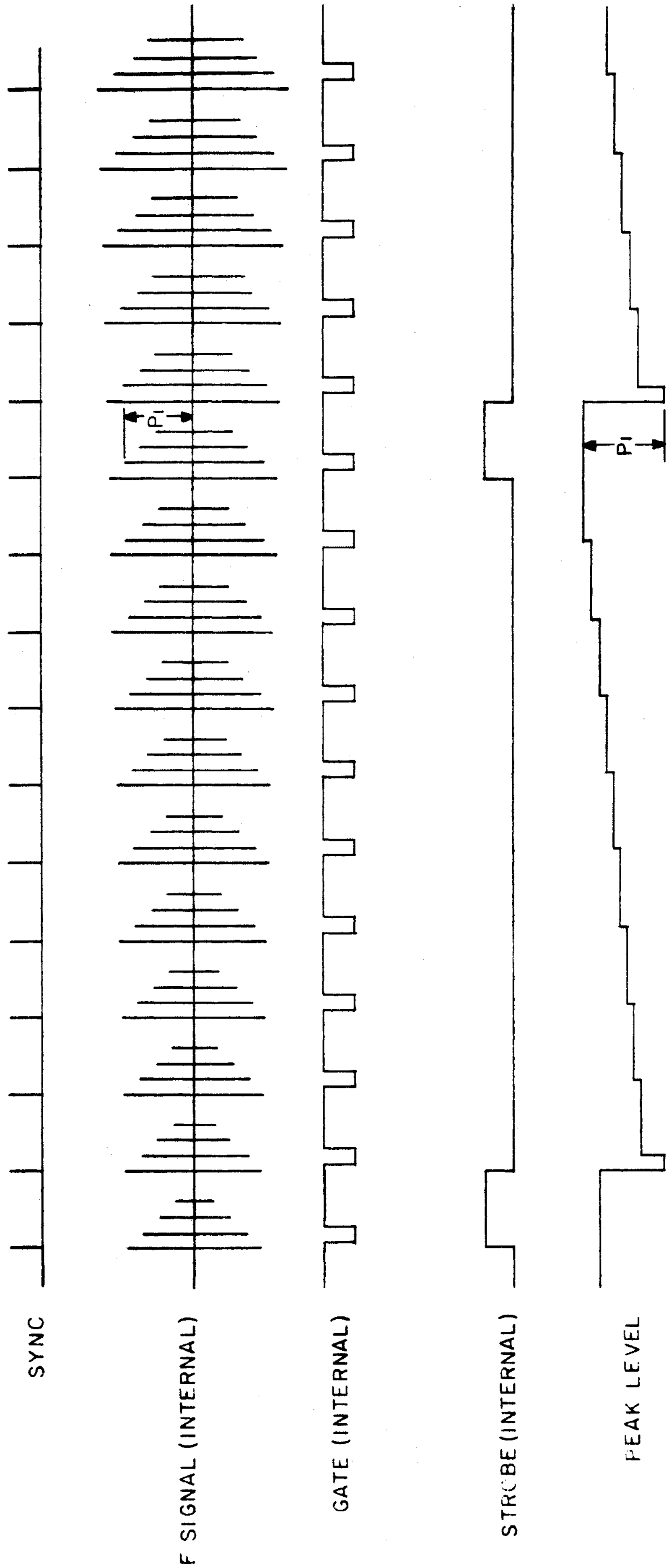

TYPICAL WAVEFORMS SHOWING STAIRCASE RESPONSE TO HIGH FREQUENCY ECHOS.

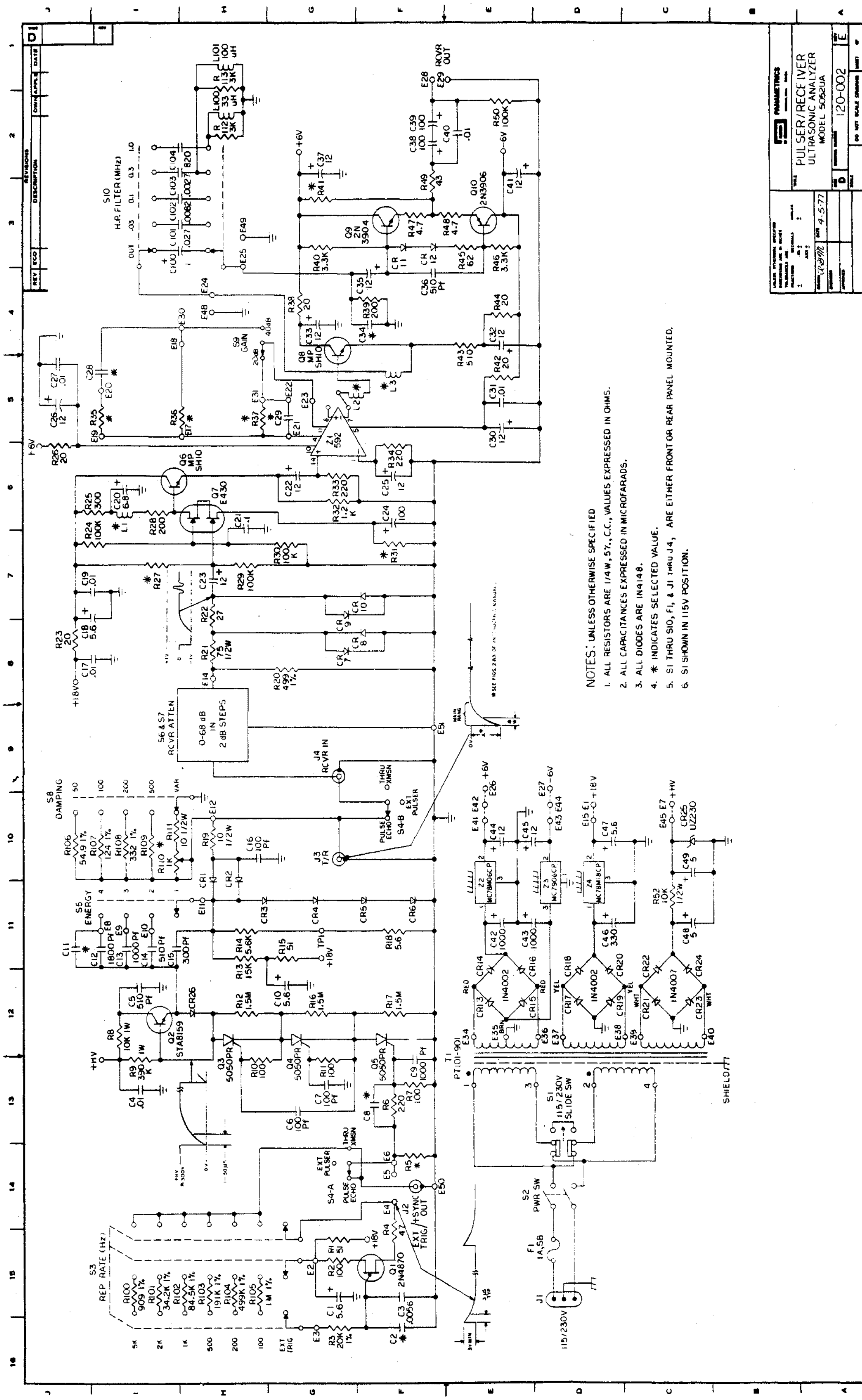
PARAMETRICS
PULSER/RECEIVER
ULTRASONIC ANALYZER
MODEL 5052UA
120-002
4-5-77
NOTES: UNLESS OTHERWISE SPECIFIED
1. ALL RESISTORS ARE 1/4 W, 5%, C.C., VALUES EXPRESSED IN OHMS.
2. ALL CAPACITANCES EXPRESSED IN MICROFARADS.
3. ALL DIODES ARE IN4148.
4. * INDICATES SELECTED VALUE.
5. S1 THRU S10, F1, & J1 THRU J4, ARE EITHER FRONT OR REAR PANEL MOUNTED.
6. S1 SHOWN IN 115V POSITION.

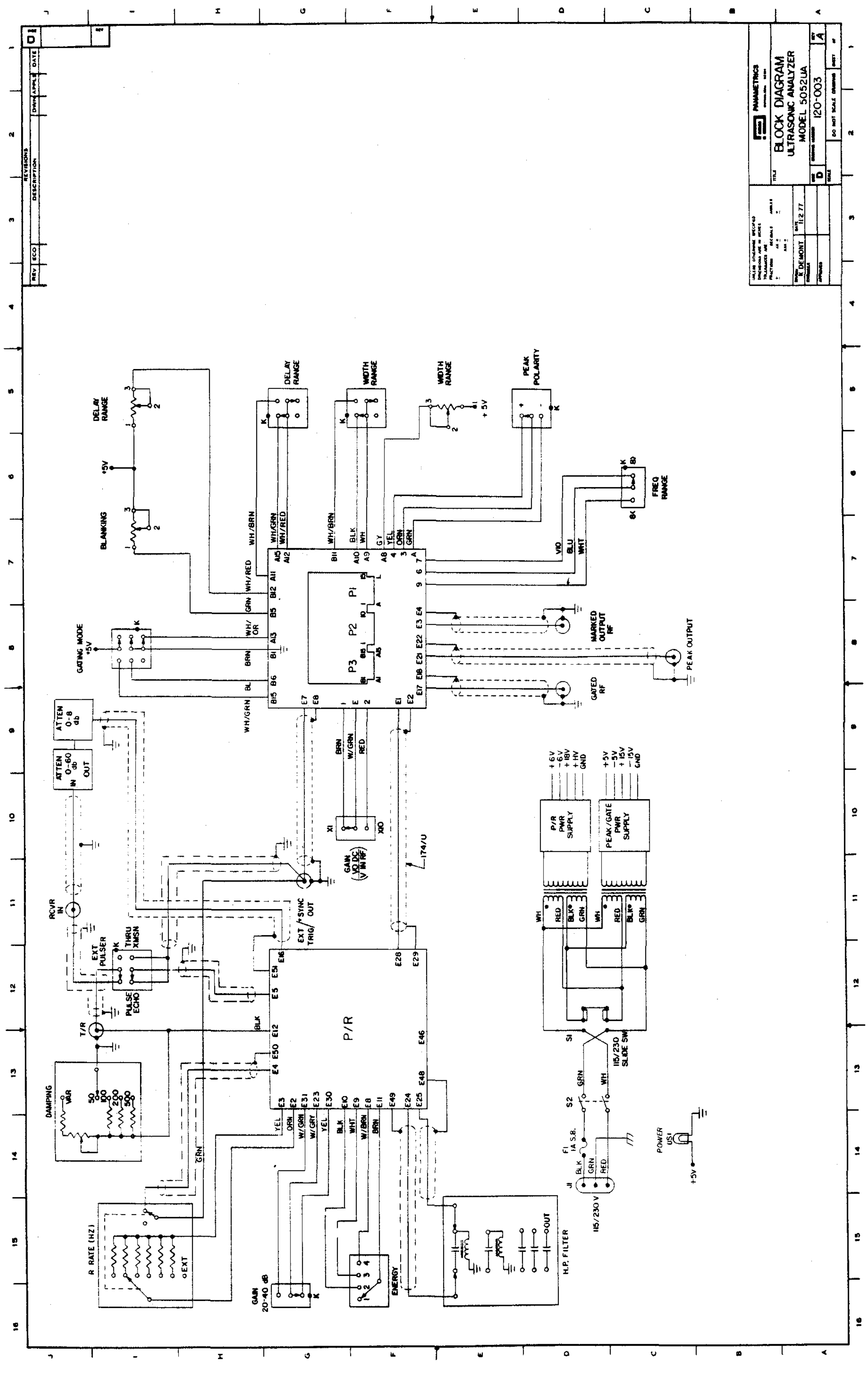
PANAMETRICS
BLOCK DIAGRAM
ULTRASONIC ANALYZER
MODEL 5052UA
120-003
REVISIONS
DELAY RANGE
BLANKING
WIDTH RANGE
PEAK POLARITY
FREQ RANGE
GATING MODE
MARKED OUTPUT RF
PEAK OUTPUT
GATED RF
ATTEN 0-8 db
ATTEN 0-60 db
RCVR IN
EXT PULSER
THRU XMSN
PULSE ECHO
T/R
DAMPING
R RATE (HZ)
GAIN 20-40 dB
ENERGY
H.P. FILTER
P/R
P/R PWR SUPPLY
PEAK/GATE PWR SUPPLY
115/230 SLIDE SW
POWER
115/230 V

PANAMETRICS 221 CRESCENT STREET, WALTHAM, MASSACHUSETTS [illegible] / [illegible] TELEX [illegible]

TRANSDUCER DESCRIPTION

P/N V312 FREQ: 10.0MHZ SIZE: .250X.000"
S/N109735 UNFOCUSSED IMMERSION

TEST INSTRUMENTATION

PANAMETRICS 5052 UA: #3
ENERGY SETTING: 1
PULSER DAMPING: 50ohms
RECEIVER ATTENUATION: 44dB
CABLE: RG-58/U LENGTH: 4FT.

LECROY9400-V2.06FT DIGITAL OSCILLOSCOPE: #2

TEST CONDITIONS

ECHO FROM FRONT SURFACE OF 1.0" SILICA
TESTED ACCORDING TO DRAWING #5978

ASTM E1065 MEASUREMENTS

PEAK FREQUENCY ------ 10.1MHZ
CENTER FREQUENCY ---- 9.75MHZ
UPPER FREQUENCY @-6dB 13.2MHZ
LOWER FREQUENCY @-6dB 6.30MHZ
BANDWIDTH ----------- 70.8%

WAVEFORM DURATION:
@-20dB LEVEL .218usec
@-40dB LEVEL .837usec

COMMENTS:

TECHNICIAN (S):

WAVEFORM

VERTICAL SENSITIVITY: 200mv/div
HORIZONTAL SENSITIVITY: .10us/div

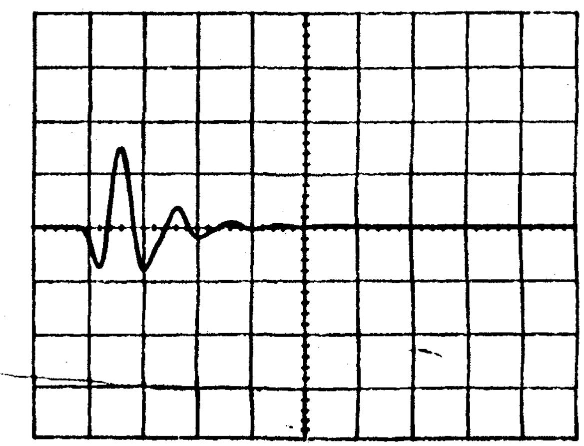

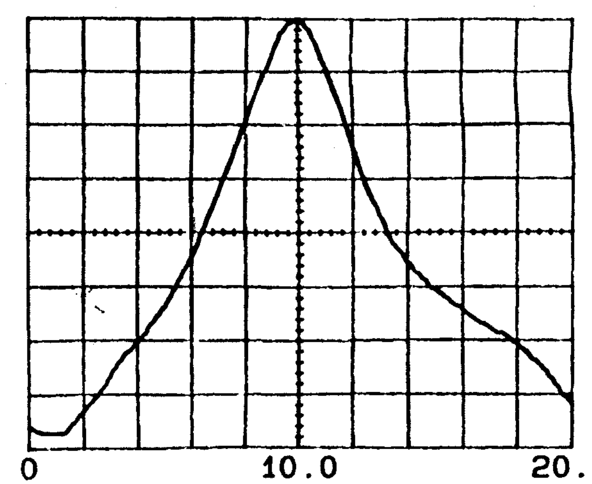

SPECTRUM
SCALE FORMAT: LINEAR (MHZ)

PANAMETRICS 221 CRESCENT STREET, WALTHAM, MASSACHUSETTS 02254 · 617 899-2719 TELEX: 923408

IMMERSION TRANSDUCER ANALYSIS FORM

PART NO. V354 SERIAL NO. 100566 FREQUENCY 20.0 MHz.

SIZE: 0.25 " DIAMETER: N/A " BY N/A ". CABLE: RG-58A/U LENGTH 4 ft.

WATER PATH 1.0 ". FOCUSSED AT N/A ". DESIGN FOCAL LENGTH N/A ".

ECHO FROM FRONT SURFACE OF 1.0 " THICK FUSED SILICA.

_____ " DIAMETER STEEL BALL.

TEST INSTRUMENTATION

_____ PANAMETRICS 5052 (PR,G) PULSER and GATE # _____

✓ PANAMETRICS 5052UA or 5030A # 6

TEKTRONIX # 5 7704A OSCILLOSCOPE MAINFRAME

lug in's # 5 7A26 DUAL TRACE AMPLIFIER

3 7B53A DUAL TIME BASE

4 7L12 SPECTRUM ANALYZER

Center frequency is determined by multiplying the horizontal scan width (4) by the number of divisions to the spectrum peak.

1 3 6

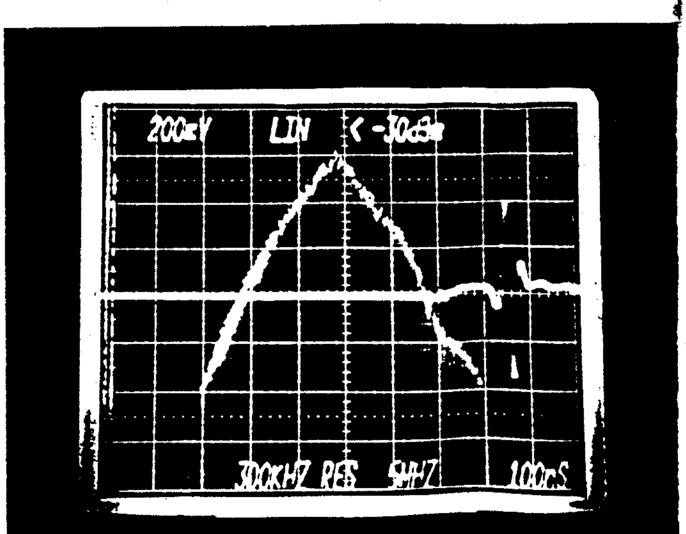

WAVE FORM

PULSER RECEIVER SETTINGS:

ENERGY SETTING: 1

RECEIVER ATTENUATION 30 dB

RECEIVER DAMPING 50 ohms

OSCILLOSCOPE SETTINGS:

1-VERTICAL SENSITIVITY/div.

2-HORIZONTAL SENSITIVITY/div.

SPECTRUM ANALYSIS

3-SCALE FORMAT

4-HORIZONTAL SCAN WIDTH/div.

5-RESOLUTION

6-INPUT ATTENUATION

TECHNICIAN [signature]

DATE 4/17/87

PANAMETRICS 221 CRESCENT STREET, WALTHAM, MASSACHUSETTS 02254 · 617 899-2719 TELEX: 923406

IMMERSION TRANSDUCER ANALYSIS FORM

PART NO. V356 SERIAL NO. 105285 FREQUENCY 30.0 MHz.

SIZE: 0.25 " DIAMETER: N/A " BY N/A ". CABLE: RG-58A/U LENGTH 4.0 ft.

WATER PATH 1.0 ". FOCUSSED AT N/A ". DESIGN FOCAL LENGTH N/A ".

ECHO FROM FRONT SURFACE OF 1.0 " THICK FUSED SILICA.

______ " DIAMETER STEEL BALL.

TEST INSTRUMENTATION

____ PANAMETRICS 5052 (PR,G) PULSER and GATE # ____

✓ PANAMETRICS 5052UA or [5030A] # 2

TEKTRONIX # 5 7704A OSCILLOSCOPE MAINFRAME

plug in's # 2 7A26 DUAL TRACE AMPLIFIER

3 7B53A DUAL TIME BASE

3 7L12 SPECTRUM ANALYZER

Center frequency is determined by multiplying the horizontal scan width (4) by the number of divisions to the spectrum peak.

1 3 6

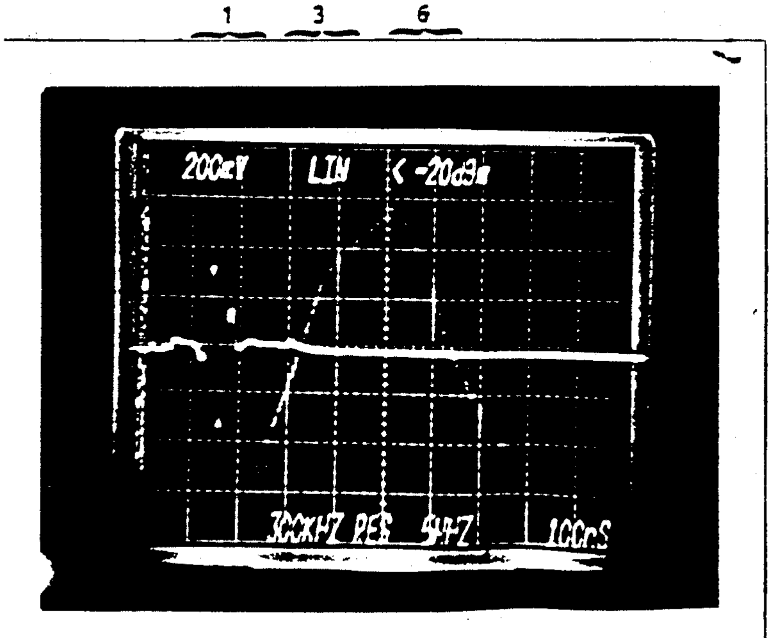

0f 5 4 2

WAVE FORM

PULSER RECEIVER SETTINGS:

ENERGY SETTING: 1

RECEIVER ATTENUATION 30 dB

RECEIVER DAMPING 50 ohms

OSCILLOSCOPE SETTINGS:

1-VERTICAL SENSITIVITY/div.

2-HORIZONTAL SENSITIVITY/div.

SPECTRUM ANALYSIS

3-SCALE FORMAT

4-HORIZONTAL SCAN WIDTH/div.

5-RESOLUTION

6-INPUT ATTENUATION

TECHNICIAN [signature]

DATE 10-6-87

PANAMETRICS 221 CRESCENT STREET, WALTHAM, MASSACHUSETTS 02254 / 617 899-2719 TELEX: 923406

IMMERSION TRANSDUCER ANALYSIS FORM

PART NO. V376 SERIAL NO. 111741 FREQUENCY 30.0 MHz.

SIZE: 0.25 " DIAMETER: — " BY — ". CABLE: RG-58a/u LENGTH 4 ft.

WATER PATH ______ ". FOCUSSED AT ______ ". DESIGN FOCAL LENGTH 1.25 OLF ".

ECHO FROM BACK SURFACE OF 0.228 " THICK FUSED SILICA.

______ " DIAMETER STEEL BALL.

TEST INSTRUMENTATION

____ PANAMETRICS 5052 (PR,G) PULSER and GATE # ____

✓ PANAMETRICS 5052UA or 5030A # 2

TEKTRONIX # 4 7704A OSCILLOSCOPE MAINFRAME

plug in's # 4 7A26 DUAL TRACE AMPLIFIER

6 7B53A DUAL TIME BASE

5 7L12 SPECTRUM ANALYZER

Center frequency is determined by multiplying the horizontal scan width (4) by the number of divisions to the spectrum peak.

1 3 6

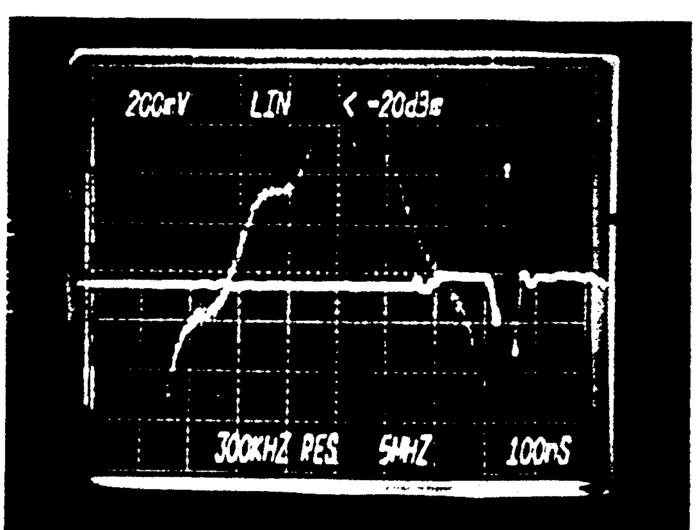

↑ 0f 5 4 2

185

WAVE FORM

PULSER RECEIVER SETTINGS:

ENERGY SETTING: 1

RECEIVER ATTENUATION 20 dB

RECEIVER DAMPING 50 ohms

OSCILLOSCOPE SETTINGS:

1-VERTICAL SENSITIVITY/div.

2-HORIZONTAL SENSITIVITY/div.

SPECTRUM ANALYSIS

3-SCALE FORMAT

4-HORIZONTAL SCAN WIDTH/div.

5-RESOLUTION

6-INPUT ATTENUATION

TECHNICIAN [signature]

DATE 6/24/88

Introduction

NOTE: This is a combined operating manual for the 4071 and 4072 2-Channel and the 4074 4-Channel Digital Storage Oscilloscopes.

Throughout the operating manual the following convention applies:-

4070 – refers to the 4071, 4072 and 4074.
4071 – refers to only the 2 channel 4071.
4072 – refers to only the 2 channel 4072.
4074 – refers to only the 4 channel 4074.

Gould's 4070 series of digital oscilloscopes have been designed with the user in mind. These highly sophisticated instruments are particularly easy to use.

To obtain a trace is especially simple – just connect the signal and press the Auto Setup button – the 4070 does the rest. Having obtained a trace, three readily accessible cursors make it easy to take timing and voltage measurements directly from the screen. The built-in plotter or an external plotter using HPGL can be used to make a hard copy of the display for future reference as well.

For the more advanced user, the 4070 series have a great deal to offer. The GPIB(IEEE488) and RS423(RS-232) interfaces, allow control by a computer, hence the oscilloscope can be left unattended whilst it continues to take measurements and plot traces as and when required. All of the operating functions can be controlled by the computer and the oscilloscope can output complete trace data to the computer for further analysis.

The 4070 incorporates a software menu system allowing functions to be easily accessed. For example, up to four control setups including attenuator, trigger, GPIB and RS423 settings can be stored in battery-backed memory for future use with the 'Save and Recall Setups' menu.

The trigger menu allows the 4070's triggering system to be controlled using a 'Trigger Configuration Diagram'. This is designed to mimic the way that most users think about complex triggering requirements. It displays a flow diagram allowing various conditional triggering options to be set and combined appropriately. Options include event counting, time delays, and trace B to wait for triggering on trace A.

The Display menu allows control of some of the 4070's most advanced facilities. For example, using this menu, it is possible to select the glitch detection function. This can be used to detect transients as brief as 5ns even on the slowest timebase ranges. It is also useful for alias detection in certain circumstances. Another option, particularly useful when a trace has been magnified in the X direction, is interpolation. The 4070 is able to perform rapid sine interpolation on captured signals. Points are calculated and inserted between the actual samples which make up the originally captured trace. The original trace data is not lost and the uninterpolated display can be retrieved at any time. The 4070 can also perform linear interpolation if required.

The oscilloscope is also fitted with a keypad interface, allowing Gould waveform processors to be connected to provide extra functions. These include automatic measurement of risetime, overshoot and frequency.

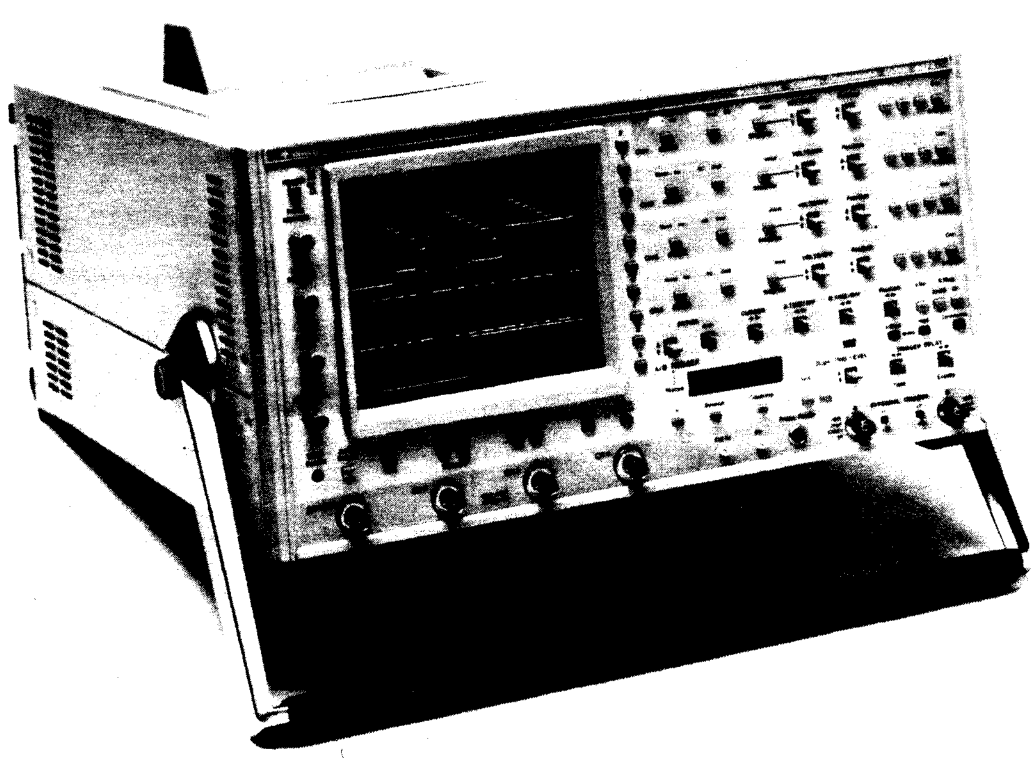

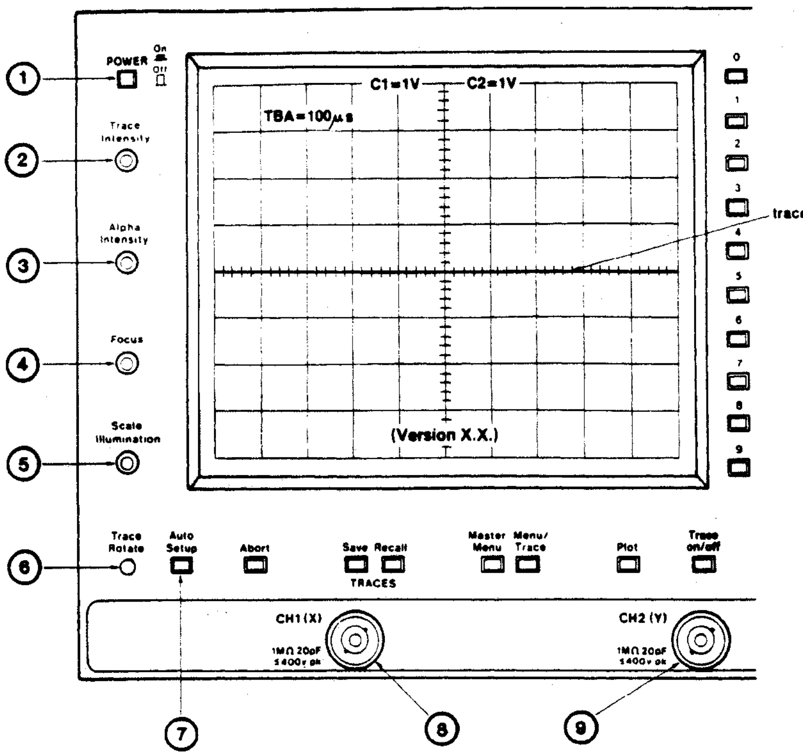

Power-on Display (4071 & 4072)

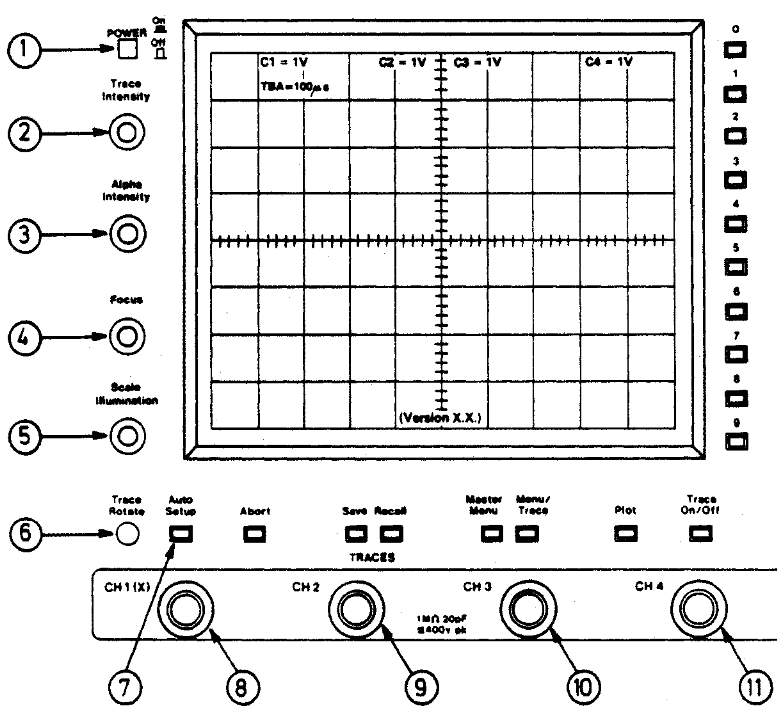

Power-on Display (4074)

APPENDIX-C

C-1 ALGORITHM:

1- **expm**: an exponential function with square matrix exponent for computing the complex exponents based on the approximation theory. Complex results are produced if Variable parameter has negative eigenvalues.

2- **besseln**: used for computing the Bessel' functions. The mode numbers are integer numbers , therefore, algorithm besseln is used in Codes 1 and 2.

C-2 Symbols:

c: speed of ultrasonic wave in the coolant.
c_p: specific heat.
κ: thermal conductivity.
k: wave number
K:eigenvalues
J: Bessel's function.
I: Ultrasonic wave intensity.
P: Ultrasonic wave pressure
r: tube radius variable, a: tube radius ($1.59*10^{-3}$ m).
t: time.
z: height (distance from transducer face or from the oart surface.
α: eigenvalues.
β: expansion coefficient.
ρ: coolant density.
ω: transducer frequency.

C-3 CODES:

The cylindrical surface finish measurement are analyzed by computer codes, based upon the empirical equations which were obtained through this research work.

Codes descriptions are presented in Chapter 7. A proper code is written for any research parameter either individually or in conjunction with some of variables.

The following codes are written in PC-MATLAB for surface finish measurement of the cylindrical parts:

<u>Code-1:</u> This code is written in PC-MATLAB, to compute the amplitudes of eigen function, lateral modes, in Fourier Bessel Series form. It also enable us to do modal analysis for ultrasonic wave propagation in lateral direction of the tube shape passage of the waveguide assembly, fundamental and lateral modes.

```
pi=3.141592654
a=1.59E-3;
alpha=[.0000001 2.41 4.41 6.40 8.83];
r=[0. .0006 .0012 .0014 1.59E-3];
z=[0. .0061 .0081 .0121 .0162];
c=1516
i=(-1)^(.5)
rho=983
omega=2*pi*10E7
for n=1:5
    JA1=besseln(1,alpha(n)*a)+besseln(3,alpha(n)*a);
    JA2=besseln(5,alpha(n)*a)+besseln(7,alpha(n)*a);
    JA=(JA1+JA2)*sin(alpha(n)*a);
    JB1=besseln(2,alpha(n)*a)+besseln(4,alpha(n)*a);
    JB2=besseln(6,alpha(n)*a);
    JB=(JB1+JB2)*cos(alpha(n)*a);
    JAB=JA-JB
  C=(a*besseln(1,alpha(n)))^(-2);
   for m=1:5
       A(n,:)=C*JAB/alpha(n)*r(m);
           K(n)=omega/c*(1-c*alpha(n)/omega)^(.5);

     end
   end
diary A.dat
r
alpha
A
diary off
diary metxy.plt
end
clg
plot(r,A(1,:),A,E(2,:),r,A(3,:),r,A(4,:),r,A(5,:))
grid
title ('LATERAL AMPLITUDE OF THE PROPAGATING MODE')
xlabel ('Tube Radius (m)')
ylabel ('Amplitude')
diary off
```

__Code-2:__ This code is written in PC-MATLAB, to compute the amplitudes of general solution, in Fourier Bessel Series form. It also enable us to do modal analysis for ultrasonic wave propagation in the tube shape passage of the waveguide assembly, fundamental and lateral modes.

```
pi=3.141592654
a=1.59E-3;
alpha=[.0000001 2.41 4.41 6.40 8.83];
r=[0. .0006 .0012 .0014 1.59E-3];
z=[0. .0061 .0081 .0121 .0162];
c=1516
i=(-1)^(.5)
rho=983
omega=2*pi*10E7
for n=1:5
    JA1=besseln(1,alpha(n)*a)+besseln(3,alpha(n)*a);
    JA2=besseln(5,alpha(n)*a)+besseln(7,alpha(n)*a);
    JA=(JA1+JA2)*sin(alpha(n)*a);
    JB1=besseln(2,alpha(n)*a)+besseln(4,alpha(n)*a);
    JB2=besseln(6,alpha(n)*a);
    JB=(JB1+JB2)*cos(alpha(n)*a);
    JAB=JA-JB
  C=(a*besseln(1,alpha(n)))^(-2);
   for m=1:5
       A(n,:)=C*JAB/alpha(n)*r(m);
           K(n)=omega/c*(1-c*alpha(n)/omega)^(.5);
     for l=1:5
       t(l)=z(l)/c;
       E(n,:)=abs(A(n,:)/(exp(-i*omega*t(l)).')*cos(K(n)*z(l)))

        end
     end
   end
diary E.dat
r
alpha
E
diary off
diary metxy.plt
end
clg
plot(r,E(1,:))
grid
title ('AMPLITUDE OF THE FUNDAMENTAL PROPAGATING MODE')
xlabel ('Tube Radius (m)')
ylabel ('Amplitude')
diary off
```

Code-2: This code is written in PC-MATLAB, to compute the amplitudes of general solution, in Fourier Bessel Series form. It also enable us to do modal analysis for ultrasonic wave propagation in the tube shape passage of the waveguide assembly, fundamental and lateral modes.

```
pi=3.141592654
a=1.59E-3;
alpha=[.0000001 2.41 4.41 6.40 8.83];
r=[0. .0006 .0012 .0014 1.59E-3];
z=[0. .0061 .0081 .0121 .0162];
c=1516
i=(-1)^(.5)
rho=983
omega=2*pi*10E7
for n=1:5
    JA1=besseln(1,alpha(n)*a)+besseln(3,alpha(n)*a);
    JA2=besseln(5,alpha(n)*a)+besseln(7,alpha(n)*a);
    JA=(JA1+JA2)*sin(alpha(n)*a);
    JB1=besseln(2,alpha(n)*a)+besseln(4,alpha(n)*a);
    JB2=besseln(6,alpha(n)*a);
    JB=(JB1+JB2)*cos(alpha(n)*a);
    JAB=JA-JB
  C=(a*besseln(1,alpha(n)))^(-2);
   for m=1:5
       A(n,:)=C*JAB/alpha(n)*r(m);
           K(n)=omega/c*(1-c*alpha(n)/omega)^(.5);
     for l=1:5
       t(l)=z(l)/c;
       E(n,:)=abs(A(n,:)/(exp(-i*omega*t(l)).')*cos(K(n)*z(l)))

        end
     end
   end
diary E.dat
r
alpha
E
diary off
diary metxy.plt
end
clg
plot(r,E(2,:),r,E(3,:),r,E(4,:),r,E(5,:))
grid
title ('AMPLITUDE OF THE PROPAGATING MODE')
xlabel ('Tube Radius (m)')
ylabel ('Amplitude')
diary off
```

<u>Code-3:</u> This code is written in PC-MATLAB, to compute the ultrasonic energy attenuation in term of concentration oil volume fraction in the coolant.

```
pi=3.141592654
rho1=924;
rho2=998;
c1=1650;
c2=1482;
nu1=61.0*10^(-4);
nu2=.001;
Cp1=1874;
Cp2=4179;
k1=.148;
k2=.2068*10^(-3);
beta1=.68*10^(-3);
beta2=.2068*10^(-3);
a=.7*10^(-6);
phi=[1 2 3 4 5 6 7 8 9 10];
omega=[10 20  30]*2*pi;
To=293;
for n=1:10
for m=1:3
A=(beta1/(rho1*Cp1)-beta2/(rho2*Cp2))^2;
B=sqrt(rho1*Cp1*k1*rho2*Cp2*k2)/(sqrt(rho1*Cp1*k1)+sqrt(rho2*Cp2*
k2))
alphat(n,m)=phi(n)'*sqrt(omega(m))/a*c2*To*rho2*A*B*100;
end
  end
    end
diary alphat.dat
phi
omega
diary off
diary metxy.plt
end
clg
plot(phi, alphat)
grid
title('ULTRASONIC ENERGY ATTENUATION IN EMULSION (THEORETICAL)')
xlabel('VOLUME FRACTION OF INTERLUBE (%)')
ylabel('ATTENUATION (%)')
```

Code-4: This code is applied to analyze the part surface condition. It shows a relation between feedrate and scattering angle. This code is written in Pc-MATLAB.

```
PI=3.141592654
feedrate=[.637 1.273 1.911 2.548 3.185 3.822 4.459 4.775]*10^(-3);
a=0.0005;
for m=1:8;
x(m)=1/4*feedrate(m);
delta(m)=0.02*x(m) ;
f(m)=1384*(2*feedrate(m))^(-1);
A(m)=a*cos(2*PI*f(m)*x(m));
thetas(m)=abs(atan(delta(m)/A(m))*180/PI)
end
 end
    end
diary thetas.dat
delta
feedrate
a
thetas
diary off
diary metxy.plt
end
clg
plot(feedrate,thetas)
grid
xlabel('FEEDRATE (in/rev.)')
ylabel('SCATTERING ANGLE (DEGREE)')
title('ULTRASONIC SCATTERING ANGLE V.S. SURFACE CONDITION')
diary off
```

__Code-5:__ This code is used to analyze the part surface condition. It shows a relation between cutting depth and scattering angle. This code is written in PC-MATLAB.

```
PI=3.141592654
feedrate=4.775*10^(-3);
a=[0.00025 0.0005 .00075 .001 .00125 .0015 .00175 .002];
for n=1:8
x=1/4*feedrate;
delta=.02*x;
f=1384*(2*feedrate)^(-1);
z(n)=a(n)*cos(2*PI*f*x);
thetas(n)=abs(atan(delta/z(n))*180/PI)
end
 end
    end
diary thetas.dat
delta
feedrate
a
thetas
diary off
diary metxy.plt
end
clg
plot(a ,thetas)
grid
xlabel('CUTTING DEPTH (in.)')
ylabel('SCATTERING ANGLE (DEGREE)')
title('ULTRASONIC SCATTERING V.S. SURFACE CONDITION')
diary off
```

__Code-6:__ This code demonstrates scattering angle variation in term of the feedrate parameter, when the cutting depth parameter is also a variable parameter. This code is written in PC-MATLAB.

```
PI=3.141592654
feedrate=[.637 1.273 1.911 2.548 3.185 3.822 4.459 4.775]*10^(-3);
a=[.00025 .0005 .00075 .001 .00125 .0015 .00175 .002];
for m=1:8;
for n=1:8
x(m)=1/4*feedrate(m);
delta(m)=.02*x(m) ;
f(m)=1384*(2*feedrate(m))^(-1);
A(m,n)=a(n)*cos(2*PI*f(m)*x(m));
thetas(m,n)=abs(atan(delta(m)/A(m,n))*180/PI)
end
 end
    end
diary thetas.dat
delta
feedrate
a
thetas
diary off
diary metxy.plt
end
clg
plot(feedrate,thetas)
grid
xlabel('FEEDRATE (in/rev.)')
ylabel('SCATTERING ANGLE (DEGREE)')
title('ULTRASONIC SCATTERING V.S. SURFACE CONDITION')
diary off
```

<u>Code-7:</u> This code is used to compute the ultrasonic intensity attenuation versus distance increasing. The analysis is done only for a 10 MHZ transducer. This code is written in PC-MATLAB.

```
PI=3.141592654
omega=10*10^6*2*PI
c=1516;
rho=983;
i=(-1)^.5;
z=[.016154 .03175 .034290 .034925 .038100];
for n=1:5;
A=exp(-2*395.2*.034290)
p(n)=7.4*10^17/((omega/c)*z(n))*A;
t=1.;
P(n)=p(n)*expm(i*(omega*(z(n)/c-t)));
I(n)=abs(P(n)^2/(2*rho*c))
end
  end
    end
       end
diary I.dat
z
P
omega
I
diary off
diary metxy.plt
end
clg
plot(z,I)
grid
xlabel('NORMAL DISTANCE FROM THE TRANSDUCER FACE (m)')
ylabel('INTENSITY (Watt/m.m)')
title('ULTRASONIC INTENSITY V.S. DISTANCE (Z)')
diary off
```

Code-8: This code is used to compute the ultrasonic intensity attenuation for wave propagation in term of the distance variation, from transducer face to the part surface. This analysis is also done for 10 MHZ, 20 MHZ and 30 MHZ transducers.

```
pi=3.141592654
omega=[10^7  2*10^7  3*10^7]*2*pi;
c=1516;
rho=983;
i=(-1)^.5;
z=[.016154 .03175 .03429];
t=1;
for n=1:3;
for m=1:3;
k(m)=omega(m)/c
A=exp(-2*395.2*(.03429))
Pi(n,m)=((7.4*10^17)/(k(m)*z(n)))*exp(i*(k(m)*z(n)-omega(m)*t))*A;
Ii(n,m)=abs(Pi(n,m)^2/(2*rho*c));
end
    end
       end
diary Ii.dat
Pi
Ii
z
t
omega
diary off
diary metxy.plt
end
clg
plot(z,Ii)
grid
xlabel('NORMAL DISTANCE FROM THE TRANSDUCER FACE (m)')
ylabel('INTENSITY (watt/m.m)')
title('ULTRASONIC INTENSITY V.S DISTANCE (Z) ')
diary off
```

Code-9: This code is used to compute the ultrasonic intensity attenuation for echo signal, from the part surface to the transducer face. A 10 MHZ transducer is employed in this computation. The code is written in PC-MATLAB.

```
pi=3.141592654
omega=10^7*2*pi;
c=1516;
rho=983;
i=(-1)^.5;
z=[.016154 .03175 .03429 .034925 .038100];
t=1;
for n=1:5;
k=omega/c;
A=exp(-2*395.2*(.03429));
Pi(n)=(7.4*10^17/(k*z(n)))*exp(i*(k*z(n)-omega*t))*A;
Ii(n)=abs(Pi(n)^2/(2*rho*c));
Pr(n)=(6.93*10^17/(k*(-z(n))))*exp(-i*(k*z(n)+omega*t))*A;
Ir(n)=abs(Pr(n)^2/(2*rho*c));
Im(n)=(Ii(n)-Ir(n))
end
  end
    end
       end
diary Im.dat
Pi
Pr
Ii
Ir
z
t
omega
Im
diary off
diary metxy.plt
end
clg
plot(z,Im)
grid
xlabel('NORMAL DISTANCE FROM PART SURFACE (m)')
ylabel('INTENSITY (watt/m.m)')
title('ULTRASONIC INTENSITY V.S DISTANCE (Z) ')
diary off
```

Code-10: This code is used to compute the ultrasonic intensity attenuation for echo signal, from the part surface to the transducer face. This analysis is also done for 10 MHZ, 20 Mhz and 30 MHZ transducers.

```
pi=3.141592654
omega=[10^7  2*10^7  3*10^7]*2*pi;
c=1516;
rho=983;
i=(-1)^.5;
z=[.016154 .03175 .03429];
t=1;
for n=1:3;
for m=1:3;
k(m)=omega(m)/c;
A=exp(-2*395.2*(.03429));
Pi(n,m)=((7.4*10^17)/(k(m)*z(n)))*exp(i*(k(m)*z(n)-omega(m)*t))*A;
Ii(n,m)=abs(Pi(n,m)^2/(2*rho*c));
Pr(n,m)=((6.93*10^17)/(k(m)*(-z(n))))*exp(-i*(k(m)*z(n)+omega(m)*
t))*A;
Ir(n,m)=abs(Pr(n,m)^2/(2*rho*c));
Im=(Ii-Ir)
end
  end
    end
       end
diary Im.dat
Pi
Pr
Ii
Ir
z
t
omega
Im
diary off
diary metxy.plt
end
clg
plot(z,Im)
grid
xlabel('NORMAL DISTANCE FROM PART SURFACE (m)')
ylabel('INTENSITY (watt/m.m)')
title('ULTRASONIC INTENSITY V.S DISTANCE (Z) ')
diary off
```